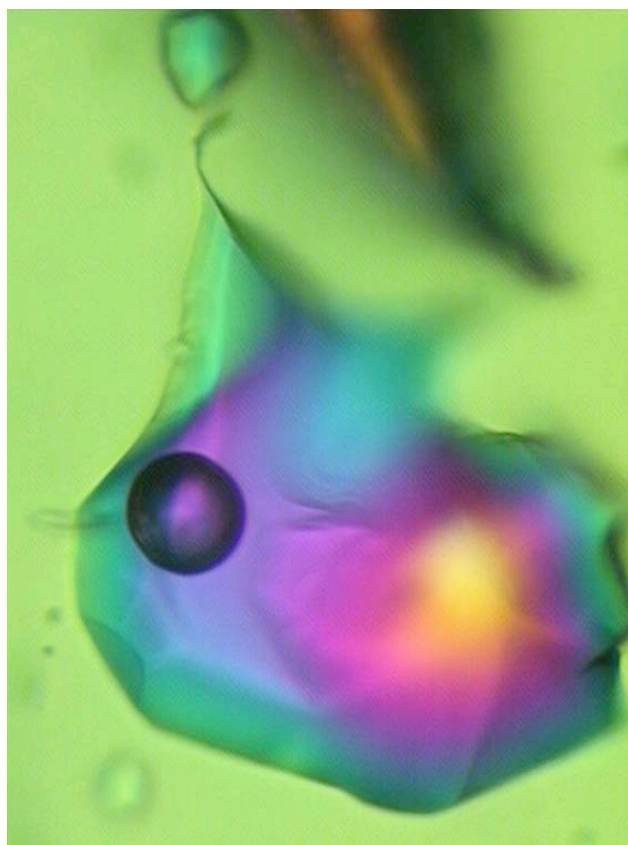# ECROFI XXI

Abstracts

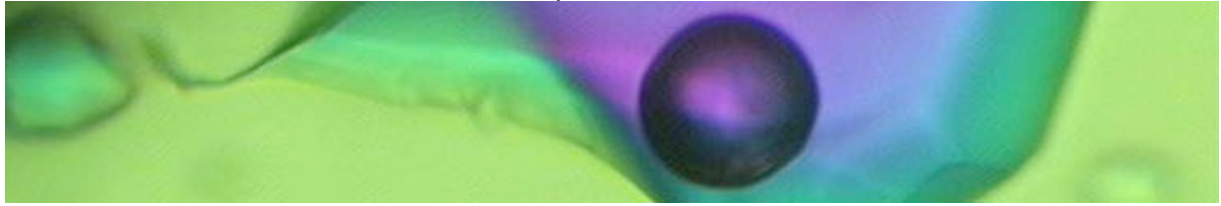9-11 August 2011

Montanuniversitaet Leoben
Austria

21st Biennial Conference   -   European Current Research on Fluid Inclusions

9 - 11 August 2011
Leoben
Austria

ECROFI XXI

Abstracts

Edited by:

Ronald J. Bakker
Miriam Baumgartner
Gerald Doppler

Cover photo: Image of a fluid inclusion (ca. 50 μm diameter) in quartz with crossed nicols, illustrating the birefringence character of quartz in a thick-section.

Organizing Committee ECROFI XXI

Ronald J. Bakker
Miriam Baumgartner
Judith D. Bergthaler
Gerald Doppler

Chair of Resource Mineralogy
Department of Applied Geology and Geophysics
Montanuniversitaet Leoben
Austria

http://ecrofixxi.unileoben.ac.at

http://fluids.unileoben.ac.at

The "Fluid Inclusion Team" from Leoben. from left to right Ronald J. Bakker,
Gerald Doppler, Miriam Baumgartner, and Amir M. Azim Zadeh

Preface

The ECROFI (European Current Research on Fluid Inclusions) has now reached the age of majority (21), and is part of a family: with her little sister PACROFI, and the newly born ACROFI, which are named after the continents where they take place, i.e. Pan-American (PA), Asian (A), and European (E). The ECROFI meetings have been the most successful in this series, because many participants come from Europe. Up to 180 participants attended these meetings in the past. Traditionally, the ECROFI meetings are held biennially, alternating with the PACROFI. Since 2006, the ACROFI is organized in the same year as the PACROFI

ECROFI meetings are visited by wide range of Earth-scientists investigating the role of fluids and melts within the Earth. For ECROFI XXI (21) we have invited scientific presentations on almost anything related to the development and application of research into fluid- and melt inclusions, including the following fields:

- Advances in analytical techniques
- Experimental studies
- Theoretical studies (e.g. fluid phase relations, equations of state)
- Diagenetic fluids
- Petroleum fluids
- Geothermal systems
- Fluid flow
- Deep crustal and mantle fluids
- Ore deposits
- Melt inclusions and igneous processes
- Fluids in tectonics
- Paleoclimate
- Extraterrestrial fluids
- Waste disposal
- Novel fields

Fluid inclusion research has become a thoughtful science in the 1960's and finally became subjected to the empirical scientific method. The experimental method was actively applied since the 1980's, but is restricted to only a few universities. The importance of fluid inclusion research is well known within the community of "fluid inclusionists", but lacks attention elsewhere. It is, therefore, not as successful as, for example, isotope research. Nevertheless, approximately 300 manuscripts with fluid inclusion studies are published every year, mainly within ore deposit research. The quality of these manuscripts must be under permanent surveillance, using international standards for scientific work, fundamental principles of chemistry and physics, and a lot of common sense. The ECROFI meetings are valuable for innovations, discussions and research quality improvements within the fluid inclusion community, and, moreover, they are strong signals to "fluid inclusion aliens" that our community is alive and kicking.

Groetjes

Ronald J. Bakker

History of the ECROFI (European Current Research on Fluid Inclusions)

Chronological list of ECROFI meetings

I	13-15 September 1969	Naturhistorisches Museum, Bern (Switzerland)
II	2-3 October 1970	Universitá di Milano (Italy)
III(?)	4 December 1975	Centre National de la Recherche Scientifique (CNRS) Paris (France)
III or IV	14-17 December 1976	University of Durham (England)
IV (?)	26-29 September 1978	Société Française de Minéralogie et de Cristallographie and CNRS, Nancy (France)
V	February 1979	Universität Karlsruhe (Germany)
VI	22-24 April 1981	Rijks-Universiteit Utrecht (Netherlands)
VII	6-8 April 1983	Université de Orléans (France)
VIII	10-12 April 1985	Universität Göttingen (Germany)
IX	4-6 May 1987	Universidade do Porto (Portugal)
X	6-8 April 1989	Imperial College, London (England)
XI	10-12 April 1991	Universitá di Firenze (Italy)
XII	14-16 June 1993	Uniwersytet Warszawski, Warsaw (Poland)
XIII	21-23 June 1995	Institut de Ciències de la Tierra "Jaume Almera", CSIC Barcelona-Sitges (Spain)
XIV	1-4 July 1997	Ecoles des Mines and CREGU, Nancy (France)
XV	21-24 June 1999	Geoforschungszentrum (GFZ) Potsdam (Germany)
XVI	2-4 May 2001	Universidade do Porto (Portugal)
XVII	5-7 June 2003	Eötvös University, Budapest (Hungary)
XVIII	6-9 July 2005	Università degli Studi, Siena (Italy)
XIX	17-20 July 2007	Universität Bern (Switzerland)
XX	23-25 September 2009	Universidad de Granada (Spain)
XXI	9-11 August 2011	Montanuniversität Leoben (Austria)

The use of quantities, units and symbols in fluid inclusion research

Bakker, Ronald J.

Resource Mineralogy, Department of Applied Geology and Geophysics, University of Leoben, Peter-Tunner Str. 5, Leoben, Austria

Publications, manuscripts and presentations, which include studies of fluid and melt inclusions, reveal a wide variety of units and symbols that are not conform with the SI (international system of units). This may cause confusion if these studies are communicated towards the chemical, physical, and mathematical society. Moreover, even within the community of fluid inclusion researchers quantities, symbols and units may be misunderstood. Recently, Diamond (2003) presented a glossary with terms and quantities of importance for fluid inclusion studies, and Kerkhof & Thiery (2001) introduced a variety of quantities to characterize the behaviour (i.e. a series of phase change) of carbonic fluid inclusions during heating in microthermometrical experiments. These recommendations are still absent in many publications. Several modifications have to be applied to these considerations to make them SI conform, which are presented in this study. The main objective of this study is to stimulate the awareness of fluid inclusion researchers of the existence of an internationally accepted code to present quantities in scientific papers.

The international system of units (published by the Bureau International des Poids et Mesures, 2006) is the main tool for worldwide unification of measurements, and contains fundamental standards and scales for the measurements of the principal physical quantities. The IUPAC (the 'greenbook', 2nd edition, 1998) has adopted the same objectives as the BIPM to improve the international exchange of scientific information and describes a large variety of *coherent derived quantities* from SI. The *coherent derived quantities* are mainly used in fluid inclusion research. They provide clear rules about the use of units and symbols, and recommendations about style in geological sciences.

1. Basic quantities

The basic quantities of the SI are given in Table 1 (see also: The international System of Units (SI). Bureau International des Poids et Mesures, 8th edition, 2006). The use of the correct form of symbols for units is obligatory, whereas symbols for quantities are <u>recommendations</u>. Authors may use a symbol of their own choice for a quantity, for example in order to avoid a conflict arising from the use of the same symbol for two different quantities. In such cases, the meaning of the symbol must be clearly stated. However, neither the name of a quantity, nor the symbol used to denote it, should imply any particular choice of unit.

Quantity name	Symbol for quantity (italic)	Unit name	Unit Symbol (upright)
length	l, x, r, etc	metre	m
mass	m	kilogram	kg
time	t	second	s
electric current	I	ampere	A
thermodynamic temperature	T	Kelvin	K
amount of substance	n	mole	mol
luminous intensity	I_V	candela	cd

Table 1. SI base quantities and units

1.1 Mass

The unified atomic mass unit, symbol u or m_u (also known as dalton, symbol Da) is the atomic mass of one ^{12}C atom divided by 12:

$$u = m_a(^{12}C)/12 \approx 1.66053886 \cdot 10^{-27} \text{ kg}$$

Subscripts, superscripts or text in brackets can be used to illustrate further information of a specific quantity. The subscript 'a' specifies that the mass of atoms is expressed in this equation, and the specific isotope is given in brackets. The use of subscripts and superscripts in the text within subscripts and superscripts should be omitted. The quantity relative atomic mass has the symbol A_r

$$\text{For example: } A_r(^{16}O) = m_a(^{16}O)/m_u = 16$$

This quantity is also known as *"atomic weight"*. The word *"weight"* is used sometimes for mechanical force, sometimes for mass. This

ambiguity must be put to an end, therefore, the *CIPM*[1] (see also BIPM, 2006) declared that: 1. The kilogram is the unit of mass; 2. The word *"weight"* denotes a quantity of the same nature as a *"force"*: the weight of a body is the product of its mass and the acceleration due to gravity; in particular, the standard weight of a body is the product of its mass and the standard acceleration due to gravity. This is a major deficiency within geological sciences because electron microprobe analyses as well as salinities of aqueous fluid inclusions are usually given in *"weight fractions"* (symbol wt. %). There are no acceptable logical arguments for ignoring the international standards, or for the continuation of using the word *"weight"* when mass is the proper name for the quantity involved.

1.2 Thermodynamic temperature

The melting of ice occurs at 273.15 K, and 0.1 MPa. The difference between a measured temperature and this reference value is called Celsius temperature, symbol *t*. The unit of the quantity Celsius is degree Celsius, symbol ˚C, which is by definition equal in magnitude to the Kelvin.

$$t = T - T_0$$

$$t/˚C = T/K - 273.15$$

The basic quantity time has the same symbol, but it is hardly ever used in fluid inclusion studies. The subscript *"C"* can also be used to specify the Celsius temperature:

$$T_C$$

1.3 Amount of substance

The amount of substance is defined to be proportional to the number of specified elementary entities (e.g. atoms or molecules) in a sample. The relation between the number of molecules (*N*, dimensionless) and the amount of substance (*n*, mole) is given by the Avogadro constant (*N*$_A$ unit is mol^{-1}).

$$n = N/N_A$$

$$N_A \approx 6.02214179(30) \cdot 10^{23} \text{ mol}^{-1}$$

For example: $n(CO_2) = N(CO_2)/N_A$

The quantity *"amount of substance"* or *"chemical amount"* has been used for a long time without a

proper name. It was simply referred to as the *"number of moles"*. This practice should be abandoned, because it is wrong to confuse the name of a physical quantity with the name of a unit. In a similar way it would be wrong to use *"number of kilogram"* as a synonym for *"mass"*. The length of the word *"amount of substance"* is somewhat large, therefore, it can be shortened by using only (1) *"amount"* or (2) *"substance"*. When there is no risk of confusion, it can be left out completely.

For example:

the amount of substance of CO_2 is 25 mol
the amount of CO_2 is 25 mol

and not:

the number of moles of CO_2 is 25 mol

2. Derived quantities

Derived quantities have units that are products of powers of the base units. The most common quantities in fluid inclusion research are given in Table 2.

Derived quantity	Symbol (italic)	Unit name	Unit symbol
area	A	square metre	m^2
volume	V	cubic metre	m^3
molar volume	$V_m (= V/n)$	cubic metre per mole	$m^3 \text{ mol}^{-1}$
concentration (amount concentration)	$c (= n/V)$	mole per cubic metre	mol/m^3
density (mass density) or mass concentration	$\rho (= m/V)$	kilogram per cubic metre	kg/m^3
specific volume	$v (= V/m)$	cubic metre per kilogram	m^3/kg
force	f	metre kilogram per square second	$m \text{ kg s}^{-2}$
		or newton	N

Table 2. Derived quantities

---

[1] Comité International des Poids et Mesures

Derived quantity	Symbol (italic)	Unit name	Unit symbol
pressure, stress	p	kilogram per metre per square second	$kg\ m^{-1}\ s^{-2}$
		or pascal	Pa $= N/m^2$
energy, work, amount of heat	$G,\ H,\ A,$ *etc.*	square metre kilogram per square second	$m^2\ kg\ s^{-2}$
		or joule	$J = N\ m$

Table 2. continued

2.1 Pressure

Pressure is expressed in Pascal (unit name), but can also be expressed in bar (with symbol bar), which is a non-SI unit, and which was selected as a standard pressure for tabulating all thermodynamic data. One bar is per definition 0.1 MPa (10^5 Pa). The use of Pascal is preferred.

2.2 Solubility of salt in aqueous liquid solutions

The solubility of NaCl in water can be expressed as a concentration, and as a molality (symbol b):

$$b_{solute} = n_{solute}/m_{solvent}\ (\text{in mol kg}^{-1})$$

The solvent is water, and the solute is a salt e.g. NaCl and KCl.

For example:

$$b(NaCl) = 16.2\ \text{mol kg}^{-1}$$
$$b_{NaCl} = 16.2\ \text{mol kg}^{-1}$$

Dissociation of salt molecules or chemical reactions is usually ignored in the characterisation of the composition of aqueous liquid solutions in fluid inclusion research. The behaviour of multi-component fluid systems that involve H_2O and salts is in general described in terms of associated salt molecules. Partial dissociation of NaCl in aqueous solutions results in the formation of a variety of ions: $NaCl^0$, Na^+ and Cl^- ions in distinct concentrations. Complete dissociation results in the formation of equal numbers of Na^+ and Cl^- ions that are equal to the amount of NaCl. For example, one kilogram of average seawater contains 965 g H_2O, 10.7 g Na^+ and 19.25 g Cl^-, consequently the molality of an associated NaCl complex is 0.482 mol kg^{-1}, in the presence of excess Cl^- ions.

3. Fractions, dimensionless quantities

A fraction is a number that is not a whole number, and varies between 0 and 1. Fractions can be used in solutions (mixtures) for amount of substance, mass, and volume (Table 3).

Quantity	Symbol (italic)
mass fraction	w
volume fraction	$\phi,\ \varphi$
amount fraction	$x,\ y$

Table 3. Fractions

The definitions of these fractions are:

$$w(i) = \frac{m(i)}{\sum_j m_j}$$

$$\varphi(i) = \frac{V(i)}{\sum_j V_j}$$

$$x(i) = \frac{n(i)}{\sum_j n_j}$$

For a condensed phase x is used for mass fraction (e.g. liquid), and for a gaseous mixtures y may be used (e.g. vapour). Mass fractions are often erroneously described as *"weight fraction"* (see paragraph 1.1), which should be omitted because weight is per definition a force (in newton), and mass is expressed in kg. The term *"ppm"*, meaning 10^{-6} relative value, or 1 in 10^6, or parts per million, is also used. This is analogous to the meaning of percent as parts per hundred. The terms "parts per billion", and "parts per trillion", and their respective abbreviations *"ppb"*, and *"ppt"*, are best avoided, because their meanings are language dependent. In English-speaking countries, a billion is now generally taken to be 10^9 and a trillion to be 10^{12}; however, a billion may still sometimes be interpreted as 10^{12} and a trillion as 10^{18}. The abbreviation *"ppt"* is also sometimes read as parts per thousand, adding further confusion.

In mathematical expressions, the internationally recognized symbol % (percent) may be used with the SI to represent the number 0.01. Thus, it can be used to express the values of dimensionless quantities. When it is used, a space separates the number and the symbol %. In expressing the values of dimensionless quantities in this way, the symbol % should be used rather than the name "percent". When any of the terms % and ppm are used it is important to state the

dimensionless quantity whose value is being specified.

For example:

the mass fraction
$w = 0.12$
$w = 12$ %
$w = 120$ g/kg

the amount fraction
$x = 3.7 \cdot 10^{-2}$
$x = 3.7$ %
$x = 37$ mmol/mol

Numerical values of physical quantities, which have been experimentally determined, are usually subject to some <u>uncertainty</u>. The experimental uncertainty should always be specified. The magnitude of the uncertainty may be represented as follows:

For example:

$l = (5.3478 \pm 0.0065)$ cm
$l = 5.3478$ cm ± 0.0065 cm

4. Writing unit symbols and names, and expressing the values of quantities

Symbols for quantities are generally single letters set in an italic font, although they may be qualified by further information in subscripts or superscripts or in brackets (in upright fond). Thus V is the recommended symbol for volume, V_m for molar volume, $V_{m, A}$ or $V_m(A)$ for molar volume of phase A.

Unit symbols are mathematical entities and not abbreviations. Therefore they are not followed by a period except at the end of a sentence, and one must neither use the plural nor mix unit symbols and unit names within one expression, since names are not mathematical entities. It is not permissible to use abbreviations for unit symbols or unit names, such as *cc* (for either cm^3 or cubic centimetres).

In forming products and quotients of unit symbols the normal rules of algebraic multiplication or division apply. Multiplication must be indicated by a space or a half-high dot ($\cdot$). When multiplying the value of quantities either a multiplication sign ($\times$), or brackets should be used, not a half-high dot. When multiplying numbers only the multiplication sign ($\times$) should be used. Division is indicated by an oblique stroke (/) or by negative exponents. In general, the sign $\times$ can be mistaken for the symbol of the quantity 'amount of substance fraction' (x),

and it is therefore recommended to use the space or dot.

For example:

N m or N·m (for a newton metre)
J/(mol K) or J mol^{-1} K^{-1} or J·mol^{-1}·K^{-1}

and not:

Nm or N×m

Within the text, for example, the equation $T = 293$ K may equally be written $T/K = 293$. The numerical value always precedes the unit, and a space is always used to separate the unit from the number. Thus the value of the quantity is the product of the number and the unit, the space being regarded as a multiplication sign. The symbol °C for the degree Celsius is preceded by a space when one expresses values of Celsius temperature t. Only when the name of the unit is spelled out would the ordinary rules of grammar apply, so that in English a hyphen would be used to separate the number from the unit.

For example: a 35-cm^3 vessel

The decimal marker is the point on the line. If the number is between +1 and -1, then the decimal marker is always preceded by a zero. For numbers with many digits, the digits may be divided into groups of three by a thin space, in order to facilitate reading.

4.1 State of aggregation

The components within fluid inclusions can be present in several states of aggregation (phases), in general, in the liquid, vapour and super-critical state. The following two- or three-letter symbols (Table 4) are used to represent the states of aggregation of chemical species for specific quantities. The letters should be printed in upright font without a full stop (period) in a superscript.

Phase	Symbol	Microthermometry
vapour	vap	V
liquid	liq	L
supercritical fluid	scf	SCF
solid	sol	S
clathrate	cla	

Table 4. States of aggregation

Phase	Symbol	Microthermometry
crystalline	cr	
amorphous solid	am	
vitreous substance	vit	
solution	sln	
aqueous solution	aq	

Table 4. continued

For example:

V_m^{liq} = molar volume of the liquid phase
x_a^{liq} = 0.3, or $x^{liq}(a)$ = 0.3
x_a = 0.3, or $x(a)$ = 0.3

If the name of the specified component (a) is rather large, i.e. more than 3 letters, the notation with brackets is preferred. The Greek letter symbols α, β, may be similarly used to denote phase α, phase β, etc., in a general notation. Phase changes that occur in fluid inclusions in microthermometrical experiments can be illustrated with single-letter symbols V, L and S.

Both *"gas"* and *"vapour"* have been used to indicate the lower density aggregation state. It is preferred to use *"vapour"* for this phase, whereas *"gas"* refers to components or a mixture of components.

4.2 Tables and figures

It is often convenient to write the quotient of a quantity and a unit for the heading of a column in a table, so that the entities in the table are all simple numbers. For example, a table of the natural logarithm of vapour pressure against temperature, reciprocal temperature, and molar volume may be formatted as shown below.

T/K	10^3 K/T	V_m/cm^3 mol^{-1}	ln(p/MPa)
573.15	1.7447	22.47	1.8073
600.00	1.6667	23.03	2.1920
623.15	1.6048	23.55	2.4907

Table 5. Example table.

The axes of a graph may also be labelled in this way, so that the tic marks are labelled only with numbers, as in Figure 1.
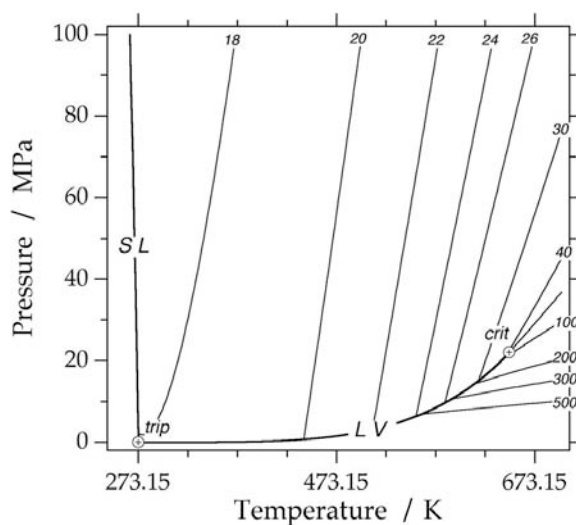

Fig. 1. Example phase diagram of H_2O, with curves of equal molar volume (18 to 500 cm^3·mol^{-1}).

5. Quantities in fluid inclusion research

Temperature is an important quantity in fluid inclusion research, because microthermometry reveals a variety of phase changes at specific temperatures, including homogenization and melting temperatures (Table 5, see also Diamond, 2003; v.d. Kerkhof & Thiery, 2001). All temperatures involve a process where two phases are unified in one phase by homogenization or dissolution upon heating. In addition, freezing of inclusions can also be analysed at specific temperatures. All temperatures are expressed in degree Celsius or Kelvin.

Quantity	Symbol of quantity	Phase transition
homogenization temperature	T_h	LV → L
		LV → V
		LV → SCF
		LLV → LV[a]
		LLV → LL[a]
		LLV → LSCF[a]
		SLV → SL[a]
dissolution temperature[b]	T_m	SV → LV
		SL → L[c]
		SL → LV[d]
		SLV → LV
		SLL → LL
nucleation temperature	T_n	LV → SV
		LL → SL
		LV → S

Table 5. The main quantities in microthermometry

a)   These   processes   are   *"partial homogenizations"*, e.g. CO_2 liquid and vapour phases may homogenize in the presence of an aqueous liquid solution that wets the walls of the inclusion.

b) The process of *"melting"* refers to pure substances,   and   corresponds   to *"dissolution"* in multi-component systems.

c) This process of dissolution is in principle also a homogenization of two phases.

d)   This   process   is   also   known   as "metastable melting", when a vapour phase appears simultaneously with the complete dissolution of a solid phase.

5.1 Style

The   general   style   of   expressing   these temperatures:

$$T_{process}\text{(phase transition)}$$

where it is important to note that the subscript is in upright font and the symbol of the quantity in italic font. Specific solid phases can be indicated with their proper name, and specific phase transition can be indicated with symbols.

For example:

T_m(IceV→LV), or T_m(Ice)
T_h(HaliteL→L), or T_h(Halite)
T_h(LV→L), or T_h(total)

The word *"total"* does not include the mode of homogenization,   it   requires,   therefore,   extra information.

5.2 Eutectic temperature

The eutectic temperature, symbol T_e, the minimum temperature of liquid stability, is a variety of T_m. In binary   systems   (i.e.   two   components),   this temperature corresponds with the dissolution of one solid phase and the simultaneous appearance of a liquid phase, whereas the other solid phase(s) remain(s) present (e.g. Ice + Hydrohalite + Vapour → Ice + Liquid + Vapour). The value of T_e can be correlated to a specific system, for example, -21 ˚C is indicative for the binary H_2O-NaCl system, but is very difficult to detect optically (see also Bakker, 2004).

5.3 Nucleation temperature

Nucleation temperature is usually measured during cooling   experiments,   and   represents   a spontaneous phase changes of an undercooled metastable   phase   assemblage   to   a   stable assemblage. The value of T_n depends on the size and shape of the inclusion and the velocity of cooling, and it can only be reproduced within a range of several degrees Celsius. The value of T_n is indicative for the salinity of the fluid system, e.g. highly saline aqueous solutions have lower T_n values than solutions with lower salinities. Some brines fail to nucleate solid phases, even at -190 ˚C (see also Bakker, 2004).

5.4 Decrepitation

The strength of the host mineral around fluid inclusions   can   be   characterized   by   the *"decrepitation"* temperature (symbol T_d). At this temperature,   cracks   are   formed   in   the   crystal around fluid inclusions with high internal fluid pressures. When the extensions of these cracks remain inside the crystal, the fluid inclusions has suffered an uncontrolled increase in total volume, otherwise, fluid can be lost from the inclusions. The value of T_d is also affected by the shape and size of fluid inclusions, and their distance to the crystal surface (or grain boundary).

5.5 Equivalent mass

The term "equivalent" has a general application in chemistry. In fluid inclusion research, it is used to describe the mass of one equivalent entity (e.g. NaCl)   that   produces   a   specific   dissolution temperature of ice, salt-hydrates, or salt in a liquid aqueous   solution   of   unknown   composition. Equivalent is abbreviated with eq and it is put in front of the base unit symbol. For example, a liquid solution with $b(CaCl_2)$ = 1.0 mol kg^{-1} will have a T_m(Ice) of -6.0 ˚C; the same temperature is obtained from a solution with b(NaCl) = 1.7 eq mol kg^{-1}. As a fraction, this solution has a w(NaCl) of 9.2 eq %. Alternatively, the type of percentage can be further specified with its quantity, e.g. 9.2 eq mass%.

For example:

w(NaCl) = 9.2 eq %
the mass fraction of NaCl is 9.2 eq %
the solution contains 9.2 eq mass% NaCl

The eutectic temperature of the binary H_2O-NaCl system is -21.2 ˚C, therefore, lower dissolution

temperatures cannot be transformed in NaCl mass equivalents. $CaCl_2$ or $ZnCl_2$ can be selected as equivalent entities for dissolution temperatures below -21.2 °C.

5.6 Fluid inclusion types

Fluid inclusions are usually classified according to their fluid properties, shapes, and distributions. The main component of a fluid inclusion can be used as a specification in the type-name.

> For example:
>
> a H_2O-rich fluid inclusion
> a water-rich fluid inclusion

The type names can also be related directly to their behaviour in microthermometric experiments (Boiron et al., 1992). The upper case letters L and V are symbols for inclusions that homogenize in the liquid phase and vapour phase, respectively. The lower case letters w and c are symbols for the compositions: H_2O-rich (±salt) and CO_2-rich (±CH_4 and N_2), respectively.

For example, a Lw inclusion is a water-rich fluid inclusion with total homogenization in the liquid phase. The presence of salt may depress the dissolution temperature of ice. A Lcw inclusion may reveal clathrate, ice and CO_2 dissolution temperatures, because it is composed of H_2O and CO_2, with or without minor amounts of CH_4, N_2 and NaCl. The total homogenization of this inclusion occurs in the liquid phase.

Lc and Vc fluid inclusions are gas-rich that homogenize in the liquid and vapour phase, respectively. Kerkhof & Thiery (2001) have further classified these types of inclusions in the CO_2-CH_4-N_2 fluid system according to their complex behaviour at low temperatures as H-type (liquid-vapour homogenization) and S-type (solid-liquid or solid-vapour homogenization).

5.7 Fluid properties

The properties of fluids can be described in terms of n, T, V, and p. Alternatively, x, T, V_m, and p are used (see also Bakker, 2003). These properties can be expressed in an equation of state, i.e. a mathematical formula that relates these quantities, e.g.:

$$p = \frac{RT}{(V_m - b)} - \frac{a}{V_m^2}$$

or

$$p = \frac{nRT}{(V - nb)} - \frac{n^2 a}{V^2}$$

where R is the gas constant, and a and b are van der Waals constants (see also Bakker, 2009). The symbols for temperature and volume are written in capital italic font, whereas the symbols for pressure and amount of substance (and fractions) are written in normal italic font.

References

Bakker, R.J. (2003) Package FLUIDS 1. Computer programs for analysis of fluid inclusion data and for modelling bulk fluid properties. *Chemical Geology,* v. 194 , 3-23.

Bakker, R.J. (2004) Raman spectra of fluid and crystal mixtures in the systems H_2O, H_2O-NaCl and H_2O-$MgCl_2$ at low temperatures: application to fluid inclusion research. *Canadian Mineralogist*, vol. 42, 1283-1314.

Bakker, R.J. (2009) Package FLUIDS. part 3. Correlations between equations of state, thermodynamics and fluid inclusions. *Geofluids*, vol. 9, 63-74.

Boiron, M.C., Essarraj, S., Sellier, E., Cathelineau, M., Lespinasse, M., Poty, B. (1992) Identification of fluid inclusions in relation to their host microstructural domains in quartz by cathodoluminescence. *Geochimica et Cosmochimica Acta*, vol. 56, 175-185.

Bureau International des Poids et Mesures (2006) The International System of Units. 8th Edition, Organisation Intergouvernementale de la Convention du Metre, 95-180.

Diamond, L.W. (2003) Glossary: Terms and Symbols used in Fluid Inclusion studies. In: Fluid Inclusions: Analysis and Interpretation (I. Samson, A. Anderson, D. Marshall) Mineralogical Association of Canada Short Course Series Vol. 32, 363-372.

Kerkhof, A.M. van den, Thiery, R. (2001) Carbonic inclusions. *Lithos*, vol. 55, 49-68.

Mills, I., Cvitas, T., Homann, K., Kally, N., Kuchitsu, K. (1998) Quantities, Units and Symbols in Physical Chemistry. International Union of Pure and Applied Chemistry (IUPAC), Physical Chemistry Division, Second Edition, Blackwell Science, pp 167.

European Current Research on Fluid Inclusions (ECROFI-XXI)
Montanuniversität Leoben, Austria, 9–11 August, 2011. Abstracts, p. 12

12

Session Index

In alphabetical order according to first author

Theoretical Studies on Fluid and Mineral Properties

Experimental Studies

Advances in Analytical Methods

Diagenetic and Petroleum Fluids

Ore Deposits

Deep Crustal and Mantle Fluids

Melt Inclusions and Igneous Processes

Paleoclimate and Groundwater

16

Oral and Poster Abstracts

in alphabetical order according to first author

Composition and evolution of magmas producing alkaline salic rocks (trachydacite and pantellerite) of the Dzarta Khuduk bimodal volcanic association, Central Mongolia

Andreeva, Irina A.

Institute of Geology of Ore Deposits, Petrography, Mineralogy and Geochemistry Russian Academy of Sciences (Igem Ras), Staromonetny 35, 119017, Moscow, Russia

The composition, evolution, and origin of the melts that produced trachydacite and pantellerite of the Late Paleozoic bimodal volcanic association at Dzarta Khuduk, central Mongolia, were studied by examining melt inclusions with the use of electron microprobe and ion probe.

The Dzarta Khuduk magmatic complex in the western part of the Northern Gobi Rift Zone is restricted to a number of narrow grabens of latitudinal strike. The complex comprises alkaline granosyenite and nordmarkite of a small (~15 km^2) massif, alkaline granitoid and basalt dikes, and volcanic piles of basalt, trachydiorite, comendite, pantellerite, alkaline and subalkaline trachydacite, and their tuffs. The age of the complex was evaluated by U-Pb, Ar-Ar, and Rb-Sr techniques at 211 Ma. The volcanic fields have a complicated facies structure, primarily because of the local predominance of mafic or acid rocks, a fact suggesting that these sites were close to corresponding volcanic centres. The complex includes three ancient volcanos and corresponding isolated volcanic fields of Dzarta Khuduk, Unege Betogin and Ulziit.

One of the largest massifs of acid volcanics is Dzarta Khuduk paleovolcano, whose fragments occur over an area of more than 120 km^2. The bottom of the volcanic pile is not exposed, and judging by rock relations observable 1.5 km north of the volcanic field boundary, the lower portions of the vertical section most probably consist of basalt. The paleovolcano is made up of alternating alkaline trachydacite, comendite, pantellerite, their tuffs and ignimbrite. The volcanic pile has a thickness of 600 m and is cut by subvolcanic comendite bodies and agpaitic syenite massifs. The rocks of the paleovolcano are dominated by fluidal and eutaxitic lavas at subordinate amounts of ignimbrite; the lavas have aphyric or porphyritic textures and are often altered and silicified (mostly in the proximity of subvolcanic bodies). The mineralogical and chemical composition of the unaltered rocks corresponds to those of acid alkaline rocks of the K-Na series, with an agpaitic coefficient (Ka) > 1 and with elevated concentrations of F, REE, Rb, and Zr. Silicified lithologies are enriched in REE (up to a few mass%).

Primary crystalline and melt inclusions were found in anorthoclase from trachydacite and quartz from pantellerite and pantellerite tuff. The identified minerals of crystalline inclusions in the trachydacite are hedenbergite, F-apatite, and pyrrhotite, and those in the pantellerite are F-arfvedsonite, fluorite, ilmenite, and the rare REE diorthosilicate chevkinite. Melt inclusions in anorthoclase from the trachydacite consist of glass, a gas phase, and daughter minerals (F-arfvedsonite, fluorite, villiaumite, and anorthoclase as a rim on the walls of the inclusions). Melt inclusions in quartz from the pantellerite contain glass, a gas phase, and fine-crystalline salt aggregates of Li, Na, and Ca fluorides (griceite, villiaumite, and fluorite) (Andreeva et. al, 2007). To our knowledge, griceite has been reported in the literature only once from sodalite inclusions in hornfels of the Mont Saint-Hilaire massif, Quebec (Canada) (Van Velthuizen J., Chao G., 1989). Melt inclusions in clasts of quartz crystals from the pantellerite tuff are originally homogeneous silicate glasses.

The thermometry of melt inclusions in phenocrysts in the trachydacite and pantellerite indicates that they crystallized at temperatures of 1060 - 1030 °C. It was also determined that inclusions in quartz from the pantellerite show evidence of immiscibility between silicate and salt (fluoride) melts at a temperature of 800 °C.

Homogeneous melt inclusions in anorthoclase from the trachydacite have a trachydacite or rhyolite composition and contain 68 to 70 mass% SiO_2, 12 to 13 mass % Al_2O_3, 0.34 to 0.74 mass% TiO_2, 5 to 7 mass% FeO, 0.4 to 0.9 mass% CaO, 9 to 12 mass% $Na_2O + K_2O$ at a agpaitic coefficient (Ka) = 0.92 to 1.24. The glasses of homogenized melt inclusions in quartz from the pantellerite and pantellerite tuff have a rhyolite composition. Compared to the glasses of melt inclusions in anorthoclase from the trachydacite, glasses of melt inclusions in quartz from the pantellerite are richer in SiO_2 (72 to 78 mass%) and poorer in Al_2O_3 (7.8 to 10.0 mass%). They contain 0.14 to 0.26 mass% TiO_2, 2.5 to 4.9 mass% FeO, 9 to 11 mass% $Na_2O + K_2O$, and 0.9 to 0.15 mass% CaO. The agpaitic coefficient is 1.2 to 2.05. Homogeneous melt inclusions in quartz from the pantellerite tuff contain 69 to 72 mass% SiO_2, and the concentrations of other major components, for example, TiO_2, Al_2O_3, FeO, and CaO, are close to the concentrations of these elements in the homogeneous glasses of melt inclusions in quartz from the pantellerite. The Na_2O and K_2O concentrations are 4 to 10 mass%, the agpaitic coefficient is 1 to 1.6.

The glasses of melt inclusions of each rock group have different concentrations of volatile components. Their H_2O concentrations are 0.08 mass% (in anorthoclase from the trachydacite), 0.4 to 1.4 mass% (in quartz from the pantellerite), and up to 5 mass% (in quartz from the pantellerite tuff). The F concentrations in glasses of melt inclusions in phenocrysts of the trachydacite are not higher than 0.67 mass%, and those in quartz form the pantellerite and pantellerite tuff reach 2.8 and 1.4 mass%, respectively. The Cl concentrations in glasses of melt inclusions in minerals in the trachydacite reach 0.2 mass%, and those in glasses in inclusions in quartz from the pantellerite tuff are up to 0.5 mass%.

The trace-element composition of the glasses and homogenized melt inclusions in minerals from the rocks suggests that trachydacite and pantellerite were produced by profoundly differentiated rare-metal silicate alkaline melts with high Li, Zr, Rb, Y, Hf, Th, U, and REE concentrations. The composition of homogeneous melt inclusions in minerals from the rocks provides an insight into the magmatic processes that led to concentrating trace elements (including REE) in the rocks. The leading role there in was played by the crystal fractionation and liquid immiscibility that involved salt (fluoride) melts. It was also determined that all of the melts underwent differentiation in spatially separated magmatic chambers, which predetermined differences in the evolution of the trachydacite and pantellerite melts. Late in the course of differentiation, when the magmatic systems were saturated in ore elements, salt Na-Ca fluoride melts were segregated and extracted much Li.

REFERENCES

Andreeva I.A., Kovalenko V.I., Yarmolyuk V.V., Listratova E.N., Kononkova N.N. (2007). *Doklady Earth Sciences.* 414 (4): 655-660.

Van Velthuizen J., Chao G. (1989). *Canadian Mineralogist.* 27: 125-127.

Basaltic melts in olivine phenocrysts from alkaline pumice of Southern Primorye

Andreeva, Olga A.[*], Naumov, Vladimir B.[**], Andreeva Irina, A.[*] and Kovalenko, Vyatcheslav I.[*]

*Institute of Geology of Ore Deposits, Petrography, Mineralogy, Geochemistry, Russian Academy of Sciences (IGEM RAS), Staromonetny 35, Moscow, 109017, Russia
**Vernadsky Institute of Geochemistry and Analytical Chemistry, Kosygina 19, Moscow 119991, Russia

A large intraplate volcanic province was formed in the Late Cenozoic within Central and Eastern Asia. Subalkaline and alkaline magmatism is mainly typical for it. Acid magmatic rocks are a rare exception. In the far eastern part of the province, they are related only to the formation of the large Pektusan volcano located at the boundary between China and Northern Korea and composed of alkaline trachyte and rhyolite. The presence of such a volcano in this province is not only a large geological problem it also determines the high volcanic danger in the region as well. In particular, its historical eruption 969 ± 20 AD was accompanied by an outburst of a huge mass of pyroclastic products, which reached the Islands of Japan.

Based on the study of mineral inclusions we consider the peculiarities of the composition of a melt registered in olivine from alkaline pumices of one of the Pektusan volcano eruptions and estimate the mechanisms that could result in its catastrophic eruptions.

The studied pumices produced by the Pektusan volcano were collected in the territory of Southern Primorye, in the Tyumen-Ula River area. The Pektusan volcano is composed of lavas and pyroclastic rocks of trachyte–comendite–rhyolite composition intruded by volcanic necks and dykes of alkaline basalt, trachybasalt, and trachyandesite. According to the geochronological data, the formation of the volcano proceeded over >3 Ma. Alkaline pumices were removed by the Tyumen-Ula River starting close to the Pektusan volcano to the Sea of Japan and later dispersed by sea currents along the coast.

Pumices are composed of light-grey glass with a refractive index of 1.506 ± 0.002 and a small portion (2 to 3 vol%) of phenocrysts of sanidine, ferrohedenbergite, magnetite, olivine, apatite, ilmenite, zircon, and chevkinite. According to the chemical composition, pumices correspond to trachyrhyodacite. The total concentration of alkalis in them reaches up to 9.5 mass%, with an insignificant prevalence of sodium over potassium. Pumices are characterized by high concentrations of niobium, zirconium, and REE). These pumices are unusual, since olivine in them is magnesium-rich with the composition of Fo74 to Fo79. It is characterized by a high CaO concentration (up to 0.22 mass%) as well.

Coexisting primary melt, crystalline, and fluid inclusions were studied in olivine phenocrysts. Crystalline inclusions in olivine comprise chrome-spinellid, titanomagnetite, picroilmenite, and clinopyroxene (?). Chrome-spinellid inclusions contain 8.8 to 16.7 mass% Cr_2O_3, 8.5 to 12.0 mass% Al_2O_3, and 7 to 8 mass% MgO at a FeO concentration of 48 to 57 mass%. The studied chrome-spinellids are characterized by an extremely high TiO_2 concentration reaching 10.5 to 14.0 mass%, which allowed us to characterize them as titanium chrome-spinellids. Titano-magnetite contain 65 to 70 mass% FeO and 13 mass% TiO_2. The chemical composition of ilmenite is characterized by very high concentrations of MgO (up to 9.6 mass%), which corresponds to the composition of picroilmenite. In addition to ore minerals, crystalline inclusions comprised an unusual silicate phase with the composition close to clinopyroxene. This phase is characterized by extremely high concentrations of TiO_2 and P_2O_5 (6 and 4 mass%, respectively). Thus, the mineral association registered in olivine is not typical for trachyrhyodacite.

Primary melt inclusions in olivine are located irregularly and have a shape close to oval and sizes from 30 to 150 µm. They are usually partly crystallized and contain residual glass,

daughter minerals and a gaseous phase. Residual (not heated) glasses in melt inclusions contain high concentrations of alkalis ($Na_2O + K_2O$) up to 5.2 mass%, CaO up to 5 mass%, P_2O_5 up to 1.3 mass% at concentrations of 60 to 64 mass% SiO_2 and 21 mass% Al_2O_3. As a whole, the compositions of residual glasses from melt inclusions plot on the andesite field in the classification SiO_2 – ($Na_2O + K_2O$) diagram. Daughter minerals of melt inclusions comprise augite, ilmenite, titanium chrome-spinellid and apatite. As a whole, the set of daughter minerals in melt inclusions is close to the mineral association registered in olivine as crystalline inclusions. According to our thermometric data, the melt inclusions homogenize at 1040 to 1230 ºC.

In addition, several two-phase fluid inclusions containing liquid and gaseous carbon dioxide were registered in two olivine phenocrysts. Homogenization into the liquid phase occurs at 29.0 °C, which provides evidence a high density in the inclusions (0.63 g/cm^3). The pressure calculated from PVT data of CO_2 in a temperature interval of 1040 to 1230 °C is 2600 to 3000 bar, which corresponds to a depth of 10 to 13 km.

Examination of the glasses under an electron microscope allowed us to reveal a significant difference between their composition and that of the pumice. The chemical composition of homogeneous glasses from melt inclusions corresponds to the composition of basalt and is characterized by high concentrations of 2.2 to 3.5 mass% TiO_2 and up to 0.7 mass% P_2O_5 at a SiO_2 content of 44 to 52 mass% and 12 to 18 mass% Al_2O_3. The concentration of alkalis ($Na_2O + K_2O$) in the melts is quite high as well (4.0 to 6.6 mass%) with a strong prevalence of Na_2O over K_2O. The comparison of the compositions of the melt inclusions and those of the alkali basalts of Pektusan volcano show their obvious similarities (Table 1). Similarly to the studied melts, alkaline basalts are characterized by high TiO_2 concentrations. As was mentioned above, the formation of the Pektusan volcano with alkaline pumices of Primorye as products occurred in intracontinental conditions. The studied peculiarities of the composition of glasses from homogenized melt inclusions in olivine demonstrate clear characteristics of intraplate

magmas, particularly the high concentrations of TiO_2, P_2O_5, and K_2O. Thus, the results of the study of inclusions allow us to consider that olivine observed in alkaline pumices as phenocrysts is a non-equilibrium mineral and most likely a crystalline fragment of the basalts. The identity of the composition of glasses from melt inclusions in olivine from basalts supports this assumption. The presence of high-titanium and high-magnesium minerals, namely titanium chrome-spinellid and picroilmenite in olivine, is quite consistent with the suggested assumption as well.

This allows us to assume participation of the processes of mixing of melts with contrasting compositions in the formation of alkaline pumices. Portions of basaltic magma together with olivine crystals contained in it were incorporated in the mobile acid melt, which provided degassing and foaming of magma. An increase in pressure in the magmatic chamber could catalyze the explosive eruption, which resulted in an outburst of trachyte pumices containing phenocrysts of xenogenic olivine. Thus, pumices of Primorye are most likely hybrid rocks formed as a result of mixing of acid and basic magmas.

	1	2	3
SiO_2	43.89	47.32	46.77
TiO_2	3.55	2.67	3.06
Al_2O_3	12.36	13.85	14.78
FeO	18.92	13.62	12.81
MnO	0.32	0.17	0.21
MgO	6.47	7.79	4.51
CaO	7.7	7.16	6.96
Na_2O	3.03	3.07	3.71
K_2O	1.41	1.55	2.18
P_2O_5	0.79	0.59	0.64
Cl	0.03	0.03	-
S	0.13	0.08	-
H_2O	-	-	0.48
Total	98.6	97.9	99.91*

Table 1. Chemical composition of glass in melt inclusions contained in olivine from pumice from Primoye and basalt from Pektusan volcano
Note: 1, 2 – glasses in melt inclusions; 3 – basalt (the analytical total is reported with regard for 3.80 mass% LOI (Sakhno, 2007)).

REFERENCES
Sakhno, V.G. (2007). *Dokl. Ros. Akad. Nauk* 417 (3): 528-534.

Ore-bearing hydrothermal systems of deposits from Magnitogorsk metallogenic zone, South Urals: fluid inclusion data

Ankusheva Natalia N. and Zaykov Victor V.

Institute of Mineralogy, Urals Branch, Russian Academy of Sciences, Miass, Russia

The formation of VMS and Au-bearing deposits is caused by hydrothermal fluids activity. Their general features are volcanogenic-sedimentary complexes location, Cu-Zn-massive sulphide and Au mineralization, sericite-quartz metasomatic zones and prevalence seawater as fluid source. The aim of our work is to give an overview of the results of fluid inclusion studies of the hydrothermal systems from Magnitogorsk paleo-island arc to establish the history of hydrothermal activity from the bottom to top of this geological structure.

Fluid inclusion data are obtained from barite, calcite and quartz by the use of cryo- and thermometric methods (Borisenko, 1977; Bodnar, Vityk, 1994). We used own and published data.

Magnitogorsk paleo-island arc consists of structural complexes of Urals paleo-ocean suburb (Puchkov, 2000). According to geodynamic reconstructions there are West-Magnitogorsk paleoisland arc, Sibay inter-arc basin and East-Magnitogorsk paleoisland arc. Paleoisland arc ages are different: the west is formed in Eifelian, and the east in Givetian (Artyushkova and Maslov, 1998).

Au-polymetallic VMS deposits in rhyolite-basalt complex of the Baymak ore region are located in the bottom of West-Magnitogorsk paleoisland arc (Zaykov, 2006)

Hydrothermal systems of Tash-Tau and Vishnevka deposits consist of streaky-disseminated ores, sulphide ores of feeder channels filled with calcite and quartz, and quartz veins in supra-ore dacites. NaCl with additions of $MgCl_2$ and $CaCl_2$ with total salinities between 2 and 8 eq mass% NaCl prevail in these hydrothermal systems. The temperatures of homogenization for sulphide-quartz veins from Tash-Tau deposit are between 250 and 300 °C; for feeder channel ores between 160 and 170 °C; for quartz and calcite veins in dacites, andesites and rhyolites from Vishnevka deposit between 120 and 200 °C (Zaykov and Ankusheva, 2008).

Fluid inclusions data of the Balta-Tau deposit are obtained from quartz and barite in streaky-disseminated ores (Holland et al., 2003). The temperatures of homogenization are 140 to 180 °C. First melting temperatures are indicative for the salt systems of $NaCl–H_2O$ and $NaCl–KCl–H_2O$ with total salinities between 3 and 4.5 eq mass% NaCl.

In Severo-Uvaryash deposit barite from Au-bearing sulphide-barite ores in rhyodacites was studied. In Utrenneye deposit Au-bearing streaky-disseminated chalcopyrite-sphalerite and impregnated sphalerite ores with calcite in breccial chloritized rhyolites were studied. In the Zvezdnoye ore mineralization quartz and barite from sulphide veinlets in sericite-quartz metasomatites were studied. Au-bearing barite-quartz-carbonate-sulphide veins from these deposits are formed due to hydrothermal fluids with salinities of 1.8 mass% (Utrenneye deposit) up to 11.9 eq mass% NaCl. (Severo-Uvaryazh deposit). First melting temperatures are indicative for the salt systems $NaCl-Na_2SO_4–H_2O$ (Severo-Uvaryazh deposit), $NaCl–H_2O$ and $NaCl–MgCl_2–H_2O$ (Utrenneye and Zvezdnoye deposits). The temperatures of homogenization are between 145 and 170 °C (Zaykov et al., 2010).

Yanzigitovo Mn-bearing deposit in Sibay inter-arc basin is located on the south flank of anticline structure hosted VMS deposits. Hematite-quartz edifice is located in the top of rhyolite-basalt stratum. It is 20 m thick and has a length of 15 to 200 m (Telenkov and Maslennikov, 1995). Dendritic, net-shaped and zonal hematite-containing quartz veins were studied. It is established that hematite-quartz rocks of the Yanzigitovo deposit are formed due to NaCl-fluids with salinities between 2.7 and 6 mass% in a temperature range of 200 to 230 °C.

In the bottom of East-Magnitogorsk paleoisland arc Cu-Zn VMS deposits of Verchne-Uralian ore region are located (Uselga, Chebachye, Talgan, Zapadno-Ozernoye). Fluid inclusion data in ore minerals (barite, quartz, carbonates and sphalerite) and peri-ore rocks indicate temperatures of the ore forming fluid of 110 to 360 °C and salinities of 1 to 10 eq mass% NaCl, with a chloride salt composition and a mixture of hydrocarbonate and sulphide salts (Karpukchina and Baranov, 1995).

The hydrothermal system of Lissy Gory Au-bearing ore field is located in andesite-basalt and siliceous strata in the top of East-Magnitogorsk paleoisland arc. It includes Au-bearing quartzitized zones and hematite-quartz edifices. They formed in NaCl-fluids with salinities of 1.5 to 7 eq mass% NaCl. The temperatures of homogenization are 120 to 290 °C (Ankusheva, 2007).

Thus, all these data allow to describe the history of hydrothermal activity which formed the sulphide and gold mineralization in the Magnitogorsk metallogenic zone.

Massive sulphide forming fluids of the bottom of Magnitogorsk paleoisland arc system (both West and East parts) are similar and have complex salt composition. There are NaCl, KCl, $MgCl_2$ and $CaCl_2$. These fluids are characterized by higher salinities that are caused by magmatic component. The total salinity interval is up 1.8 to 11.9 eq mass% NaCl that is lower and higher than the seawater salinity (*ed. 3.5*).

New fluid inclusion data of hydrothermal systems from Magnitogorsk paleoisland arc system are comparable with data of modern Au-containing sulphide fields from island arc systems of Pacific Ocean. Fluid inclusion data from these localities illustrate salinities of 3.4 to 5.8 (Binns et al., 1993) and 2.7 to 6.9 eq mass% NaCl (Bortnikov et al., 2004) in barite from barite-silica-sulphide chimney Franklin Mountain from Woudlark Basin; 5.3 to 7.2 eq mass% NaCl in barite and anhydrite from sulphide edifice Vensky Wood from Manus Basin and 1.6 to 4.2 in the opaline silica (Bortnikov et al., 2004); 5 eq mass% NaCl in sphalerite from barite-sulphide chimney Vay Lily field, Lau Basin (Herzig et al., 1993); 2.2 eq mass% NaCl (liquid) and 1.74 to 1.98 eq mass% NaCl (vapour) obtained by direct measurements, Brandon field, Rappa Nuy, latitude 21°S, EPU (Von Damm et al., 2003). The temperatures of homogenization are up to 128 ºC in opaline silica in Vensky Wood edifice to 316 ºC in barite of Franklin Mountain edifice (Bortnikov et al., 2004).

According to comparative analysis the salinity of mineral-forming fluids in VMS-bearing fields of paleoisland arc structures from the South Urals is close to modern analogues, and in the systems both seawater and magmatic fluid circulated. The fluid salinity of hematite-quartz edifices from Magnitogorsk paleoisland arc system has confined variations which decrease the role of the magmatic component during final stages of ore hydrothermal system development.

REFERENCES

Ankusheva N. (2007) *Metallogeny of Ancient and Modern Oceans*: 38–46.

Binns R., Scott S. (1993) *Economic Geology*. 88: 2122-2153.

Bodnar R., Vityk M. (1994) in *Fluid inclusions in minerals: methods and applications*: 117 130.

Borisenko A. (1977) *Geology and Geophysics*. 8: 16–28.

Bortnikov N., Simonov V., Bogdanov Yu. (2004) *Ore Deposits Geology*. 1. 46: 74–87.

Herzig P., Hannington M., Fouquet Y. et al. (1993) *Economic Geology*. 88. 8: 2182–2209.

Holland N., Roberts S., Herrington R., Boyce A. (2003) *Mineral Exploration and Sustainable Development*. 1:123–126.

Karpukchina V., Baranov E. (1995) *Geochemistry*. 1: 48–63.

Von Damm K., Lilley M., Shanks III. et al. (2003) *Earth and Planetary Science Letters*. 206: 365–378.

Zaykov V., Ankusheva N., Melekestseva I. (2010) *Metallogeny of Ancient and Modern Oceans*: 166–170.

Zaykov V., Ankusheva N. (2008) *XIII All-Russian Thermobarogeochemistry Conference*: 41-44.

Artyushkova O., Maslov V. (1998): ? 156

Puchkov V. (2000): ? 146.

Telenkov O., Maslennikov V. (1995) ? 200.

Zaykov V. (2006) ? 429.

Late magmatic crystallization in the tourmaline-bearing miarolitic granitic pegmatites (by example of Shakhdarinskaya and Leskhozovskaya veins, SW Pamir, Tajikistan)

Astrelina Elena*, Smirnov Sergey*,**, Ragozin Alexey**, Karmanov Nikolay** and Konovalenko Sergey***

*Novosibirsk State University, Pirogova, 2, Novosibirsk, Russia
**V.S. Sobolev Institute of Geology and Mineralogy SB RAS, pr. Koptuga, 3, Novosibirsk, Russia
***Tomsk State University, pr. Lenina, 36, Tomsk, Russia

Introduction

Late stages of granitic magma crystallization are frequently accompanied by separation of aqueous fluids, which assist in ore deposit formation. Miarolitic granitic pegmatites are natural laboratories that allow to study this process in detail. However, some features of the late-stage magmatic crystallization should vary depending on initial magma composition. This should lead to different P-T paths and various styles of phase transitions.

Pegmatites of SW Pamirs

Pegmatie veins Shakhdarinskaya (ShV) and Leskhozovskaya (LeV) are located within 1.5 km from each other on the right bank of the Shakhdara river in the SW Pamir. Both veins consist of quartz-two-feldspar pegmatite with schorl and contain small miarolitic cavities with elbaitic coloured tourmaline. Some of miarolitic cavities are surrounded by quartz-tourmaline plagioclase or quartz-lepidolite-plagioclase paragenesis with abundant apatite and accessory phenakite (near-miarolitic assemblage). Quartz-two-feldspar pegmatite is a major constituent of the veins. Mineralogy and texture make it similar to tourmaline-rich coarse-grained granite. In the majority of models this mineral paragenesis is attributed to magmatic crystallization. Miarolitic cavities contain well formed quartz and feldspar crystals and are believed to form from hydrothermal solution. Thus, miarolitic mineralization corresponds to hydrothermal crystallization stage. The mineral paragenesis surrounding the miarole thus may represent the transitional stage from magmatic to hydrothermal crystallization. This work represents the features of late magmatic crystallization in two tourmaline bearing granite pegmatites on the basis of fluid and melt inclusion studies in quartz from magmatic, transitional and hydrothermal assemblages. This study was focused on phase transitions and chemical compositions of coexisting phases, which participated in pegmatite crystallization and formed mineralogically different mineral assemblages.

Fluid and melt inclusion study

Fluid and melt inclusions in quartz were studied by microthermometry, Raman spectroscopy, SEM EDS, EMPA and LA-ICP-MS methods. Quartz from quartz-two-feldspar pegmatite contains rare primary fluid and extremely scarce melt inclusions both in ShV and LeV. However, the amount and size of inclusions increase in quartz of quartz-two-feldspar pegmatite in vicinity of miarolitic cavities in LeV. Primary fluid inclusions from quartz-two-feldspar pegmatite of ShV consist of H_2O-CO_2 fluid, while in LeV primary fluid inclusions contain aqueous solution with daughter sassolite. These inclusions were found to accompany silicate melt inclusions that are composed mostly of mica and feldspar, and aqueous fluid. In contrast to quartz-two-feldspar pegmatite quartz from near-miarolitic assemblage of both veins contains numerous fluid and melt inclusions. In quartz from LeV these inclusions have much in common with those from quartz-two-feldspar pegmatite, while in quartz from ShV both types of inclusions are larger and more abundant. Primary fluid inclusions in quartz from ShV similarly to quartz-two-feldspar assemblage contain large CO_2 bubbles with an aqueous rim. The aqueous rim contains daughter crystals of sassolite and an unidentified phase. Fluid inclusions in quartz of LeV also represent

aqueous solution with daughter sassolite and unidentified phase. Miarolitic quartz also contains fluid and melt inclusions. Melt inclusions are less numerous than in the near-miarolitic assemblage and confined to root part of crystals. Miarolitic fluid inclusions from veins consist of gas, aqueous solution and daughter sassolite, Cs and Rb pentaborates (ramanite) and an unidentified phase, similar to that of inclusions from the near-miarolitic assemblage. Melt inclusions in quartz of magmatic and transitional stage were heated in the autoclave at 2.5 kbar. Their homogenization temperatures were 600 to 615 °C for both veins. Quenched glasses of inclusions are depleted in SiO_2, compared to evolved granite (62 mass% for ShV and 67.8 mass% for LeV) and have elevated Al_2O_3 contents (14.0 mass% for ShV and 13 mass% for LeV). Unlike to the evolved granite the studied glasses from ShV are depleted in Na and K but strongly enriched in Cs (up to 3.4 mass %Cs_2O). The glasses hosted in the quartz from LV have K and Na contents at the level of evolved granite but are less enriched in Cs (up to 0.16 mass% of Cs_2O). Similarly to glasses of melt inclusions in pegmatitic quartz from tourmaline-bearing pegmatites of other regions of the world, melt inclusions from ShV and LeV are enriched of B_2O_3, F and H_2O. H_2O contents were estimated at 10 to 15 mass%. Fluid compositions recorded by fluid inclusions change from quartz-two-feldspar to miarolitic assemblage. Fluid inclusions in quartz of ShV show a strong decrease in the CO_2 contents and an increase in boron concentrations, which is manifested in the appearance of sassolite daughter phases (up to 14 mass% of H_3BO_3). The concentration of boron in the fluid of LV increases from 16 to 19 mass% H_3BO_3 in quartz-two-feldspar pegmatite to 22 to 25 mass% H_3BO_3 in the miarolitic quartz. LA-ICP-MS studies of individual fluid inclusions showed that they are enriched in B, Na (up to 3.4 mass%), K (up to 0.6 mass%), Cs (up to 0.4 mass%), Li (up to 0.3 mass%), W (up to 0.1 mass%), As (up to 2.3 mass%) and Sb (up to 0.1 mass%). Elevated amounts of Be, Ta, Sn and Nb were recorded. SEM EDS measurements of dry residues of opened fluid inclusions indicate the presence of trace amounts of Cl in the solution. Trace element compositions of fluid inclusions from both veins are similar. On the basis of the study one can conclude that the fluid have tendency to increase concentrations of B, As, Sb, Na, W and probably Li.

Discussion and conclusion

Classic models, based on examination of the P-Q type system silicate – H_2O and granite – H_2O, envisage pegmatite formation through three subsequent stages: magmatic, where silicate melt and aqueous fluid are present; pneumatolytic, where supercritical fluid is a major mineral forming medium; and hydrothermal, where crystallization proceeds from subcritical aqueous fluids. This suggests that quartz from the first stage should contain coeval fluid and melt inclusions, from the second stage only crystal-rich fluid inclusions, and from the third stage two or three-phase fluid inclusions. Our study showed that besides mineralogical and textural difference quartz from three subsequent mineral assemblages contain both fluid and silicate melt inclusions. The study of fluid and melt compositions showed that silicate melts and aqueous fluids changed systematically their compositions from quartz-two-feldspar pegmatite to miarolitic quartz. From the data obtained in this study one can conclude that three phases, i.e. silicate melt, aqueous fluid and crystallizing minerals, coexisted in the course the magmatic crystallization. The compositions of fluid and melt evolved due to element re-distribution between all three phases.

According to Valyashko (1990) and Ravich (1974) this way of phase transformations is possible when volatiles of flux components are added to the system with P-Q type phase diagram transforming it into the diagram without critical phenomena on the saturation curve.

REFERENCES
Valyashko V. M. (1990) *M.: Nauka*, - 270 p.
Ravich M. I. (1974) *M.: Nauka*, 150 p.

Practical application of synthetic fluid inclusions: production of calibration standards

Azim Zadeh, Amir M., Bakker, Ronald J.

Resource Mineralogy, Department of Applied Geosciences and Geophysics, University of Leoben, Peter-Tunner-Str. 5, Leoben, Austria

Synthesis of fluid inclusions in natural materials, mainly quartz is an experimental technique that was refined and widely applied by Bodnar & Sterner (1987). The method is based on the relatively fast healing process of microcracks in minerals at high temperature and pressure. The distorted crystals do not heal perfectly (Fig. 1), and a huge amount of fluid inclusions is synthesized. The fluid that is present at experimental conditions is trapped accidentally, and it is completely isolated from the system around the crystal. The generated fluid inclusion trails mark the position of the former crack.
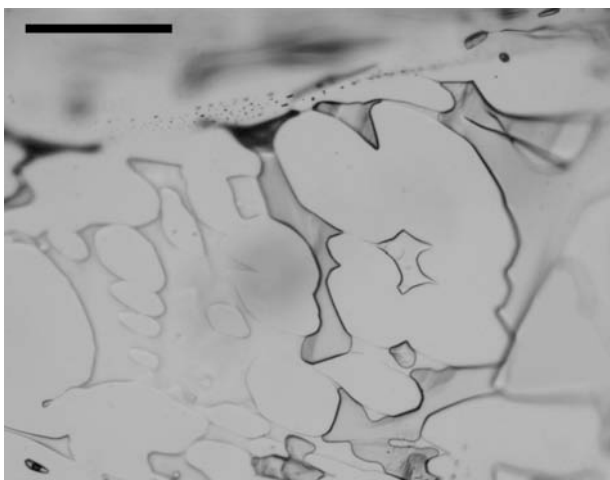
Fig. 1. Quartz growth within crack, the clear spots mark the positions where top and bottom of the crack are connected with new crystals, fluid inclusions form in between these crystals. Scale bar is 100 µm.

The hydrothermal laboratory of the University of Leoben has been optimized for the generation of synthetic fluid inclusions. The method of Bodnar & Sterner (1987) has been further refined in this laboratory, with e.g. internal thermocouples to be able to control the starting and ending conditions of a specific experiment.

The experiment set-up allows well-defined T-P-t paths and can be adapted to calculated isochoric paths of specific fluids. The hydrothermal laboratory is equipped with 10 externally heated cold-seal pressure vessels, and maximum experimental conditions are 800 °C and 1000 MPa.
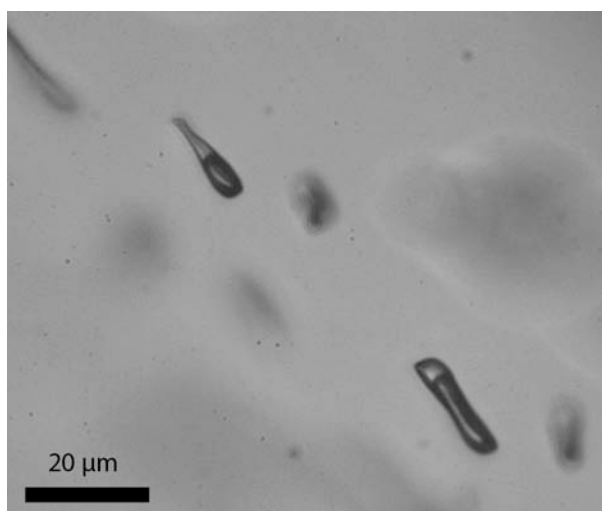
Fig. 2. Elongated synthetic H_2O fluid inclusions with critical density.

A large variety of fluids can be used in these experiments, consequently, many different types of standard fluid inclusions with well-defined compositions and densities can be produced. Thermodynamic properties of these fluid systems can be used to calibrate numerous analytical instruments (microthermometry, Raman spectroscopy, laser-ablation methods). The most common fluid systems for the calibration of microthermometry are **a**. pure H_2O fluid with a critical density (Fig. 2), $T_m(SV{\rightarrow}LV) = 0.0 \pm 0.1$ °C (melting of ice) and $T_h(LV{\rightarrow}L) = 374.0 \pm 0.5$ °C (critical homogenization); **b**. CO_2-H_2O fluids (Fig. 3), $T_m(SSV{\rightarrow}SLV) = -56.6 \pm 0.2$ °C (melting of CO_2) and $T_m(SLV{\rightarrow}LLV) = 9.9 \pm 0.1$ °C (melting of clathrate); **c**. H_2O salt (e.g. NaCl) fluid with an

eutectic composition (Fig. 4), T_m(SSV→SLV) = -21.2 ± 0.2 ˚C (eutectic melting).

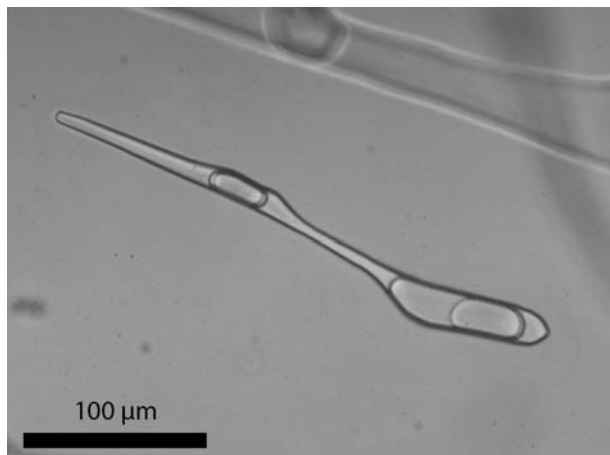*Fig. 3. Elongated synthetic H_2O-CO_2 fluid inclusion with three phases, two CO_2 bubbles (L+V) separated by an aqueous liquid solution.*

Fig. 4. Synthetic H_2O-NaCl fluid inclusions of variable sizes and shapes with an eutectic composition (23.3 mass% NaCl)

The uncertainties of thermodynamically fixed temperatures of phase changes in fluid systems are defined by the precision of the stage that is used in microthermometry. The production of mixed H_2O-gas fluids is based on the use of solid silver-oxalate for CO_2 (explosive decomposition at 140 ˚C) and solid silver-azide for N_2 (explosive decomposition at 250 ˚C). The fluid inclusions in Figure 2, 3 and 4 were synthesized at 550 ˚C - 72 MPa, 600 ˚C - 400 MPa and 600 ˚C - 220 MPa, respectively.

REFERENCES

Bodnar RJ, Sterner SM (1987) In: *Hydrothermal Experimental Techniques (ed. GC Ulmer & HL Barnes),* 423-457.

P-T conditions of fluid trapping at Hohentauern/Sunk sparry magnesite deposit (Eastern Alps, Austria)

Azim Zadeh, Amir M.*, Bakker, Ronald J.*, Ebner, Fritz**

*Resource Mineralogy, Department of Applied Geosciences and Geophysics, University of Leoben, Peter-Tunner-Str.5, A-8700 Leoben, Austria

**Geology and Economic Geology, Department of Applied Geosciences and Geophysics, University of Leoben, Peter-Tunner-Str.5, A-8700 Leoben, Austria

The Carboniferous of the Veitsch nappe in the Graywacke Zone (Eastern Alps/Austria) is the type region of the "Veitsch type" sparry magnesite. The Hohentauern/Sunk deposit, at the structural base of the Veitsch Nappe, is one the best known magnesite deposits. Sparry magnesite of the Hohentauern/Sunk deposit is characterized by pinolite (Fig. 1), rosette and banded (zebra) textures. All geological, petrographical and geochemical features support a diagenetic dolomitization of the carbonate host rocks followed by the magnesite formation via metasomatic replacement and redolomitization. The magnesite forming fluid with high salinity has a marine/evaporitic origin.

Fig. 1. Handspecimen of sparry magnesite (pinolite) from Sunk, Austria

Fluid inclusions are relatively abundant in the magnesite, but generally less than 5 μm in size. At room temperature two phase (L+V) and three phase (L+V+S) inclusions have been recognized. The liquid-rich inclusions display a Raman spectrum typical for H_2O and in some cases of gas rich inclusions CO_2. Commonly, fluid inclusions contain solid daughter crystals, identified as dolomite by Raman spectroscopy.

The results of the chemical composition of the extracted inclusion fluid of the magnesite samples using crush-leach technique show very low Na/Br (22 to 77) and Cl/Br (60 to 119) ratios. Their compositions lie at the end of the evaporation trend on the Na/Br and Cl/Br molar ratio diagram. The position of the plots at the end of the evaporation trend and the extent of fractionation indicate that the highly saline fluids were the product of evaporitic concentration predominantly of seawater. The fluid compositions of magnesite samples indicate evaporitic bittern brines to be the original fluid source.

The inclusions in the magnesite show different homogenization temperatures (T_h) around 150°C to 190 °C and a well defined mode around 170 – 180 °C and a broader range of T_h at 350 °C . Final ice melting temperatures (T_m) were observed mainly between -30 °C and -10 °C with a clear peak centered on -20 °C to -15 °C. They have a well defined mode around -20 °C which indicates a substantial content of NaCl in the fluids. The salinity of the fluid was calculated in the H_2O-NaCl system (Bodnar 1993) with the use of *BULK* software from the computer package *FLUIDS* (Bakker 2003). Microthermometric data indicate that fluids trapped in primary fluid inclusions in Hohentauern/Sunk magnesite are brines characterized by high and variable bulk total salinities (22.4 eq mass% NaCl) belonging to the H_2O-NaCl system. The observed variation in homogenization temperatures (T_h) and final ice melting temperatures (T_m) of the fluid inclusions from sparry magnesite may be interpreted as the result of local mixing of two fluids with different salinities. As a result, the study of fluid inclusions of sparry magnesite indicates a high salinity of the

Mg-rich solutions which transformed the dolomite protolites.

Possible *P-T* conditions of fluid trapping are estimated using the intersection point of isochores with the lithostatic thermobaric gradients. We consider that the timing for magnesite mineralization and fluid trapping coincides with HT/LP metamorphism (peak around 270 ± 30 Ma), magmatism and extensional tectonics which are characteristic for some segments of the Austroalpine crystalline basement in which a geothermal field gradient of 45 °C/km and geobarometric gradients of 27.1 MPa are supposed (Schuster et al. 2001, Schuster & Stüwe 2008). The isochore intersection with the general lithostatic gradient at the time of magnesite mineralization is around 245 °C and 136 MPa, which corresponds to a depth of approximately 5 km. The calculated temperature is the maximum achievable temperature for the fluids. Therefore, the real trapping temperature is most probably between the measured T_h with a mode at 170 °C and a temperature of 245 °C for lithostatic pressure with a geothermal field gradient of 45 °C/km. This temperature is similar to the temperature (247 °C) calculated by the Na-K geothermometer (Azim Zadeh, 2009).

REFERENCES

Azim Zadeh A. M. (2009) *PhD thesis*, Montanuniversität, Leoben, 181 pp.

Schuster R, Stüwe K. (2008) *Geology*, 38: 175-178.

Schuster R., Scharbert S., Abart R., Frank W. (2001) *Mitteilungen der Geologie und Bergbau Studenten Österreichs*, 40: 111-141.

Fluid inclusion in quartz from the Aligudarz Granitoids, NW Iran

Bagheriyan, Siyamak

Islamic Azad University, Tiran Branch, Isfahan, 85318, I.R. Iran

The Aligudarz granitoid plutons intruded into meta-sediments in the Sananday-Sirjan zone, NW of Aligudarz city (west Iran). Based on petrography and geochemistry, the Aligudarz granitoid has been classified as granite, granodiorite and S-Type pegmatite with the mineral assemblage of quartz, plagioclase, K-feldspar, biotite and muscovite. The intrusion has thermally metamorphosed the country rocks up to the albite-epidote-hornfels facies. Fluid inclusions studies in the quartz veins of the Aligudarz granitoid show four types of fluid inclusions (Fig.1): 1) low saline aqueous inclusions; 2) high saline inclusions (Fig. 2); 3) CO_2-H_2O rich inclusions; and 4) carbonic inclusions. The density data obtained from the fluids indicate entrapment temperatures of 580 to 636 °C at pressures of 3.9 to 5.1 Mbars. These conditions nearly coincide with the obtained mineral P-T estimations. There are partial melting processes during the formation of the S-Type Aligudarz granitoids.
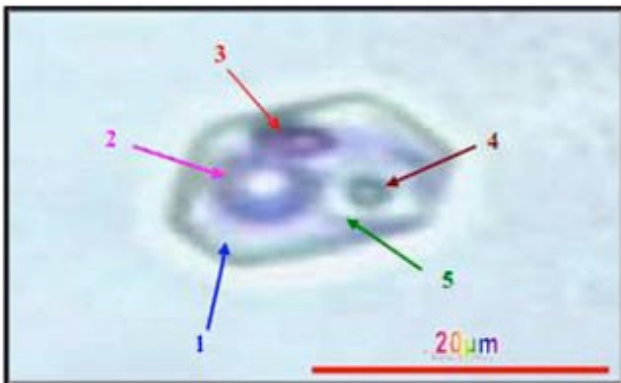

Fig. 2. Fluid inclusion in a quartz vein of the Aligudarz granitoid (high saline inclusion)
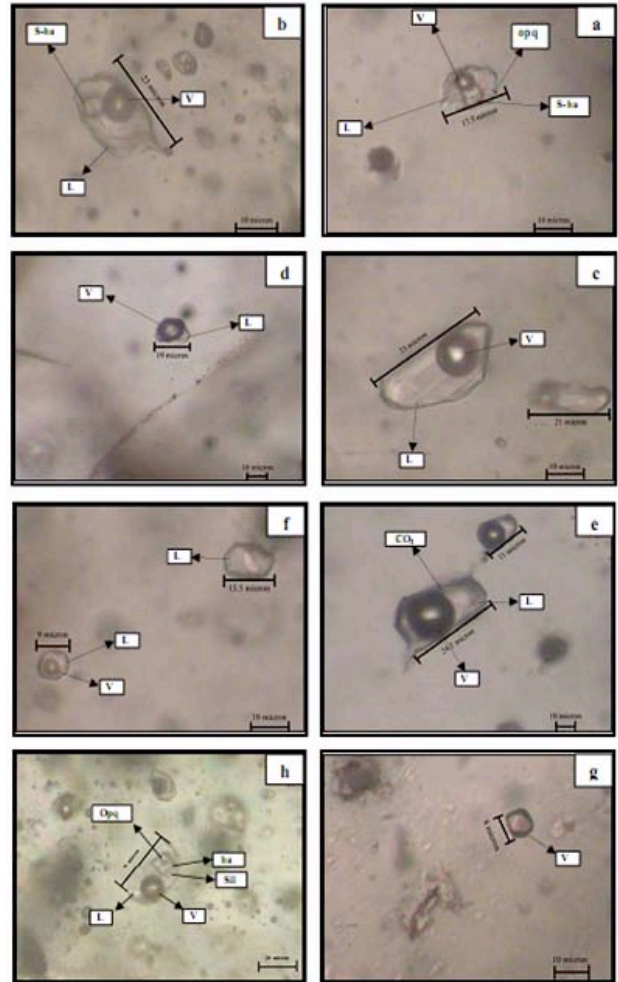

Fig. 1. a-b: three-phase fluid inclusions (L+V+S); c: two phase fluid inclusions (L+V), rich of liquid phase; d: two-phase fluid inclusions (L+V), rich of vapour phase; e: two-phase fluid inclusions (L+V) including two phases of non-mixed vapour; f: liquid single phase fluid inclusion (L) and two phase inclusion (L+V); g: single phase of fluid inclusion (V); H: multi-phase fluid inclusion (L+V+ha+sil+opg)

Accuracy, precision and uncertainty of peak position estimations of CO₂ and CH₄ in Raman spectra

Bakker, Ronald J.

Resource Mineralogy, Department of Applied Geosciences and Geophysics, University of Leoben, Peter-Tunner-Str. 5, Leoben, Austria

Raman spectra of gases, such as CH_4 and CO_2 are characterized by specific peak positions in the range 2910 to 2920 cm^{-1} and 1260 to 1440 cm^{-1}, respectively. A typical CH_4 spectrum consists of one peak that may vary a few wavenumbers (2911.5 to 2917.5 cm^{-1}) according to internal pressure or density of the gas (e.g. Lin et al., 2007). The CO_2 spectrum consists of a Fermi double, one peak at 1279.7 to 1285.3 cm^{-1} and the other at 1384.6 to 1388.3 cm^{-1} (e.g. Rosso & Bodnar, 1995), also dependent on the density of the gas. According to these studies, the assumed precision of peak position estimations is about 0.02 cm^{-1}. Consequently, direct measurements of these peak positions can be used to calculate precisely the density of gases.

The present study will illustrate the relationship between precision, accuracy and spectral resolution of Raman spectra measured with a LABRAM and LABRAM HR (Jobin Yvon, Horiba).

First, the detector is a limiting factor for the resolving power of a spectrograph. A spectrum is a series of pixels defined by a certain wavenumber and intensity. Wavenumbers in-between these pixels cannot be detected and are assigned to one of the bordering pixels. The wavenumber distance between two pixels is 0.46 cm^{-1} for the LABRAM HR and 1.35 cm^{-1} for the LABRAM with a 1800 gratings. By definition, the spectral resolution is the minimum wavenumber difference between two lines in a spectrum that can be distinguished, and it cannot exceed the pixel distance values.

Second, the accuracy of a spectrum can only be improved by adequate calibration. The peak position of neon light or minerals such as silicon and diamond can be used as calibration material. A single peak of the signal of neon light is composed of about 7 and 12 pixels, for LABRAM and LABRAM HR respectively (Fig.1). The diamond peak is composed of about 25 and 65 pixels. Comparison of a measured spectrum with these standard values permits an improvement of the accuracy, but the uncertainty of standard values has to be taken into account.
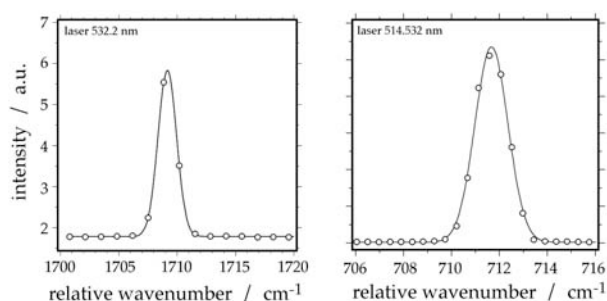

Fig.1. Raman spectra of two neon-"lines" with LABRAM (left) and LABRAM HR (right).

The detected signal in a range of pixels of the detector is mathematically fitted to distribution equations in order to illustrate the interpolated peak position. A variety of distribution equations are available, e.g. Gaussian and Lorentzian. It was suggested that this mathematical treatment of data could improve the precision by about 30 times compared to that estimated by the detector pixel resolution (e.g. Lin et al., 2007). Unfortunately, the obtained peak position in between two pixels depends on the type of distribution equation that is selected. For example, Gaussian peak fitting results in 1709.16 cm^{-1} for neon (using 532.2 nm laser), whereas Lorentzian peak fitting to the same data result in 1709.38 cm^{-1}. This least-square fitting method is already a part of data-treatment, which provides secondary data, or interpreted data. The R^2 coefficient of these fitting procedures may approach 1, which mainly illustrates that the background signal is perfectly reproduced because it contains the majority of the pixels, whereas the pixels of the peak signal are usual highly deviating from distribution equations. The FWHH of this

standard is 1.83 cm^{-1} for the LABRAM and 0.69 cm^{-1} for the LABRAM HR, which is in principle the resolving power of the spectrograph. Ones again, the example illustrates that the detector pixel resolution is a limiting factor for the precision and accuracy.

The spectrum of CO_2 from synthetic fluid inclusions is tested in this study to evaluate the precision, accuracy and uncertainty of peak positions. Inclusions with known densities (Fig.2) were measured at selected temperatures, above and below homogenization conditions of CO_2 phases. The Fermi double of the CO_2 spectrum allows the use of differential peak position estimation, which reduces the uncertainties according to calibration with standards.
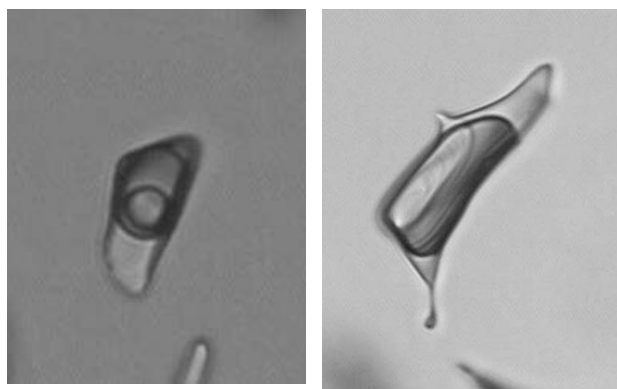
Fig. 2. Synthetic fluid inclusions (±20 µm length) at room T with a CO_2 density (inner phases) of 0.6381 g·cm^{-1} (left) and 0.1535 g·cm^{-1} (right).

The peak positions of the Fermi double of the vapour CO_2 phase are highly affected by the presence of a liquid CO_2 phase, and vice versa (Fig. 3, black arrows). The interference of vapour and liquid CO_2-"lines" does not allow an unambiguous data treatment with least-squares fitting methods. Therefore, measurements should be performed above homogenization conditions, preferentially at 40 °C. Repeated measurements at the same conditions result in a variation in wavenumber of maximally 1 cm^{-1}. The variation of the CO_2 spectrum is controlled by the parameters temperature, pressure and molar volume. Mathematical calculations of the density of CO_2 from Raman spectra must, therefore, include all of these parameters, similar to the equation of state of CO_2. The liquid and vapour equilibrium line

indicates a high uncertainty (short dashed curve in Fig. 3) due to the previously mentioned deviations. The homogeneous fluids measured at variable temperatures indicated a variation with internal pressure, and an uncertainty of about 0.3 cm^{-1} (Fig. 3). Previous work on Raman spectra analyses of CO_2 spectra (Rosso & Bodnar, 1995; Fall et al., 2011; Wang et al., in press) is inconsistent with the present study. Both the values of differential peak positions and precision are distinctively different. The present study illustrates that the use of a simple polynomial equation to calculate the density of CO_2 directly from the peak difference gives incorrect values. From the most optimal estimation of the uncertainty in a measurement, i.e. 0.3 cm^{-1}, the recalculated uncertainty in CO_2 density is about ± 0.2 g·cm^{-1} which exceeds about 20% of the estimated value. According to the resolving power of the spectrograph, this uncertainty increases to about 50 %.
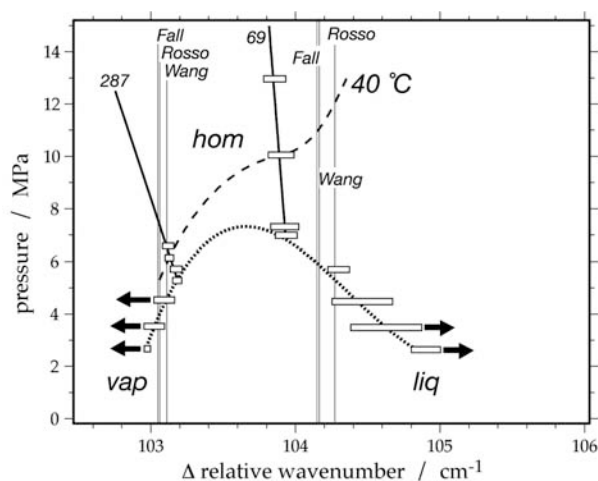

Fig. 3. Peak position difference of the Fermi double of CO_2 as a function of pressure, density (in molar volume: 69 and 287) and temperature (40 °C).

REFERENCES
Fall A, Tattich B, Bodnar RJ (2011) *Geochim. Cosmochim. Acta* 75: 951-964.
Lin F, Bodnar RJ, Becker SP (2007) *Geochim. Cosmochim. Acta* 71: 3746-3756.
Rosso KM, Bodnar RJ (1995) *Geochim. Cosmochim. Acta* 59: 3961-3975.
Wang et al. (in press) *Geochim. Cosmochim. Acta.*

The relationship between salinity, dissolution temperatures of halite, and volume fraction of the vapour phase in the binary H_2O-NaCl system

Bakker, Ronald J.

Resource Mineralogy, Department of Applied Geosciences and Geophysics, University of Leoben, Peter-Tunner-Str. 5, Leoben, Austria

Phase transitions observed in fluid inclusions during microthermometrical experiments can only be interpret in terms of composition and density if adequate and accurate equations, either empirical or theoretical, of the fluid that is trapped are available. The equations should be able to reproduce experimental properties of the specific fluid systems, moreover, they should be able to produce "reasonable" interpolated and extrapolated data.
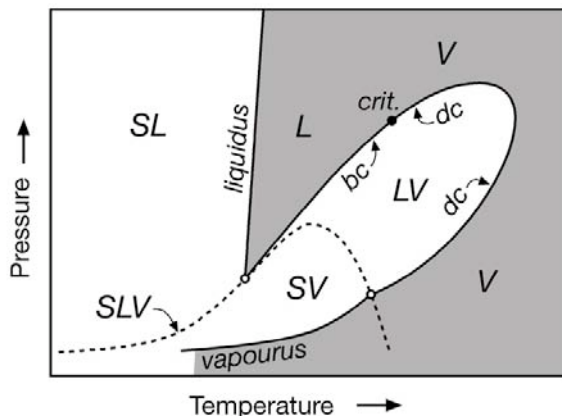

Fig. 1. Schematical isopleth of the H_2O-NaCl system illustrating a variety of phase assemblages. The shaded area contains a homogeneous fluid.

Dissolution of halite crystals in a brine occurs along the liquidus of this binary system (Fig. 1). The liquidus shifts to higher temperatures if the bulk salinity increases. The "starting point" of the liquidus is located on the SLV curve (halite + brine + vapour), and it extends to high pressures in a relatively small temperature interval. The dissolution of halite crystals in fluid inclusions can occur in two differently developing phase assemblages upon heating:

1. SLV → SL → L
2. SLV → LV → L (or V)

The first type of dissolution occurs on the liquidus, the second type of dissolution occurs on the SLV curve, and not on the liquidus. In principle, the dissolution temperature of both types cannot be used to calculate salinities directly. According to equilibrium thermodynamics, two parameters (or variables) have to be estimated or measured to define binary systems in inclusions, such as H_2O-NaCl. In practise, the nearly pressure-independent extension of the liquidus allows an approximate estimation of salinity with the definition of the SLV curve for type 1 dissolution. The intersections of isochores within the immiscibility field and the SLV curve (which mark the dissolution temperature of halite, Fig.2) are occasionally close to the "starting point" of the liquidus, therefore, the salinity is also approximately estimated by the definition of the SLV curve for type 2 dissolution.
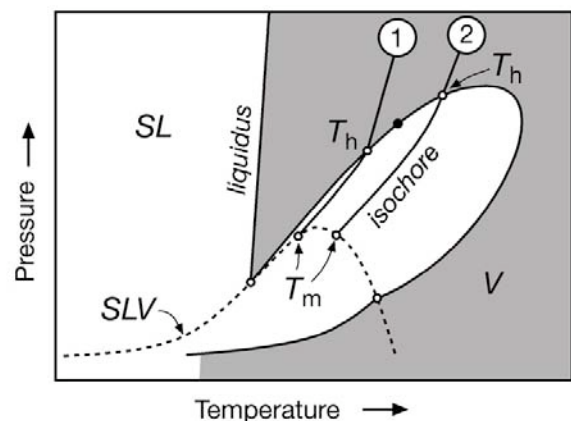

Fig. 2. Schematical isochores in a H_2O-NaCl system illustrating total homogenization (T_h) in to the liquid phase (1) and in to the vapour phase (2). T_m indicates dissolution temperatures of halite.

Figure 2 illustrates that the dissolution temperature of halite can be substantial higher for inclusions with lower bulk densities and the same bulk salinity, and thereby violating the above

mentioned simplification for type 2 dissolution. In other words, the size of the vapour bubble is also a factor that defines the bulk salinity of a fluid inclusion that reveals a total homogenization temperature that is higher then the dissolution temperature of halite (type 2, Fig. 3).
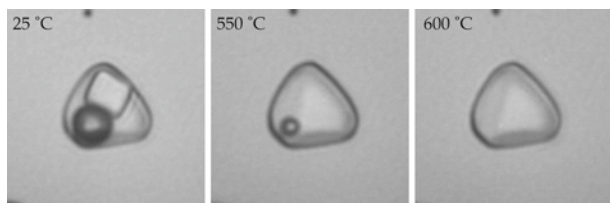

Fig.3. Microthermometrical heating experiment of a highly saline fluid inclusion of type 2 dissolution.

An equation of state for the H_2O-NaCl system according to Anderko & Pitzer (1993) is the only equation that can be used to calculate an isochore within the immiscibility field of a system with specific bulk salinity. It can, therefore, be used to calculate the intersection conditions of the SLV curve and variable bulk densities (Fig.4).
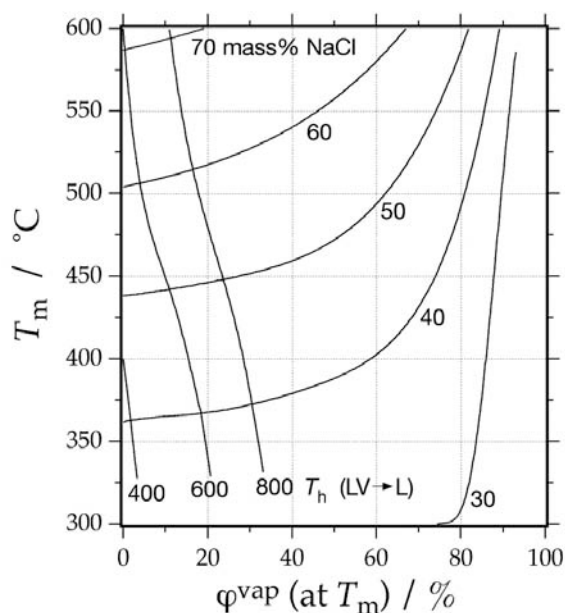

Fig.4. Relationship between T_m of halite (SLV→LV) and the volume fraction of the vapour bubble at T_m. at selected salinities. Nearly vertical curves represent equal total homogenization temperatures (LV→L) in ˚C.

Figure 4 is calculated with the software "LonerAP" which is part of the package FLUIDS (Bakker, 2003). The temperature limits in Figure 4 are in principle the limitation of the heating-freezing stage (i.e. 600 ˚C). Moreover, microthermometry above 600 ˚C may result in decrepitation of fluid inclusions because internal pressures may reach values above 100 MPa. Therefore, the estimation of vapour bubble volume fractions according to the method of Bakker & Diamond (2006) or a simplified estimation of volume fractions directly from area fractions at the temperature of dissolution of halite is a reliable method to obtain bulk salinities

The equation of state from Anderko & Pitzer (1993) is based on experimental data of vapour-liquid equilibria and density data in the homogeneous liquid region. In addition, the activity of NaCl along the liquidus is also included in modelling this fluid system. The properties of the SLV-curve are approximately reproduced with this equation of state, with a maximum relative deviation of 5% from experimentally obtained values. Below 300 ˚C, this equation of state cannot be applied, which is according to the temperature limits indication of the original paper. At lower salinities, below about 35 mass% NaCl, isochores in the immiscibility field are nearly parallel to the temperature-pressure conditions of the SLV-curve, which prevents the estimation of a straight-forward relationship between T_h and T_m.

Combining the equation of state for the H_2O-NaCl system from Anderko & Pitzer (1993) and knowledge about the SLV curve allows the determination of both bulk salinity and density of a fluid entrapped in inclusions, and can be used to estimate isochores within and outside the immiscibility field of the system. This equation of state can also be used for the ternary H_2O-NaCl-KCl system.

REFERENCES

Anderko A., Pitzer K.S. (1993) *Geochim. Cosmochim. Acta* 57: 1657-1680.

Bakker R.J. (2003) *Chem. Geol.* 194: 3-23.

Bakker R.J., Diamond L.W. (2006) *Am. Min.* 91: 635-657.

Influence of cracking of crude oil in hydrothermal systems on formation of various types of oil-and-gas deposits

Balitsky, Vladimir S.*, Pironon Jacques **, Penteley, Svetlana V. ***, Novikova, Maria A.*, Balitskaya, Liudmila V.* and Bublikova Tatiyana, M*

*Institute of Experimental Mineralogy RAS, Osepian St, 4, Chernogolovka, Moscow District, Russia
**Université de Lorraine, G2R-CREGU laboratory – BP 239 • F-54506 Vandœuvre lès Nancy
***17, Allée des Noires Terres, 54850 Messein, France

Cracking of crude oil and of its heavy fractions is one of the principal processes of obtaining benzine and other oil-products. It is shown that sometimes the cracking took place in natural conditions. Precisely this fact explains the particularities of so-called hydrothermal oil's composition, which can be find in zones of spreading and in the fields of volcanic and thermal activities where the temperatures often achieve 400 °C and more (Simoneit, 1995; Bajenova & Lein, 2002). Experimental works have proved principal possibility of crude oil cracking in the hydrothermal systems (Bjoroy et al., 1992; Huang et al, 2001). The most convincing experiences related to such studies were a comparison of initial oil with residual oil and with hydrocarbons in synthetic fluid inclusions formed in the same systems (Teinturier et al., 2003).

In the present work the experimental study of crude oil cracking is attempted to understand its influence for formation of different types of oil & gas deposits. The investigations were carried out in a complex. The main attention was kept on fluid inclusions in quartz grown simultaneously with interaction of hydrothermal solutions and crude oil in a large range of temperatures and pressures.

Experiences were run by the hydrothermal method of thermal gradient, which was described in previous works (Balitsky et al., 2005, and others). Initial oil-water mixtures were prepared from oils with neutral, alkalescent and alkaline solutions. Oil part in the mixtures varied from 0.01 to 50 vol%.

The temperatures of experiences were set from 220/260 °C up to 490/500 °C where the first value is the temperature of the upper part of autoclave and the second is the temperature of the bottom. The filling of autoclaves ranges from 50 to 80 %. More than 100 experiences with duration time between 14 to 30 days were carried out. The products of experiments were studied by optical microscope, X-ray, fluorescence, microprobe and were characterised by IR-spectra and by chromatograms. Fluid inclusions were studied in polished slices of quartz. Phase transformations in inclusions were observed in-situ during heating and cooling them in micro thermometric equipment THMSG-600 (Balitsky et al., 2007). Composition of oil fractions was defined by the boiling temperature and was characterised by local IR-spectra.

Fluid inclusions of quartz obtained at 220 to 320 °C are characterised by three-phase state with phase relation from L1≥G>L2 till L2≥L1>G, where L1 is the water solution, G is the gas phase (water vapour) and L2 is oil (Fig. 1).
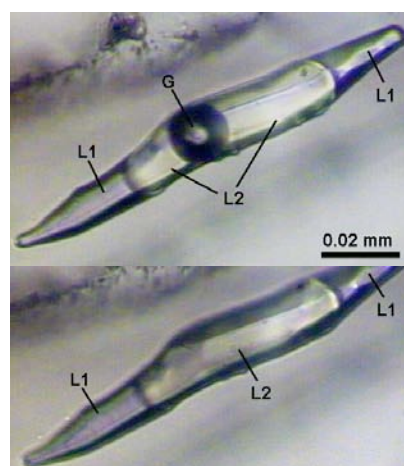

Fig. 1. Three-phase gas-liquid aqua-hydrocarbon inclusion in quartz, formed at 280 °C (upper picture), and the same inclusion in the two-phase state at 230 °C (bottom picture). Fragment of micro-thermogram.

The composition of initial and residual oils has not changed. During heating of inclusions up to 230 - 330 °C the gas phase disappears with the transformation of fluid to two-phase state liquid with a different L1/L2 ratio. Water-oil fluid existence can be evidence without a free gas-phase in earth crust under noted TP-parameters. Such fluids must be found at depths of about 3.5 to 4.5 km on the basis of average values of geothermic gradients and hydro- and litho-static pressures.

Fluid inclusions in quartz obtained at higher temperatures (330 to 490 °C) and saturation vapour pressures and more are characterised by different phase transformations. Such inclusions are polyphased under room conditions. Fluid in them can be essentially liquid (L1≥G>L2>SB) or essentially gaseous (G>>L1>L2>SB), where L1 is the water solution; L2 are liquid hydrocarbons, mainly light oil fractions (benzene, kerosene); G are gaseous hydrocarbons, essentially methane; and SB is solid bitumen.

At the beginning of heating inclusions up to 250 - 290 °C dissolved liquid hydrocarbons in gas hydrocarbons form a bi-phase fluid (L1>G). Then homogenization of the fluid at 365 to 372 °C occurs (Fig. 2).
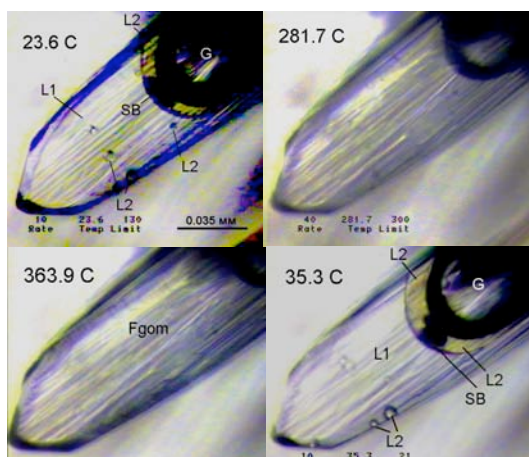

Fig. 2. Fragment of micro-thermogram: Formation of bi-phase aqua-hydrocarbon fluid (L1>G) at 280 °C followed by its homogenization at 363.9 °C. Inclusion's cooling gives a restoration of all disappeared phases. Temperature of inclusion's formation is 490 °C.

This is a principle difference of such type of inclusions from bi-phase aqua-oil fluid inclusions formed at lower TP-parameters. The heavy oil fractions in high temperatures solutions (above 330 °C) undergo cracking. Formation of light hydrocarbon fractions is fixed with their boiling temperature from 60 till 240 - 270°C in inclusions. Gas hydrocarbons, especially methane, and the presence of solid bitumen is also observed. Chromatograms' comparison of oil and its heavy fractions before and after experiments definitely evidences the hydrocarbon cracking both, by appearance of light fractions and by the increase of their quantity. The heating of such fluids up to critical point of water, transforms them into a homogeneous supercritical state. It indicates the possibility of the existence of light and medium oil fractions and their migration as supercritical fluids in the earth crust. This process probably demonstrates the conditions of formation of gas condensate and oil condensate deposits.

Thus, the investigations show the principle phase compositions and phase states of aqua-hydrocarbon fluids formed at temperatures lower than 320°C and above 330°C at saturated vapour pressure and more. Such differences are related with crude oil cracking, which results in the appearance of light oil fractions (benzene and kerosene), gaseous hydrocarbons and solid bitumen. That is clearly observed by the influence of high temperatures on primary aqua-oil inclusions formed in quartz at temperatures between 280 - 320 °C (Fig. 3).
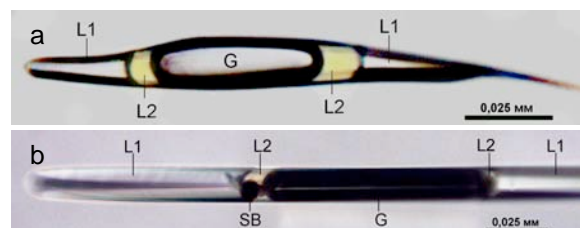

Fig. 3. a An inclusion formed in quartz at 280 °C: L1 – water solution, G – water vapour, L2 – hydrocarbons identical to the composition of oil used as initial charge; b The same kind of inclusion after high-temperature (400 °C) treatment within 12 days: L1 – water solution, G – gas, mainly methane, L2 - light oil fractions as well benzene and kerosene, and residual asphalts (SB).

Thermo-baric parameters in the earth crust depend on real thermo-gradients and hydro- and litho-static pressures. Such parameters inevitably reach with depth the values, which lead to hydrocarbon cracking. This fact has an important meaning on hydrocarbon composition and formation of corresponding types of oil and gas deposits.

REFERENCES

Balitsky V.S., Pironon J., Penteley S.V., Novikova M.A., and Balitskaya L.V. (2011) *Doklady Earth Sciences*, p. 383–386.

Bazhenova O.K., Lein A.Yu. (2002) V kn.: Organicheskaya mineralogiya. *Materialy Rossiiskogo soveshchaniya po organicheskoi mineralogii.* SPb: SPbGU, p. 95–96. (in russian)

Behar F., Kressman S., Rudkiewicz J.L., Vandenbroucke M. (1992) *Organic Geochemistry*, 19, p. 173-189.

Huang W.-L., Otten G.A. (2001) *Organic Geochemistry*, 32, p. 817-830.

Simoneit B.R.T. (1995) Osnovnye napravleniya geokhimii. M.: Nauka, c. 236-259. (in russian)

Teinturier S., Elie M., Pironon J. (2003) *Journal of Geochemical Exploration*, 78-79, p. 421 - 425.

Exotic pegmatite fluids: a pre-cursor for orogenic gold mineralization.

Banks David.*, Bodnar Robert** and Bozkaya Gulcan***

*University of Leeds, School of Earth and Environment, Leeds, LS2 9JT, U.K
**Virginia Polytechnic Institute & State University, Dept. of Geosciences, Blacksburg, VA, 24061, USA
***Cumhuriyet University, Department of Geological Engineering, Sivas, TR-58140, Turkey

The Alto Ligonha region of Mozambique contains economically important pegmatites in a NE-trending zone covering some 10 000 km^2.The pegmatites are emplaced in schistose rocks and are thought to be related to late Pan-African syn-tectonic equigranular granites c. 500 Ma. The largest pegmatite in the region is at Muiane, which has recently been re-opened for Li and Ta exploitation, and has been estimated to be some 1600m long, 360m wide and have a thickness or over 150m (Hutchinson and Claus, 1956). The pegmatite is zoned with a central quartz core, going outwards to a lepidolite unit, a quartz plumose muscovite unit, a massive perthite unit and finally a plagioclase unit. It is essentially a Li-dominated pegmatite with significant proportions of spodumene, lepidolite, eucryptite and petallite. There are also significant concentrations of pollucite, a rare Cs mineral.

Fluid inclusions were examined in a number of samples from the quartz core using microthermometry, SEM, Raman and LA-ICP-MS. They are aqueous-CO_2 showing variable H_2O/CO_2 ratios in different fluid inclusion assemblages (FIA). Within each assemblage the ratio is however quite consistent, the dominant type being, by volume fraction, ca. 0.4 CO_2 with lesser numbers of ca. 0.9 high density CO_2 inclusions. Many of the inclusions are extremely large, reaching ca.300 μm with the CO_2 phase reaching ca. 100 μm. Many of the inclusions contain solid phases some of which are daughter minerals and others which are probably trapped phases.

Microthermometry reveals that $T_m(CO_2)$ is between -57.7 and -56.6 °C (average -56.9 °C), T_m(cla) is between -8.2 and -3.9 °C corresponding to an average salinity of 5 eq mass% NaCl, CO_2 homogenizes to liquid between 30.1 and 31.1 °C (average 30.9 °C, effectively the critical temperature). The CO_2 is effectively pure with little

other gases present which was confirmed by Raman analysis which did not detect any other species in the CO_2 liquid or vapour. Total homogenization was not always achieved in the H_2O-CO_2 inclusions as decrepitation frequently occurred at temperatures in excess of 250°C, a small number of inclusions did homogenize between 210 and 300 °C. Some of the solids (As-species) dissolved at 100 to 150 °C.

The composition of the solids in the inclusions was determined by opening the inclusions and analyzing the solids using the SEM. As well as the As- and Sb-phases (Fig. 1.) many other elements were detected in the solids, Bi, Sn, Cs, Ag, Mn, Zn, Cu, Ta, Ba, Ca, P, F, Cl, Br, S. Some solids could tentatively be identified as native Bi, mangano-tantalite, calcite and gypsum.
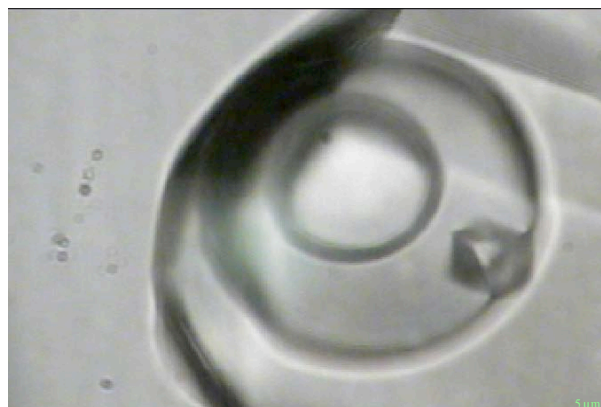

Fig. 1. Large H_2O-CO_2 inclusion with an octahedral daughter mineral. Raman spectroscopy identified the solid as arsenolite (As_2O_3).

Raman identification proved to be more definitive, positively identifying two As_2O_3 phases, arsenolite (cubic structure, low temperature phase) and claudetite (orthorhombic structure, high temperature phase) which have equivalents

as Sb_2O_3 in senarmontite and valentinite, respectively (White et al., 1967). Sb-phases are found as zones within the As-oxides as well as individual minerals (Fig. 2.). In addition, we identified the rare mineral hambergite ($Be_2BO_3(OH,F)$) in the H_2O-CO_2 inclusions which was previously reported from Muine in crystals of morganite (Thomas & Davidson, 2010). Many other solids remain unidentified.
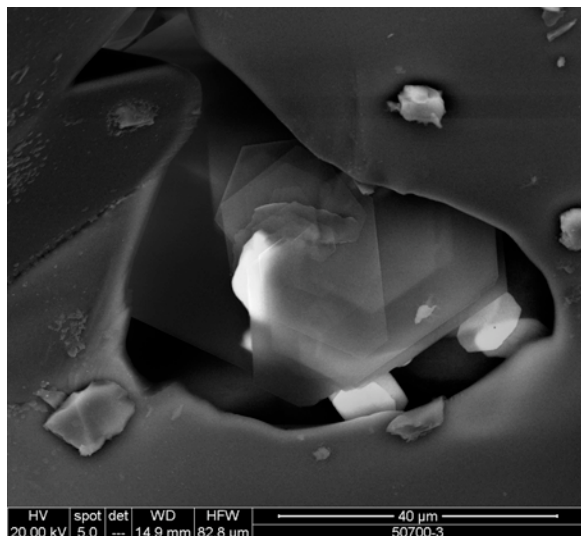

Fig. 2. SEM image of opened inclusion. The inclusion contains a zoned Al-Si polymorph, with additional As and Sb (brightest phase) daughter(?) minerals.

LA-ICP-MS analysis was carried out on the different FIA's and the composition of the inclusion fluids strongly reflects the mineralogy of the pegmatite. The maximum concentrations of Li (6,000 ppm), B (18,000 ppm) and Cs (5,000 ppm) are reflected in the presence of spodumene, lepidolite, eucryptite, petallite, tourmaline and pollucite. However, the extremely high maximum concentrations of As (210,000 ppm) and Sb (2,000 ppm) are not reflected in the bulk mineralogy of the pegmatite. Relatively low concentrations of Mn (50 ppm) and Fe (300 ppm) may be due to unusually oxidising conditions. Based on the K/Na ratios the fluid inclusion compositions can be placed in two groups. Fluids with a high K/Na ratio have low concentrations of Li, Rb, Sb, As and B and higher concentrations of Zn, Bi and Cs compared to the fluid with the lower K/Na ratios. Sr, Cu, Pb, P, Mn, Mo and Ag did not correlate with K/Na. It is likely that this represents

a fluid evolution controlled by the precipitation sequence of minerals within the pegmatite. As Muiane is a Li-pegmatite it is reasonable to assume the low K/Na, high Li, B, Cs, Sb and As fluid was the parental fluid and a decrease in Li was due to precipitation of the Li-minerals in the pegmatite. It is also likely that precipitation of pollucite and tourmaline are related to decreasing Cs and B.

Many of the inclusions are large enough that the CO_2 phase can be sampled relatively independently of the aqueous phase. The significance of this is that high concentrations of Au are associated with the release of CO_2 and subsequent analysis of the aqueous portion reveals no detectable Au. However it is not clear how the Au is transported in these fluids as there is no H_2S, as would be expected if Au was transported as a bi-sulphide complex. There is also no association with the presence of As_2O_3 in the inclusions as inclusions without a daughter mineral also have a significant Au signal in many instances. An alternative is that Au nano particles are in effect stuck to the CO_2 phase when they precipitated during H_2O-CO_2 phase separation.

The compositions of these pegmatite fluids show many of the characteristics associated with orogenic Au-deposits, the typical enrichment of As, Sb, B, Bi, only a slight enrichment in Pb, Zn and Cu, low salinity and substantial CO_2 concentrations. Mineralizing fluids derived from oxidised granitic magmas have been considered as possible sources of Au-bearing fluids for this type of mineralization and the presence of As and Sb oxides as daughter crystals, cassiterite and mangano-tantalite plus the lack of any reduced gas species indicates that these pegmatite fluids were oxidising. Therefore, these evolved granitic fluids may be the precursors of fluids that transport and precipitate ore metals in orogenic Au deposits.

REFERENCES

Hutchinson R.W., Claus R.J. (1956) *Economic Geology*, 51, 757-708.

Thomas R., Davidson P. (2010) *Mineralogy and Petrology.* 100, 227-239.

White, W.B., Dachille, F and Roy, R. (1967) *Zeitschrift für Kristallographie*, 125, 450 - 458.

The inevitable use of Raman spectroscopy to identify the major salt components in single fluid inclusions

Baumgartner, Miriam and Bakker, Ronald J.

Resource Mineralogy, Department of Applied Geosciences and Geophysics, University of Leoben, Peter-Tunner Str.5, Leoben, Austria

INTRODUCTION

The determination of fluid composition is one of the major tasks in fluid inclusions research. Microthermometry is the most common analytical technique and is the only non-destructive method, which can be applied to obtain directly qualitative and quantitative information on the salts dissolved in the fluid. Multi component salt systems show various complex phase assemblages at low temperatures (ice and salt-hydrates). The final melting of ice and salt hydrates can be used to determine the salinity, if the phase can be clearly identified. Nevertheless, various salt hydrates show similar optical properties and they are difficult to distinguish by purely optical means. In addition, optical observations cannot be applied to microcrystalline aggregates of hydrates and ice, which may regularly occur in frozen inclusions. Eutectic and peritectic reactions are additionally used to define the salt systems, as they occur at specific temperatures in dependence of the salt composition. Those temperatures are difficult to monitor accurately and the theoretic temperatures of phase transitions may occur in relatively small temperatures ranges (e.g. $CaCl_2$-H_2O eutectic at -49.8 °C and $CaCl_2$-KCl-H_2O eutectic at 50.5 °C; Borisenko, 1977). The approach presupposes the presence of stable phase assemblages and the availability of reliable data of phase transitions and relationships. Due to metastabilites, precipitation of stable phase assemblages in salt-H_2O fluid inclusions is often inhibited and expected phase transitions do not occur. Therefore, microthermometry cannot be adequately interpreted by optical means only. Raman spectroscopy has to be used to overcome the difficulties in identifying stable and metastable phase assemblages. The presence of brine, ice and salt-hydrates can be verified by specific Raman bands, which occur in the stretching region of water (e.g. Dubessy, 1992, Bakker 2004). In addition, Raman spectroscopy at selected temperatures is the only method which can be used to identify phase changes in inclusions of Raman active materials, e.g. melting of hydrates.

METASTABLITIES

Fluid inclusions containing a $NaCl$-$CaCl_2$-H_2O mixture (see Fig. 1) freeze to a glassy matrix during cooling to -90 °C. During heating the matrix re-crystallize into a microcrystalline aggregate. Optically the inclusions seem to be completely frozen and in theory the salt-hydrates hydrohalite ($NaCl\cdot2H_2O$) and antarcticite ($CaCl_2\cdot6H_2O$) should be stable with ice below the eutectic point of -49.8 °C.
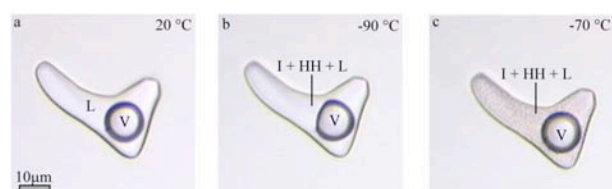

Fig. 1. Freezing of $NaCl$-$CaCl_2$-H_2O inclusions. V-vapour, L – liquid, I – Ice, HH – hydrohalite
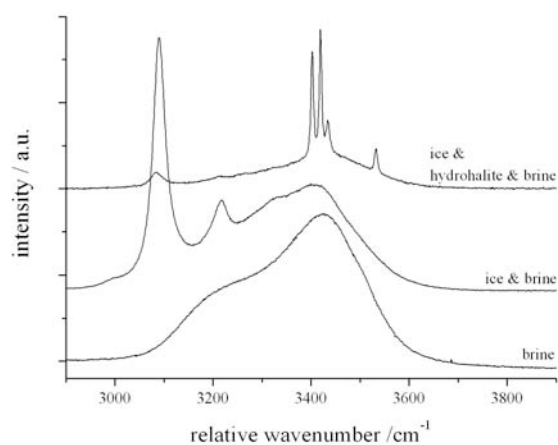

Fig. 2. Raman spectra of ice, hydrohalite, and brine at -190 °C.

Raman spectra (Fig. 2) taken from the inclusion, reveal the presence of ice, hydrohalite and brine at temperatures down to -190 °C. This inclusion contains a metastable phase assemblage at low temperature and the eutectic reaction cannot be observed in this inclusion.

EUTECTIC REACTIONS

The volume fraction of salt-hydrates in inclusions may be very small and nucleation and melting may not be observed accurately. For example, inclusions containing 16 mass% $MgCl_2$ and 5 mass% NaCl freeze to a mixture of fine grained mass. At temperatures below the eutectic of -35 °C (see Fig. 3a) it is not obvious if the inclusion is completely solidificated, respectively single hydrate crystals are difficult to identify. Raman spectroscopy allows to detect already small amounts of the hydrate phase (see Fig. 4) and offers the possibility for an exact estimation of the eutectic point, with measuring the phase assemblage simultaneously during heating the inclusion (see Fig 3b and 3c).
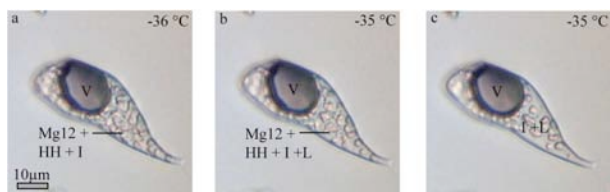

Fig. 3. Eutectic melting of $NaCl-MgCl_2-H_2O$ inclusions. V – vapour, L – liquid, I – ice, Mg12 – $MgCl_2 \cdot 12H_2O$, HH - hydrohalite
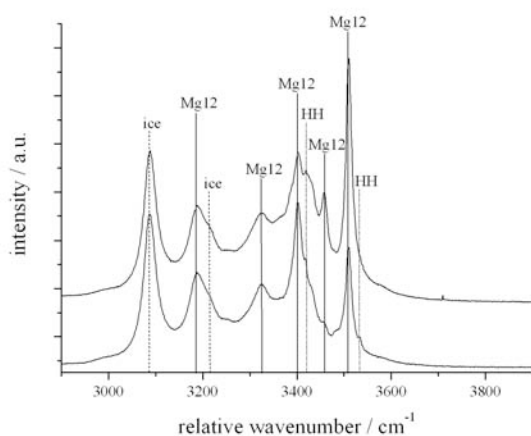
Fig. 4. Raman spectra of ice, $MgCl2 \cdot 12H_2O$ (Mg12) and hydrohalite (HH) at -190°C.

PHASE TRANSITIONS

Not only the change of state, e.g. melting of phases, also solid-solid transitions may occur in fluid inclusions and may be easily overseen by microthermometry. For example, the transition of sinjarite ($CaCl_2 \cdot 2H_2O$) into α-tetrahydrate ($CaCl_2 \cdot 4H_2O$) is only evident by a change in the Raman spectrum of the hydrate phase (Fig. 5 and 6; see Baumgartner and Bakker, 2010).
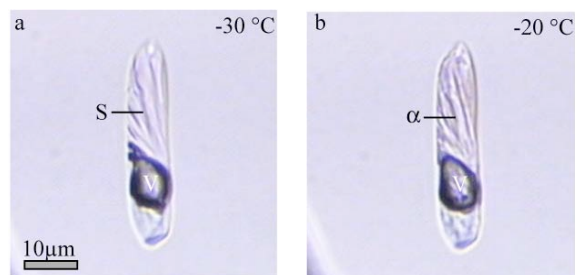

Fig. 5. Inclusion containing sinjarite (S) at -34 °C, which react between -29 to -25 °C into α-tetrahydrate (α).
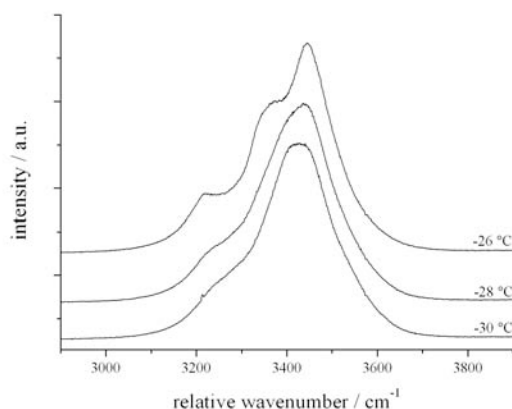
Fig. 6. Raman spectra of the phase transition sinjarite (spectrum at -30 °C) into α-tetrahydrate (spectrum at -28 °C).

REFERENCES

Bakker R.J. (2004) *Can. Min.* 42: 1283-1314

Baumgartner M., Bakker R.J. (2010) *Chem. Geol.* (2009) 265: 335-344

Borisenko A.S. (1977) *Geol. Geofiz.* 18/8: 16-27

Dubessy J. et al. (1992) *Chem. Geol.* 37: 137-150

Preliminary results of experimental re-equilibration studies of natural H₂O-CO₂-NaCl-bearing fluid inclusions in quartz

Baumgartner, Miriam, Doppler, Gerald and Bakker, Ronald J.

Resource Mineralogy, Department of Applied Geosciences and Geophysics, University of Leoben, Peter-Tunner Str.5, Leoben, Austria

INTRODUCTION

Experimental diffusion studies with fluid inclusions are performed under hydrothermal conditions to obtain diffusion rates of water related species through the quartz crystal. Synthetic fluid inclusions are synthesised under well defined experimental conditions und re-equilibrated with an external fluid at elevated temperatures and pressures (see Doppler et al., this volume). In addition to synthetic inclusions natural, negative-crystal shaped inclusions (Fig. 1A) in quartz veins in gneisses from the Alpeiner Scharte (Olperer, Tauern Window, Austria) are used for re-equilibration studies. Before re-equilibration, those inclusions were analysed accurately by optical investigation (estimation of volume fractions, size and shape of the inclusions), microthermometry and Raman spectroscopy to characterize their bulk fluid properties.

NATURAL FLUID INCLUSIONS

The fluid in natural inclusions belongs to the ternary $NaCl-CO_2-H_2O$ system. Solid phases such as mica, most probably muscovite, and an unknown hairy-like phase are found in some inclusions. The perfect shape of the fluid inclusions and the perfectly spherical vapour bubble do not allow an optical observation of separated CO_2 liquid and vapour phase, i.e. the CO_2 liquid phase is hidden in the dark rim of the vapour bubble. Therefore, the density of the vapour phase (CO_2) was determined after the method described by Fall et al. (2011) by measuring the distance between the main Raman peaks of CO_2 at about 1285 cm⁻¹ and 1388 cm⁻¹ at 40 °C. Salinity calculations were performed with the computer program Q2 (Bakker, 1997). From the obtained data, the fluid composition is calculated to about 74 mass% H_2O, 19 mass% CO_2 and 7 mass% NaCl. The total molar volume of the inclusions is about 25

cm³/mol. According to these fluid properties the specific isochore of fluid trapping was calculated by using the program ISOC (Bakker, 2003). Re-equilibration experiments are performed along this specific isochore to beware of pressure difference and of inclusion stretching and/or decripitation.

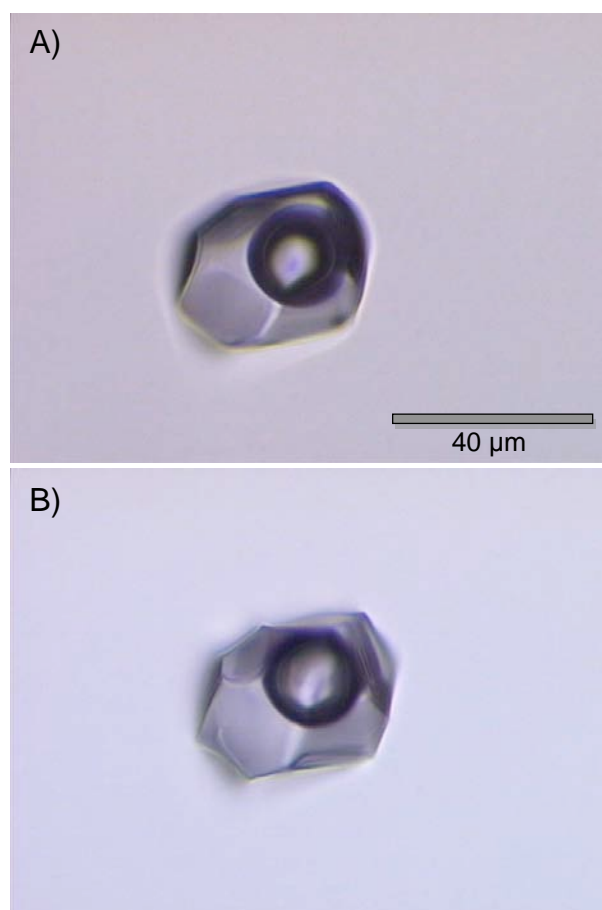*Fig. 1. A) Natural NaCl-CO₂-H₂O inclusions before re-equilibration. B) Fluid inclusions after re-equilibration with pure H2O.*

RE-EQUILIBRATION EXPERIMENTS

First experiments were carried out at 600 °C and about 400 MPa with 1) pure water and 2) D_2O as external fluid. D_2O does not play a role in

natural fluid systems, but it is used as tracer for diffusion studies because it has similar properties as H_2O, and it is easily identified by Raman spectroscopy by its specific vibrational modes between 2200 and 2800 cm^{-1}.

Differences in the chemical potential (concentration of species) are known as the controlling parameters of diffusion. In theory, CO_2 and NaCl outward diffusion through the quartz crystal should occur in both experiments. As the CO_2 molecule and also the atomic radii of Na^+ and Cl^- (dissolved in the aqueous solution) are relatively large compared to atomic distances in the crystal lattice of quartz, no efficient transport is assumed within 19 days of re-equilibration. In addition Na^+ and Cl^- occur as charged ions, which also decelerate the transport out of the inclusions due to adsorption processes.

The difference in water fugacity at experimental conditions for the pure water re-equilibration is chosen to be very little (about 217 MPa in the external fluid and 182 MPa in the fluid inclusions; calculated with the software LONER AP and LONER HKG, Bakker, 2003) and therefore no significant fluid flow is assumed. Preliminary results illustrate minor changes in fluid composition. Nevertheless, inclusions shape may modify during re-equilibration as it is shown in Figure 1.

Fluid inclusions which were re-equilibrated with D_2O show modifications in fluid composition. Minor amounts of D_2O are clearly identified by Raman spectroscopy (see Fig. 2). The amount of D_2O transported into the inclusion varies. The intensity of variation is mainly caused by the position of the inclusion in the quartz sample (3-dimensional distance from the quartz surface) and the total volume of the inclusions.

OUTLINE

Further experiments with different compositions of the external fluid at different experimental conditions (temperature and pressure) will be carried out to obtain new data of diffusion rates in natural quartz-fluid systems in order to create new diffusion models and compare them with already established ones.
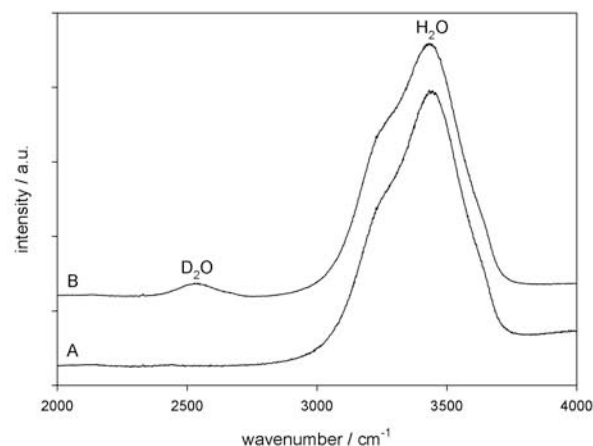

Fig. 2. A) Raman spectrum of H_2O measured in a fluid inclusion before re-equilibration. B) Raman spectrum of D_2O-H_2O mixture after 19 days of re-equilibration.

Bakker R.J. (1997) *Comp. & Geosc.* 23, 1 - 9
Bakker R.J. (2003) *Chem- Geol.* 194, 3 - 23
Doppler G. et al. (2011) *this volume,* 72-73.
Fall A. (2011) *Geochim. Cosmochim. Acta* 75, 951-96

Advantage of the use of Focused Ion Beam technique to specify mantle fluid inclusions

Berkesi, Márta*, Guzmics, Tibor*, Szabó, Csaba* and Dubessy, Jean**

*Lithosphere Fluid Research Lab, Eötvös University, Budapest (ELTE), Hungary
**UMR G2R et CREGU, Nancy University, Nancy, France

Introduction

It is known that within the fluid inclusions solids (referred to as daughter phase) may crystallize as a result of cooling and/or reaction with the host mineral. If the volume proportions of the daughter phases are not known, the fluid composition determined can be misinterpreted. However, in situ measurement of the daughter phases can be complicated and ambiguous with conventional techniques because of their size and/or composition. In this study we report our results using FIB (focused ion beam) - SEM (scanning electron microscopy) technique on investigation of daughter phases in orthopyroxene-hosted fluid inclusions in mantle xenoliths from the Pannonian Basin.

Samples

Double-polished 100 microns thick orthopyroxenes (enstatite) were prepared from mantle xenoliths that were collected from two different alkali basaltic edifices (Szentbékkálla and Tihany) of the Bakony-Balaton Highland Volcanic Field, Central Pannonian Basin, Hungary. The mantle xenoliths from this region have been a subject of detailed petrologic, geochemical and deformation studies over the last decade (e.g. Szabó et al., 2004). Migrating fluid was trapped in orthopyroxenes at lithospheric mantle condition (Berkesi et al., 2009) forming negative crystal shaped inclusions that occur mostly along healed fractures. Their size varies between 2 and 30 microns, and it was found that the smaller the inclusion the more representative their fluid composition.

Previously, the fluid phases were studied revealing C-O-H-S fluid system (Berkesi et al., 2009). Although there are evidences on the presence of different daughter phases detected by Raman microspectroscopy (magnesite and quartz in orthopyroxene-hosted fluid inclusions), there was no information of their volume percentages because of their poor visibility.

Fluid inclusion exposing procedure by FIB technique

FIB-SEM measurements were carried out in a FEI QUANTA 3D FIB-SEM apparatus having both secondary and backscattered electron detector together with silicon drift X-ray energy dispersive spectrometer (EDS), operating at the Eötvös University, Budapest. Identification of daughter phases were mostly based on their morphology on the secondary electron images and the brightness on the backscattered electron images together with study of EDS spectra. Depending on the size of fluid inclusion, an optimal extent was removed by the ion beam and therefore, we could look at the exposed part of the inclusion by SEM and analyze with EDS. For example, we found that ~100-200 nm large steps are sufficient for 5 microns large orthopyroxene-hosted fluid inclusions to have accurate volume proportions of daughter phases. The actual progress of the inclusion exposing process is monitored acquiring secondary electron images of the sample.

Results

In accord with previous Raman analysis, magnesite and quartz have been found within the fluid inclusions. These daughter phases have sizes between 200 and 2000 nm occurring as cluster on some parts of the inclusion walls. Either the magnesite or quartz is mainly euhedral or subhedral. In addition, subhedral S-bearing solid phase (Fe-sulphide) has also been identified, sizing in a range between 400 and 1000 nm (Fig. 1). The presence of sulphide allows us to understand the role of H_2S fluid molecule found by

Raman microspectroscopy in the mantle fluid inclusions (Frezzotti and Peccerillo, 2007; Berkesi et al., 2009; Hidas et al., 2010). The vol% of the magnesite is ranging from 3.3 to 8.0, quartz from 2.6. to 6.2 vol.%, whereas the sulphide remains between 1.3 and 1.9 vol%.
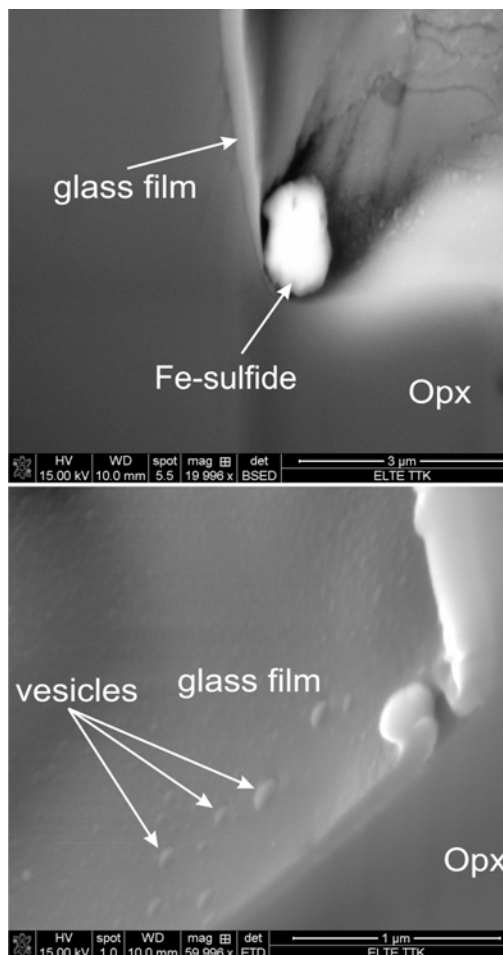

Fig. 1. Daughter phases identified by FIB-SEM in the mantle fluid inclusions. Upper image-backscattered electron image of Fe-sulphide daughter phase. Lower image-secondary electron image of the glass film having numerous spherical-shaped vesicles on its surface. Opx-orthopyroxene

One of the most interesting feature observed was a thin film covering the whole wall of the fluid inclusions in less than 1 vol%. They have a feature that is typical also for the volcanic glasses, showing numerous spherical-shaped holes (vesicles) on the surface as a result of the exsolution of volatiles (Fig. 1). The EDS analysis revealed that the glass has higher Si/Mg and richer in Fe, Ca and in some cases in Al than the host orthopyroxene. The thickness of the thin glass layer is around 100-200 nm, therefore remains invisible by using any other analytical method (optical microscopy, heating-freezing stage and Raman microspectroscopy).

Concluding remarks

Volume proportions of daughter phases, which have not been detected by using any other routinely used analytical technique for fluid inclusion studies, were identified by using the FIB-SEM technique on mantle fluid inclusions.

The acquired results of this study contribute to 1) precise quantification of the bulk fluid composition and 2) better understanding the mechanisms of the post-entrapment processes.

Acknowledgement

REFERENCES

Berkesi M., Hidas K., Guzmics T., Dubessy J., Bodnar R. J., Szabó C., Vajna B. & Tsunogae T.(2009) *J. Raman Spectrosc.* 40: 1461-1463.

Frezzotti M.L.; Peccerillo A. (2008) *Earth. Planet. Sci. Lett.* 262: 273-283

Hidas K., Guzmics T., Szabó C., Kovács I., Bodnar R.J., Zajacz Z., Nédli Z. Vaccari L. & Perucchi A. (2010) *Chem. Geol.* 274: 1 - 8.

Szabó C., Falus G., Zajacz Z., Kovács I., Bali E. (2004) *Tectonophysics* 393: 119–137

Alteration of oil by gas: experiments in fused silica capillary capsules to interpret natural petroleum inclusion pattern

Bourdet, J.*, Eadington, P.J.*, Burruss, R.C.** and Chou I.-M.**

*CSIRO, CESRE, 26 Dick Perry Ave., Kensington, 6151, WA, Australia
**US Geological Survey, 956 National Center, Reston, VA 20192, USA

Reservoir case studies showed that the fluorescence of oil inclusion assemblages of current or palaeo-gas zone has patterns that are not seen in zones that have only been invaded by oil (Eadington *et al.*, 2008; Bourdet *et al.*, 2010). It is suspected that a fraction of the oil is retained in the pores around grains when oil is drained by gas and that molecules from this residual oil partitioned in gas. To reproduce the alteration of oil by gas (gas-washing), we sealed small amounts of crude oil (59º, 42º or 33º API) and excess pure gas (methane, ethane, propane or CO_2) in fused silica capillary capsules (FSCCs, Chou *et al.*, 2008), with and without water. The UV-visible fluorescence spectra of oil phase(s) enclosed within the FSCCs were acquired using Hg lamp excitation with a narrow-band 365 nm filter at temperatures of 20 to 100 ºC. Raman and FT-IR spectra of the gas, oil and solid phases were measured at 20 ºC.

The 33° API oil (yellow fluorescence, Fig. 1 and Fig. 2) formed with ethane and propane a new immiscible fluorescent liquid phase with a blue fluorescence, a large amount of semi-solid residues with dark orange fluorescence while the oil fluorescence become whiter or the oil disappeared. Without water solid residues are not present in FSCC with ethane, while they are abundant in the capillary with ethane and water. The oil with methane kept the same fluorescence colour. Temperature has a small effect on the fluorescence spectra of liquids and solids. Temperature slightly increases the fluorescence intensity of the new immiscible liquids at low (400-450 nm) and high wavelength (500-700 nm) while the fluorescence of the residual oil is red-shifted. Experiments with 59°and 42° API oils (fluorescing blue, Fig. 3) do not show immiscible hydrocarbon liquids. The fluorescence of those crude oils displays red-shifts in the presence of gas that are accentuated with increasing temperatures. Solid

residues are negligible. Methane has a similar or stronger effect compared to ethane and propane with those oils. Slight increases of the fluorescence spectrum at short wavelength occur for the 42º API crude oil with gas.
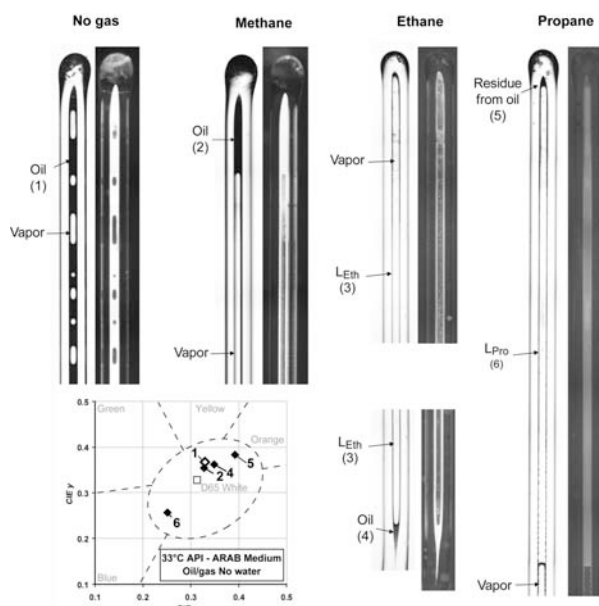

Fig. 1. *Paired photomicrographs (bright field and 365 nm illumination) of FSCCs enclosing Arab medium oil (33º API), or Arab medium oil mixed with methane, ethane or propane. The graph plot the CIE chromaticity indexes of oil or semi-solids observed in capsules.*

FT-IR and Raman spectra showed that at room temperature methane dissolves in the oil and concentrate in the vapour phase. The pressures estimated using the Raman methane peak position technique created for the system CH_4-H_2O (Lu et al., 2007) are between 95 and 200 bars. Ethane and propane dissolve in the oil, vaporise in the vapour phase and form a new immiscible liquid with heavy oil (33º API). Pressures are not measurable as yet for those gas, but the intensity

of the FT-IR and Raman scatter signals in the vapour phase were weaker for ethane than methane, and the propane peaks were very low. This suggests that their concentrations in the vapour phase are low at room temperature and the pressure is probably low. Vapour pressures for pure ethane and pure propane at 20 ºC are respectively at 34 bar and 10 bar (Danesh, 1998). Propane is the most effective gas to precipitate semi-solid residues; water band is always associated with the FT-IR signals of the semi-solid residues.
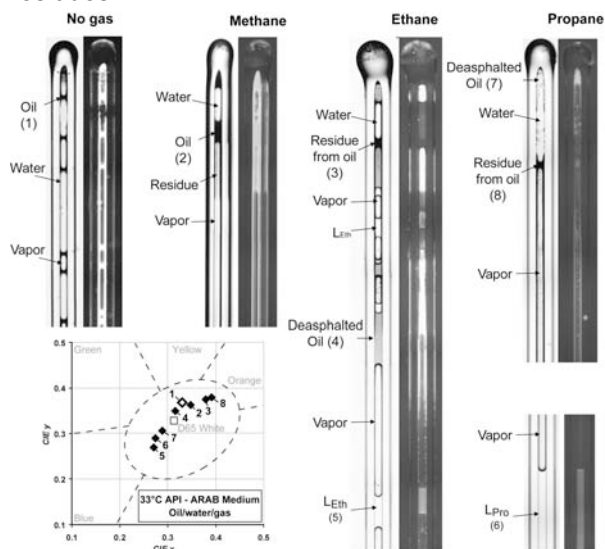

Fig. 2. *Paired photomicrographs (bright field and 365 nm illumination) of FSCCs enclosing Arab medium oil (33º API) with water mixed with methane, ethane or propane. The graph plot the CIE chromaticity indexes of oil or semi-solids observed in capsules.*

We interpret factors contributing to changes in the residual oil as: (1) decrease of fluorescence at short wavelengths (red-shift) is due to partitioning of low molecular weight aromatic molecules into the vapour phase or into the new immiscible liquid phase; (2) decrease of fluorescence response at long wavelengths (blue-shift) is due to loss of high molecular weight aromatics by precipitation of solid residues; (3) increase of fluorescence response at short wavelengths (blue-shift) is due to desorption of aromatics and resins from asphaltene. In the lowest API gravity oil, water has effects on precipitation of semi-solid residue and stability of oil phase.
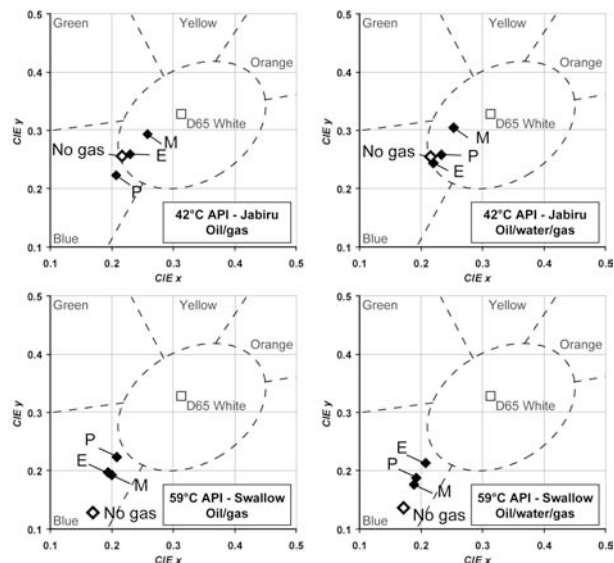

Fig 3. *CIE chromaticity indexes plots of the oil in capsules prepared with 42º and 59º API crude oils, with or without water, mixed with gas (M: methane, E: ethane, P: propane).*

The change of the fluorescence colour of the residual oil in presence of an excess of gas appears to be due to a combination of these phenomena. Their intensity depends on the initial composition of the oil. Pressure and nature of the gas present in the vapour phase has probably an impact on aromatic-bearing molecules solubility in vapour, however this assumption suggested by this study requires further experiments. These results are consistent with the variant attributes of oil inclusion assemblages trapped in palaeo-oil zones that were displaced by gas and support the concept of gas-washing of residual oil.

REFERENCES

Bourdet J., Eadington P.J., Kempton R.,Mills D., Liu K. (2010) *Geochim. Cosmochim. Acta* 74: A109.

Chou I.M., Song Y.C., Burruss R.C. (2008) *Geochim. Cosmochim. Acta*, 72: 5217 - 5231.

Danesh A. (1998) Elsevier, *Developments in Petroleum Science* 47, p. 388, Amsterdam.

Eadington P.J., Kempton R., George S., Volk H., Bourdet J., Coehlo C.E.S. (2008) *Geochim. Cosmochim. Acta* 72: A236.

Lu W., Chou I.M., Burruss R.C., Song Y., (2007) *Geochim. et Cosmochim. Acta* 71 : 3969 - 3978.

Assessment of UV-Raman for analysis of petroleum inclusions

Bourdet, J.*, Burruss, R.C.**, Bodnar, R.J.*** and Eadington, P.J.*

*CSIRO, CESRE, 26 Dick Perry Ave., Kensington, 6151, WA, Australia
**US Geological Survey, 956 National Center, Reston, VA 20192, USA
***Department of Geosciences, 4044 Derring Hall, Virginia Tech, Blacksburg, Virginia 24061, USA

Detection of hydrocarbon components in fluids or solids is useful for investigation of the petroleum potential of a basin. For this purpose, FT-IR or Raman spectrometry techniques are the two most commonly used methods for analysis of fluid inclusions. Raman spectroscopy offers a laser spot size of 1 to 2 micrometers which allows work at the scale of individual phases in a fluid inclusion. However, using visible excitation, fluorescence of aromatic compounds precludes analysis of petroleum-bearing fluids because fluorescence emission is orders of magnitude more intense than Raman scatter. Aromatic compounds present in oil and gas fluoresce in the UV, visible and near-infrared, depending on the excitation wavelength and the number of aromatic rings. Benzene is the smallest aromatic molecule and its fluorescence emission maximum is at the shortest wavelength of the aromatics at about 280 nm. In order to avoid fluorescence, UV-Raman uses short wavelength excitation from a frequency-doubled argon ion laser at 244 nm, below the fluorescence maximum of benzene. A Raman band at 3000 cm^{-1} relative to excitation at 244 nm has an absolute wavelength of 263 nm. UV-Raman scatter can be detected between the excitation wavelength and the wavelength of fluorescence emission. This work examines the potential offered by UV-Raman for analysis of petroleum inclusions. We present spectra acquired on pure paraffinic oils and on petroleum inclusions (oil and condensate).

Pure paraffinic oil contains exclusively n-alkanes. Its spectrum (Fig. 1A) shows typical C-H bands with two dominant groups, one between 1550 and 750 cm^{-1} and the other between 2600 and 3150 cm^{-1}. They represent C-C stretching, bending and twisting bands and C-H stretching bands, respectively, with additional features from Fermi resonance. The spectrum of oil in a paraffin-rich natural oil inclusion (Fig. 1B), enclosing a solid wax phase at 20 ºC (T$_m$= 66 ºC), shows a main band at around 1610 cm^{-1}, two bands at 1380 and 1435 cm^{-1} and a minor band at 1230 cm^{-1}. Two wide bands with low intensities are located at about 2925 and 3210 cm^{-1}.
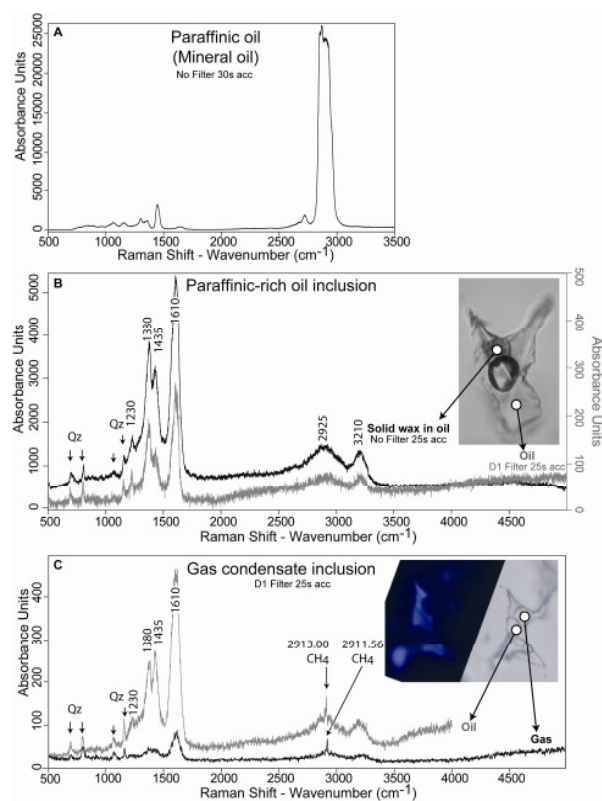

Fig. 1. (A) UV-Raman spectra of paraffinic oil (mineral oil), (B) of oil and wax in oil inclusions and (C) of oil and gas phase in a gas condensate inclusion.

The main differences observed between oil and wax in the oil is the ratio between the 1380 and the 1435 cm^{-1} bands and the increasing intensity of the baseline at high wavenumber. None of the C-H vibration Raman bands observed in the pure paraffin oil are present in the oil inclusion spectra. The spectrum of a rim of oil in a gas condensate inclusion (Fig. 1C) is very similar

to that of the paraffin-rich natural oil inclusion (heavier oil). Once again the 1380/1435 ratio is different. The dissolved CH_4 peak is visible at 2913 cm^{-1}. The gas phase (Fig. 1C) has a smooth spectrum with wide peaks at about 1400, 1610, 2925 and 3210 cm^{-1}. The vapour CH_4 peak is also clearly identified, this time at 2911.5 cm^{-1}. All the bands observed in the petroleum inclusion spectra, except methane and quartz, can be attributed to vibration of graphite in ordered and disordered forms. It appears that those vibrations mask all CH or C=C bands produced by hydrocarbon molecules. Since the ordered/disordered carbon bands are not present in the pure paraffinic oil, those are interpreted to be related to the aromatic/resin/asphaltene molecules present in natural oil.

Fluorescence of inclusion oils was measured using UV-Raman. Heavy oil (1), light oil (2) and two-phase trapping gas condensate inclusions (3 and 4) were used (Fig. 2a, b, c). The spectra were recorded between 250 and 650 nm using low laser power (D1 filter) and a 2400 grooves/mm grating displaying an approximate 10 nm window. Each wavelength window was collected once for 1 second. During acquisition the signal intensity in consecutive windows changed (increase or decrease) in the 300-450 nm area, but the general shape of the spectrum was preserved. All the spectra (Fig. 2) show periodicity in the baseline probably due to filters in the system.

Fluorescence of the heavier oil shows a symmetric low intensity spectrum with a maximum at about 405 nm (1, Fig. 2). The light oil produces a higher intensity spectrum with a maximum at about 385 nm (2, Fig. 2). The liquid in the liquid-rich gas condensate inclusion homogenizes to liquid (vapour volume fraction of 10 % at 20 ºC) and produces a spectrum similar to the light oil from the oil zone but its intensity is less than half and the maximum intensity is at about 375 nm (3, Fig. 2). The oil phase present as a rim in the gas-rich gas condensate inclusion homogenizes to the gas (vapour volume fraction >60 % at 20 ºC) and shows a low intensity left-skewed spectrum with a maximum intensity at 340 nm (4, Fig. 2). The gas-rich and the oil-rich spectra of the two-phase trapping assemblage are similar up to 340 nm. Above this wavelength, the oil-rich signal is more

intense. This means that their low-weight aromatic compositions are similar and the oil-rich inclusion is enriched in medium to heavy-weight aromatic molecules. Similarities of the spectra of the oil-rich gas condensate from the gas zone and the light oil from the oil zone indicate a similar overall composition.
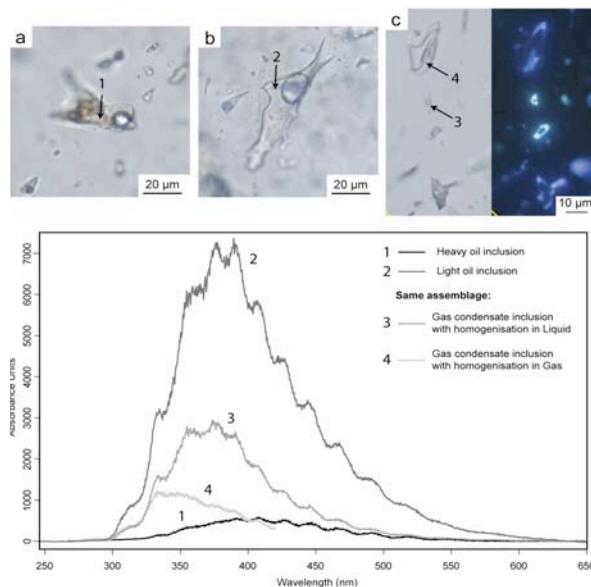

Fig. 2. *Fluorescence spectra of petroleum inclusions using UV-Raman (244 nm). Photomicrographs shows the petroleum inclusions used to measure fluorescence spectra. Oil inclusions in photos a and b are from the oil zone, while oil and gas inclusions on photo c are from the gas-zone in the same reservoir.*

During the Raman scatter spectra acquisition (D1 filter, 25s, 2 acc) a brownish spot formed that fluoresces with an orange colour (observed subsequently with a 365 nm UV lamp). A slight red-shift of the whole inclusion fluorescence colour of the heavier oil inclusions has been noticed following laser irradiation. This suggests that irradiation of petroleum inclusions with focused 244 nm laser light causes some photochemical alteration of the inclusions.

Detection of Raman bands of hydrocarbon molecules in oil inclusions using a 244 nm laser are masked by carbon bands related to molecules containing aromatic rings. Methane has been detected in gas-rich inclusions. The 244 nm laser produces a fluorescence spectrum that can be used to characterise oils.

Epithermal mineralization in Western Turkey: nature and origin of the fluids

Bozkaya, Gulcan*, Gokce, Ahmet*, Banks, David** and Bodnar, Robert J.***

*Cumhuriyet University, Department of Geological Engineering, Sivas, TR-58140, Turkey.
**University of Leeds, School of Earth and Environment, Leeds, LS2 9JT, U.K.
***Virginia Polytechnic Institute & State University, Dept. of Geosciences, Blacksburg, VA, 24061, USA.

The Biga Peninsula in Western Turkey is part of the Tethys metallogenic belt. There are diverse styles of mineralization present in the peninsula, but the most important are the epithermal Au-Ag deposits, porphyry Au-Cu-Mo deposits and epithermal Pb-Zn-Cu-Au. This study focuses on five Pb-Zn-Cu deposits that share many features, but are hosted in different lithologies. The Bagirkacdere deposit is hosted by Palaeozoic metamorphic rocks, Arapucandere is hosted by Permo Triassic clastic and calcareous rocks and Koru, Balcilar and Kumarlar are hosted by Tertiary volcanic rocks. The mineralization is in veins containing galena, sphalerite, chalcopyrite, pyrite, marcasite, covellite, bornite and fahlore as ore minerals, with quartz, calcite, barite and specular hematite as gangue minerals (Bozkaya, et. al, 2008, Bozkaya, 2009, Bozkaya, 2011). The numerous deposits in the region have been well studied and the mineralogy, paragenesis, structure and alteration are reasonably constrained. What is less clear is the age of many of the deposits (although this is now being addressed) and the nature and source of the mineralizing fluids, especially the salinity and composition. Fluids have been suggested to be dominantly magmatic, dominantly meteoric or some mixture of the two. The purpose of this study is the identification of the source of the different components of the mineralizing fluids in order to better constrain a model of fluid circulation. Data were obtained from microthermometry, Raman spectroscopy, stable isotopes, LA-ICP-MS and crush leach. Numerous FIA's were identified in the different samples, but the inclusions were typically small ca. <20µm. Almost all were L+V and on freezing the vapour bubble frequently disappeared and did not return prior to final Ice melting, making the determination of salinity impossible in these circumstances.

However, sufficient samples provided good salinity and homogenization temperatures. Only in the Arapucandere deposit was there clear evidence of V-dominated inclusions. The salinity and homogenization temperatures for the different deposits are as follows, Bagirkacdere: salinity (mass% NaCl) range 0.18 to 1.6, with an average of 0.49, T_h range 180 to 301°C, with an average of 236 °C; Arapucandere: salinity range of 0.18 to 1.4 with an average of 0.63, T_h range from 262 to 304.8 °C with an average of 277 °C; Koru: salinity range of 0.18 to 4.02 with an average of 1.43, T_h range from 129.7 to 159.3 °C with an average of 147 °C; Balcilar: salinity range of 3.86 to 8.54 with an average of 4.42, T_h range from 115.1 to 300 °C with an average of 155 °C; Kumarlar: salinity range from 3.54 to 8.81 with an average of 5.82, T_h range 246 to 285.7 °C with an average of 283 °C. Raman spectroscopy did not detect any gases in the vapour bubble of the L-V and V-only inclusions. Stable isotope compositions ($\delta^{18}O$ and δD) of fluid inclusions, quartz and baryte associated with ore minerals were measured to determine the source of the water (Fig.1). Bagirkacedere plots on the MWL with Arapucandere, Balcilar and Koru showing a shift to more positive $\delta^{18}O$ values. Kumarlar partially plots in the magmatic box, but the majority of the data coincides with those from the other deposits. The data could suggest mixing between meteoric and magmatic water in varying amounts, but we suggest that there is little magmatic fluid involved and the ^{18}O shift to more positive values is the result of the intense WRI present at the deposits. Crush-leach analysis of the inclusions in quartz and baryte was used to determine Na, K, Cl and Br in the inclusions with the aim of using primarily Cl/Br as an indicator of the source of the salinity.
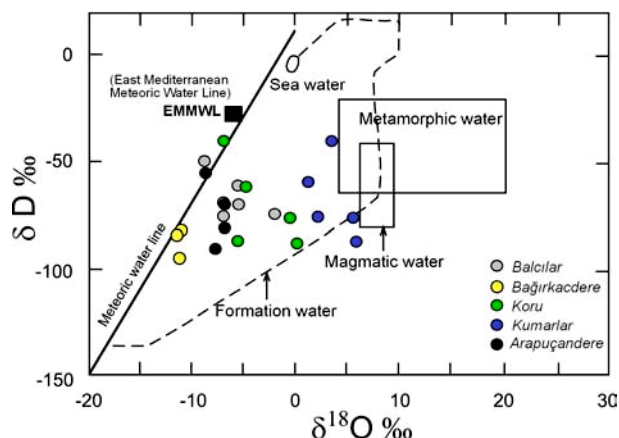
Fig. 1. Summary diagram showing the variation in $\delta^{18}O$ and δD isotopic compositions of the hydrothermal fluids in deposits from the Biga Peninsula, Turkey.

Although this is a bulk technique, microthermometry showed there to be one dominant fluid in the samples. The main limitation on the analyses was the low yield of elements from the dilute fluids. Therefore the errors on the Cl/Br ratio may be as high as 50 %. Cl/Br for Balcilar averages 20,000, Koru averages 24,000, Arapucandere averages 10,000 and Bagirkacedre averages 450, much lower than the other deposits.

The Cl/Br of the deposits is extremely high and such ratios are a clear indication that the source of Cl was from dissolution of halite. The Cl/Br molar ratio of halite is c. 20,000 but can be higher if recrystallization of the salt has taken place. However the Cl/Br ratios normally found are between 3000 and 10 000, due to some of the Br-rich bittern fluid existing in inclusions or in pore spaces. The Cl/Br ratio does not indicate any significant magmatic source for the salinity as values for volcanic gases are typically less than 1500. LA-ICP-MS analysis was carried out using a Geolas Ar-F excimer laser system coupled to an Agilent 7500c Quadrupole mass spectrometer. The inclusions were analysed individually or as groups or a few small inclusions. The elements determined were Li, Na, Mg, K, Ca, Mn, Fe, Cu, Zn, Sr, Ag, Ba, Pb. The fluids in all deposits are dominated by Na with Mg, K and Ca being approximately the same. Figure 2. shows the variability of Na, K and Mg in inclusions from each deposit. The variability is exaggerated by using the Na value divided by a factor of 10 otherwise all samples would plot in the Na apex. However, there

are slight differences apparent between each of the deposits which does not correlate with the local host rocks and may be more indicative of the composition of the source rocks that underwent extensive WRI.
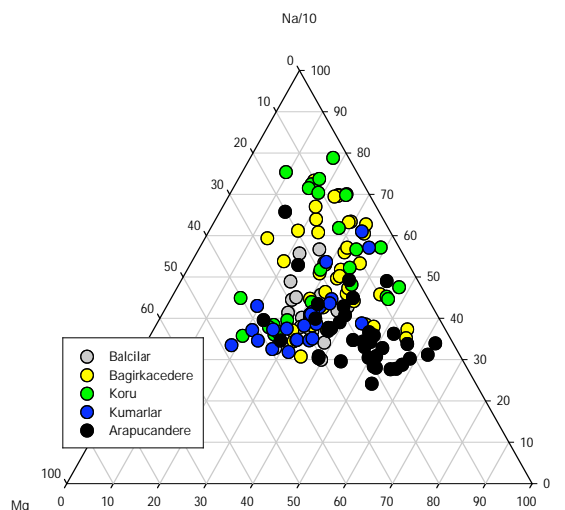

Fig. 2. Ternary plot of LA-ICP-MS analyses of inclusions from the different deposits. Although the variability within a deposit seems large, individual samples are much less variable.

The ratios of Mn, Fe Cu, Zn and Pb are similar in all the deposits. Despite the low salinity of the fluids their concentrations are still significant, reaching maximum values of approximately 100 ppm for Mn, Zn and Pb, 400 ppm for Fe, and 250 ppm for Cu. The data presented here support a common model for these deposits which although mineralogically similar are hosted in different lithologies. The salinity of the fluids is low, but the temperature is high and there is evidence of boiling in at least one deposit. Compositionally the fluids are very similar in both major and minor components with significant concentrations of ore metals despite the low salinity of the fluids. The source of the salinity is derived from dissolution of halite and the water is dominantly meteoric although the isotopic composition has been modified to different extents due to the varying intensity of WRI.

REFERENCES
Bozkaya, G., Gokce, A., Grassineau, N. (2008). *IGR*, 50:9:848-862.
Bozkaya, G.(2009) *JGE*, 101:1:8
Bozkaya, G. (2011) *IGR*, 53:116-129.

Coherent anti-Stokes Raman scattering (CARS) microscopy of fluid inclusions: multimodal 3D, chemically selective imaging and spectroscopy

Burruss, Robert C.*, Slepkov, Aaron D.**, Pegoraro, Adrian F.** and Stolow, Albert**

*US Geological Survey, Reston, VA 20191 USA
**National Research Council of Canada, Ottawa, Ontario, Canada

3D images and spectra of hydrocarbon and aqueous fluid inclusions have been recorded for the first time with coherent anti-Stokes Raman scattering (CARS) and associated nonlinear optical microscopy methods, second harmonic generation (SHG) and two-photon excitation fluorescence (TPEF). Laser scanning confocal microscopy (LSCM) with CARS is primarily used for biomedical imaging of lipids using the C-H stretching vibration (Pegararo, et al., 2010) suggesting that it should be able to image CH_4 in fluid inclusions. The CARS microscope uses a single ultrafast laser source that simultaneously generates SHG and TPEF images with the CARS image (Pegoraro, et al., 2010). All three signals are generated in the same focal volume and are collected on separate detectors, creating high-resolution 3-D images that complement the chemically-specific CARS image. The TPEF signal images the distribution of aromatic hydrocarbons and the SHG signal is sensitive to crystallographic disorder and internal surfaces in host minerals providing 3D images of inclusion shape, microfractures and grain boundaries. In the current configuration of the CARS system, images and spectra can be recorded from 2100 to 4500 cm^{-1}, providing observations for N_2, H_2S, CH_4, H_2O, and H_2. The coherent properties of the CARS signal provide orders of magnitude more signal than conventional spontaneous Raman scattering, allowing images to be acquired at about 5 microseconds/voxel. Image volumes of 350 x 350 x 100 micrometers can be recorded in minutes and hyperspectral image volumes can be recorded in less than 10 minutes.

We tested the system with CH_4-rich, CH_4-H_2O, and petroleum inclusions in sedimentary, igneous, and metamorphic rocks. 3D images of CH_4 and water clearly identify aqueous inclusions with CH_4-rich vapour bubbles that coexist with one-phase CH_4-rich inclusions (Fig. 1). In crude oil inclusions, CARS spectra of CH_4 (Fig. 2) are clearly separated from fluorescence emission of the oil.
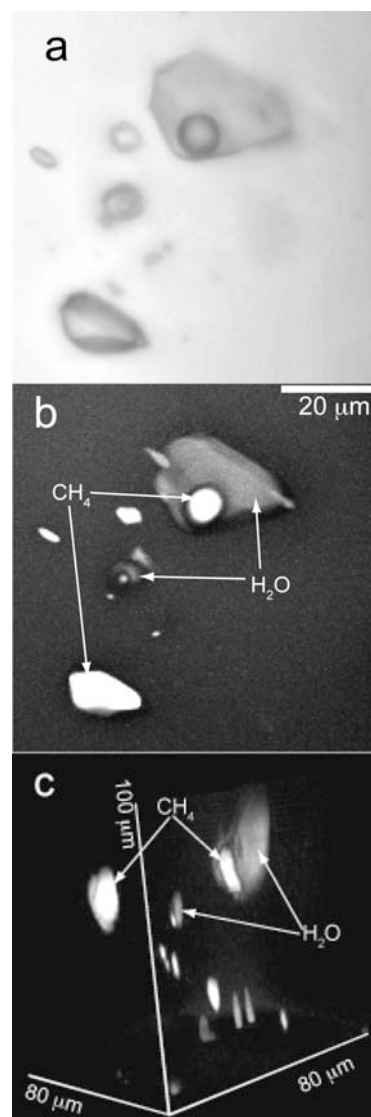

Fig. 1. CH_4-rich and CH_4- H_2O inclusions imaged in CARS. (a) Transmitted light, flattened Z-stack of multiple focal planes. (b) Flattened Z-stack, CARS image, white, CH_4 at 2910 cm^{-1}; medium grey, H_2O at 3450 cm^{-1}. (c) 3D projection of (b) rotated clockwise approximately 90°.
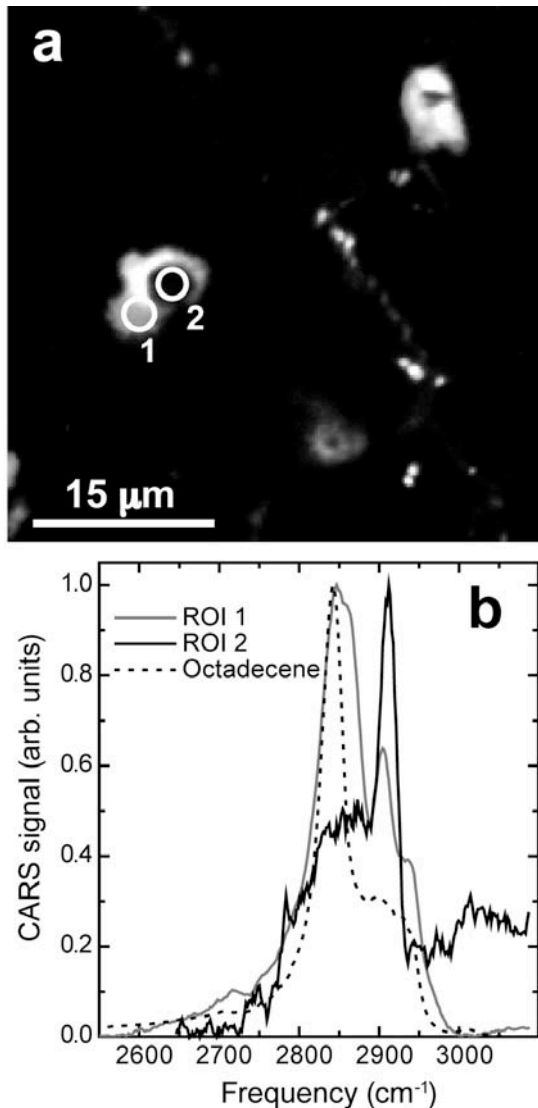
Fig. 2. Combined CARS (~2830 cm^{-1}) and TPEF (grey to white) image of 2-phase oil inclusions in calcite (a) with regions of interest (ROI) where CARS spectra (b) were recorded. Spectrum of the liquid phase (ROI 1, grey curve) has a peak for CH$_4$ in solution in the oil, whereas the spectrum of the vapour phase (ROI 2, black curve) has a more intense peak for CH$_4$ at slightly higher wavenumber. The dashed curve is a reference spectrum of octadecene.

This allows the pressure sensitive peak position of CH$_4$ (Lu, *et al.*, 2007) in oil inclusions to be recorded for the first time, providing crucial input to PVT models of oil migration. Surprisingly, some CH$_4$-rich inclusions in metamorphic and igneous rocks show TPEF signals that indicate the presence of aromatic hydrocarbons associated with CH$_4$ in these environments. Healed
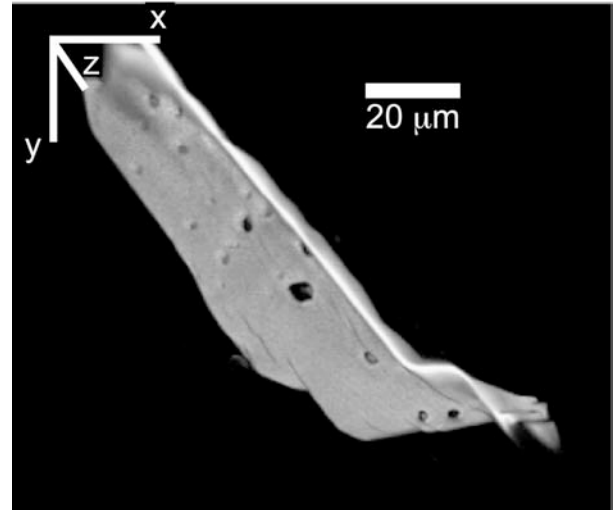
microfractures are visible in SHG (Fig. 3) allowing identification of distinct generations of CH$_4$-rich inclusions associated with specific fracture orientations.

Fig. 3. 3D projection of SHG image of healed microfracture in quartz (grey) decorated with CH$_4$-rich fluid inclusions (dark grey, CARS).

We believe these initial results demonstrate the broad potential of multimodal CARS microscopy to take fluid inclusion studies to new dimensions of chemical and spatial detail. In addition to analysis of fluid inclusions, these imaging methods are applicable to a wide range of geoscience applications in biogeochemistry, geobiology, mineralogy, and diagenesis.

REFERENCES

Pegoraro *et al.* (2010) *App. Phys.* 49, F10-F17.
Lu, *et al.* (2007) *Geochim. Cosmo. Acta* 71, 3969 - 3978.

Fluid inclusion study of Ponte Segade rare-element deposit, northern of Galicia, Spain: Preliminary results

Canosa, Francisco, Fuertes-Fuente, Mercedes and Martín-Izard, Agustín

Department of Geology, University of Oviedo, Jesús Arias de Velasco s/n 33005, Oviedo, Spain

Introduction

The Ponte Segade deposit is a recently discovered rare element mineralization, probably related to an evolved granite-pegmatite system in north-western Spain. This work presents a preliminary fluid inclusion study of on the Ponte Segade deposit to determine the composition of fluids involved in the mineralizing processes.

Geological setting

The Ponte Segade Deposit is located in the NW of the Iberian Peninsula (northern Galicia), between the villages of Viveiro (Lugo) and Ortigueira (A Coruña). Geologically, this area is in the Variscan Iberian Massif which has been divided into six zones (Julivert *et al.*, 1972), the inner one being the "Central Iberian Zone" (CIZ) where Ponte Segade deposit is located. In the CIZ, two main units were designated the Esquisto-Grauváquico Complex and the Ollo de Sapo Antiform Unit. The latter, lower Ordovician in age, is composed of augen-gneisses, porfidic schists, quarzites and slates. Variscan synkinematic S type granitoids intrude the Ollo de Sapo Antiform Unit, the Ponte Segade Deposit being related to these intrusions.

Ponte Segade deposit

The rare-element mineralized area of Ponte Segade comprises cassiterite-rich quartz veins, pegmatites and albite-rich leucogranites that are the result of magmatic differentiation from muscovite peraluminous synkinematic granites, widespread in the district. The cassiterite-rich quartz veins are tabular bodies whose thickness varies between 2 cm and 4 m and are boudinage bodies when they cut the augen-gneisses of the Ollo de Sapo Formation. These veins have the highest proportion of ore-bearing minerals, which are cassiterite, beryl, columbite-tantalite, wodginite, microlite and different sulphides. The pegmatites are tabular and lenticular intragranitic

bodies that are hosted by albite-rich leucogranites. Two types, the zoned pegmatites and layered aplite-pegmatite, have been distinguished according to their mineralogical and petrographical features. In this case, the main ore minerals are beryl, cassiterite, arsenopyrite, columbite-tantalite, wodginite, microlite, and molybdenite in zoned pegmatites, while in layered aplite-pegmatite they are elbaite, montebrasite, eosphorite, beryl and cassiterite.

Fluid inclusion study

Microthermometric studies were performed on fluid inclusion wafers (150-300 µm in thickness) using a microscope equipped with a Linkam THMSG-600 stage in the Ore Deposit Laboratory of the Geology Department of Oviedo University (Spain). The samples used for this study are quartz from cassiterite-rich quartz veins and beryl from zoned pegmatites. From petrography and microthermometric studies, 4 types of aqueous-carbonic (Lw-c_1, Lw-c_2, Lw-$(c)_1$ and Lw-$(c)_2$) and 2 types of aqueous (Lw$_1$ and Lw$_2$) fluid inclusions have been found. The nomenclature of fluid inclusion types used in this work is modified from Cathelineau *et al.* (1993).

Aqueous-carbonic fluid inclusions

The Lw-c_1 type is present in quartz of cassiterite-rich quartz veins. These fluid inclusions are characterized by irregular morphology with a size of between 18 and 19 µm. They occur in isolation. According to Roedder´s criteria, they could have a primary origin. They show a volumetric fraction of the aqueous phase (φ_{liq}) around 60 %. The melting temperature of CO_2 is -58.2 ± 0.2 ºC. The homogenization temperature of CO_2 varies between 8.7 and 10.7 ºC to the vapour phase. The eutectic temperature is observed around -20.8 ºC. The melting temperature of ice is close to -4.6 ºC and the melting temperature of clathrate, T_m(cla), is 10.3 ± 1 ºC. The total

homogenization temperature varies from 335 to 347 ºC to the liquid phase. The Lw-c_2 type is present in beryl from zoned pegmatites. These fluid inclusions have an elongated morphology and the size ranges between 25 and 62 μm. Their distribution is isolated. Thus, we consider their origin was likely to have been primary. The φ_{liq} varies from 30 to 60 %. The $T_m(CO_2)$ is between -57.3 and -56.6 ºC. $T_h(CO_2)$ is observed between 13.5 and 15.1 ºC to the vapour phase. $T_m(ice)$ ranges from -4.1 and -3.7 ºC and $T_m(cla)$ varies from 8.1 to 9 ºC. The $T_h(total)$ is around 355 ºC to the liquid phase. The Lw-$(c)_1$ type only appears in cassiterite-rich quartz veins. This typology occurs mainly in two ways, as several planar arrays of fluid inclusions with negative crystal shape that cut different quartz crystals. These planar arrays could be healed microfractures. Moreover, they occur in isolation with irregular morphology. The size ranges from 7 to 31 μm. From the petrographic features, it is probable that they could be secondary in origin. The φ_{liq} is around 60 %. Te is near to -20.8 ºC. The $T_m(ice)$ ranges from -5.3 to -4.3 ºC and $T_m(cla)$ has been measured between 10.2 and 10.8 ºC. $T_h(total)$ is next to 315 ºC to the liquid phase. The Lw-$(c)_2$ type is present in quartz from cassiterite-rich quartz veins and beryl from zoned pegmatites. The morphology is irregular or rounded and between 12 and 60 μm in size. The fluid inclusions appear isolated and, more scarcely, as intragranular alignments. Thus, we consider that they may be primary and/or pseudosecondary in origin. The φ_{liq} ranges between 70 and 80 %. Te is observed around -20.8 ºC. $T_m(ice)$ is close to -4 ºC and $T_m(cla)$ is around 8.7 ºC in fluid inclusions of beryl. In the quartz fluid inclusions, $T_m(ice)$ is between -6.8 and -5.5 ºC and $T_m(cla)$ ranges from 9.1 to 9.8 ºC. In these fluid inclusions $T_h(total)$ is near to 318 ºC to the liquid phase.

Aqueous fluid inclusions

The Lw$_1$ type appears in quartz of cassiterite-rich quartz veins and in beryl from zoned pegmatites. In quartz, these fluid inclusions are elongated or rounded morphology and appear as transgranular linear arrays. The size is between 12 and 27 μm. In beryl, they often occur isolated with irregular shapes and their size varies from 30 to 61 μm. According to Roedder´s criteria, we consider that they may be primary in beryl whereas in quartz, they could be secondary. The φ_{liq} is near to 80 %. T_e is around -20.8 ºC. The ranges of $T_m(ice)$ are -6.2 to -3.8 ºC in fluid inclusions in quartz and -4.8 to -0.3 ºC if they appear in beryl. $T_h(total)$ has a wide range of variation between 154 to 364 ºC to the liquid phase. The Lw$_2$ type occurs in quartz from cassiterite-rich quartz veins. These fluid inclusions are elongated and appear as transgranular planar. They also occur isolated with rectangular or rounded morphology. Their size varies between 20 and 50 μm. From the petrographic characteristics, we classified them as secondary in origin. The φ_{liq} is around 90 %. T_e is between -45.5 and -42.5 ºC. $T_m(ice)$ ranges between -21.7 and -18.2 ºC. $T_h(total)$ varies from 110 to 119 ºC to the liquid phase.

Conclusions

From this preliminary fluid inclusion study, the rare-element mineralization of Ponte Segade seems to be related to the aqueous-carbonic fluids that were trapped by the undoubtedly primary fluid inclusions (i.e. Lw-c_1 and Lw-c_2) found in quartz from the cassiterite-rich quartz veins and in beryl from the zoned pegmatites. However, further studies must be done in order to establish the composition and evolution of the fluids associated with this mineralization.

REFERENCES

Cathelineau M., Boiron M.C., Essarraj S., Dubessy J., Lespinasse M., Poty B. (1993)*. Eur J Mineral* 5: 107-121.

Julivert M., Fontbote JM., Ribeiro A., Nabais Conde L. (1972) *Mapa Tectónico de la Península Ibérica y Baleares a escala 1:1.000.000. Memoria explicativa*: 1, 113 (1974). Instituto Geológico y Minero de España (IGME).

Metastable melting behaviour in fluid inclusions in sphalerite from the Angouran Zn(Pb) deposit (NW Iran)

Daliran, Farahnaz*, Bakker, Ronald J.**

*Institute for Applied Geosciences, Karlsruhe Institute of Technology, 76128 Karslruhe, Germany
**Resource Mineralogy, Department of Applied Geosciences and Geophysics, University of Leoben, Peter-Tunner-Str. 5, Leoben, Austria

The Angouran Zn(Pb) ore deposit in Northwestern Iran consists of a Zn-rich sulphide ore (38 mass% Zn) and Zn-rich hypogene zinc carbonate ore (smithsonite) that formed in two successive mineralization stages. Microthermometric measurements of the primary (L+V) fluid inclusions in sphalerite (Fig. 1) yielded unusually low first melting temperatures, commonly below -59 to -66 °C (Daliran et al., 2009).

Fig. 1. L+V fluid inclusion in sphalerite (15 µm in diameter).

Because optically the formation or melting of salt-hydrates were not identified, these low temperatures were interpret as an indication of the presence of $ZnCl_2$ in the ore-forming brines (Daliran et al., 2009). The eutectic temperature of the binary H_2O-$ZnCl_2$ system is about -62 °C (Linke, 1965). The final melting temperatures of these fluid inclusions are -33 to -21 °C, commonly between -24 and -26 °C, suggesting the presence of a highly saline brine. Total homogenizations (LV→L) occur between 150 and 155 °C and occasionally up to 160 °C. The primary fluid inclusions in sphalerite are commonly irregularly shaped, but locally negative crystal shapes occur (Fig. 1).

To properly understand the behaviour of these fluid inclusions in microthermometric experiments at low temperatures, cryogenic Raman spectroscopy was applied at the Montanuniversitaet of Leoben.

Laser Raman spectroscopy studies reveal the presence of ice and hydrohalite at low temperatures (e.g. -140 °C, Fig. 2).
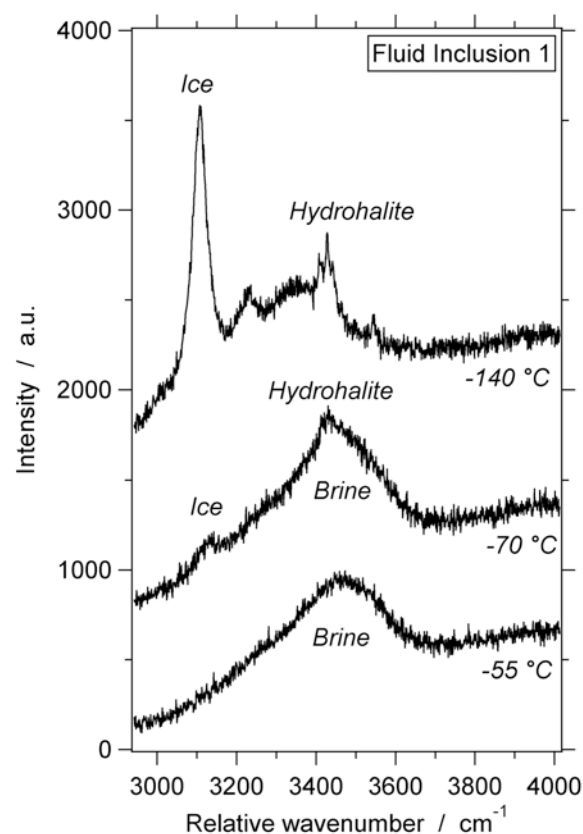

Fig. 2. Raman spectra of a fluid inclusion at -140 °C, -70 °C and -55 °C

At -70 °C, the Raman spectrum reveals the presence of ice, hydrohalite and a brine, which indicates that the melting has already started

before it is optically noticed. At -55 ˚C, both ice and hydrohalite have completely melted in part of the inclusions, whereas ice is still present in other inclusions, illustrating a variation in salinities.

In conclusion, the optically observed "first melting" is not corresponding to phase changes at an eutectic point of the fluid system in the inclusions, but only reflects the first amount of visible brine. The presence of $ZnCl_2$ in the brine cannot be proven with microthermometry, whereas Raman spectroscopy clearly evidenced the presence of NaCl in the fluid (in the form of hydrohalite at low temperatures). However, this brine must contain another type of salt, most probably $ZnCl_2$, which remains metastable in the liquid aqueous solution, even at extreme low temperatures.

The role of chloride complexing on metal solubilization in high salinity acid fluids is considered as the most important mechanism of Zn, Pb (and Ag), as well as Cd (e.g. Bazarkina et al., 2010), and could explain the formation of Zn-rich ore deposits, such as the Angouran deposit.

REFERENCES

Bazarkina EF, Pokrovski GS, Zotov AV, Hazemann JL (2010) *Chem. Geol.,* 276: 1-17

Daliran F (2009) *BGR Report*, 57: 75 pp.

Linke WF (1965) Solubilities: Inorganic and metal-organic compounds. Vol. 2.

LA-ICP-MS analysis of trace metals in hydrocarbon fluid inclusions associated with ore deposits.

Demange C.*, Banks D**, Boiron MC*, Dubessy J. * and Michels R.*

* Nancy Université, UMR G2R 7566 CNRS -CREGU, Vandoeuvre-lès-Nancy, France.
** School of Earth and Environment, University of Leeds, Leeds, LS2 9JT, UK.

The characteristics of low temperature MVT style mineralization are well established. The nature and source of the fluids and more recently the metal carrying capacity have been determined using LA-ICP-MS. As well as the high salinity metal carrying brines, found in these and similar types of sedimentary deposits, there is frequently an association with hydrocarbons. Hydrocarbon fluid inclusions are often described associated with ore deposits but few data are available and usually only concern the homogenization temperature, gas content and composition of the organic components (Gonzales-Partida et al., 2003).

The aim of this work is to develop LA-ICP-MS analysis of hydrocarbon fluid inclusions from different ore deposits and to determine their metal content. Organic matter may play an important role in the deposition of metals by acting as a reductant and in metal transport by forming organo-metallic complexes (Parnell, 1988). The initial tests were carried out on synthetic oil standards where the metal content is known, in order to determine the analytical conditions for the instrumentation and the reproducibility of the procedure. Subsequently, natural production oils were analysed in capillaries to validate the method and to compare with the data obtained from conventional methods of oil analysis in the literature. Finally, hydrocarbon fluid inclusions (Fig.1) and organic matter from different low temperature and MVT ore deposits have been studied.

The samples come from different locations [Asturias (Spain), Bou Jaber and Hammam Zriba (Tunisia), Encantada-Buenavista (Mexico), Jbel Tirremi and El Hammam (Morocco), North German basin, Annabel Lee mine, Tri-state MVT district (USA)] where fluorite or lead-zinc occurrences are recognized as vein and stratabound bodies. These deposits all have an association with oil or gas fields. In each, fluid inclusion studies reveals aqueous and hydrocarbon inclusions with low- homogenization temperatures (around 150°C), high salinities (>15 eq mass% NaCl) and with the general characteristics of MVT deposits as reported by Roedder (1984) and Leach and al. (2005).
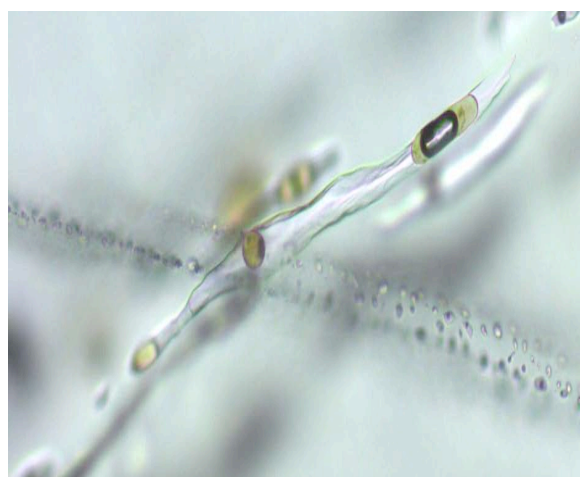

Fig. 1: Fluid inclusions with oil droplets in fluorite from Mexico.

The LA-ICP-MS system used at the University of Leeds and Nancy consists of a GeoLas Pro ArF pulsed 193 nm excimer laser system coupled with an Agilent 7500c series quadrupole mass spectrometer. For the calibration, synthetic oils (CONOSTAN 100 and 500) sealed in capillaries were used. These have been doped with the twenty-two elements chosen for the analysis, ^{11}B, ^{12}C, ^{13}C, ^{23}Na, ^{27}Al, ^{29}Si, ^{31}P, ^{34}S, ^{47}Ti, ^{51}V, ^{53}Cr, ^{55}Mn, ^{57}Fe, ^{60}Ni, ^{63}Cu, ^{66}Zn, ^{95}Mo, ^{107}Ag, ^{111}Cd, ^{118}Sn, ^{208}Pb, ^{238}U, at concentrations of 100 and 500 ppm.

The natural crude oils have metal concentrations varying from a few ppm to several hundred ppm depending on element and the origin of the oil. Two elements Ni and V tend to dominate with concentrations similar to those described in the literature for oil from the same regions of the world e.g. several hundreds of ppm

for V and Ni and less than twenty ppm for other trace metals (Tissot and Welte, 1984; Royston, 1994). In addition the metal concentration shows a good positive correlation with the sulphur concentration. Finally, for multiple analyses of each sample the V/Ni oil ratio is constant but as might be expected, distinctly different between the different oils from different locations.

The hydrocarbon inclusions from ore deposits contain higher metal concentrations (for all metals) than those measured in the crude natural oils, where there is no associated ore mineralization (Fig.2). However, the sulphur concentration shows no real difference between the two sets of oils (Fig.3). Nickel and Vanadium are no longer the dominant metals in the inclusions, Instead the metals with the highest concentrations are iron, zinc, copper, lead (up to several hundreds of ppm).

Some of the hydrocarbon inclusions from ore deposits show some unusual and interesting results. Hydrocarbon inclusions from the North German Basin have silver concentrations ranging from 100 to 800 ppm with a mean value around 300 ppm which is distinctly different to the other deposits. However in this region there are well known silver deposits and it would appear hydrocarbons have played a part in the mineralization.
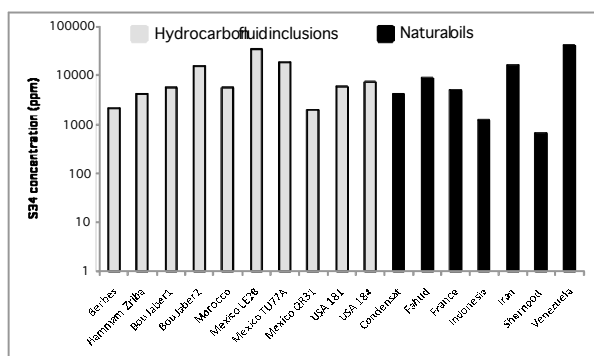

Fig. 2: Average concentrations of ^{34}S obtained from hydrocarbon inclusions from different ore deposits and from crude oils, by LA-ICP-MS.
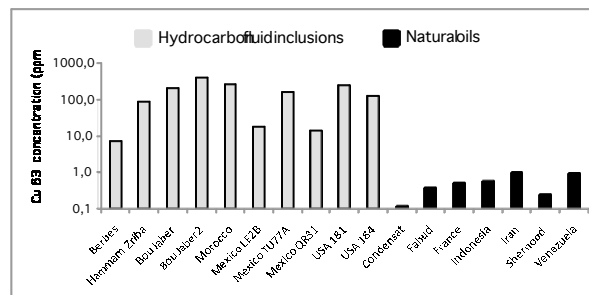

Fig. 3: Mean concentrations in ^{63}Cu obtained on hydrocarbon inclusions from the different deposits and from crude oils, by LA-ICP-MS.

This study shows how the use of LA-ICP-MS for the analysis of hydrocarbon inclusions especially the quantification of S and the metal content for MVT ore deposits can produce valid and reproducible data. The study reveals some interesting implications of the presence of organic components in the formations of low temperature ore deposits. We have shown there to be differences in the metal concentration of oil from production reservoirs and oil associated with mineralization. Our analyses oils from petroleum basins conforms to the expected concentrations for each region, but the metal concentrations in ore-related oils is up to twenty times higher.

REFERENCES

Gonzales- Partida E., Carillo-Chavez A., Grimmer J.O.W., Pironon J., Muttere J., Levresse ., (2003). *Ore Geology Reviews*, 23, 107-124.

Leach D.L., Sangster D.F., Kelley K.D., Large .R., Garven G., Allen C.R., Gutzmer J., alters S. (2005) *Economic Geology* 0th Anniversary Volume: 561-607.

Parnell J (1988) *Mineralium Deposita* 23: 191-199.

Roedder E. (1984) *Reviews in Mineralogy*, vol. 12. Mineralogical Society of America, Michigan. 644.

Royston H.F. (1994) *Geological Society, London, Special Publications* 78: 203-219.

Tissot B.P. and Welte D.H. (1984) *Second revised and enlarged edition. Springer-Verlag* Berlin Heidelberg New York Tokyo, 699 pp

Cassiterite-wolframite mineralization at Jermanice in the Krkonose-Jizera pluton (Czech Republic) – mineral chemistry, fluid inclusions, and stable isotopes

Dobes, Petr*, Vondrovic, Lukas*,**, Trubac, Jakub*,**, and Dolejs, David**

*Czech Geological Survey, Klárov 3, 118 21 Prague 1, Czech Republic
**Institute of Petrology and Structural Geology, Faculty of Science, Charles University, Albertov 6, 128 43 Prague 2, Czech Republic

Wolframite-bearing quartz veins occur at Jermanice (Czech Republic) in the Saxothuringian Zone of the Bohemian Massif, which is the largest exposure of the Variscan collisional orogen (Fig. 1a). The mineralization is situated near the intrusive contact of the Tanvald type two-mica alkali-feldspar granite of the Krkonose-Jizera batholith (318–314 Ma, Machowiak and Armstrong 2007) penetrating the chlorite-sericite phyllites with minor bodies of metavolcanics of Lower Paleozoic age (Fig. 1b).

The mineralized veins form a parallel swarm striking NNW-SSE, which crosscut the E-W oriented subhorizontal metamorphic foliation of phyllites. The veins are from a few to 25 cm thick and 50–200 m long. The veins are formed by massive milky and vuggy quartz aggregates with abundant cavities, and with minor disseminated tourmaline or with irregularly distributed wolframite crystals, up to 10 cm large. The surrounding phyllites have undergone pervasive tourmalinization.

Black coarse-grained prismatic wolframite crystals contain 59–79 mol% ferberite and 20–31 mol % hübnerite. Scheelite (with 0.1 mass% Bi_2O_3) was found along cracks in wolframite or as individual grains in quartz gangue. Cassiterite (with up to 0.7 mass% TiO_2), anhedral rutile (up to 11 mass% WO_3, 2.3 mass% FeO, and 1.85 mass% SnO_2), apatite (with 4.9 mass% F), rare stolzite ($PbWO_4$), bismutine and ilmenite are also present in the wolframite-bearing veins. Tourmaline forms grains up to 5 cm in rock matrix as well as single euhedral grains in veins. The composition is nearly elbaite with minor schorl component.

Small quartz - tourmaline ± wolframite foliation-parallel veins are composed of white or milky quartz with minor tourmaline. The primary H_2O–CO_2 inclusions in quartz had variable liquid to vapour ratio, $\varphi(liq)$ = L/L+V, CO_2–only inclusions were also observed. $T_m(CO_2)$ were measured between –57.5 and –58.4 °C, temperatures of melting of CO_2 clathrate between 7.2 and 8.4 °C, corresponding to salinity 3.3 to 5.8 eq mass% NaCl. CO_2 homogenized partly to vapour phase at 24.9 to 30.0 °C, partly to liquid phase at 12.4 to 30.0 °C, thus the CO_2 density ranged between 0.243 and 0.845 g/cm^3. Temperature of total homogenization was not measured due to variable $\varphi(liq)$. Aqueous inclusions with $\varphi(liq)$ of ~0.9 were also found in these veins. They yielded temperatures of homogenization between 154 and 186 °C, and salinity of 3.1–4.3 eq mass% NaCl.
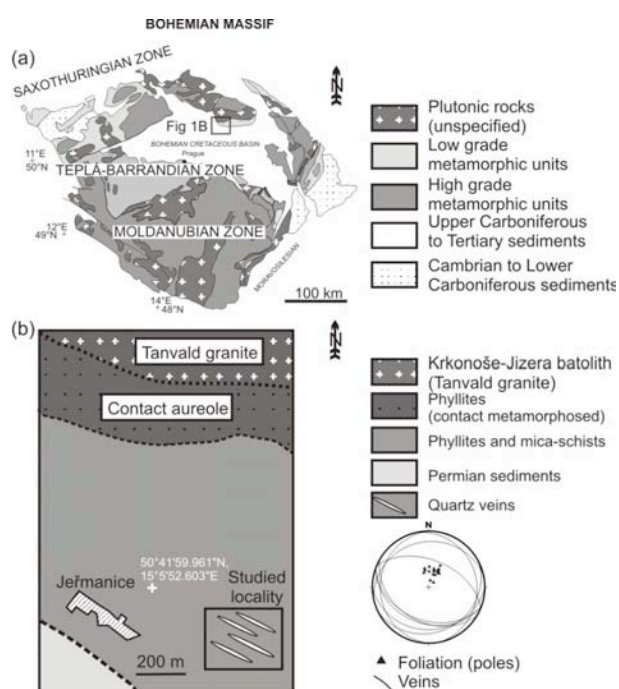

Fig. 1. (a) Bohemian Massif, (b) Geological sketch map of cassiterite-woframite mineralization

Quartz-wolframite veins crosscut the metamorphic foliation and host the wolframite ± cassiterite mineralization. Primary H_2O–CO_2 and aqueous fluid inclusions were found in euhedral quartz crystals in cavities up to 6 cm large. The aqueous-carbonic inclusions (10 to 60 µm in diameter) preferentially occur near the crystal base, show negative crystal shapes, and rather consistent liquid to vapour ratios (0.6–0.7). Temperature of melting of solid CO_2 was measured between –57.3 and –58.2 °C. These temperatures indicate only a minimal admixture of CH_4 or N_2 in gaseous phase. Temperatures of melting of CO_2 clathrate were measured between 8.0 and 9.6 °C, corresponding to low salinity of aqueous solution from 0.8 to 4.2 eq mass% NaCl. CO_2 homogenized to vapour phase, $T_h(CO_2)$ to vapour between 8.2 and 28.2 °C correspond to the density of CO_2 in the range from 0.126 to 0.292 g/cm^3. Temperatures of total homogenization fall within a narrow range between 318 and 357 °C.

Negative crystal shape of inclusions, consistent $\varphi(liq)$, and the narrow range of $T_h(CO_2)$ indicates that the inclusions were trapped at homogeneous environment (Bodnar et al. 1985), thus total T_h can be assumed to represent the minimum temperatures of trapping of inclusions. The pressure, corresponding to T_h, reached 40 to 70 MPa.

Primary H_2O inclusions can also be found at the central and peripheral part of crystals. The inclusions had relatively consistent $\varphi(liq)$ from 0.7 to 0.9, and yielded T_h from 218 to 266 °C and salinity from 4.0 to 5.6 eq mass% NaCl.

Late-stage quartz overgrowths occur on the euhedral crystals described above. They host primary aqueous fluid inclusions of oval shape (up to 60 m), with liquid to vapour ratio = 0.8–0.9. Temperatures of homogenization vary from 172 to 240 °C, the salinity of aqueous solution is between 1.1 and 7.3 eq mass% NaCl.

Oxygen stable isotopes were analyzed in vein quartz, tourmaline, and wolframite. Quartz has $\delta^{18}O_{SMOW}$ = 11.0–11.6 ‰, tourmaline gives $\delta^{18}O_{SMOW}$ = 9.3 ‰, whereas wolframite is depleted in ^{18}O, with $\delta^{18}O_{SMOW}$ = 1.0–1.6 ‰. Despite the weak alteration of wolframite to scheelite along microfractures, the quartz-wolframite thermometer of Zheng et al. (1994) yields temperatures of 240–280 °C. This temperature range is in a good agreement with the fluid inclusion features in the early quartz-tourmaline ± wolframite veins (variable $\varphi(liq)$ of inclusions and CO_2 density indicate a probable immiscibility of vapour and aqueous phase under 300 °C). The temperatures corresponding to isotopic equilibrium of quartz-tourmaline pairs are as high as 600 °C. The discrepancy in calculated temperatures has not been solved and it remains ahead for the further study.

The genesis of wolframite-bearing veins is in general connected with the pluton emplacement and thus the tungsten mineralization could be found in the pluton or host rocks (eg. Rios et al. 2003, Neiva 2008). We suppose that time constrain of quartz vein occurrence could be related with the emplacement of the Krkonose – Jizera batolith in 314 Ma (Machowiak and Armstrong 2007). Pressure build-up caused by pluton intrusion led to hydraulic fracturing of the phyllites and circulation of the solutions through the open spaces in phyllite. The cavities were filled with quartz-tourmaline and quartz-wolframite veins under estimated pressures at least 40–70 MPa and temperatures 240–360 °C. With decreasing temperature wolframite was precipitated from cooling Fe-W-bearing fluid originated from the Krkonose-Jizera batolith.

REFERENCES

Bodnar R.J., Reynolds T.J., Kuehn C.A. (1985) In: Berger B.R., Bethke P.M. (eds) *Geology and Geochemistry of Epithermal Systems. Reviews in Econ. Geology*, v. 2: 141–161.

Machowiak K., Armstrong R. (2007) *Mineralogia Polonica Special Papers* 31: 193–196.

Neiva AMR (2008) *Ore Geology Reviews* 33: 221-238.

Rios J.F., Villas R.N., Fuzikawa K. (2003) *Journal of South American Earth Sciences* 15 (7): 787-802.

Zhang Y.F., Jing-Xuuil I.U., Zhen-Sheng Ch., Huan-Bo Zhou (1994) *Economic Geology* 89: 150-157.

Epithermal gold mineralization in Costa Rica, Cordillera de Tilarán – mineralogy and fluid inclusions

Dobes, Petr*, Mixa, Petr*, Zacek, Vladimir*, Lukes, Petr*, and Quintanilla, Enrique M.**

*Czech Geological Survey, Klárov 3, 118 21 Prague 1, Czech Republic
**MINAET, Dirección de Geología y Minas, Apdo. 10104, San José, Costa Rica

Epithermal gold mineralization in quartz veins forms part of a large ore belt extending in the NW–SE direction parallel to the Cordillera de Tilarán, Costa Rica. It is confined to the Aguacate Group volcanic arc, which consists of tholeiite basalt to basaltic andesite lavas accompanied by abundant pyroclastics and breccias of andesite composition. This group of effusive rocks is of Miocene to Pliocene age (2.1 to 23.0 Ma, Bellon and Tournon 1978). The Aguacate Group is discordantly overlain by the Monteverde Formation, which is Pleistocene in age (2.2 to 1.0 Ma, Alvarado et al. 1992). The Monteverde Formation is characterized by the occurrence of more acid, calc-alkaline volcanism with dominant andesites and by the absence of regional hydrothermal alteration.

Volcanites of the Aguacate Group were intruded by granitoids of the Guacimal pluton exposed over an area of *c.* 15 × 6 km, and elongated in the NW–SE direction. Grey porphyric biotite granite is the dominant rock type of the Pluton, whereas more mafic varieties (monzodiorites to gabbros) are much less abundant. The K–Ar dating yielded ages of 7.2 to 3.9 Ma (Alvarado et al. 1992).

Epithermal gold-bearing mineralization corresponding to the SADO type (Mosier and Sato 1986) occurs exclusively in the Aguacate Group. Gold-bearing quartz veins are related to fault and fracture of steep inclinations, accompanied by pronounced hydrothermal alteration. The key tectonic zones strike NW–SE but the majority of the ore veins are controlled by local extensional structures of Riedel shear type in the NE–SW, N–S to NNW–SSE directions. The brecciation, mylonitization and healing of deformed structures suggest that three main pulses of mineralization

took place during the hydrothermal process (Mixa et al. 2011).

The age of the mineralization, is estimated in the period between the intrusion of the Guacimal Pluton and effusions of the discordant volcanic Monteverde Formation, which is devoid of mineralization (i.e. between *ca.* 6.0 and 2.1 Ma).

The gold is present as electrum (30 and 42 mass % Ag) grown as tiny inclusions up to 25 μm in size grown in quartz, pyrite and arsenopyrite. The other ore minerals are chalcopyrite, galena, sphalerite and marcasite and less abundant to scarce acanthite, pyrargyrite, greenockite, covellite, bornite and cassiterite. The principal elements exhibiting significant positive correlations with Au are Ag, Sb, As, Pb and Hg.

The Cu–Pb–Zn sulphides, which occasionally form massive vein and nest-like ores, prevail in the Guaria–Guacimal district and the Moncada mine. The gold content in this type of mineralization is low or negligible.

Three main generations of quartz suggest a multi-stage hydrothermal process. The first includes fine-grained massive quartz of grey-white, grey and grey-black colour exhibiting greasy to glassy lustre. This type of quartz forms several meters-thick veins, which are the richest in gold. The Au contents commonly range in tens ppm and exceptionally even exceed 100 ppm. The second generation is represented by coarse prismatic quartz, often forming druses filled with crystals max. 1 cm in size. This quartz type is frequently accompanied by base-metal sulphides with increased gold contents. The third generation represents the final stage of the hydrothermal ore-forming process, producing fine-grained snow-white quartz of sugary appearance. Au contents do not exceed 10 ppm.

Primary and pseudosecondary inclusions in quartz I occur mostly in the apical parts of small

euhedral quartz crystals. These inclusions show variable φ(liq) ranging from 0.5 to 0.95. Due to the variable φ(liq), the inclusions in clusters with φ(liq) of 0.9 were measured, and the temperatures of homogenization (T_h) fluctuated from 156 to 248 °C (Fig 1). The salinity of an aqueous solution varied from 0.2 to 2.9 eq mass% NaCl. NaCl is assumed to be the major compound of aqueous solutions (T_e = −22.1 °C).

The growth zones of quartz II are characterized by primary and pseudosecondary H_2O inclusions, with φ(liq) varying from 0.7 to 0.8. Rare accidental solids can be found in these inclusions. The temperatures of homogenization range between 182 and 288 °C, and the salinity of an aqueous solution is very low, not exceeding 2.1 eq mass NaCl. The eutectic temperature (T_e = -23.4 to −31.0 °C) indicates an H_2O-NaCl, ± KCl, ± $FeCl_2$, ± $MgCl_2$ type of solutions.

Fine-grained euhedral crystals of quartz III rim the coarse-grained quartz II. The primary and pseudosecondary inclusions show variable φ(liq) (0.5–0.95). Liquid-only or vapour-only inclusions were also found. Due to the variable φ(liq) the inclusions in clusters with φ(liq) = 0.8 to 0.95 were measured and the obtained T_h values range from 146 to 248 °C, and the salinity of an aqueous solution from 0.2 to 2.7 eq mass% NaCl.

Round to irregular grains of sphalerite from the Guacimal gold deposit are enclosed in quartz I. Secondary H_2O inclusions with consistent φ(liq) (0.7 – 0.8) were observed along healed microfractures in sphalerite. The T_h values of these inclusions range from 214 to 282 °C. The salinity of an aqueous solution is low (0.7–3.1 eq mass % NaCl), but slightly higher than that in inclusions trapped in quartz. The T_h of secondary inclusions corresponds to those of the primary inclusions measured in quartz II.

Coarse-grained prismatic quartz and quartz aggregates from the Moncada base-metal mine contain primary H_2O-type inclusions. They exhibit consistent φ(liq) around 0.7. The T_h values range between 248 and 278 °C, and the salinity of an aqueous solution is slightly higher, ranging from 0.5 to 4.3 eq mass% NaCl The eutectic temperatures (T_e = −25.5 to −29.4 °C) indicate H_2O–NaCl type of solution, with a small admixture of K ± Fe ± Mg chlorides.

Gold mineralization is interpreted as being the product of shallow hydrothermal circulation of dominantly meteoric waters, whose motion was triggered by the thermal gradient around the Guacimal Pluton granitic intrusion. The depth of the mineral precipitation is estimated to have varied at least between 500 and 1200 m below the paleosurface.
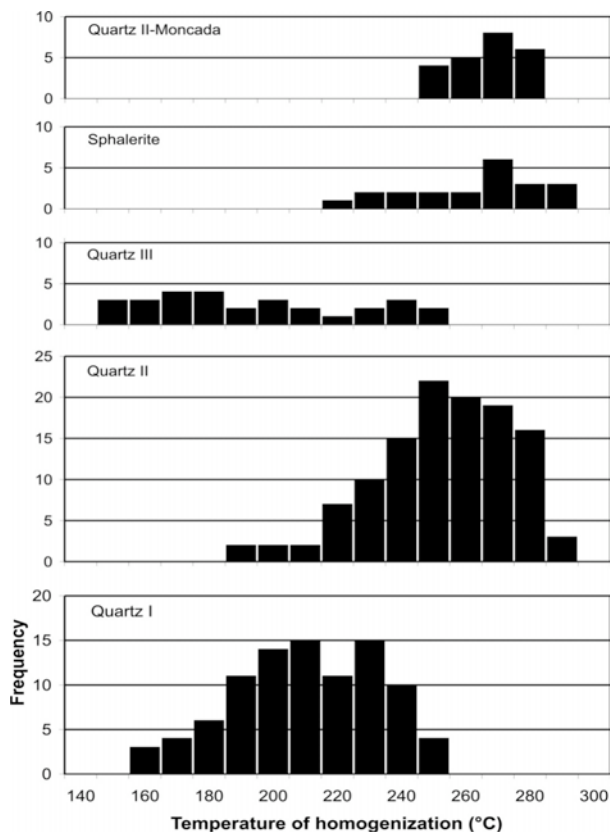

Fig. 1. Histogram of homogenization temperatures for fluid inclusions in various types of quartz and sphalerite of the Au-bearing and base-metal veins of the Aguacate Group volcanic arc

REFERENCES

Alvarado G.E., Kussmaul S., Chiesa S., Gillot P.Y., Appel H., Worner G., Rundle C. (1992) *J South Am Sci*, 6:151-168

Bellon H., Tournon J. (1978) *Bull Soc Geol France*, 20: 955-959

Mixa P., Dobes P., Zacek V., Lukes P., Quintanilla E.M. (2011) *Journal of Geosciences*, 56: 81-104.

Mosier D.L., Sato T. (1986) In: Cox D.P., Singer D.A. (eds) *Mineral Deposit Models. USGS Bul*, 1693: 155-157.

Silicate melt and fluid inclusions in the grey tuffs of Monte dei Porri, Island of Salina, Aeolian Islands, Italy.

Doherty, Angela[*,**], Bodnar, Robert.J. [**], De Vivo, Benedetto[***], Messina, Antonia[*]

[*]Dipartimento di Scienze degli Alimenti e dell'Ambiente, Università di Messina, Italy
[**]Fluids Research Laboratory, Virginia Tech (VT), Blacksburg, USA (angdoh@vt.edu)
[***]Dipartimento di Scienza della Terra, Università di Napoli Federico II), Italy

The Aeolian Magmatic Arc is an arcuate chain of volcanic islands, islets and submarine seamounts located in the southern Tyrrhenian Sea, southern Italy. The island of Salina is the second largest of the Aeolian Islands and lies in the centre of the arc. Salina exhibits the largest range in compositional variation in its erupted products across all of the Aeolian Islands, ranging from high-alumina basaltic to dacitic lava flows to rhyolitic pumice tephras erupted from 6 volcanic centres.

The Monte dei Porri eruptions were the last cone-building events on the island, occurring between 67 ka and 13 ka. They occurred after approximately 60 ka years of repose. The units consist of basaltic-andesite to dacitic lava flows interlayered with tephras. One is a red, welded agglomerate and the other, an unconsolidated, grey tuff known in the literature as the "*Grey Porri Tuff*" (Keller, 1980). The Grey Porri Tuffs are widely distributed and are comprised of up to 70 m thick deposits of scoriae and pumaceous lapilli, with many meter thick deposits identified on other Aeolian Islands and Capo Milazzo, on the northern coast of Sicily, over 30 km away (Lucchi et al. 2008).

Samples were taken at two outcrops on the flanks of Fosse della Felci volcano on the island of Salina. The first outcrop (SAL10-4a, b, c) is an unconsolidated tephra exhibiting three clear horizons defined by changes in clast size, and consists of juvenile scoria fragments of varying sizes and entrained lithics. The scoria is crystal-rich, with a phenocryst assemblage consisting of feldspar (calcic plagioclase), olivine, clinopyroxene and small amounts of quartz. The second unit (SAL10-11a, b) has two horizons consisting of rhyolitic pumice and entrained lithics. This unit is dominated by large, clear olivine, feldspar (calcic plagioclase), clinopyroxene ± quartz and

orthopyroxene. However, as will be discussed later, the origin of the quartz is yet unknown.

Silicate melt inclusions are ubiquitous in the tephra units and appear mainly as rounded, glassy inclusions with a single bubble. However, a number of inclusions in both units show more than one bubble (Fig.1), indicating that the melt was either saturated in volatiles at the time of trapping or became saturated after trapping but before the inclusion cooled through the glass transition temperature (Frezzotti, 2000). Raman spectroscopic analysis identified H_2O in the melt inclusion glass. H_2O was not detected in the bubble, and CO_2 was not detected in the glass or vapour bubbles.
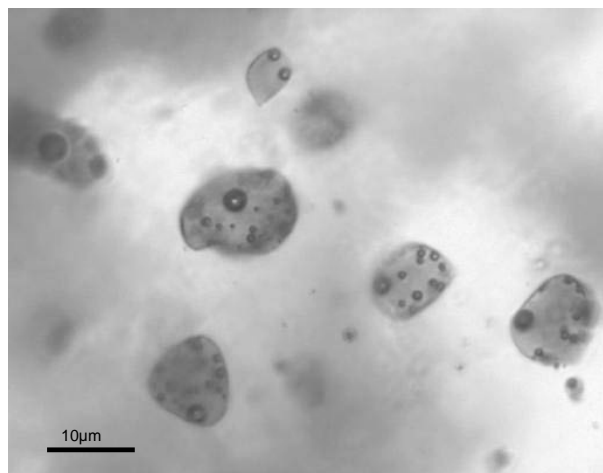

Fig. 1. Silicate melt inclusions with multiple bubbles in feldspar from scoria unit (SAL10-4b).

Silicate melt inclusions are found only rarely in olivine and pyroxene in the pumice units, but are relatively abundant in feldspar and quartz. Inclusion size is typically small, averaging ~10-15 µm in diameter. In the scoria units, melt inclusions are found in all phases but are particularly abundant in feldspar and quartz. Inclusions in the scoria units vary in size, with some particularly

large inclusions (up to 100 µm in diameter), but average inclusion size is ~10-20 µm.

Unidentified opaque minerals are present in inclusions of all phases from the scoria units. The volume ratio of the opaque phase appears to be constant in most inclusions, suggesting that the phase is a true daughter minerals. However, in some MI the opaque occupies a large volume proportion, suggesting that the phase represents a trapped solid. These two occurrences of opaques within the same group of MI suggests that the melt was saturated in that phase and that it was actively precipitating from the same melt that was being trapped as MI. If the unidentified opaque phase represents a sulphide, this would provide evidence of liquid immiscibility in the melt (Roedder, 1984).

Two-phase (liquid + vapour) fluid inclusions that occur along growth or dissolution surfaces and are interpreted to be primary are present in quartz phenocrysts in the pumice unit (Fig. 2). However, the quartz may not represent a phenocryst phase but may instead represent material that was removed from the conduit during magma ascension.

Studies are currently underway to determine the geochemistry of the melt inclusions and the homogenization temperature of the fluid inclusions.
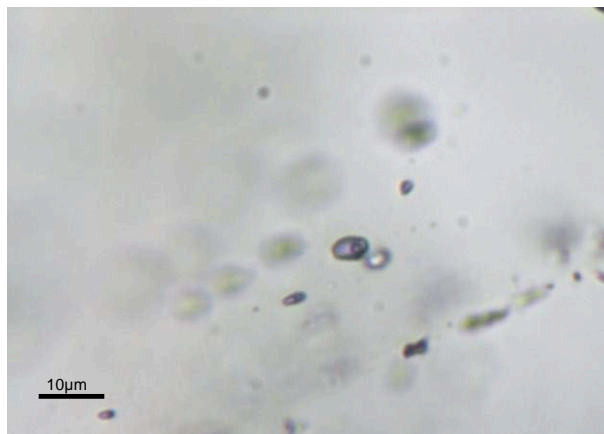

Fig. 2. Primary-appearing fluid inclusions in quartz of the pumice unit (SAL10-11a).

REFERENCES

Frezzotti M.L. (2000) *Lithos.* 55: 273-299.

Keller J. (1980) *Rend. Soc. It. Minerol. Petrol.* 36: 489-524

Lucchi F., Tranne C.A., De Astis G., Keller J., Losito R. and Morche, W. (2008) *J. Volc. Geotherm. Res.* 177:1. 49-70

Roedder E. (1984) *Rev. Min. 12*: 646p.

Fluid inclusions of the Horní Slavkov Sn-W ore deposit, Bohemian Massif, Czech Republic: evidence for non-magmatic source of greisenizing fluids?

Dolníček, Zdeněk*, René, Miloš** and Prochaska, Walter***

*Department of Geology, Faculty of Science, Palacký University, 17. listopadu 12, 771 46 Olomouc, Czech Republic

**Institute of Rock Structure and Mechanics, Academy of Sciences of the Czech Republic, V Holešovičkách 41, Prague 8, Czech Republic

***Chair of Geology and Economic Geology, Montanuniversität Leoben, Peter-Tunner-Strasse 5, 8700 Leoben, Austria

The Horní Slavkov ore deposit is one of the important occurrences of Sn-W mineralization bound to greisenized apical parts of the Variscan granitoid plutons in the Saxothuringian Zone of the Bohemian Massif. There is developed a number of post-magmatic alterations in topaz-alkali feldspar granites of the Krudum granite body (age of ca. 330 Ma) in the vicinity of Horní Slavkov, including feldspatization, greisenization and argillization. Greisenization was accompanied by crystallization of Li-micas and economic ore minerals (cassiterite, wolframite). Brittle deformation during post-magmatic stage gave rise to a suite of mineralogically distinct veins (barren quartz, quartz-cassiterite, quartz-wolframite, quartz-arsenopyrite, quartz-fluorite and quartz-hematite).

The fluid inclusion study involved petrography, microthermometry and crush-leach analyses of selected mineral phases from both rock samples (greisens) and veins. Primary fluid inclusions hosted by quartz, cassiterite, topaz and apatite from both greisens and related early veins (barren quartz, quartz-wolframite, quartz-cassiterite) are two-phase (L+V) showing three modes of homogenization which occurred within similar temperature ranges (312–405 °C, 361–408 °C, and 359–404 °C for homogenization mode to liquid, to vapour and critical, respectively). Inclusions hosted by quartz and fluorite from younger veins show systematic decrease of homogenization temperatures ranging 217–354 °C, 90–185 °C, and <100 °C for quartz-arsenopyrite, quartz-fluorite and quartz-hematite mineralizations, respectively. The eutectic temperatures ranging between -28 and -39 °C are consistent with chloridic aqueous fluids containing besides NaCl also divalent-metal chlorides. The melting temperatures of last ice indicate low bulk salinity of all fluid inclusions (0.0 to 7.1 eq mass% NaCl). In some high-T_h primary inclusions melting of clathrate was observed indicating the presence of 5–12 mol% CO_2 in these inclusions. In T_h-T_m plot, the microthermometric data define two types of trends – subhorizontal (consistent with simple cooling of a fluid phase) and diagonal (indicative for mixing of fluids with contrasting temperatures and salinities). The available fluid inclusion data indicate that greisenization was related to activity of near-critical aqueous solutions at temperatures of ~350–400 °C and pressures of ~300–600 bars.

The mineral separates from both greisens and veins have been analyzed for selected cations and anions using crush-leach method. The topaz and cassiterite (both mineral phases are essentially free of secondary low-temperature fluid inclusions) leachates show higher K/Na, Mg/Na, Ca/Na, F/Cl and NO_3/Cl molar ratios and lower Li/Na ratio then paragenetically younger quartz samples. In addition, topaz and cassiterite samples exhibit extreme variability in I/Cl (4.8×10^{-6} M to 308×10^{-6} M) and Br/Cl (0.8×10^{-3} M to 8.9×10^{-3} M) in comparison with quartz samples showing intermediate and less variable values (I/Cl = 42×10^{-6} M to 97×10^{-6} M, Br/Cl = 2.3×10^{-3} M to 5.6×10^{-3} M). All the data are negatively correlated in the I/Cl vs. Br/Cl plot implying mixing of at least two sources with contrasting I/Cl and Br/Cl signatures. The halogen data are incompatible with an idea of orthomagmatic source of fluid salinity as our data are lying outside of range reported for magmatic fluids. The

data can be easily compared to the post-Variscan post-tectonic fluids of the Bohemian Massif, which are interpreted in terms of mixing of various surficial sources (including evaporated seawater, "shield brines", and halite-dissolution fluids). The external source of at least a part of fluids at the Horní Slavkov ore deposit is suggested also from hydrogen stable isotope data showing a great variability of δD values significantly exceeding the typical "magmatic" range.

Genetic aspects of hydrothermal mineralization in the Silesian Unit (Western Carpathians, Czech Republic): comparison of igneous and sedimentary minerogenetic environments

Dolníček, Zdeněk*, Urubek, Tomáš*, Polách, Martin* and Kropáč, Kamil*

*Department of Geology, Faculty of Science, Palacký University, 17. listopadu 12, 771 46 Olomouc, Czech Republic

The study area belongs to the Silesian Unit of the Outer Western Carpathian´s Flysch Belt. The Silesian Unit is formed by dominating siliciclastic flysch marine sediments (Lower Cretaceous-to-Upper Oligocene), rare limestones (Upper Jurassic) and subordinate bodies of igneous rocks of teschenite association. The mafic and alkaline-to-subalkaline igneous rocks of the teschenite association are coincident with sedimentation of the Lower Cretaceous Těšín-Hradiště formation (Valanginian-Lower Aptian) and are widespread in the area between Hranice in Czech Republic and Bialsko-Biala in Poland. The magmatic rocks form hypoabyssal sills, dykes, pillow lavas and pyroclastics, and can be petrographically classified as teschenites, picrites, monchiquites and alkaline basalts. Igneous rocks are very variable in texture, mineral composition and chemistry, which is interpreted as a result of fractional crystallization, mixing of magmas of different origins, assimilation of sedimentary rocks and post-magmatic alterations. A typical feature of these rocks is the intense hydrothermal alteration, characterized by pervasive chloritization, serpentinization, carbonatization, silicification and zeolitization of primary magmatic mineral phases.

The recent mineralogical, fluid inclusion and stable isotope studies of amygdule and fracture mineralization in magmatic rocks revealed three stages of post-magmatic alteration which differ in both mineral association and formation conditions.

The Stage I mineralization is formed by titanite, aegirine-augite, annite, strontian apatite and analcime. Composition of this vein-type mineralization is typical for deuteric alteration which took place immediately after solidification of the host rock. Fluid inclusions indicate that the early phases (titanite and aegirine-augite) crystallized at high temperatures (390-510 °C)

from hypersaline NaCl-rich, $CaCl_2$-poor brines (47-57 mass% salts) at relatively low pressures (< 1 kbar). The origin of this mineralization is interpreted to be related to the residual fluids that remained after crystallization of silicic magma in shallow-seated setting.

The Stage II superimposed on previous stage is widespread in all rock types. It is formed by dominating coarse-grained carbonates (mainly calcite, locally also dolomite, ankerite, siderite, magnesite and/or strontianite), less occur chlorite (clinochlore-chamosite), sulphides (pyrite, marcasite, rarely sphalerite and millerite), celadonite, quartz, chalcedony and/or opal. The total range of homogenization temperatures of aqueous fluid inclusions is relatively wide (56 to 248 °C) and documents a significant temperature drop during the evolution of this mineralization. Most of the data are between 80 and 150 °C. The parent fluids are characterized by low salinity (0.2 to 3.7 eq mass% NaCl), Na-Cl or Na-Mg-Cl compositions, near-zero to highly positive fluid $\delta^{18}O$ values (between -1 and +17 ‰ SMOW), near-zero to highly negative fluid $\delta^{13}C$ values (between -17 and +1 ‰ PDB), and low content of strong REE-complexing ligands. The origin of fluids is interpreted to be predominantly in external sources, derived from surrounding sediments during diagenetic dewatering of clay minerals and/or warming-up caused by intrusions of magma.

The Stage III of mineralization is formed by fibrous calcite-dominating veinlets crosscutting both the older vein mineralization and host igneous rock. Mineralization found only at one location is composed of calcite and chlorite (clinochlore-chamosite). The homogenization temperatures of aqueous fluid inclusions present in calcite range between 83 and 155 °C. The fluids have generally low salinities (0.4 to 3.7 eq

mass% NaCl). The calculated fluid $\delta^{18}O$ values range between -1 and +6 ‰ SMOW and fluid $\delta^{13}C$ values around -12 ‰ PDB. This mineralization could have been possibly attributed to tectonic deformations connected with orogenic events in the Carpathian's realm during the Tertiary.

The hydrothermal assemblage filling joints in sedimentary flysch rocks is very simple, composed of carbonates (mainly calcite, locally also siderite); exceptionally also chlorite, dickite, quartz, pyrite and galena were recorded. Homogenization temperatures of fluid inclusions hosted by calcite exhibit relatively wide range (54 to 170 °C), however, most data are between 120 and 170 °C. The fluids have low salinities (0.4 to 2.6 eq mass% NaCl). It was not possible to determine fluid composition because no eutectic temperatures were measured. Both siderite and calcite are characterized by near-zero to positive calculated fluid $\delta^{18}O$ values (-1 to +12 ‰ SMOW) and negative fluid $\delta^{13}C$ values (-5 to -23 ‰ PDB). Chondrite-normalized REE patterns of calcite indicate crystallization under variable redox conditions and low content of strong REE-complexing ligands. The origin of the mineralization is evidently related to the diagenetic processes that took place in the host rock.

Data on fluid inclusions, stable isotopes and REE patterns of both carbonate-rich (i.e., Stage II and Stage III) hydrothermal mineralization hosted by igneous rocks and those of mineralizations present in sedimentary rocks are very similar. Our results suggest that in both environments operated fluids dominantly derived during dewatering of sedimentary sequences.

Experimental technique for re-equilibration studies of water related species through quartz

Doppler, Gerald, Baumgartner, Miriam and Bakker, Ronald J.

Resource Mineralogy, Department of Applied Geosciences and Geophysics, University of Leoben, Peter-Tunner-Str. 5, Leoben, Austria

Due to the possibility of post-entrapment compositional and density changes of fluid inclusions, the analyses of fluid properties have to be performed with particular attention. Re-equilibration processes are not yet fully understood, therefore further investigations are required to characterize all aspects of post-entrapment changes in fluid inclusions. We design our recent experimental work to test the behaviour of aqueous fluid inclusions in Brazilian quartz crystals under conditions of different pressure (p) and different fugacity (f) of water related species at a variety of temperatures.

For our purpose fluid inclusions are synthesised according to the method of Bodnar and Sterner (1987) by healing fractures which are induced by thermal shock. Fracture healing experiments, to synthesize fluid inclusions, are conducted in annealed gold capsules having an inside diameter of 3 mm and a length of 40 mm to prevent chemical intersections with the autoclaves. In our hydrothermal laboratory there are 10 autoclaves installed, in a vertical position, which are specially designed for the synthesis of fluid inclusions. Starting materials (quartz-rods) are drilled in specific crystallographic orientations. To minimize the influence of birefringence of laser light in Raman spectroscopic analyses after the experiments, rods are orientated parallel to the c-axis, according to Baumgartner and Bakker (2009).

The P-T-path followed from room temperature to final run conditions may affect fluid inclusion properties, therefore we heat up and cool down the pressure vessel along the specific isochore such that the specific volume of the fluid doesn't change. This can only be achieved with the use of an internal thermo-couple that measures the temperature directly at the sample surface. An example is illustrated in Figure 1.
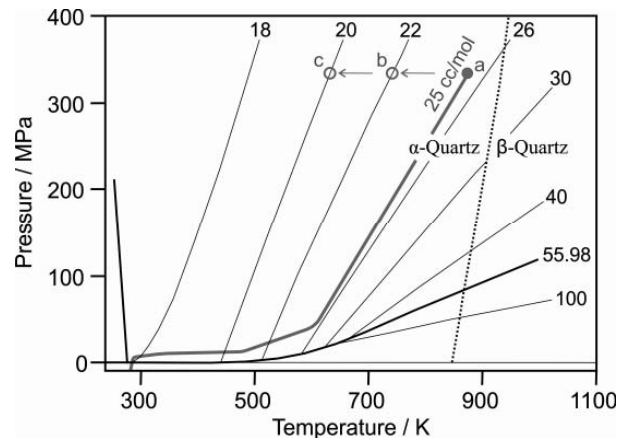

Fig. 1. Isochore diagram (in cm^3 mol^{-1}) of H_2O. Point a is the synthesis of H_2O inclusions at 337 MPa and 873.15 K which correspond to a molar volume of 25 cm^3 mol^{-1}. The grey thick line illustrates the heating and cooling conditions of the experiment.

During the experiment, both temperature and pressure are controlled by a computerized operating system that is able to stabilize the conditions within 1 °C and 2 MPa (Fig. 2). The maximum temperature and pressure of the hydrothermal experimentation are 700 °C and 1 GPa (Argon pressure).
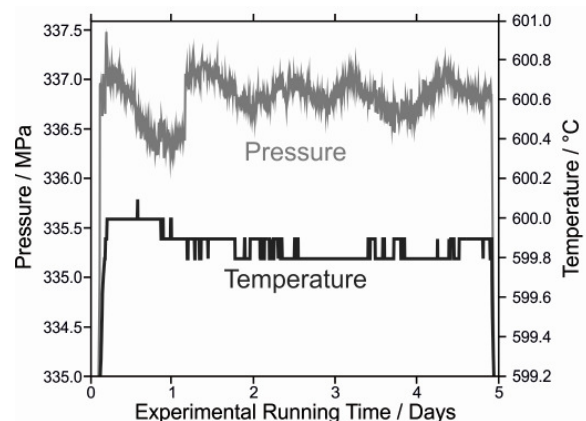

Fig. 2. Experimental run conditions with a running time of 5 days.

Fluid inclusions of known composition and density are synthesised in carefully selected inclusion-free Brazilian quartz crystals in cold seal pressure vessels under hydrothermal conditions. For performed re-equilibration studies see Doppler et al., this abstract volume. A collection of natural quartz samples with well-defined natural fluid inclusions (mixture of $NaCl$-H_2O-CO_2) is also available for experimental diffusion studies (see Baumgartner et al., this volume). After the initial experiment, the quartz cores are cut into disks of ~2750 μm in diameter and a thickness of ~500 μm, which are then polished on both sides for microscopic, microthermometric and Raman spectroscopic investigations. About 100 fluid inclusions of variable sizes, shapes and distances to the surface of each quartz disc are analyzed. We measure the T_h and T_m by using a Linkam heating-freezing stage (LINKAM MDS 600 stage and LINKAM THMSG 600 stage). The composition of the fluid inclusions is measured by an ISA JobinYvon LABRAM confocal Raman spectrometer. The morphological properties of each fluid inclusion are characterized by the total area and the perimeter. The area fractions of the vapour bubble are measured with the ImageJ software by tracing digitally around the outside edges of the shadows that define the perimeters of the bubble and the inclusion at room temperature (Bakker and Diamond, 2006).

The quartz disks with synthesized fluid inclusions are subsequently used for re-equilibration experiments. To prevent any damages during the re-equilibration experiment, we place the fragile sample in between two quartz spacers (Fig. 3).
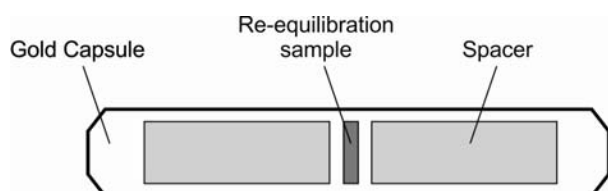

Fig. 3. Illustration of the setup of the filled gold capsule of a re-equilibration experiment.

Re-equilibration experiments are defined by four parameters: 1. fugacity of fluid components; 2. fluid pressure; 3. temperature; and 4. time. Re-equilibration conditions at the same temperature and pressure as the initial conditions (point a in Fig.1) can be performed with gradients in fugacities (or concentrations). Diffusion can be provoked without pressure differences between inclusions and the hydrothermal fluid in the capsule. Re-equilibration experiments can also be performed by varying temperature (point b and c in Fig. 1) and/or pressure, with and without a gradient in fugacities. Careful analyses of the same fluid inclusion assemblages that were selected after the synthesis, may reveal changes in shape, size, position, and fluid properties (V_m and x). The main goal of these experimental studies is to find a relationship between the parameters (including gradients in fugacity and pressure) and the fluid inclusion alterations, in order to predict the behaviour of natural fluid inclusions in specific rock exhumation P-T-t paths.

REFERENCES
Bakker, R.J. and Diamond, L.W. (2006) American Mineralogist, Volume 91, pages 635-657.
Baumgartner, M. and Bakker, R.J. (2009) Miner Petrol, 95:1-15.
Baumgartner, M., Doppler, G. and Bakker, R.J. (2011) This Abstract Volume, 44-45.
Bodnar, R.J. and Sterner. S.M. (1987) Hydrothermal Experimental Techniques, pp. 423-457. Wiley, New York.
Doppler G., Baumgartner M. and Bakker R.J. (2011) This Abstract Volume, 74-75.
ImageJ 1.43u Wayne Rasband, National Institutes of Health, USA, http://rsb.info.nih.gov/ij.

Re-equilibration studies of synthetic fluid inclusions in quartz

Doppler, Gerald, Baumgartner, Miriam and Bakker, Ronald J.

Resource Mineralogy, Department of Applied Geosciences and Geophysics, University of Leoben, Peter-Tunner-Str. 5, Leoben, Austria

Synthesised fluid inclusions in carefully selected inclusion-free Brazilian quartz crystals are used for re-equilibration experiments. Due to the possibility of post-entrapment changes of fluid inclusions, interpretations of fluid properties have to be done with particular attention. Therefore we perform re-equilibration experiments in cold seal pressure vessels under hydrothermal conditions (for applied experimental technique see Doppler et al., this abstract volume). The experiments are carried out at high experimental temperatures and pressures (max. 700 °C and 1 GPa). The experimental studies allow investigating the main factors that affect H_2O diffusion through nominally anhydrous minerals.

The present study illustrates the changes of primary synthesised H_2O-rich fluid inclusions which were exposed to D_2O during the re-equilibration process at high experimental temperatures and pressures.

The presence of D_2O in H_2O-rich fluid inclusions is detected with microthermometry and Raman spectroscopy. The melting temperatures of pure H_2O and pure D_2O are significant different, 0.0 °C and +3.8 °C, respectively. Intermediate melting temperatures can be directly reflected to relative amounts of H_2O and D_2O. Furthermore, the Raman spectrum of H_2O and D_2O are similar in shape, however, they occur in completely separated wavenumber intersections: 3000 – 3800 cm^{-1} for H_2O and 2000 – 2800 cm^{-1} for D_2O.

A variety of parameters that play an important role in diffusion experiments are examined: 1) concentration gradient (chemical potential) of H_2O (negative) and D_2O (positive); 2) distance of fluid inclusions to the quartz surface; 3) size of fluid inclusions; 4) experimentation time; (Fig. 1).

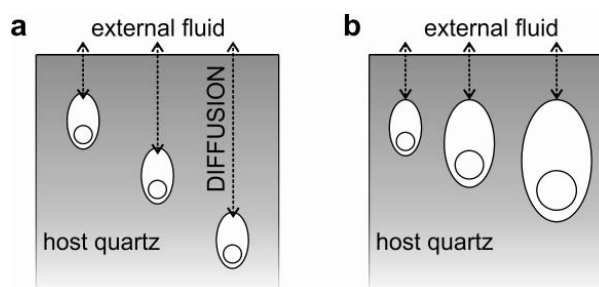Fig. 1. Schematically illustrated quartz crystal with primary synthesised fluid inclusions with known composition at *a.* variable distances to the crystal surface and *b.* variable sizes. Re-equilibration experiments are performed with a different fluid phase at the same P-T conditions and different experimentation times.

The original synthesised inclusions have a large variety of shapes (Fig. 2, definitions according to Bakker & Diamond, 2006). After re-equilibration, the original equant and regularly shaped inclusions do not change their shape, whereas elongated and irregularly shaped inclusions tend to become equant and regularly shaped during re-equilibration (arrow in Fig. 2).
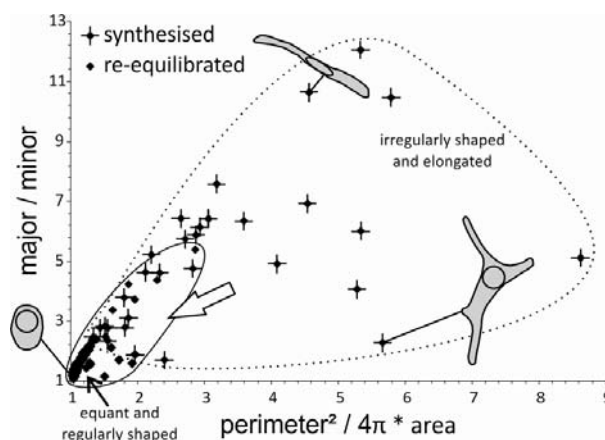

Fig. 2. Shape classification diagram (modified after Bakker & Diamond, 2006).

Analyses of re-equilibrated inclusions at variable distances to the crystal surface allow us to obtain concentration profiles in quartz. Concentration profiles of the D_2O content of fluid inclusions in quartz allow us to develop new three-dimensional diffusion models.

An example of a re-equilibration experiment is shown in Figure 3. The primary fluid inclusions have been synthesised with pure H_2O at 600 °C and 337 MPa, which corresponds to a molar volume of 25 cm³ mol^{-1}. The experimental running time for the first synthesis was nineteen days. The primary synthetic fluid inclusions were re-equilibrated with pure D_2O at the same P-T conditions for one, five and nineteen days. An example of a concentration profile, as evidenced by the melting temperature of ice T_m(SV LV), within a quartz crystal after five days is illustrated in Figure 3.
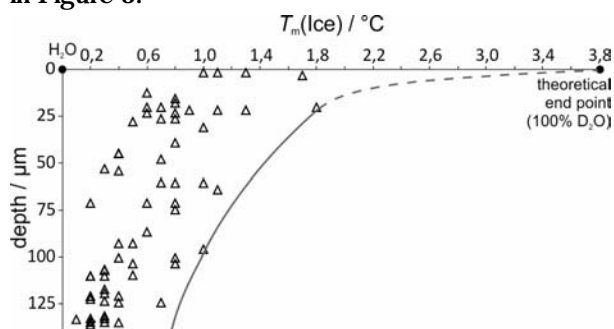
Fig. 3. Detected concentration profile as a function of distance from the surface of a quartz crystal (after an experimentation time of five days).

The performed re-equilibration experiments carried out at different running times illustrate a shift of the envelope to higher T_m values, i.e. D_2O-richer, as it is shown in Figure 4.
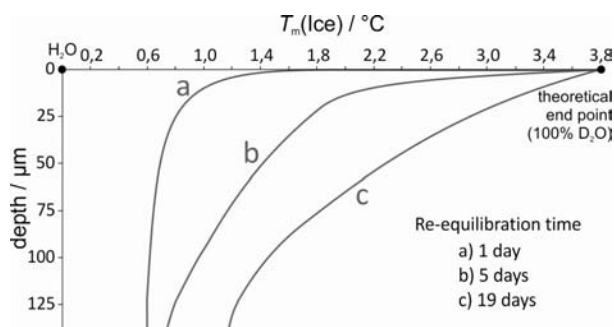

Fig. 4. The increasing running time of re-equilibration experiments illustrates the development of the concentration profile of the measured fluid phases.

Potential changes of the ambient fluid inclusions during re-equilibration correlate with the size (total volume) of the fluid inclusion. Figure 5 demonstrates again three envelopes of the detected melting temperatures of re-equilibrated fluid inclusions.
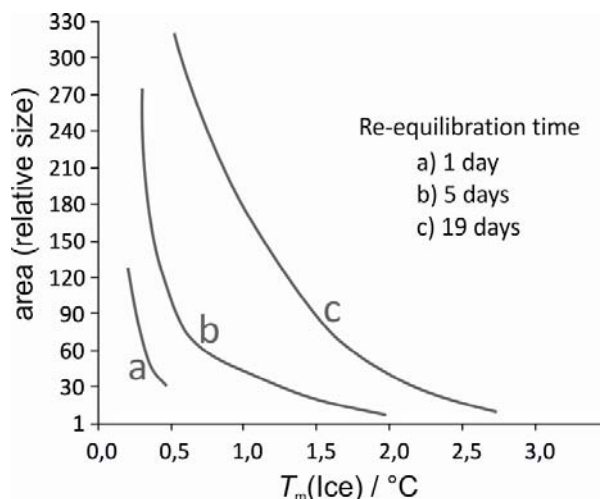

Fig. 5. Dependency of the size of the fluid inclusion to potential changes in composition during re-equilibration experiments.

These experiments have illustrated that H_2O and D_2O can diffuse relatively fast trough quartz at 600 °C and 337 MPa. Variation in re-equilibration is controlled by distance to the quartz surface, size of the fluid inclusion and experimentation time.

REFERENCES
Bakker R.J. and Diamond L.W. (2006) American Mineralogist, Volume 91, pages 635-657.
Doppler G., Baumgartner M. and Bakker R.J. (2011) This Abstract Volume, 72-73.

Preliminary fluid inclusion study of the gold-bearing quartz-vein system of the Limarinho Deposit (northern Portugal)

Doria, Armanda*, Guedes, Alexandra*, Fuertes-Fuente, Mercedes**, Cepedal, Antonia**, Campos de Lima, Alexandre*, dos Anjos Ribeiro, Maria* and Martin-Izard, Augustin**

*Centro de Geologia/DGAOT, Faculdade de Ciências, Universidade do Porto, Rua do Campo Alegre 687,Porto, Portugal
**Department of Geology, University of Oviedo, Jesús Arias de Velasco s/n 33005, Oviedo, Spain

Introduction

The Limarinho deposit (northern Portugal) is located in the Variscan Iberian Massif and is a set of Au-bearing quartz-arsenopyrite veins hosted by a Variscan S-type granite. This work presents the preliminary results of a fluid inclusion study associated with the Limarinho deposit in order to characterize the fluids involved in the mineralizing process.

Geological setting

The Limarinho deposit is located in "Galicia-Trás-Os-Montes Zone" (GTMZ), one of the axial geotectonic zones of the Iberian Massif (Julivert et al., 1972; Farias et al., 1987). The GTMZ is characterized by allochthonous mafic and ultramafic complexes, surrounded by parautochthonous (Ordovician-Lower Devonian) metasedimentary sequences (Schistose Domain). The GTMZ tectonic style is dominated by the thrust regime related to nappe emplacement with two Variscan deformation stages associated with this emplacement (D1 and D2). The tectonic evolution subsequently became a predominantly wrench regime (D3 stage) characterized by folds with subvertical axial planes and subparallel shear zones.

Variscan granitoids are widespread in the GTMZ and two main groups have been distinguished: synkinematic and post-kinematic. The former are S-type two mica granites (syn-D3: 315-310 Ma) and the latter are biotite granites that were emplaced after the main phases of crustal shortening, thus being late to post-D3 (310-280 Ma) (Noronha et al., 2000, references therein).

The late Devonian - early Carboniferous compressional event described above was followed by deformation in a brittle regime during the later stage of the orogeny, and several E-W, NW and NE trending fault systems were developed. In the studied area, these structures are mainly represented by the Régua-Verín NE trending fault system (N20ºE).

The Limarinho deposit

In this deposit the mineralized structures are a system of subvertical quartz veins with a strike of N30º-40ºE dip. Most of them have a thickness of around 2 cm, although they can reach up to 20 cm. They are hosted by peraluminous muscovite-biotite granite belonging to the synkinematic Chaves Granitic Complex. This is a syn-D3 granitic massif which is located in a D3-antiform core. These quartz-vein sets occur close to the Régua-Verín fault with a trend running almost parallel to this major fault.

Arsenopyrite is the most common sulphide in the ore-bearing quartz veins, and occurs together with base-metal sulphides, native gold, electrum and sulphosalts, mostly tellurides and bismuthides.

Fluid inclusion study

The samples used for this study are apatite and quartz from the gold-bearing arsenopyrite-rich quartz veins. From petrographic, microthermometric and micro-Raman characteristics, three types of fluids were recognized: (i) aqueous-carbonic $H_2O-CO_2-CH_4-N_2-NaCl$; (ii) aqueous with low to medium salinity $H_2O-NaCl$ (Lw_1, Lw_2) and (iii) aqueous with high salinity $H_2O-CaCl_2-NaCl$ (Lw_3).

The aqueous-carbonic fluids have been observed in intragranular fluid inclusion planes

(FIP) and clusters containing Lc-w, Vc-w, Lc-(w), Vc-(w) and Lw-c fluid inclusion types (Boiron et al., 1992; Cathelineau et al., 1993) in quartz and apatite. All of these fluid inclusions have a degree of filling (φ_{liq}), varying from ~0 to 0.70. These fluid inclusions have a melting temperature of CO_2 ranging from –59.6 to –57.2 °C, the lowest values were observed in apatite. CO_2 is the dominant species in the volatile phase ranging from 85.5 to 98.9 mol%. CH_4 is in the 0-6 mol% range and is not present in apatite fluid inclusions. N_2 content ranges from 0 to 14.5 mol %. Homogenization temperature of CO_2 to the liquid and vapour phase is in the range of 7 to 28.8 °C (the highest values were observed in apatite). The melting temperature of clathrate is in the range of 3.3 to 11.5 °C. Total homogenization temperatures, T_h(total) to the liquid phase, range from 260 to 351°C and from 335 to 365 °C, to the vapour phase.

The aqueous low to medium salinity fluids are represented by Lw_1 and Lw_2 fluid inclusions occurring as clusters and as fluid inclusion planes (FIP), respectively. The Lw_1 fluid inclusions show T_m(ice) ranging from –4.6 to –2.9 °C (calculated salinity between 4.8 and 7.3 eq mass% NaCl) (Bodnar, 1993). In these fluid inclusions the total homogenization occurs in the liquid phase between 142 and 270 °C. In the Lw_2 type the T_m(ice) ranges from -1.1 to -0.2 °C corresponding to a salinity of 0.35 to 1.91 eq mass% NaCl. Total homogenization in these fluid inclusions occur in liquid state at temperatures between 134 and 183 °C.

In the aqueous high salinity fluids (Lw_3), the eutectic temperature is around -70°C and T_m(ice) ranges from -24.3 to -24.1 °C having the highest salinity of approximately 22.4 eq mass% $CaCl_2$ (Goldstein and Reynolds, 1994). T_h(total) occurs in the liquid phase in the range from 63 to 73 °C.

Conclusions

The preliminary fluid inclusion studies carried out on quartz from the Limarinho gold deposit reveal an evolution of aqueous-carbonic fluids probably related to the earlier sulphides, to late aqueous fluids with low to medium salinity and finally to high salinity fluids. These fluids display similar features to those found in Variscan gold mineralizations from the Iberia (Noronha et al., 2000 and references therein).

REFERENCES

Bodnar R.J. (1993) *Geochim. Cosmochim. Acta* 57: 683-684.

Boiron M.C., Essarraj S., Sellier, E., Cathelineau M., Lespinasse M., Poty B. (1992) *Geochim. Consmochim. Acta* 56 : 175-185.

Cathelineau M., Boiron M.C., Essarraj S., Dubessy J., Lespinasse M., Poty B. (1993) *Eur J Mineral.* 5: 107-121.

Farias P., Gallastegui G., González Lodeiro F., Marquínez J., Martín Parra L.M., De Pablo Macía J.G., Rodríguez Fernández L.R. (1987) *Mem Fac Cienc Univ Porto* 1: 411 - 431

Goldstein R.H., Reynolds T.J. (1994) *SEPM Short Course* 31,Tulsa, 199 pp.

Julivert M., Fontbote J.M., Ribeiro A., Nabais Conde L. (1972) *Instituto Geológico y Minero de España* (IGME).

Noronha F., Cathelineau M., Boiron M.C., Banks D., Doria A., Ribeiro M.A., Nogueira P., Guedes A. (2000) *J Geochem Explor* . 71(2): 209-224.

Isotopic composition of groundwater in the southern Great Basin (USA) from late Miocene to the present: results from a pilot fluid-inclusion study

Dublyansky, Yuri*, Spötl, Christoph*, Boch, Ronny* and Lachniet, Matthew**

*Institute of Geology and Paleontology, Innsbruck University, Innrain 52, 6020 Innsbruck, Austria
**University of Nevada, Las Vegas, USA

Isotopic composition of paleogroundwater and paleoprecipitation can be derived from analyses of aqueous fluid inclusions trapped in hydrogenic minerals. Such mineral deposits are known in the southern Great Basin and can be used for characterization of the isotope paleohydrogeology of this currently arid region.

Previous studies

First results from the southern Great Basin were reported by Winograd et al. (1985), who determined δD values of inclusion water in Plio-Pleistocene calcite veins (fossil spring feeders) emplaced in clastic deposits of the Amargosa Desert and Furnace Creek (Death Valley), Late Pleistocene phreatic deposits from Devils Hole cave in Ash Meadows, and Holocene flowstone from Trout Springs cave in the Spring Mountains. The authors reported a unidirectional decline of δD from values between -50 and -70 ‰ to values ranging from -85 to -105 ‰ between the

Fig. 1. Calcite veins in fanglomerate of the Pliocene Funeral Formation in Furnace Creek wash, Death Valley, California, USA, offset by a low-angle fault.

Pleistocene and today. The decline was explained by the uplift of the Sierra Nevada, and the Transverse Ranges, which purportedly resulted in a progressively increasing rainout of the Pacific-derived precipitation.

Samples

In order to improve the record, we re-sampled the most important sites studied by Winograd and co-authors: calcite deposits at Furnace Creek (Fig. 1), Devils Hole, and Amargosa desert. In addition, we acquired data from a 17 to 20 ka-old stalagmite from Pinnacle Cave (southern Spring Mountains), and from ca. 12.9 Ma-old hydrothermal calcite and fluorite from the Diamond Queen (fluorspar) and Sterling (gold) Mines at Bare Mountain (Nevada).

Dating

Whenever possible, samples were dated by the U-series disequilibrium method. Where material was too old for U-series dating, ages were estimated from growth rates obtained on the younger parts of these samples. Ages of hydrothermal calcite and fluorite from Bare Mountain were constrained by the published [40]Ar-[39]Ar dates of the associated hydrothermal minerals.

Method

The δD values of fluid inclusion water were measured on an analytical line at Innsbruck University. Water was released by heated crushing (Dublyansky and Spötl, 2009).

Results

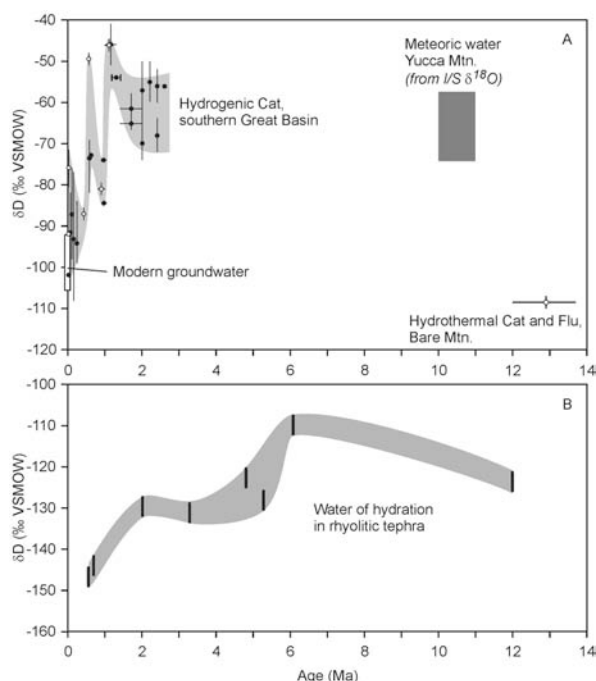The new data suggests that between ca. 11 Ma and 1.8 Ma meteoric precipitation in the

Fig. 2. Evolution of δD values in groundwater and precipitation in southern Great Basin, USA, between late Miocene and the present. A - Fluid inclusion data: black circles - Winograd et al. (1985), white circles - this study. Field for δD of the 10-11 Ma-old meteoric water at Yucca Mountain was calculated from δ^{18}O of illite/smectite using data from Feng and others (1999). B - δD of water of hydration in rhyolitic tephra (based on data of Mulch et al. 2008).

area had characteristically higher δD values as compared to modern values (Fig. 2A). The transition to the lower values of the late Holocene was not continuous, but associated with high-amplitude (30-40 ‰) oscillations.

Surprisingly, water from the late Miocene massive hydrothermal fluorite and scalenohedral calcite sampled in the Bare Mountain mines show remarkably constant values of -108±2 ‰ (n = 6), similar to modern precipitation.

The fluid inclusion isotope data show similarities with the δD values obtained from the water of hydration in tephra of different age studied

by Mulch et al. (2008). Hydration of glass occurs within the first ca. 1000 years following tephra deposition; these δD values, thus, reflect the integrated isotopic composition of local precipitation at the depositional site.

Discussion

Models relating the decline of δD values of precipitation in the southern Great Basin to the uplift of the Sierra Nevada appear no longer plausible. The Sierra formed a high topographic barrier already in the Late Cretaceous or early Cenozoic (Henry, 2009). The large-amplitude (30-40 ‰) fluctuations in the post-Pliocene part of our data may be explained by different pathways of moisture supply. In one scenario moisture from the Pacific Ocean crosses the Sierra Nevada (resulting in low δD values due to orographic rainout effects). An alternative scenario involves moisture transport from the Gulf of Mexico, skirting the Sierra Nevada from the south (little rainout, higher δD values). The specific climatic forcing responsible for the switch, though, remains to be identified.

Presently, there is no reliable fluid inclusion data for the period 2.5 to 12.5 Ma, but the search for hydrogenic deposits formed during this period of time is underway.

REFERENCES

Dublyansky Y., Spötl C. (2009) *Rapid Comm. Mass Spectrom.*, 23: 2605-2613.

Feng et al. (1999) *Earth Planet. Sci. Lett.*, 171: 95-106.

Henry C. (2009) *Geology,* 37: 575-576.

Mulch A., Sarna-Wojcicki A., Perkins M., Chamberlain C. (2008) *Proc. Natl. Acad. Sci.*, 105: 6819-6824.

Winograd I., Szabo B., Coplen T., Riggs A., Kolesar P. (1985) *Science,* 227: 519-522.

Fluid inclusions and evolution of ore fluids in the Baghkhoshk porphyry copper system, Urumieh- Dokhtar magmatic belt, Iran

Einali, Morteza*, Bakker, Ronald J.**, Alirezaei, Saeed* and Mohammadzadeh, Zahra***

*Faculty of Earth Sciences, Shahid Beheshti University, Tehran, Iran
**Department of Applied Geosciences and Geophysics, University of Leoben, Leoben, Austria
***Faculty of Basic Sciences, Tarbiat Modarres University, Tehran, Iran

The Baghkhoshk porphyry copper system is located south of the Cenozoic Urumieh-Dokhtar magmatic belt in Iran (~15 km SE of the giant Sarcheshmeh Cu-Mo-Au porphyry deposit). The hypogene mineralization in Baghkhoshk occurs within two Miocene intrusions (an older granular granodiorite and a younger porphyritic quartz-diorite) and their enclosing Eocene volcanic-sedimentary rocks. Both intrusions and their host rocks are extensively altered by hydrothermal fluids into potassic, phyllic, and propylitic assemblages. The deposit was first discovered in early 1970s, and the ore reserve was reported to be 24 million tons at 0.27 % Cu (Nedimovic, 1973). The deposit is currently under detailed exploration by deep diamond drillings. This paper presents data on the fluid inclusions and evolution of the ore fluids in the Baghkhoshk porphyry system.

Based on the mineralogy and crosscutting relationships, two main types of veinlets associated with potassic and phyllic alterations can be distinguished: 1) quartz + chalcopyrite + pyrite ± molybdenite (mineralized veinlets); and 2) quartz ± pyrite (barren veinlets).

Heating and freezing experiments were conducted on a Linkam MDS600 stage attached to an Olympus BX40 microscope in the Department of Applied Geosciences and Geophysics, University of Leoben, Austria. For freezing runs, the precision is about ±0.3 °C for melting CO_2 and ±0.2 °C for ice melting; for heating runs, the precision is about ±1 °C for critical point of H_2O. The stage was calibrated with synthetic fluid inclusions of CO_2 and H_2O. Composition of the fluid inclusions was analyzed by Raman microspectroscopy at Leoben using a LABRAM Jobin-Yvon system.

Fluid inclusions petrography

Three types of fluid inclusions were identified in various types of quartz veinlets: 1) Poly-phase inclusions; 2) Vapour-rich inclusions; 3) Liquid-rich inclusions. The poly-phase inclusions always contain vapour bubble, a saline aqueous liquid and halite (Fig. 1a). The poly-phase brine inclusions contain additional opaque daughter crystals including small red hematite flakes and triangular chalcopyrite, the former being more frequent.

The vapour-rich inclusions contain vapour + liquid ± solid phase. The solid phase is triangular chalcopyrite crystals as indicated by Raman microspectroscopy (Fig. 1b). Vapour bubbles are variable in size, but in all cases consist of > 60 % of inclusion volume.

The liquid-rich inclusions are the most abundant type in Baghkhoshk. They consist essentially of liquid and vapour with the latter forming < 30 % of inclusion volume. The boiling trails (vapour-rich+ liquid-rich inclusions) observed in the quartz veinlets associated with potassic and phyllic alteration (Fig. 1c). The barren quartz± pyrite veinlets contain only liquid-rich inclusions.

Microthermometry:

The liquid-rich inclusions, homogenizing by vapour disappearance, display a wide range of homogenization temperatures, varying from 128.5 to 383.8 °C, with most measurements are between 200-250 °C and 300-375 °C. Liquid-rich fluid inclusions have salinity values between 0.35 to 24.24 eq mass% NaCl, with most measurements in the range 4 to 10 eq mass% NaCl. The salinity and homogenization temperatures of barren veinlets are 2 to 4 eq mass% NaCl and 200-240 °C, respectively.

The poly-phase inclusions, homogenizing by vapour disappearance, display homogenization

temperatures from 191.8 to 382 °C, with a mode of 300 to 375 °C. The halite melting temperature in the poly-phase inclusions varies from 173.1 to 248.9 °C, and the salinity varies between 32.5 and 35 eq mass% NaCl.

The vapour-rich inclusions, homogenizing by liquid disappearance, range in T_h from 325.8 to 434 °C, with a mode at 400 – 425 °C. The salinities are low, 4 to 8 eq mass% NaCl.
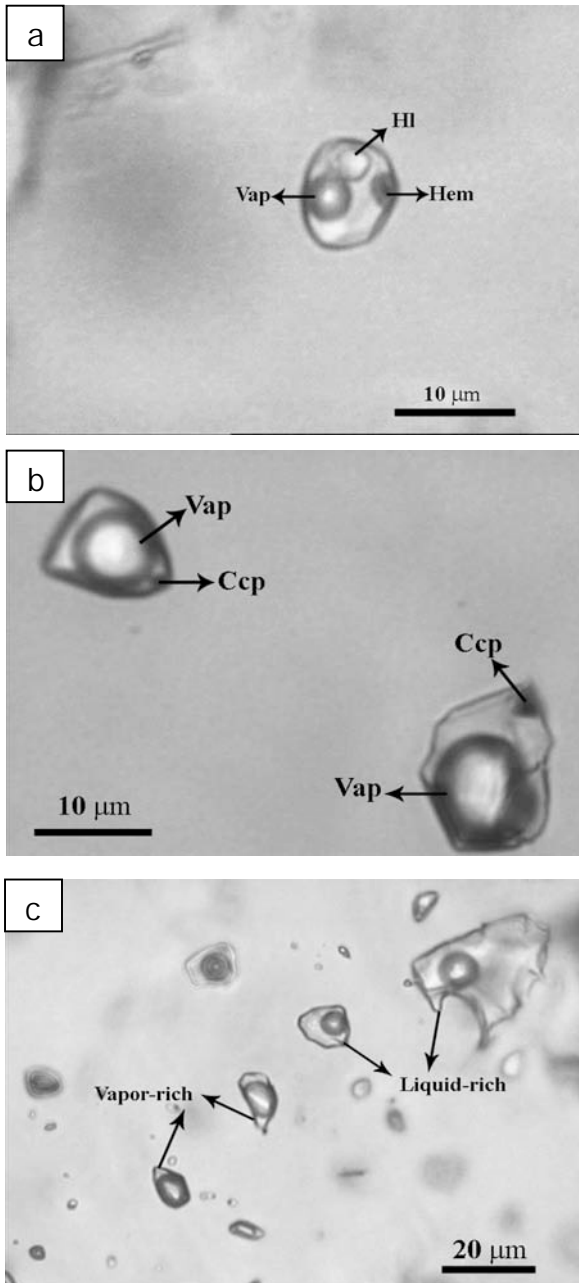

Fig. 1. Three main types of fluid inclusions at Baghkhoshk: a) Poly-phase inclusion; b) Vapour-rich inclusions; C) Boiling trail.
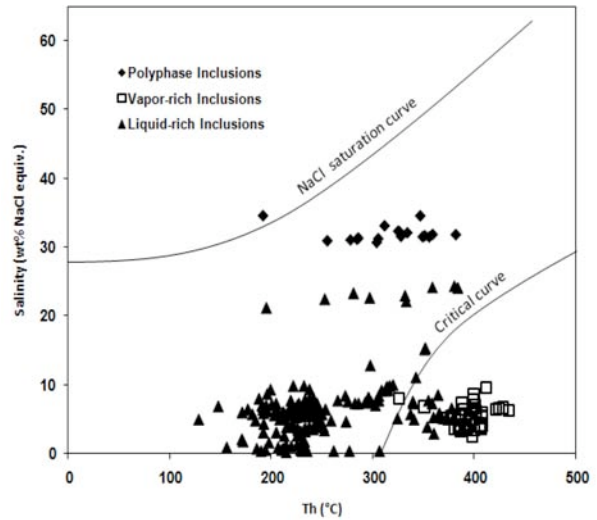
Fig. 2. Distribution of salinity and T_h values for various fluid inclusion types in Baghkhoshk. The NaCl saturation and critical curves from Ahmad and Rose (1980).

Results:

The ore deposits at Baghkhoshk developed from fluids with originally low-moderate salinities (6 to 8 mass% NaCl) at temperatures varying from 350 to 425 °C.

Our observations demonstrate that boiling occurred during potassic and phyllic alterations. Fluid inclusion evidence indicates that phase separation (boiling) was important and likely the main cause of heat loss and ore deposition (*c.f.* Hezarkhani and William-Jones, 1998).

The temperature and salinity of the fluids associated with phyllic alteration decreased from 375 °C to 200 °C and 32.5 - 35 to 4 - 10 eq mass% NaCl, respectively. This could be explained by mixing with a low temperature fluid (likely meteoric water).

REFERENCES

Ahmad S.N., Rose A.W. (1980) *Econ. Geol.* 75: 229-250.

Hezarkhani A., William-Jones A.E. (1998) *Econ. Geol.* 93: 651-670.

Nedimovic R. (1973) *Geol. Surv. Iran Rep* 53:247.

Laser Raman microspectroscopy with fluid inclusions from the Darrehzar porphyry copper deposit, Kerman, Iran

Einali, Morteza*, Bakker, Ronald J.**, Alirezaei, Saeed* and Azimzadeh, Amir Morteza**

*Faculty of Earth Sciences, Shahid Beheshti University, Tehran, Iran
**Department of Applied Geosciences and Geophysics, University of Leoben, Leoben, Austria

The Darrehzar porphyry copper deposit is located in the southern part of the Cenozoic Urumieh- Dokhtar magmatic belt in Iran (~8 km SE of the giant Sarcheshmeh Cu-Mo-Au porphyry deposit). Mineralization in Darrehzar is associated with two Miocene porphyritic bodies of diorite and granodiorite compositions, and their enclosing Eocene volcano-sedimentary rocks.

Both intrusions and their host rocks are extensively altered by hydrothermal fluids into potassic, phyllic, propylitic and argillic assemblages. The ore reserve in Darrehzar has been estimated to be about 67 Mt at an average copper grade of 0.37 % (NICICO, 2008). The hypogene ore occurs in quartz-sulphide stockworks, as well as disseminations. This paper presents laser Raman data of fluid inclusions in quartz from the quartz-sulphide veinlets associated with potassic and phyllic alteration zones in Darrehzar. All experiments were carried out at the Leoben University (Austria) using a LABRAM Jobin-Yvon system.

Fluid inclusions and laser Raman study:

Based on the phases present at room temperature, four major types of fluid inclusions have been identified in the quartz-sulphide veinlets in the potassic alteration zone. They include vapour-rich, liquid-rich, halite-bearing, and halite-sylvite-bearing inclusions. The same types of fluid inclusions, excluding the halite-sylvite-bearing inclusions, occur in the quartz -sulphide veinlets in the phyllic alteration zone.

Several solid phases including chalcopyrite, hematite, magnetite, molybdenite, pyrite, rutile and siderite were identified by laser Raman microspectroscopy in the salt-bearing inclusions. Chalcopyrite and hematite are the dominant solid phases in the inclusions, and appear to be true daughter minerals. Hematite mainly occurs as reddish flaky crystals (Fig. 1a), and chalcopyrite mostly occurs as triangular crystals (Fig. 1b). Magnetite and pyrite were observed in the salt-bearing inclusions as relatively large irregular bodies and appear to be captured phases (Fig. 1b). Flaky molybdenite crystals were recognized only in the halite-bearing inclusions in the potassic alteration.

Siderite ($FeCO_3$) is abundant in salt-bearing and vapour-rich inclusions. This mineral mostly occurs as greenish rounded translucent crystals (Fig. 1a-c).

Chalcopyrite and hematite are the only daughter minerals identified in the vapour-rich inclusions (Fig. 1a-c). Anhydrite was identified as transparent tabular crystals (Fig. 1d), only in the vapour-rich inclusions, associated with both phyllic and potassic alterations.

Most liquid-rich inclusions devoid solid phases; some high salinity liquid-rich inclusions were found to contain chalcopyrite, hematite and siderite. The occurrence of various gases, CO_2, SO_2, N_2 and CH_4, was investigated by laser Raman in various types of the fluid inclusions. The vapour-rich inclusions were identified to have CO_2 in their bubbles. Some salt-bearing inclusions contain minor CO_2, and the liquid-rich inclusions are devoid of the gas.

Conclusions:

The identification of chalcopyrite, magnetite, molybdenite, siderite, anhydrite (Fig. 2a-d) hematite and pyrite in the fluid inclusions of Darrehzar deposit shows that ore fluid was rich in copper, molybdenum, iron, sulphur, chlorine, and CO_2. This metal-Cl-S-CO_2 rich fluid is a suitable source to generate a mineralized porphyry system.
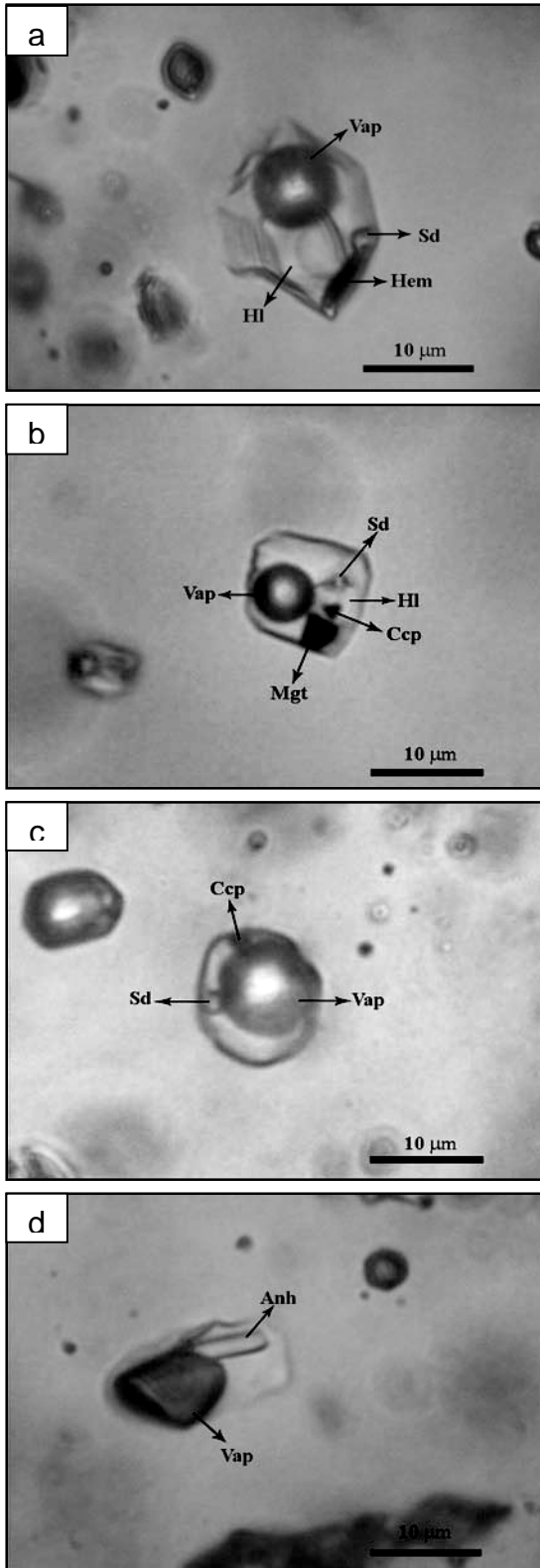
Fig. 1. Solid phases identified in the fluid inclusions from Darrehzar porphyry system (Abb. Hl: halite, Vap: vapour, Hem: hematite, Sd: siderite, Ccp: chalcopyrite, Mlb: molybdenite, Mgt: magnetite, Anh: anhydrite).
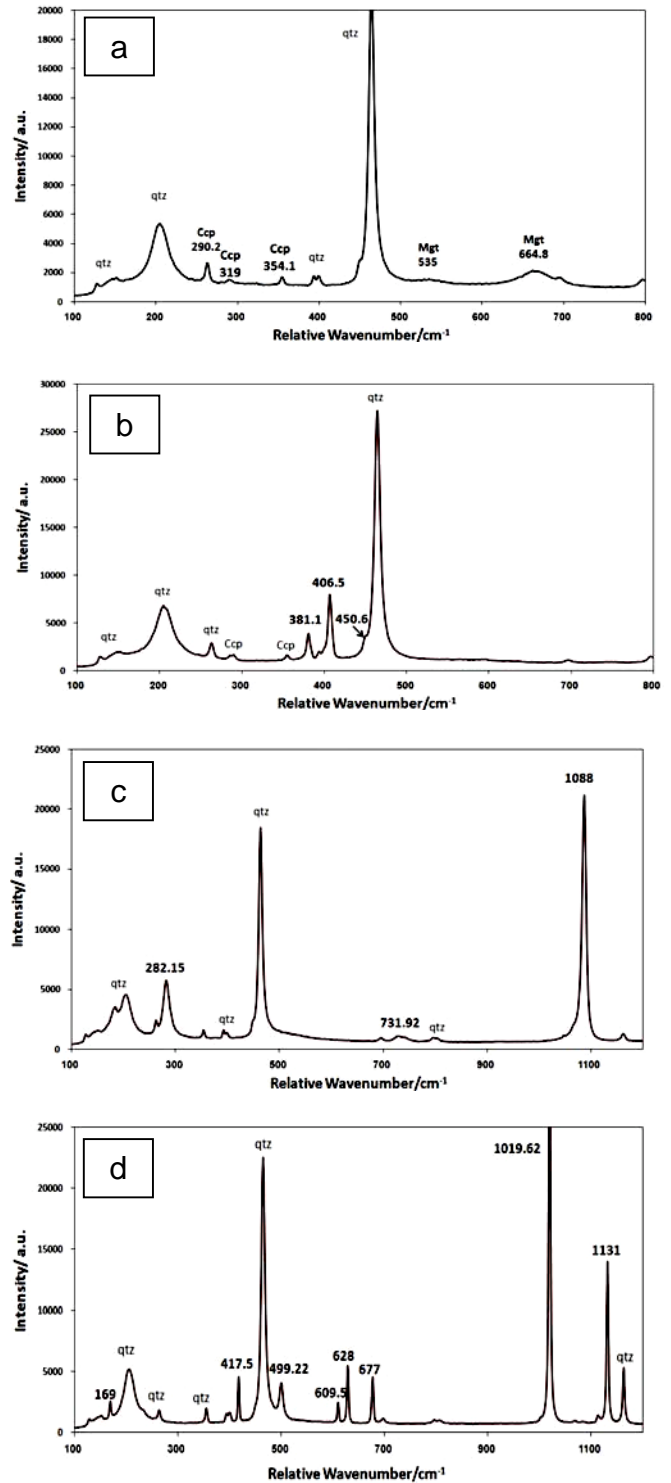

Fig. 2. Raman spectrum of a) chalcopyrite and magnetite, b) molybdenite, c)siderite, d) anhydrite in the fluid inclusions from Darrehzar porphyry copper deposit .

REFERENCE

NICICO (2008) *Darrehzar ore reserve estimates*. Internal report [In Farsi].

Application of the Linkam TS1400 X-Y heating stage to MI studies

Esposito, Rosario*, Bodnar Robert J.*, Klebesz Rita*,**, Bartoli Omar***, Klyukin Yury I.****, Moncada Daniel* and Doherty Angela*, *****

* Virginia Polytechnic Institute & State University, Department of Geosciences, Blacksburg, VA, USA
**Università di Napoli Federico II, Dipartimento di Scienze della Terra, Naples, Italy
***Unibersità degli Studi di Parma, Dipartimento di Scienze della Terra, Parma, Italy
****Institute of Geology and Geochemistry of UB, RAS, Yekaterinburg, Russia
*****Università degli Studi di Messina, Dipartimento Elementi e Ambiente, Messina, Italy

The volatile (H_2O, CO_2, SO_2, etc.) content in a magma chamber beneath a volcano determines the energy of the volcanic eruption. The only direct way to determine what the volatile content in the melt was before an eruption is by measuring the volatile abundances in melt inclusions (MI). For this reason, in the last decades the number of publications describing the use of melt inclusions (MI) to determine the pre-eruptive volatile contents of magmas has increased significantly. Unfortunately, MI are often partially or totally recrystallized as found, depending on the MI P-T path following trapping. In order to rehomogenize the melt and to obtain the original volatile content of MI, many researchers use a heating stage equipped with a quenching system and mounted on an optical microscope (e.g. the Vernadsky stage). In this study we tested the recently developed Linkam TS1400 XY heating stage to homogenize crystallized MI.

In this study, several experiments have been performed on recrystallized melt inclusions (MI) contained in phenocrysts from eruptions in the Phlegrean Volcanic District (PVD), and from the Sarno eruption at Monte Somma-Vesuvius in Southern Italy. Recrystallized MI from the PVD are hosted in olivine, clinopyroxene and sanidine. These phenocrysts were contained in trachybasalt to trachyte magmas which can be high in volatile contents. Recrystallized MI from the Sarno eruption are hosted in clinopyroxenes which have formed from a basaltic magma. The Sarno eruption is considered to be one of the most explosive eruptions in all the Somma-Vesuvius history.

During the heating experiment, a constant flow of argon gas was introduced into the sample chamber at a flow rate of 0.5 liter/min (± 5 %). The heating rates used for these experiments were as follows: 100 °C/min from 25 to 900 °C; 50 °C/min from 900 to 1000 °C; 25 °C/min from 1000 to 1100 °C; 10°C/min from 1100 to 1200 °C; 5 °C/min from 1200 to 1340 °C. These heating rates were used to produce equilibrium melting and minimize diffusion of components out of most MI.

In all experiments, it was possible to homogenize the MI and, importantly, to quench the melt to a glass after homogenization. In some experiments, the sample was heated to around 1340 °C. At that temperature, the field of view became darkish-red in colour and it was difficult to observe the MI behaviour. At lower temperatures the optics were excellent. The quality of the optics at high temperature depends on two factors: the thickness of the phenocryst and the volume percentage of inclusions (solid and or melt) relative to the volume of the phenocryst.

In most of the experiments, the MIs were homogenized completely (crystals + bubbles) and remained homogeneous during quenching to room temperature to produce a glass. In some cases, the MI were heated to relatively high temperature and the solids all melted but the bubble did not dissolve back into the melt before the optics deteriorated and it was no longer possible to observe the MI behaviour. When the MI was quenched, the single bubble remained in the MI and grew larger during cooling. The bubble in these MI may represent a trapped vapour bubble (i.e. the MI trapped a volatile-saturated melt plus a vapour bubble) and thus the bubble should not be expected to dissolve back into melt.
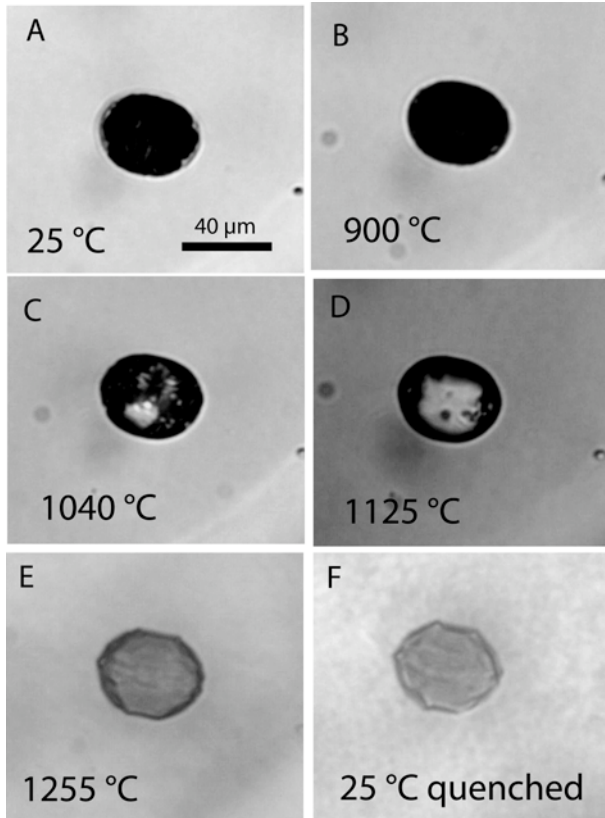
Fig.1. Heating experiment performed on an olivine phenocryst from a scoriae sample from the Solchiaro eruption of the Phlegrean volcanic district (PVD). The MI is around 40 µm in diameter and has an ellipsoidal shape. A) At room temperature (25 °C), the MI is partially recrystallized. Some daughter crystals are visible at the olivine-MI interface. B) At 900 °C daughter crystals at the olivine/inclusion interface are smaller relative to those at room temperature. C) At 1040 °C it is possible to distinguish between vapour bubbles, solid and melt phases. D) At 1125 °C, the melt inclusion contains mostly a silicate melt phase. A vapour bubble is clearly observed at this temperature. E) At 1255 °C, the MI contains 100% silicate melt. Note that at this temperature the MI assumes a negative crystal shape. Also, the "wrinkles" at the MI-host interface reflect dissolution of olivine into the melt. F) After homogenization at 1262 °C, the MI was quenched to a homogenous glass. During the quenching some crystallization of olivine at the olivine/glass interface may have occurred.

Coupled pore fluid pressure oscillation and natural fracture opening in tight-gas sandstone reservoirs: Piceance Basin, Colorado, USA

Fall, András*, Eichhubl, Peter*, Laubach, Stephen E.* and Bodnar, Robert J.**

*Bureau of Economic Geology, Jackson School of Geosciences, The University of Texas at Austin, Austin TX 78713, USA

**Department of Geosciences, Virginia Tech, Blacksburg, VA 24061, USA

Continuous gas charge of low-permeability tight-gas sandstones in the Piceance Basin, Colorado, creates a dynamic system where pore pressure increases locally and temporarily to near lithostatic pressures, and fractures the rocks. The natural opening-mode fractures are partially cemented with crack-seal quartz cement bridges that precipitate synkinematically with fracture opening. Coexisting aqueous and hydrocarbon gas fluid inclusions trapped in crack-seal cement increments record pressure, temperature, and fluid composition (P-T-X) conditions during subsequent fracture opening and cementation. Methane concentrations of the aqueous fluid inclusions can be used as proxy to determine the pore pressure variations during fracture opening. Combining homogenization temperatures with burial history models allows determining the timing of fracture opening and cementation in these systems.

The Upper Cretaceous Mesaverde Group in the Piceance Basin is considered a basin-centred continuous gas accumulation where gas charge of the low-permeability sandstone occurs during peak gas generation at maximum burial conditions. This model contrasts with other low-permeability gas reservoirs where gas accumulates in conventional traps prior to maximum burial and significant permeability reduction. We tested aspects of the basin-centred gas model as it applies to the Piceance Basin by determining the timing of fracture growth and associated temperature, pressure, and fluid composition conditions using microthermometry and Raman microspectrometry of fluid inclusions. Trapping temperatures of methane-saturated aqueous fluid inclusions record systematic temperature trends that increase from ~140 °C to 185 °C and then decrease to 158 °C over time, indicative of fracture growth during maximum burial conditions. The CH_4 Raman symmetric stretching (v_1) peak position of the vapour bubble was used to determine the pressure of the aqueous inclusions at room temperature (Lin et al., 2007). Based on microthermometry, fluid pressure at room temperature, and equation of state modelling, the pressures at trapping were calculated for the observed inclusions (Becker et al., 2010). Pore fluid pressures for methane-rich inclusions of 55-110 MPa indicate fracture growth under near-lithostatic pressure conditions consistent with fracture growth during active gas maturation and charge. Lack of systematic pore pressure trends over time (Fig. 1) suggests dynamic pressure conditions and is consistent with episodic gas charge from deeper source rocks along connected fracture and fault systems (Cumella and Scheevel, 2008). The natural fracture network creates pathways that allow upward gas migration in high-pressure cells to form a continuous gas-saturation interval in the absence of a top seal in the deep-central parts of the Piceance Basin.

Comparison of trapping temperatures with burial and thermal maturity models suggests that gas generation, active gas charge in high-pressure cells, and natural fracture growth lasted for 33 Ma., and ended at ~8 Ma in the Piceance Basin.
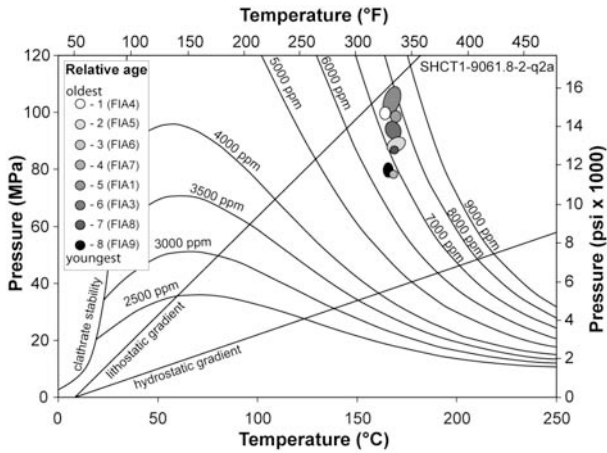
Fig. 1. P-T diagram illustrating trapping pressure oscillation of aqueous fluid inclusions in a single quartz bridge cement of a natural opening-mode fracture in the southern Piceance Basin, Colorado. Methane concentrations of the FIAs range from ~6500 ppm to 8000 ppm corresponding to trapping pressures from ~75 MPa to 110 MPa. Also shown are isopleths of methane concentrations in the H_2O-NaCl-CH_4 system for the 2 mass % NaCl-CH_4 pseudobinary (Duan and Mao, 2006), and thermobaric gradients representing a geothermal gradient of 43 °C/km over the hydrostatic and lithostatic gradients of 9.9 MPa/km, and 24.8 MPa/km, respectively.

REFERENCES

Becker, S. P., Eichhubl, P., Laubach, S. E., Reed, R. M., Lander, R. H., Bodnar, R. J. (2010) *GSA Bulletin* 122: 1081-1093.

Cumella, S. P., J. Scheevel (2008) *in* S. P. Cumella, K. W. Shanley, W. K. Camp, eds., *AAPG Hedberg Series* 3: 137 – 155.

Duan, Z., Mao, S. (2006) *Geochim. Cosmochim. Acta* 70: 3369-3386.

Lin, F., Bodnar, R. J., Becker, S. P. (2007) *Geochim. Cosmochim. Acta* 71: 3746 - 3756.

Genesis of the Weishan REE deposit in the Shandong Province, eastern China: evidences from Rb-Sr isochron age, LA-MC-ICPMS Nd isotopic composition and fluid inclusions

Fan, Hong-Rui*, Lan,Ting-Guang*, Hu, Fang-Fang* and Yang, Kui-Feng*

*Key Laboratory of Mineral Resources, Institute of Geology and Geophysics, Chinese Academy of Sciences, Beijing 100029, PR China

Weishan REE deposit, a pegmatite-type REE deposit related to alkaline rocks, is located at Luxi Block, south-eastern North China Craton. According to muscovite Rb-Sr isochron, it formed at the age of 119.5 Ma, which belonged to the early Cretaceous large-scale mineralization in the North China Craton. LA-ICPMS Nd isotopic compositions of bastnaesite and monazite indicate that the source of the REE minerals is the enriched lithospheric mantle. Observation of fluid inclusions in quartz, fluorite and barite shows that four types of inclusions can be identified, including (1) H_2O inclusions, (2) pure CO_2 inclusions, (3) H_2O+CO_2 inclusions and (4) H_2O+CO_2+daughter mineral inclusions. The H_2O inclusions are secondary inclusions while others are primary inclusions. The daughter minerals in H_2O+CO_2+daughter mineral inclusions include thenardite, barite, celestine, calcite, aphthitalite and glauberite. The homogenization temperature and capture pressure of H_2O+CO_2 and H_2O+CO_2+daughter mineral inclusions range from 205 ℃ to 433 ℃ and 120 MPa to 200 MPa, respectively. Coupled with the existence of abundant daughter minerals and sulphur stable isotopic compositions, it can be deduced that the initial ore-forming fluids were high-temperature, moderate-pressure and high-concentration orthomagmatic fluids, which were characterized by enrichment of HCO_3^-/CO_3^{2-}, SO_4^{2-} and F^- and multicomponent (e.g., Na^+, K^+, Ca^{2+}, Ba^{2+}, Sr^{2+} and REE^{3+}). The coexistence of C, HC and HCD inclusions and the wide range of liquid/vapour ratios between these inclusions suggest that fluid unmixing may have occurred during ore-forming process. REE were most probably transported as $REEF^{2+}$ and precipitated through fluid boiling. Fluids mixing, which contributed little to the REE precipitation, also happened in the late stage of the ore-forming process.

In situ laser ablation ICP-MS analyses of fluid inclusions, Serra Norte jaspilite-hosted high grade iron ore, Carajás Mineral Province, Brazil

Figueiredo e Silva, Rosaline C.*, Hagemann, Steffen**, Banks, David*** and Lobato, L.M.*

*Department of Geology, Federal University of Minas Gerais, Av. Antônio Carlos 6627, Pampulha 31270 901, Belo Horizonte, Minas Gerais, Brazil
**Centre for Exploration Targeting, School of Earth and Environmental Sciences, University of Western Australia 6009, Crawley, Australia
***School of Earth and Environment, University of Leeds, Woodhouse Lane, Leeds LS2 9JT, UK

In situ laser ablation ICP-MS analyses conducted on fluid inclusions trapped in quartz and carbonate veins and breccias from Serra Norte Carajás iron ore deposits revealed a saline Ca-rich fluid evolving to low saline Na-rich fluid from early to advanced hydrothermal alteration stages. In order to better constrain and understand the hydrothermal processes that lead to the upgrade of protore jaspilite to form hard, high-grade iron ores in the Serra Norte deposits, we have investigated the composition of hydrothermal fluids from five major veins-breccias types of quartz ± carbonate ± oxide ± sulphide located in the distinct hydrothermal alteration zones: V1 from distal; V2 and V3 from intermediate; and V4 and V5 from proximal hydrothermal alteration zones.

The elements Na, Ca, K, Mg, Fe, Mn, Li, Sr, Ba, Cu, Zn and Pb were identified and quantified in all vein-breccia types. With respect to the contents of the cations Na, Ca, K and Mg, V1 veins display slightly higher content when compared to V2b and V3 veins (Figs. 1A to C), and fluid inclusions from the latter two are compositionally similar. In V5 veins the trace element contents is significantly lower when compared to all other vein types (Fig. 1D). The majority of the analyzed fluid inclusions in all vein types are Na-rich, followed by Ca and K. Exception are fluid inclusions in V3 veins, where Na is followed by K (Fig. 1C). Magnesium contents are higher in V2b veins than in all other veins. Lithium and Sr contents are similar in all vein types (Fig. 1), except in V1 veins that display slightly higher Li contents than the other veins, with Sr concentration higher than Li. The V2b and V5 veins display the lowest Sr contents, and Li is

only detected in two inclusions of V5 veins. Figure 1 shows that Fe is present in most fluid inclusions from all vein types, with proximal V5 displaying the lowest concentrations when compared to early (distal) and intermediate stages V1, V2 and V3 quartz veins. Fluid inclusions in V1a and V2 veins have higher Fe and Mn contents when compared to other vein types, but only slightly higher concentrations than V3 veins. Among the base metals, Cu is the main element in V1 veins, followed by V3 veins. The next most important is Zn, in both distal V1 and intermediate V2 and V3 veins. Copper, Zn and Pb decrease slightly from V2b to V5 veins (Fig. 1), and somewhat higher in overall values in V1a and V2a veins (Fig. 1). There is a significant decrease in Cu concentrations from V1a to V2a veins, and the lowest contents are observed in V2b and V5 veins. Copper is detected only in some inclusions of V1 veins.

Fluid inclusions trapped in calcite from V1b vein breccias and kutnahorite from V4 ore breccias have also been analyzed, although Ca, Mn and Fe were not considered since these elements are part of carbonate composition. In carbonate samples the sequence is Na > K > Zn > Li > Cu > As > Pb > Ag > Cs. The most outstanding depiction from Figure 1 is the significant decrease in all elements from the distal V1 to the proximal V5 veins. A decrease in Fe in the fluid is accompanied by the advanced hematite precipitation in the proximal alteration zone, which is compatible with iron having been extracted from the fluid to form hematite (Fig. 1D). The overall decrease in all elements analyzed in V5 veins, in conjunction with the decrease in the total fluid salinity, suggests the significant influx of

meteoric water causing dilution of the original fluid in the high-grade ore zone. Calcite is widely distributed in V1 veins, mainly in the N4E deposit, but is not in present in V2 veins. This supports the assertion that the high contents of this element, as shown in Figure 1, must reflect the high Ca concentration in the fluids, suggesting an original Ca-rich fluid, in accordance with the low eutectic temperature of –50 °C. Of note is the presence of Li in the studied fluid inclusions, mainly from the early hydrothermal stage V1 type, which likely suggests a magmatic component in the hydrothermal fluids. According to Seitz and Woodland (2000), Li may be used as an indicator of magmatic processes such as partial melting, crystal fractionation and accumulation.

The presence of the base metals Cu-Pb-Zn in fluid inclusions, mainly Cu in V1, V2 and V3 veins from the distal and intermediate alteration zones, is compatible with a magmatic fluid. The lower concentration of these metals in the proximal V5 veins helps corroborate the LA-ICPMS analyses obtained on paragenetically different hematite types from high-grade iron ore, which also show low Zn, and some Pb and Cu (Figueiredo e Silva et al., 2009). The gradual dilution of the base metal signature in fluid inclusions from early to late stage veins and breccias also serves to support the influx of surface water into the high-grade ore zone.

Relative to the distal and proximal alteration zones, the laser ablation ICP-MS data of the intermediate-stage V2-V3 veins (Figs. 1B-C) display oscillating distribution patterns of most elements with concentrations that cover a much wider range than those elements observed for fluid inclusions from the distal alteration zone (Fig. 1A). Furthermore, various other characteristics of the intermediate alteration zone, including mineral assemblages, microthermometric fluid inclusion data including low to high salinity values, and variation of eutectic temperatures, together strongly suggest mixing of magmatic fluid and meteoric water. This results in the dilution of fluid composition, including the magmatic trace element Li. Some of the more abundant elements (mainly Na, K, Ca, Fe, and Mg) maintain their initial concentration in the fluid, as they likely were transported through the vein and breccias system

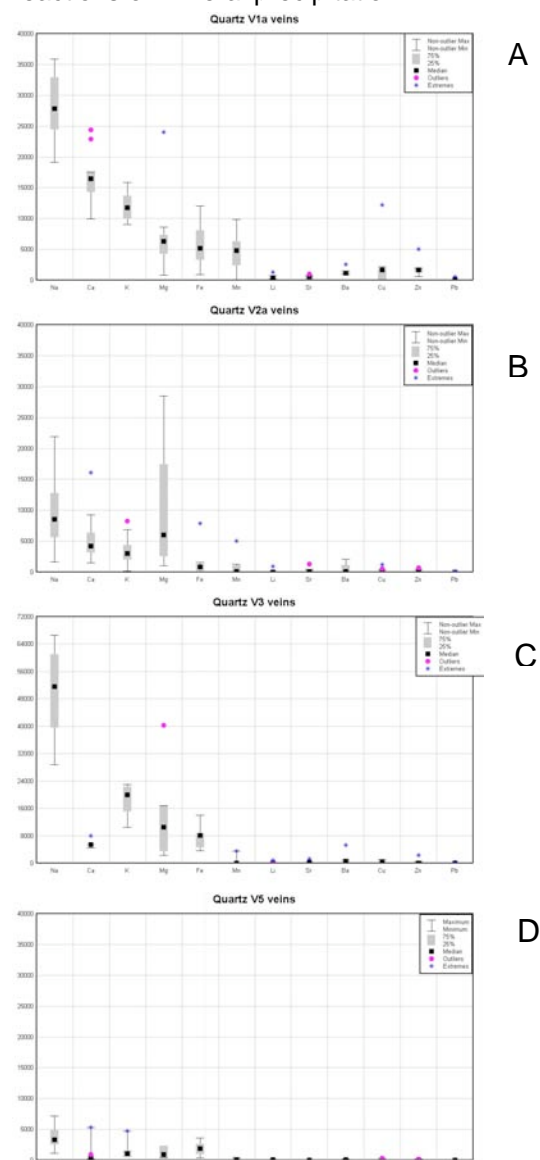without significant mass transfer via fluid-rock reactions or mineral precipitation.

Fig. 1. *Metal concentrations obtained from LA-ICPMS analyses of fluid inclusion assemblages and individual fluid inclusions: A. quartz from V1a vein-breccias; B. quartz from V2a veins; C. quartz from V3 veins; D. quartz from V5 veins located in high grade hard iron ore. Error bars show 1σ variability within an assemblage of similar inclusions.*

REFERENCES

Figueiredo e Silva, R.C., Hagemann S.G., Lobato, L.M., Danyushevsky, L. (2009) *Proceedings, SGA, Townsville, Australia,*2: 570-572.

Seitz, H.M., Woodland, A.B. (2000) Chemical Geology, 166: 47.

Raman-spectroscopic investigations of fluid and melt inclusions from the South Kawishiwi Intrusion, Duluth Complex, Minnesota, U.S.A. – the role of gas rich late-magmatic hydrothermal fluids in the formation of Cu-Ni-PGE mineralization

Gál, Benedek*, Molnár, Ferenc*, Mogessie, Aberra** and Peterson, Dean M.***

*Department of Mineralogy, Eötvös Loránd University, Pázmány P. s. 1/C, Budapest, Hungary, 1117
**Institute of Mineralogy and Petrology, Karl-Franzens University of Graz, Universitätplatz 2, Graz, Austria, 8010
***Duluth Metals Ltd., 130 West Superior Street, Duluth, Minnesota, USA, 55802

The Duluth Complex is a set of intrusive series of rocks which are the products of the 1.1 Ga old Midcontinent Rift system of North America. One of the troctolitic intrusions that host the vast majority of unexploited Cu-Ni-PGE mineralization is the South Kawishiwi Intrusion. Mantle-derived troctolitic melts intruded from a deep-seated chamber system into their current position through a magmatic plumbing system. During their ascent, they had reacted with metasedimentary rocks and this process triggered sulphide saturation producing an immiscible sulphide melt phase (Miller et al., 2001).

During formation of the South Kawishiwi Intrusion, the intruding sulphide-laden melts subsequently reacted with granitoid footwall rocks as well, resulting in contamination with a felsic partial melt component (Molnár et al., 2010). Combined analysis of primary fluid and melt inclusions provides a strong tool to understand and evaluate different components of this late magmatic – early hydrothermal stage of the ore-bearing system.

In the present study, we have investigated mostly pegmatitic, quartz-rich, sulphide-bearing samples close to the basal contact of the intrusion. Macroscopic textures of the rock samples and micropetrographic features of coeval fluid and melt inclusions in quartz show that the crystallizing melts have exsolved a magmatic fluid phase. That fluid coexisted with the late stage silicate and sulphide melt phases. Negative crystal-shaped primary fluid inclusions usually form groups in the centre of quartz grains and are dominated by relatively low density, near critical CO_2 (Fig. 1.). Raman-spectrometry confirmed minor amounts of methane and N_2 inferred from the slight decrease of the triple point of the

inclusions (~-57.2 °C) compared to pure CO_2. After heating and total homogenization of inclusions well above 300 °C, small amount of H_2O was also detectable by Raman-microspectrometry.
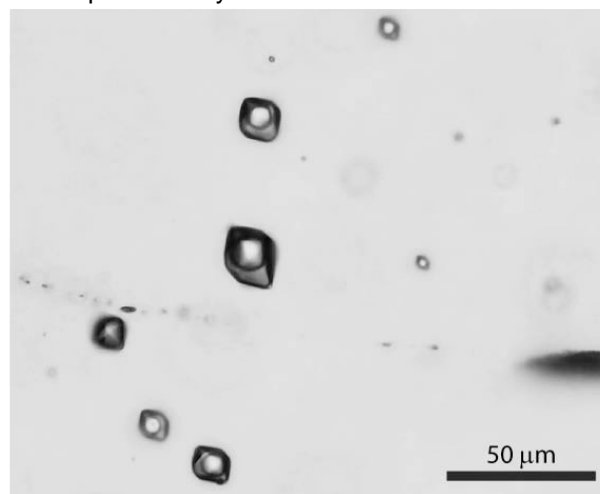

Fig. 1. Primary CO_2-rich, CH_4, H_2O and N_2-bearing fluid inclusions in quartz from a felsic rock sample close to the basal contact of the intrusion.
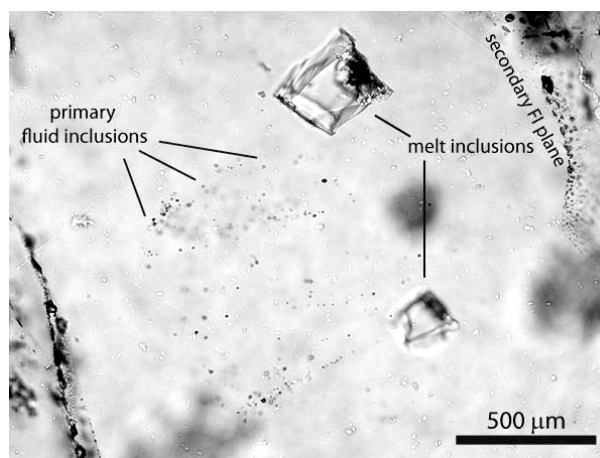

Fig. 2. Primary, coeval melt- and fluid inclusions rich in CO_2 in quartz from the same sample as Fig.1.

Coeval melt inclusions in quartz appear to represent a fractionated silicate melt (Fig. 2). Daughter minerals in melt inclusions (identified by SEM and Raman investigations) are potassic feldspar, plagioclase, biotite, muscovite, apatite, calcite, and Zr- and REE-bearing phases.

Petrography of secondary fluid inclusion assemblages suggest that the primary fluids have evolved and separated to different components. One generation of later stage fluids played a role in local mobilization of metals because gas-rich, secondary fluid inclusions occur together with chalcopyrite in microcracks of pegmatitic quartz (Fig. 3). In these inclusions, gas phases identified by Raman-microspectroscopy were dominantly CH_4 with subordinate amounts of N_2 and H_2O (latter was only detectable after heating the inclusions). CO_2 is absent from this generation of secondary inclusions.
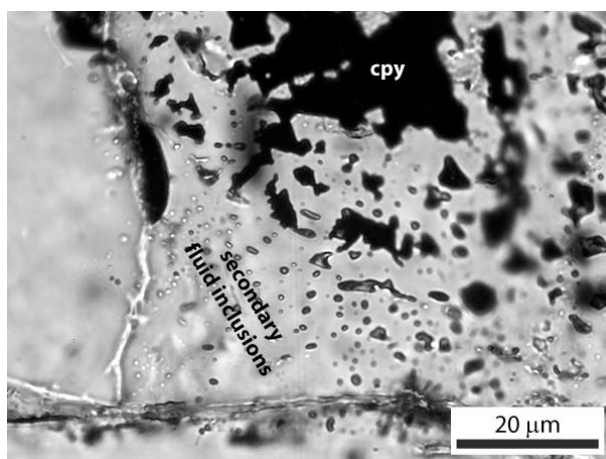
Fig. 3. Secondary vapour-rich fluid inclusions aligned along a healed microcrack partly filled by chalcopyrite in quartz

Felsic patches in the troctolitic rocks often exhibit miarolitic cavities which are filled by euhedral biotite, calcite, prehnite, chlorite and chalcopyrite. In the surroundings of these cavities occurrences of CO_2-rich, methane-bearing fluid inclusions were detected in potassic feldspar. They likely represent a different stage in fluid evolution.

	Inclusions type	Environment
I.	Primary, $CO_2+CH_4+N_2+H_2O$	with melt inclusions, in qtz
II.	Secondary, $CH_4+N_2+H_2O$	along cpy-filled microcracks in qtz
III.	Primary/secondary, $CO2+CH_4$	associated with cpy-bearing miarolitic cavities in kspar

Table 1. Fluid inclusion generations that represent metal-mobilizing fluids from pegmatitic, quartz-rich samples.

Features listed above imply that gas-rich fluids, probably evolved from the segregated magmatic fluid component, had a potential in mobilizing metals, copper in particular (Table 1).

Presence of extremely Cl-rich apatite crystals ($X^{Cl}>0.8$) that crystallized in thin chalcopyrite and PGE-mineral bearing veinlets suggests that there was a potential of the development of a highly saline aqueous fluid as well which in turn was capable of PGE-transport in the form of chloro-complexes. Late-stage remobilization of PGEs is clearly implied by textures of platinum group minerals. The timing and the spatial variation of these processes are still under investigation.

REFERENCES

Miller, J.D. Jr., Green, J.C., Severson, M.J., Chandler, V.W., Hauck, S.A., Peterson, D.M., and Wahl, T.E. (2002) *Minn. Geol. Survey Report of Inv.* 58: 106-139.

Molnár, F., Peterson, D, Arehart, G.B., Poulson, S.,Hauck, S.A. (2010) *Acta Min.-Petr., Abstract Series, vol. 6., Abstracts of IMA 2010 Budapest,* p. 228.

Hydrothermal quartz and calcite in gypsum pseudomorphs: Tera Group, Tithonian-Berriasian, Cameros Basin.

González-Acebrón, L.*, Goldstein, R.H.** Mas, J.R.* and Arribas, J.***

*Dpto. Estratigrafía. Facultad de Ciencias Geológicas. Universidad Complutense de Madrid – IGEO (CSIC), Madrid, Spain.
**Department of Geology, University of Kansas, Lawrence, Kansas, USA.
***Dpto. Petrología y Geoquímica. Facultad de Ciencias Geológicas. Universidad Complutense de Madrid – IGEO (CSIC), Madrid, Spain.

This study is focused on Tithonian-Berriasian fluvial and lacustrine-palustrine deposits in a rift basin located in Northern Spain. Analysis of the lacustrine deposits reveals an evolution from (1) shallow carbonate ramps in lakes, to (2) shallow alkaline ephemeral lakes, and then (3) carbonate lakes rich in organic matter. This evolution in facies indicates that these lakes evolved from open to more closed hydrologic conditions. The cause may be a tectonic one, with progressive rift development and faulting leading to progressive isolation. Limestones and dolostones formed in the alkaline lakes contain abundant lenticularly shaped gypsum pseudomorphs. Lenticular gypsum is considered to form early and displacively in association with evaporative conditions in the lake system. They are replaced by quartz and non-ferroan calcite (Ca-2, Fig. 1-3). The corrosion of the quartz by Ca-2 indicates that Ca-2 postdates quartz. Quartz contains solid inclusions of a former phase of non-ferroan calcite (Ca-1) anhydrite and less commonly celestine (Figs 2-3). Where Ca-2 is a replacement phase, it also contains solid inclusions of anhydrite and in a few examples celestine (Fig. 1-3). Solid inclusions are typically oriented, 40-80 µm-size, rectangular in shape, and preserving some crystal faces. Small pyrite crystals (10-100 µm) are commonly observed in the limestone host rock and in the inner boundaries of the pseudomorphs, probably indicating they predate both quartz and Ca-2. The solid inclusions in quartz and Ca-2 are probably relicts of earlier diagenetic processes. This suggests that gypsum was converted to anhydrite during burial.
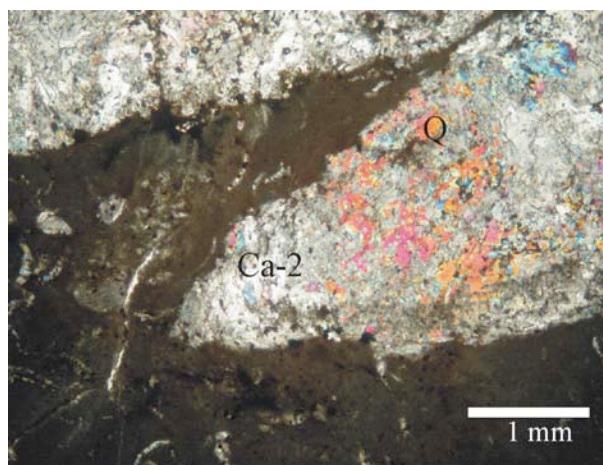

Fig. 1. Gypsum pseudomorph replaced by quartz (Q) which has subsequently been replaced by non ferroan calcite (Ca-2). (crossed polarized light)
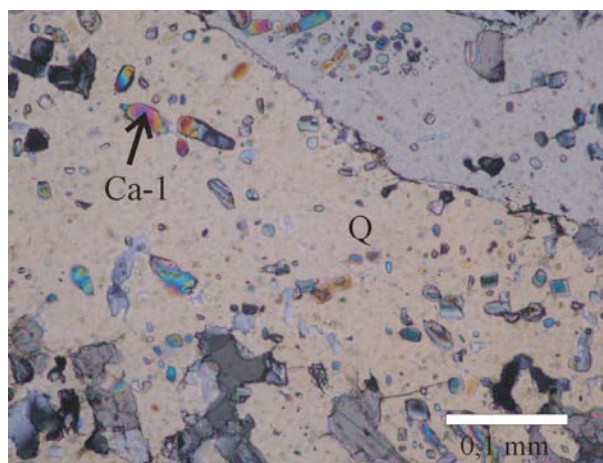

Fig. 2. Gypsum pseudomorph replaced by quartz with abundant solid inclusions of calcite (Ca-1), anhydrite and celestine. (crossed polarized light)

The quartz contains biphasic fluid inclusion assemblages (FIAs) of secondary origin with inclusion sizes ranging between 2-14 µm. No petrographically paired vapour-rich and vapour-

poor inclusions were observed, indicating that there is no evidence for necking down after a phase change. In addition, no vapour-dominant inclusions were found, evidence against heterogeneous entrapment (e.g. Goldstein and Reynolds 1994). In FIA's, inclusions have highly variable liquid to vapour volume ratios. Homogenization temperatures (T_h) measured in these FIA's are inconsistent and range from 147 to 351 ºC, with higher T_h in the deeper samples. Final melting of ice measurements, T_m(ice), are between -4.9 and -1.6 ºC. Final melting temperatures of clathrate are typically between 5 and 10ºC
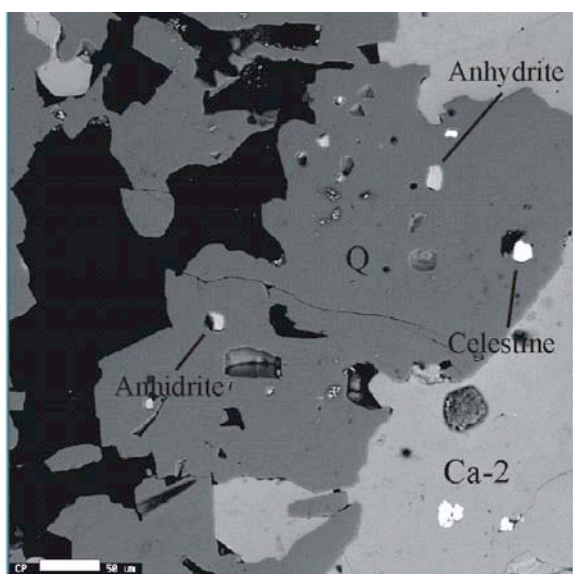
Fig. 3. Gypsum pseudomorph replaced by quartz (Q) with solid inclusions of anhydrite and celestine. Notice the corrosion of quartz by Ca-2 (BSE image).

Ca2 contains FIA's with all-liquid fluid inclusions of secondary origin. They have very irregular shapes and variable sizes (1-16 µm), and are probably related to uplift and unroofing. In addition, secondary biphasic FIA's have fluid inclusions with small size (typically 2-6 µm) and highly variable liquid to vapour volume ratios. Again, no petrographic pairing or vapour-dominant inclusions were found. T_h measured in these FIA's range from 108-352 ºC with T_m(ice) of -0.1 ºC.

As demonstrated by the high T_h values and the inconsistency of FIA's measured in secondary fluid inclusions in quartz (147-351 ºC) and calcite (108-352 ºC), both minerals experienced high temperatures after their formation and after entrapment of originally lower temperature FIAs. The temperatures are in the same range as other re-equilibrated fluid inclusions measured in thick quartz veins in the same area, related to a Cretaceous hydrothermal process that affected this part of basin (Barrenechea et al., 2001; González-Acebrón et al., 2010). The observations indicate early gypsum precipitation associated with an evaporitic depositional environment. This was followed by anhydrite replacement, likely during burial heating. Later, the anhydrite was partially replaced by Ca-1 in associated with a burial thermal regime and intermediate temperatures. It is possible that intermediate temperature thermochemical sulphate reduction led to pyrite precipitation as well. After all of these intermediate-temperature processes, both anhydrite and Ca-1 were partially replaced by quartz and this by Ca-2 during higher temperature hydrothermal processes in association with a CO_2-H_2O fluid. Progressive heating and different heat fluid flow pulses produce the re-equilibration of the FIAs. This was followed by uplift and cooling.

Despite the secondary nature of the fluid inclusions, and their thermal re-equilibration, these data contribute significantly to understand the geologic history of this system.

REFERENCES

Barrenechea, J., Rodas, M., Frey, M., Alonso Azcárate, J., Mas, J.R. (2001) *Clay Minerals*. 36(3):325-333.

Goldstein RH, Reynolds TJ (1994) *SEMP Short Course* 31. 192 p.

González-Acebrón, L., Goldstein, R.H., Arribas, J., Mas, R. (2010) *Int J Earth Sci* (available online).

A new heating/cooling stage designed for fluid inclusions measurements in large stalagmite sections

Greminger, Andrea[*], Krüger, Yves[*,****], Marti, Dominik[*], Hidalgo, Rita[*,****], Luder, Andres[*], Hiltbrunner, Beat[**], Fleitmann, Dominik[***,****] and Frenz, Martin[*]

*Institute of Applied Physics, University of Bern, Sidlerstrasse 5, CH-3012 Bern
**Institute of Astronomy, University of Bern, Sidlerstrasse 5, CH-3012 Bern
***Institute of Geological Sciences, University of Bern, Baltzerstrasse 1 & 3, CH-3012 Bern
****Oeschger Centre for Climate Change Research, University of Bern, Zähringerstrasse 25, CH-3012 Bern

In order to measure homogenisation temperatures of fluid inclusions in stalagmites the samples have to be broken to small pieces to fit on the Linkam THMSG 600 microscope heating/freezing stage that is currently used for microthermometric measurements. However, this makes a reconstruction of the chronological succession of the fluid inclusions difficult and requires extensive documentation. Therefore we have constructed a new microscope heating/cooling stage (Fig. 1) that is suitable for measurements of large sections fixed on a 300 µm thick carrier glasses with 28x48 mm standard dimensions. The stage is designed for a temperature range between 0 and 35 °C.

translation of the sample. Additionally the preparation of the stalagmite samples is simplified because the sections remain on the 300 µm thick glass substrate that is used for sawing.

Fig. 2 shows a cross section through the stage with the upper and the lower copper block. Twin core heating elements (1) are used to heat against permanent cooling of -10 °C (2) realised by a cooling cryothermostat (Lauda RP 885). The stage can be used with a high NA objective (3) and condenser (4) whereby v-seals (6) tighten the measurement chamber. The sample (5) can be moved in x-y directions by micrometer screws. The temperature is measured by PT-100 sensors in each block and regulated by a PID (proportional-integral-derivative) controller.

Fig. 1. Overview of the system with the cooling thermostat and the microscope heating/cooling stage. To load the stalagmite sections the upper block of the stage can be removed without disengaging connecting pieces.

The new stage makes the temporal reconstruction of fluid inclusion data more precise and efficient as the sections can be systematically scanned for suitable inclusions by a precise x-y
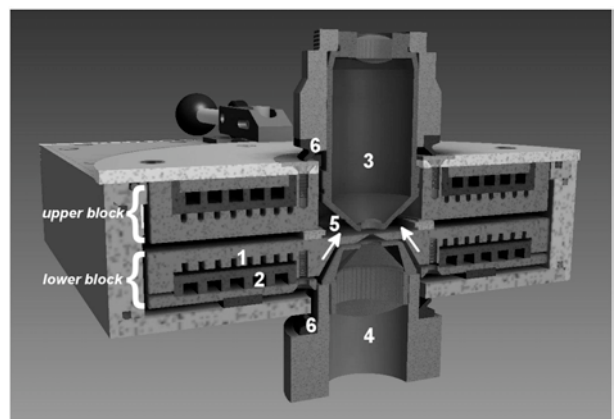

Fig. 2. Cross section of the heating/cooling stage. The objective and the condenser lens can be inserted into the copper blocks. The upper block is removable to load the sample. (1) heating elements, (2) cooling channels, (3) oil immersion objective fixed in a nylon jacket with v-seal (6), (4) condenser (NA 0.9) fixed in a nylon jacket with v-seal (6), (5) sample holder.

Since we use immersion oil to make the section transparent for microscopic observation we can use an oil immersion objective (NA 1.3) that provides improved optical resolution and image quality compared to the commonly used long working distance objectives (see Fig. 3). Additionally the oil immersion objective provides significantly higher transmission for the 800 nm wavelength of the femtosecond laser that is used to nucleate the vapour bubble. Thus the available pulse energy is increased and vapour bubble nucleation can be induced in larger depths within the section (cf. Krüger et al., 2007).
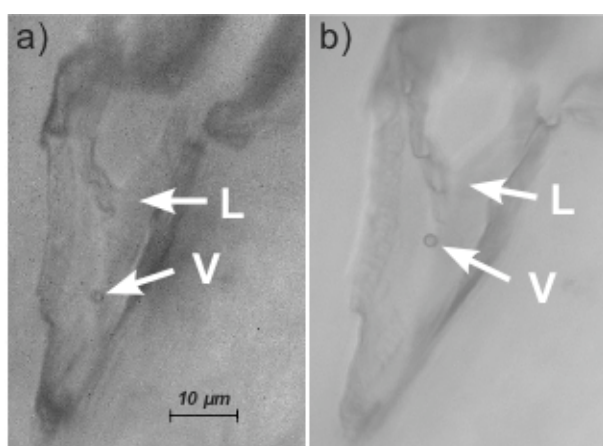
Fig. 3. Microphotographs of a two-phase inclusion in a stalagmite after laser-induced vapour bubble nucleation, (a) imaged by an Olympus LMPlanFL 100x/0.80 LWD objective, and (b) imaged by an Olympus UPLFLN 100x/1.30 oil immersion objective.

For temperature calibration of the stage a PT-100 temperature sensor was used to simulate the sample under measurement conditions. Because of the contact between objective and sample via the oil film, the calibration of the stage has additionally to account for variation of the room temperature.

REFERENCE

Krüger, Y., Stoller, P., Riĉka, J., Frenz, M., (2007). *Eur J Min* 2007, 19, 693–706.

Melt inclusions in co-precipitated perovskite, nepheline and magnetite in Kerimasi pyroxene-nephelinite, Tanzania

Guzmics, Tibor*, Berkesi, Márta*, Mitchell, Roger H.**, Milke, Ralf*** and Szabó, Csaba*

*Lithosphere Fluid Research Lab, Eötvös University Budapest, 1117 Budapest, Pázmány P. stny. 1/C Hungary
**Lakehead University, Thunder Bay, ON P7B 5E1 (Canada)
***Free University, Habelschwerdter Allee 45, 14195 Berlin (Germany)

Carbonatite and associated silicate rocks occurred in more than 500 localities in the Earth (Wooley and Kjarsgaard, 2008). Besides scientific aspects (e.g., Kjarsgaard 1998, Lee and Wyllie, 1998; Guzmics et al., 2008) many of them have great economic potential (e.g. Groves and Vielreicher, 2001). Evolution path(s) of their parental melt(s) is still ambiguous and questions have remained unanswered over the years, although, immiscible silicate and carbonate melts hosted in co-precipitated minerals of alkaline silicate rocks have been already studied (e.g. Nielsen et al., 1997; Mitchell, 2009; Guzmics et al., 2011).

In this study we have investigated a statistically significant number of melt inclusions hosted in coexisting perovskite, nepheline and magnetite in a clinopyroxene-nepheline-perovskite-magnetite-melilite rock collected at the Southern slope of Kerimasi Volcano, Tanzania. The rock shows typical igneous texture. Apatite and calcite can also be found as accessories. Nepheline hosts silicate melt inclusions however, perovskite and magnetite host melt inclusions containing droplets of immiscible carbonate and silicate melts. In general, all rock-forming minerals can be found in melt inclusions as daughter minerals; however, nepheline and clinopyroxene are the most common.

Microthermometric experiments were undertaken on nepheline- and perovskite-hosted melt inclusions. Melt inclusions show minimum temperatures for fluid-melt homogenization (into the melt phase) at 1050 °C. Many of melt inclusions were not homogenized, but decrepitated above 1100 °C. Melting of the last solid phase (e.g. clinopyroxene in nepheline-hosted melt inclusions) was detected between 1040 and 1050 °C. Using the minimum homogenization temperature (1050 °C), heating-quenching experiments were carried out on perovskite-, magnetite- and nepheline-hosted melt inclusions in furnace.
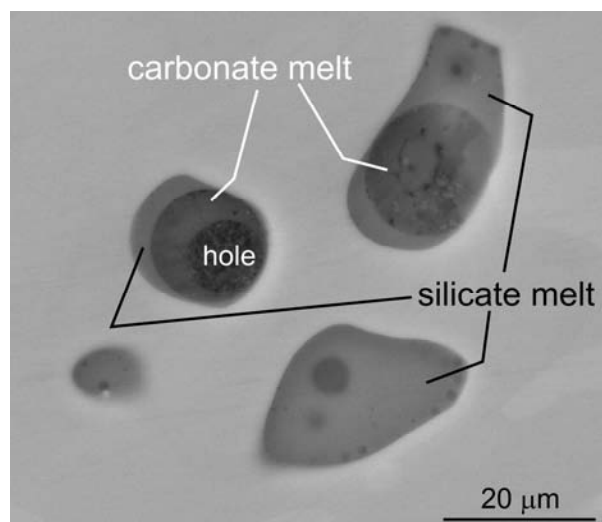

Fig. 1. Quenched (after heating to 1050 °C) melt inclusions in perovskite, backscattered electron image.

In general, nepheline-hosted melt inclusions showed quenched silicate melt and fluid bubble whereas, perovskite- and magnetite-hosted melt inclusions contained quenched silicate melt, carbonate melt and fluid bubble. These are interpreted as heterogeneously entrapped phases as their proportions are highly variable among the melt inclusions (Fig. 1). Microprobe measurements on quenched products have also been carried out for their major element composition.

Our results show, that at the early stage of melt evolution a carbonated olivine-nephelinite melt existed. We can follow evolution of this melt in a high number of melt inclusion showing enrichment in CaO and depletion in SiO_2 and

Al_2O_3, which was mainly controlled by co-precipitation of nepheline and clinopyroxene. Eventually, this chemical evolution led up to immiscibility between two alkali-rich melts: an MgO and FeO-rich silicate melt and a CaO- and P_2O_5-rich carbonate melt. Latter one could be physically separated from the system and became the parental melt of Kerimasi calcio-carbonatite (e.g., Guzmics et al. 2011). Our study suggests that immiscibility, occurred at crustal environment, can be responsible for observations worldwide namely; most of carbonatite rock is calcio-carbonatite (e.g. Le Bas, 1977).

Acknowledgement

REFERENCES

Groves D.I., Vielreicher N.M. (2001) *Miner. Dep.* 36: 189-194.

Guzmics T., Mitchell R.H., Szabó Cs., Berkesi M., Milke R., Abart R. (2011) *Contrib. Mineral. Petrol.* 161: 177–196.

Guzmics T., Zajacz Z., Kodolányi J., Werner H., Szabó C. (2008) *Geochim. Cosmochim. Acta* 72:1864–1886.

Kjarsgaard B.A. (1998) *J. Petrol.* 39: 2061–2075.

Le Bas M.J. (1977) John Wiley, London, 347 pp.

Mitchell R.H. (2009) *Contrib. Mineral. Petrol.* 158: 589–598

Lee W-J., Wyllie P.J. (1998). *J. Petrol.* 39: 2005 2013.

Nielsen T.F.D., Solovova I.P., Veksler I.V. (1997) *Contrib. Mineral. Petrol.* 126: 331–344.

Woolley A.R., Kjarsgaard B.A. (2008) Geological Survey of Canada, Open File 5796

Paleohydrothermal evolution of the 3.24 Ga Panorama Zn-Cu volcanic-hosted massive ide system, Pilbara craton, Western Australia

Hagemann, Steffen G.*, Huston, D.** and Drieberg, S.*

*Centre for Exploration Targeting, School of Earth and Environmental Sciences, University of WesternAustralia 6009, Crawley, Australia
**Geoscience Australia, GPO Box 378, Canberra, ACT 2601, Australia

The 3.24 Ga Panorama VMS District, located in the Pilbara craton of Western Australia contains discrete volcanogenic zinc-copper deposits over a strike length of about 30 km with ide mineralization exhibiting a typical upward and outward zonation from copper-rich to zinc (lead)-rich (Vearncombe et al., 1995). Indicated and inferred resource estimates for the Sulphur Springs deposit are 2.8 Mt at 10.7% zinc and 0.6% copper and 2.5 Mt at 4.0% copper and 1.1% zinc (Morant, 1998). Base metal mineralization at Sulphur Springs occurs as Zn-rich mineralization within the Marker Chert, as a much larger Zn- and Cu-rich accumulation in the dacite immediately beneath the Marker Chert, and as a stringer-style Cu-bearing zone at the base of the massive ide lens (Vearncombe et al., 1995).

The Panorama VMS District is exposed as a cross-section through subvolcanic granite intrusions and a coeval submarine volcanic sequence that hosts Zn-Cu mineralization. The near-complete exposure across the district, the very low metamorphic grade, and the remarkable preservation of primary igneous and volcanic textures provides an unparalleled opportunity to examine the P-T-X-source evolution of an ancient VMS ore-forming system and to assess the role of the subvolcanic intrusions as heat sources and/or metal contributors to the overlying VMS hydrothermal system.

Detailed mapping of the Panorama VMS District has revealed seven major vein types related to the VMS hydrothermal system or to the subvolcanic intrusions. (1) Quartz-chalcopyrite veins, hosted in granophyric granite immediately beneath the granite-volcanic contact, formed prior to main stage VMS hydrothermal convection, and were precipitated from mixed H_2O-CO_2-NaCl-KCl fluids with variable salinities (2.5 to 8.5 eq mass% NaCl); (2) quartz-sericite veins, ubiquitous across the top 50m of the volcanic sequence, were formed from an Archean seawater with a salinity of 9.7 to 11.2 eq mass% NaCl at temperatures of 90° to 135°C. These veins formed synchronous with the regional feldspar-sericite-quartz-ankerite alteration during seawater recharge into the main stage VMS hydrothermal convection cells; (3)

quartz-pyrite veins hosted in granophyric granite; (4) quartz-carbonate-pyrite veins hosted in andesite-basalt, also formed from relatively unevolved Archean seawater (5.5 to 10.1 eq mass% NaCl; 150° to 225°C), but during the collapse of the VMS hydrothermal system when cool, unmodified seawater invaded the top of the subvolcanic intrusions; (5) quartz-topaz-muscovite greisens; (6) quartz-chlorite-chalcopyrite vein greisens; and (7) hydrothermal Cu-Zn-Sn veins are hosted in the subvolcanic intrusions. Primary H_2O-NaCl-$CaCl_2$ fluid inclusions in the vein greisens were complex high temperature hypersaline inclusions (up to 590°C and up to 56 eq mass% NaCl). The H_2O-CO_2-NaCl fluid inclusions in the Cu-Zn-Sn veins have variable salinities, ranging from 4.9 to 14.1 eq mass% NaCl, and homogenization temperatures ranging from 160° to 325°C. The hydrothermal quartz veins and magmatic metasomatic phases in the subvolcanic intrusions were formed from a magmatic-hydrothermal fluid that had evolved through wallrock reactions, cooling, and finally mixing with seawater-derived VMS hydrothermal fluids.

Interpretation of the physico-chemical conditions of the Panorama fluids has led to a model of continuous interaction between seawater and volcanic rocks within a thermally waxing and waning system. Four end-member fluids precipitated the veins mapped in the Panorama VMS District: Archean seawater, VMS hydrothermal, magmatic-hydrothermal, and magmatic brine. These end-member fluids have been variably modified by fluid-rock reaction, phase separation, and fluid mixing. Volcanic-hosted veins and veins hosted in altered granophyric granite were formed from slightly modified Archean seawater. The granite-hosted veins were formed from magmatic-hydrothermal fluids exsolved from the crystallizing inner phase granite. Due to temperature and density contrasts, the magmatic brine phase exsolved from the granophyric granite remained stratified and isolated from the overlying lower temperature seawater-hydrothermal convection cells in the volcanic sequence. Therefore, this metal-bearing

magmatic brine played no role in the formation of the overlying VMS deposits. The VMS deposits were precipitated from hot (>300°C) highly evolved seawater that had undergone significant low- and high-temperature reaction with the volcanic rocks to modify its chemical composition and leach metals from the volcanic strata and underwent phase separation to increase its volatile content and decrease its salinity relative to unmodified Archean seawater. The chemistry and isotopic compositions of the VMS hydrothermal fluids can be adequately explained as evolved and phase separated seawater, and no magmatic fluid component is required.

REFERENCES

Morant, P. (1995) The Panorama Zn-Cu VMS deposits, Western Australia: *Australian Institute of Geoscientists Bulletin*, 16: 75-84.

Vearncombe, S., Barley, M. E., Groves, D. I., McNaughton, N. J., Mikucki, E. J., and Vearncombe, J. R. (1995) 3.26 Ga black smoker-type mineralisation in the Strelley Belt, Pilbara Craton, Western Australia: *Journal of the Geological Society of London*, 152: 587-590.
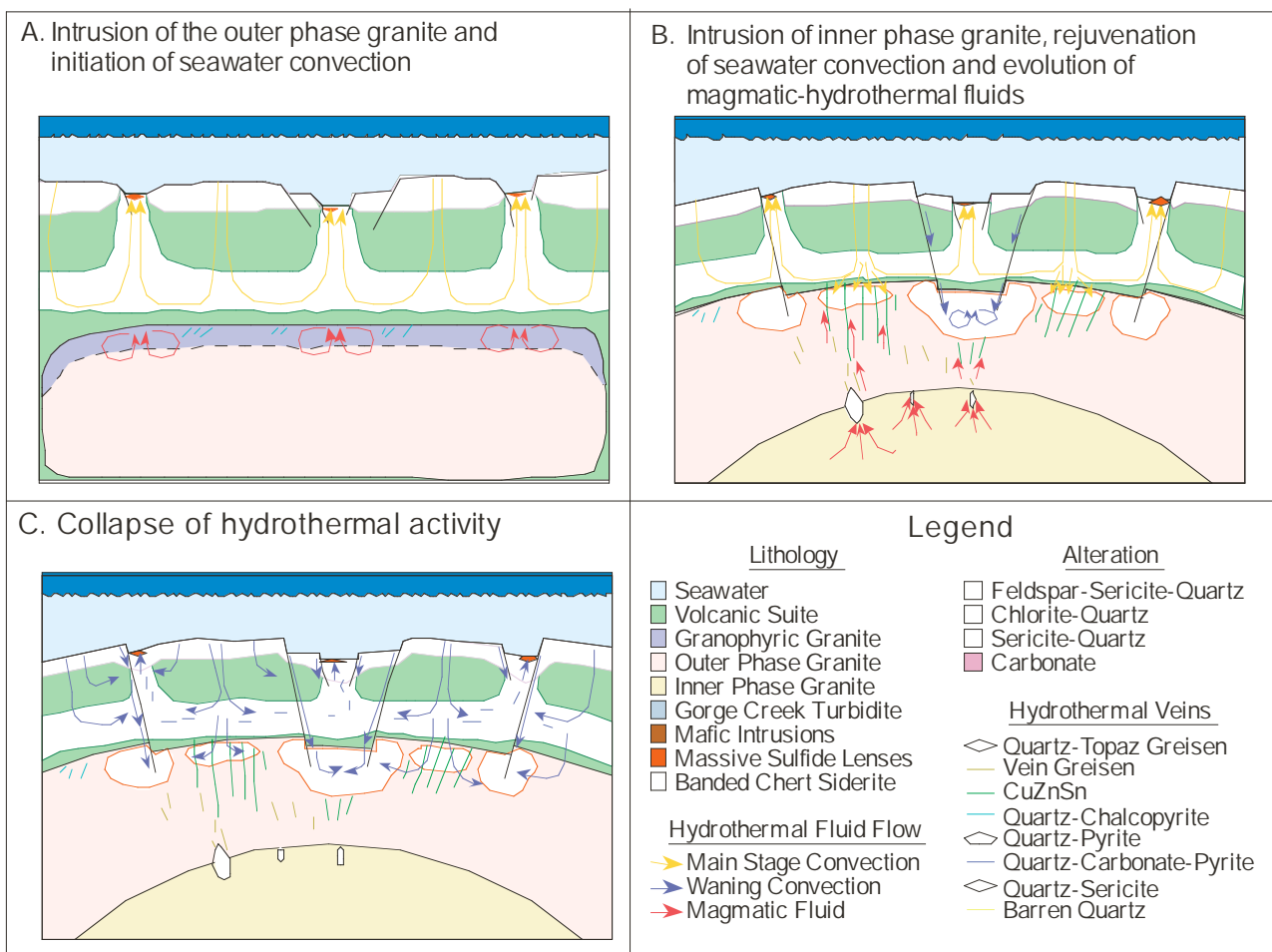
Fig. 1 Inferred hydrothermal evolution in the northern part of the Panorama volcanic hosted massive ide hydrothermal system: (A) Intrusion of outer phase of Strelley Monzogranite and initiation of seawater convection, (B) Intrusion of inner phase of Strelley Monzogranite, rejuvenation of seawater convection, and evolution of magmatic-hydrothermal fluids, and (C) Collapse of hydrothermal activity.

Correcting stalagmite fluid inclusion homogenisation temperatures for the effect of surface tension

Hidalgo Staub, Rita[*,***], Krüger, Yves[*,***], Frenz, Martin[*] and Fleitmann, Dominik[**,***]

[*]Institute of Applied Physics, University of Berne, Sidlerstrasse 5, CH-3012 Bern
[**]Institute of Geological Sciences, University of Berne, Baltzerstrasse 1&3, CH-3012 Bern
[***]Oeschger Centre for Climate Studies, University of Berne, Zähringerstrasse 25, CH-3012 Bern

We evaluate a new method to determine paleotemperatures (mean annual surface temperatures) from liquid-vapour homogenisation temperatures (T_h) of fluid inclusions in stalagmites. Our approach is to determine the density of fluid inclusions by measuring the liquid-vapour homogenisation temperature after inducing vapour bubble nucleation in the initially monophase inclusion. This is achieved by ultra short laser pulses to overcome the metastable state of water (Krüger et al. 2007). Fluid inclusions in stalagmites are primary inclusions containing remnants of the drip water from which the calcite precipitated under atmospheric pressure. Therefore their T_h is expected to equal the stalagmite formation temperature i.e. the cave air temperature. An important precondition being that the density of the fluid inclusions remains unaltered, it is important to avoid large fluid overpressure and to minimise mechanical stress during sample preparation.

MEASUREMENTS

To test our paleothermometer T_h measurements were carried out using 300–400 μm thick sections of an actively growing stalagmite from Milandre Cave (Switzerland). The observed homogenisation temperatures ($T_{h\ obs}$) display a large variability with a maximum around the actual cave temperature of 9.5 °C (see Fig. 1). The position of this maximum is, however, coincidental, because $T_{h\ obs}$ values are influenced by various parameters.

$T_{h\ obs}$ values above 9.5°C result from density changes in the fluid inclusions induced by mechanical stress during sample preparation. Therefore these inclusions do not represent the original fluid density and are not considered for the determination of the stalagmite formation temperature (T_f).
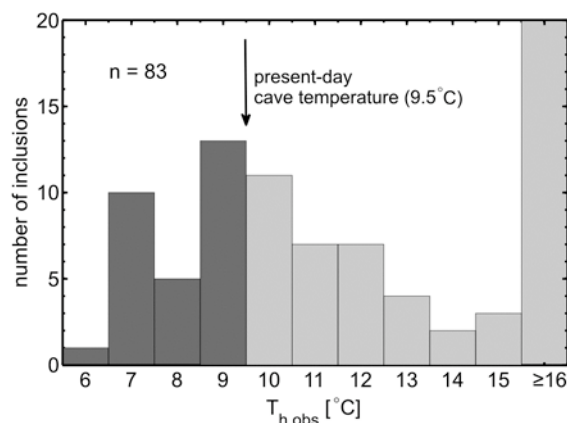

Fig. 1. Distribution of $T_{h\ obs}$ values measured in a recent stalagmite from Milandre Cave. Temperatures in light grey are higher than the actual cave temperature and result from density alterations in the inclusions. Temperatures in dark grey are from fluid inclusions that have potentially preserved their density. $T_{h\ obs}$ above 16°C were not determined in order to avoid overheating (and large overpressure in other inclusions).

$T_{h\ obs}$ values lower than 9.5°C can be explained by the effect of surface tension on liquid-vapour homogenisation. Surface tension leads to a collapse of the vapour bubble below the nominal homogenisation temperature. The extent of this effect depends on the inclusion volume as well as on the fluid density. Being negligible in large inclusions of low density it can amount to a temperature difference of several degrees in small inclusions with high bulk density. Thus, to determine T_f we have to correct the measured $T_{h\ obs}$ values for the effect of surface tension.

CORRECTION OF SURFACE TENSION EFFECT

To compensate for the effect of surface tension we applied a correction algorithm to derive the nominal homogenisation temperature (T_h and

the inclusion volume from $T_{h\,obs}$ and the vapour bubble radius measured at a known temperature. Fig.2 shows the result of this correction. Marti et al. have described the thermodynamic relations between bulk density, inclusion volume and the vapour bubble radius at a defined temperature (see abstract in this conference volume). Their model predicts that fluid inclusions with T_f of 9.5°C with a volume of less than $35000\,\mu m^3$ are too small for a stable vapour bubble to exist. Therefore we can eliminate these values in the diagram as the density in these inclusions must have been altered.
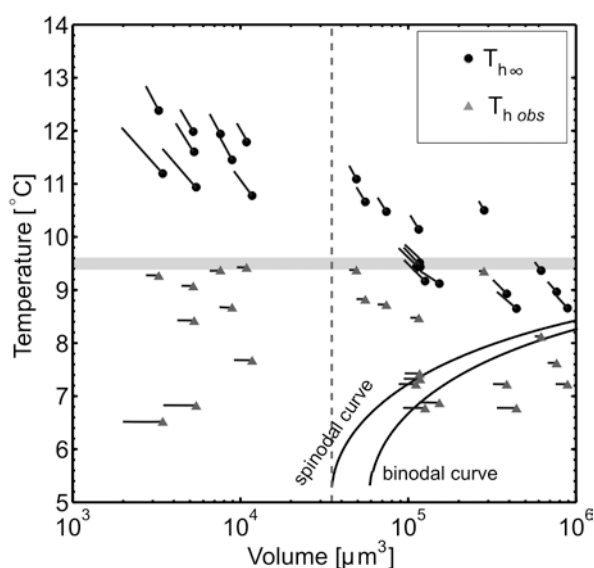
Fig. 2. Temperature-volume diagram showing the results of the surface tension correction. Grey triangles denote $T_{h\,obs}$, black dots the corrected temperatures T_h. The horizontal bar indicates the stalagmite formation temperature of 9.5°C. The correction is made on the assumption that $T_{h\,obs}$ corresponds to the spinodal temperature with error bars indicating the uncertainty arising from the bubble metastability. The solid curves denote the spinodal and binodal temperatures for a formation temperature of 9.5°C. The spinodal curve ends at 5.1°C at the minimum inclusion volume of $3500\,\mu m^3$ (dashed line) predicted by the model. Median of corrected T_h 9.42°C.

The model also shows that due to surface tension the bubble passes through a metastable state (beginning at the binodal temperature) before it becomes unstable and collapses (at the spinodal temperature). However, the bubble may also collapse before approaching the spinodal temperature and therefore the actual $T_{h\,obs}$ is not clearly defined. This leads to an uncertainty in the calculated volume and T_h shown in Fig.2.

A second error rises from the uncertainty in vapour bubble radius determination due to microscopic resolution and scattering effects around the vapour bubble.

CONCLUSION

Only the lowest $T_{h\,obs}$ values originate from inclusions that have preserved the original fluid density. These values have then to be corrected for the effect of surface tension in order to determine the stalagmite formation temperature. In the presented example this procedure yields a stalagmite formation temperature (median value) of 9.42°C, which is close to the present day cave temperature. Based on these results we expect an accuracy in paleotemperature determination of ±0.5°C.

REFERENCES

Krüger Y., Stoller P., Ricka J. and Frenz M. *Eur. J. Mineral.* (2007), 19, 693 706.

Krüger Y., Marti D., Hidalgo Staub R.; FleitmannD., Frenz M. (in press) *Chemical Geology*.

Marti D., Krüger Y., Fleitmann D., Ricka J., FrenzM. (submitted) *Fluid Phase Equilibria*.

Marti D. et al. (2011) *ECROFI-XXI Abstracts*

Potential concentration measurements of HCO_3^- and pH estimates in natural fluid inclusions by Raman spectroscopy: a case study from Libcice Gold Deposit

Hrstka, Tomas.*, Dubessy, Jean** and Zacharias, Jiri***

*Institute of Geology AS CR, v.v.i., Rozvojová 269, CZ-165 00 Prague 6 – Lysolaje, Czech Republic
**G2R(UMR 7566), Faculté des Sciences, Université Henri Poincaré-Nancy Université, BP-70239, 54506Vandoeuvre-les Nancy Cedex France
***Charles University in Prague, Faculty of Science, Institute of Geochemistry, Mineralogy and MineralResources, Albertov 6, Praha 2, CZ-128 43

Unusual fluid inclusion composition has been reported earlier at the Libcice orogenic gold deposit. (Zacharias, 2002 and Hrstka et al., 2011). Bicarbonate(HCO_3^-)-rich H_2O-CO_2 fluids (with minor amounts of CH_4-N_2-H_2S-C_2H_6) and H_2O fluids were recorded by this earlier study. Based on the high variability of FIA and expected variable HCO_3^- content these fluids has been identified as ideal candidate for HCO_3^- quantification in natural fluid inclusions. Quantitative calculations of the concentration of Raman active ions such as: HCO_3^-, CO_3^{2-}, SO_4, PO_4^{3-}, and HS^-, can lead us to important information about pH, f_{O2}, f_S fugacity as well as other parameters of the paleofluid (Dubessy et al., 1989, 2008). The concentration of SO_4; HS^- polyatomic species in natural paleofluids was measured and quantified for some species (Dubessy et al., 2002), but not many data have been reported for the HCO_3^-.

This study reports on high temperature Raman measurements made in order to confirm the abnormally high concentrations of bicarbonate in Libcice paleofluids and also on the first attempts to validate the individual Raman peaks for future quantitative analysis of HCO_3^- in aqueous-carbonic paleofluids. The pH calculation in quartz hosted natural fluid inclusions based on the pH controlled equlibria of (HCO_3^-)/(CO_3^{2-}) (with main Raman peaks at about 1017 cm^{-1} and 1064 cm^{-1}, respectively) were also evaluated. The high concentration of HCO_3^- in the fluids was confirmed by the presence of a peak at 1014cm^{-1} and at 1360cm^{-1} even at the temperatures above total homogenization). Proportions of the IR peak integrated areas were measured in order to receive the relative concentration of HCO_3^- in the aqueous solution.
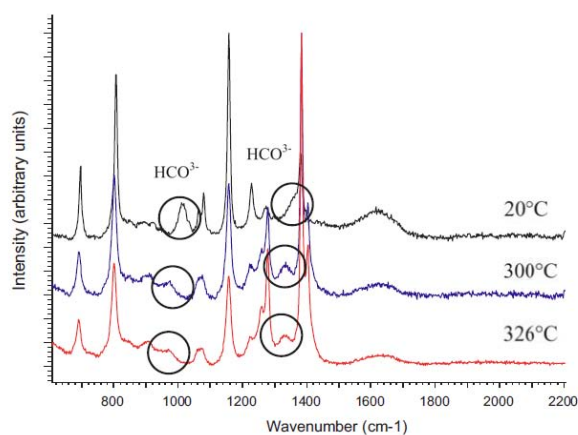

Fig. 1. Example Raman spectra of bicarbonate-rich aqueous phase present in H_2O-CO_2 fluid inclusions at variable temperatures. Two major areas used for HCO_3^- identification and quantification are highlighted. Note the Raman peak shift with temperature.

For the low temperature measurements the peak area ratio was suggested as the most practical to estimate concentrations, whereas the peak height ratio seems more applicable for temperatures above 100 °C. The spectrum of quartz matrix and the possibility of spectral subtraction of quartz from the inclusion spectra were tested to overcome the peak overlap of quartz and CO_3^{2-} at around 1066 cm^{-1}. Based on our results, the Libcice paleofluids were estimated to pH 7 - 8.5. The extremely high variation in relative peak intensity of the monitored part of quartz spectrum was confirmed even within a single grain. Other peak parameters were tested to establish the best potential calibration strategies for quantitative Raman measurement of bicarbonate in natural fluid inclusions both at room and at elevated temperatures. This research is important for the future pH calculation development and high

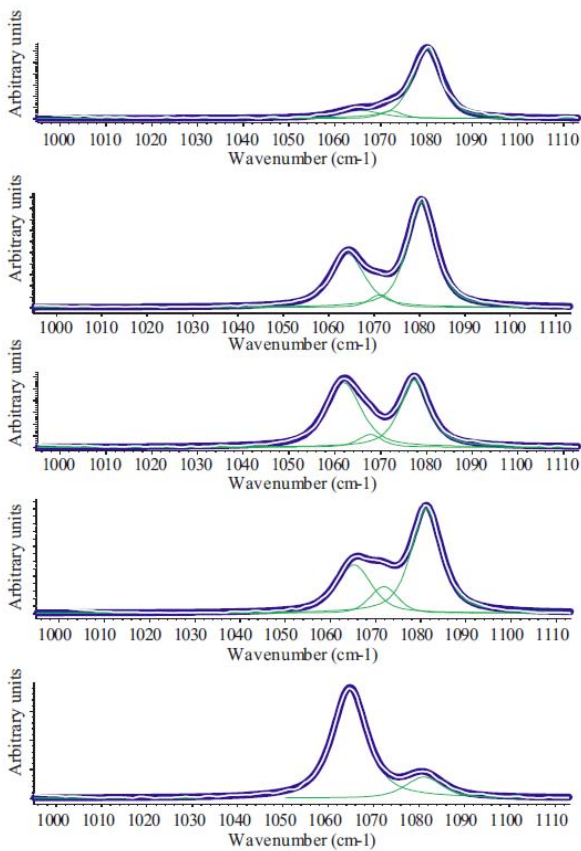temperature Raman spectroscopic study of fluid inclusions/paleofluids.

Fig. 2. Example Raman spectra of the quartz matrix showing variation in the region of interest for CO_3^{2-} quantification and potential pH calculation of paleofluids. Note the presence of variable matrix peak intensities in the area of 1064 cm^{-1} which is also an area of major CO_3^{2-} peak.

REFERENCES

Hrstka T., Dubessy J., Zacharias J. (2011, Chemical Geology-Volume 281,Issues 3-4, 24 February 2011, Pages 317332

Dubessy J., Poty B., Ramboz C., 1989. Europian Journal ofMineralogy 1, pp. 517-534.

Dubessy, J., Ding, J., Leisen, M. and Robert, P.,2008. PACROFIIX USGS, Reston, USA.

Zachariáš, J. 2002Journal of the Czech GeologicalSociety, volume 47, issue 3-4,123 – 132

Ore-forming fluids, stable isotope and mineralizing age of the Hubazhuang gold deposit in the Jiaodong Peninsula, eastern China

Hu, Fang-Fang, Fan, Hong-Rui, Cai, Ya-Chun, Yang, Kui-Feng and Lan, Ting-Guang

Key Laboratory of Mineral Resources, Institute of Geology and Geophysics, Chinese Academy of Sciences,Beijing 100029, PR China

Hubazhuang gold deposit is a typical pyrite- and polymetallic sulphide-quartz lode deposit in the Muping-Rushan gold belt of Jiaodong Peninsula, and gold occurs mainly in pyrite- and polymetallic sulphide-quartz vein. Fluid inclusion studies show that in the different altered wall rocks and gold ores of different mineralization stages there are three major types of fluid inclusions: CO_2-rich fluid inclusions, CO_2-H_2O fluid inclusions and aqueous fluid inclusions. CO_2-rich fluid inclusions occur mainly in the early mineralizing stage (stage I); the main mineralizing stage (stage II) contains CO_2-H_2O fluid inclusions and aqueous fluid inclusions; there are only the aqueous fluid inclusions in the late mineralizing stage (stage III). Microthermometric study shows that in stage the homogenization temperatures and salinities range respectively from 260 to 360 and 1.02 to 7.38 % NaCl, and stage the range is 180 to 269 and 1.74 to 13.07 % NaCl, then stage III is 104 to 189 and 0.88 to 8.81 % NaCl. The fluids in stage I were medium-high temperature, volatile-rich and low salinity fluid system. During stage II the fluids evolved to a CO_2-H_2O-NaCl fluid system with medium-low temperature, low volatile and wide range of salinity. Finally in stage the temperature, salinity and volatile content all decreased. The study of hydrogen and oxygen stable isotope indicates that in stage the mineralizing fluids were mainly magmatic water, but during stage II the mineralizing fluids were mixed fluids which originated mainly from meteoric water. Sulphur isotope of the main mineralizing stage reveals that ore-forming materials may mainly come from the wall rocks which were leached by the meteoric water. Temperature decline and fluid immiscibility are the main reason of the gold precipitation. Rb-Sr isochron of sericite in altered rocks shows that the mineralizing age of Hubazhuang gold deposit is 126.5±5.6Ma.

Fluids associated with the Au-Ag and Ag-Pb-Zn mineralizations of the Blanice graben tectonic zone, Bohemian Massif

Hübst, Zdenek*, Islakaeva, Zemfira*, Zacharias, Jiri* and Selmi, Moustafa*,**

*Institute of Geochemistry, Mineralogy and Mineral Resources, Faculty of Science, Charles University, Albertov 6, Prague, Czech Republic
**Geology Department, Faculty of Science, Suez Canal University, Ismailia, Egypt

Numerous small-sized Ag-Pb-Zn vein type (intermittently mined from the 14th to the 17th century) and two late orogenic-gold (electrum) deposits (about 6 t of gold was mined at the Roudný deposit between 1895 – 1930) are hosted by the Blanice graben in the central part of the Bohemian Massif. This, about 200 km-long NNE-SSW trending tectonic zone (also called the Kouřim – Blanice – Kaplice – Rödl fault zone) crosses all the Moldanubian Units and extends from east of Prague to Linz in Austria. The faults of the Blanice graben have been repeatedly reactivated; the oldest identified tectonic activity is inferred to be Permo-Carboniferrous in age (Stephanian C to Autunian), as has been inferred from the isolated islets of coal-bearing sediments. The major tectonic movements in the Blanice graben must, therefore, be of Permian age or younger. The only geochronological data on the tectonic evolution of the Blanice graben are those of Košler et al. (2001; 270±2 Ma, representing a minimum intrusive age for the microdiorite dike swarm parallel with the strike of the Blanice graben, but located outside the graben structure) and of Brandmayr et al. (1995; 288-281 Ma, ductile deformation in the Austrian part of the Blanice graben).

Up to five different fluid types, were recognized in the quartz and carbonate gangue of the Au-Ag Roudny deposit (Zachariáš et al., 2009). The early fluids represent $H_2O-CO_2\pm CH_4-N_2$ low salinity (<3.9 % NaCl) fluids (400-330 °C) with isotopic signatures consistent with a metamorphic origin ($\delta^{18}O_{fluid}$ = +4.7 to +2.9 ‰ SMOW), while the late fluids are of aqueous-only type. The salinity of aqueous fluids evolves from about 24 % NaCl (350-250 °C; probably electrum-bearing) to about 7 to 9 % NaCl (250-70 °C; Ag-Pb-Zn bearing and post-ore fluids).

The Ag-Pb-Zn vein type deposits are represented by quartz-carbonate-barite gangue with Ag-rich galena, pyrrargyrite, proustite, salerite, chalcopyrite and minor pyrite. Arsenopyrite is almost absent; carbonates correspond to dolomite, Fe-dolomite and to calcite. The studied samples (the Rudolfov, Stara Vozice, Stribrna Skalice, Zvestov and Hriva deposits) represent variations in fluid composition along the strike of the Blanice graben of more than 70 km.

Fluids are of aqueous type only, having relatively constant range of homogenization temperatures (from ~200 to ~130 °C; L+V=L), but differing mutually in the salinity (from 10 to 0 % NaCl) for individual deposits. The data suggest almost isothermal mixing between low and moderate salinity fluids. Isotope composition of carbonates indicate more or less constant oxygen composition ($\delta^{18}O_{fluid}$ = +3 ‰ SMOW), coupled with gradual decrease in the $\delta^{13}C_{fluid}$ from about -7 to about -22 ‰ CDT.

Minor variations in total homogenization temperatures of inclusions and constant oxygen isotope composition of fluids points to compositionally homogeneous parent fluid, probably of deep metamorphic origin.

REFERENCES

Brandmayr M., Dallmeyer R.D., Handler R.,Wallbrecher E. (1995) *Tectonophysics*248: 97-116.

Kosler J., Kelley S.P., Vrana S. (2001): *Int. J. EarthSci. (Geol. Rdsch.)* 90: 379-385.

Zacharias J., Paterova B., Pudilova M. (2009):*Econ. Geol.* 104: 53-72.

Calciocarbonatite melts in plagioclase megacrysts and xenoliths from Plio-Pleistocene alkali basalt (Slovakia)

Hurai, Vratislav*, Huraiová, Monika** and Thomas, Rainer***

*Geological Institute, Slovak Academy of Sciences, Dúbravská cesta 9, Bratislava, Slovakia
**Department of Mineralogy and Petrology, Comenius University, Mlynská dolina, Bratislava, Slovakia
***Helmholtz-Zentrum Potsdam, GFZ, Telegrafenberg D 320, Potsdam, Germany

Quenched carbonatite melts occur in basaltic diatreme near Hajnáčka village in the Lučenec basin of southern Slovakia. The 2.60–2.75 Ma old diatreme (Konečný *et al.,* 1995; Vass *et al.,* 2000) together with spatialy associated monogenic maars and lava flows belong to the alkali basalt volcanic province of the intra-Carpathian back-arc basin (the Pannonian basin) originated during post-rift thermal subsidence following aMiocene subduction. The alkali basalts were generated during crustal thinning, astenosphere updoming and partial melting of metasomatised mantle (Konečný *et al.,* 2002; Seghedi *et al.,* 2004). Carbonatite melts occur in inclusions in plagioclase megacrysts, interstitial glass in anorthoclasite xenoliths, as separate carbonatite xenoliths, and isolated globules in kaersutite from clinopyroxene-rich cumulates.

Oligoclase megacrysts ($An_{24-26}Or_{5-6}$), up to 6 cm in diameter, contain rounded melt pockets, composed of ~65 vol% of Ca-carbonatite globules tightly packed in silica-undersaturated (larnite-normative) melilititic glass matrix. About 50 % of the globules contain phosphate-rich domains and almost pure Ca-phosphate globules occupy ~1 % of the inclusion volume (Fig. 1).

Anorthoclasite xenoliths are composed of alkali feldspar (Or_{29-51}) and interstitial Ca-carbonatite melt with dispersed calcite crystals (Fig. 2). Mg-rich ilmenite, apatite and aegirine-augite are present in accessory amounts. Nb-rutile (3.57 % Nb_2O_5) and hedenbergite crystallized as breakdown products of Mg-ilmenite and aegirine-augite, respectively.

Carbonatite xenoliths are composed of quenched Ca-carbonatite glass trapped between radial aggregates of elongated calcite crystals. No other silicate phases have been observed in the carbonatite xenoliths.
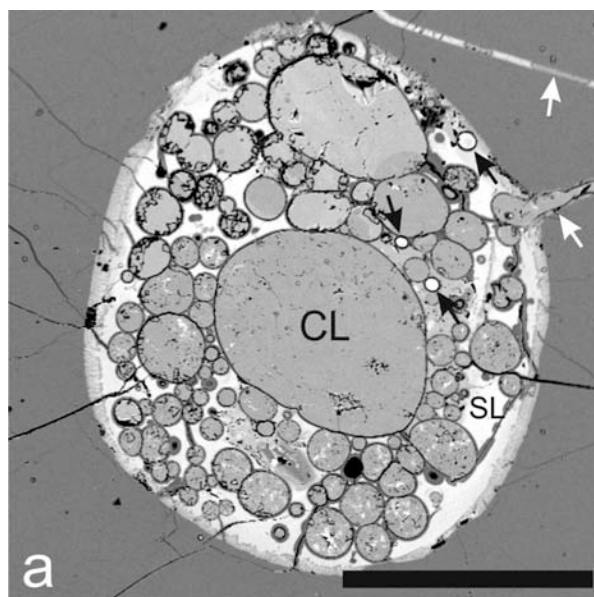

Fig. 1. Back-scattered electron image of a glass pocket in oligoclase megacryst. Variably sized calcio-carbonate globules (CL) are dispersed in alumino-silicate glass matrix (SL). Many carbonate globules contain irregular white phosphate-rich domains, and black arrows indicate three isolated Ca-phosphate globules. White arrows designate cracks with deformed Ca-carbonate globules bulging out into the glass pocket. Black bar scale represents 500 µm.

Textural phenomena rule out the possibility that carbonate globules in plagioclase megacrysts could represent resorbed calcite crystals. Moreover, variable volumes of P-rich domains in the carbonate globules unequivocally document partial immiscibility between the Ca-carbonate and the Ca-phosphate endmember melt phases. Compositions of the coexisting carbonate crystals and melts in megacrysts and xenoliths differ significantly, showing preferential partitioning of Sr in calcite crystals, and P and Mg in the carbonatite melt phase.
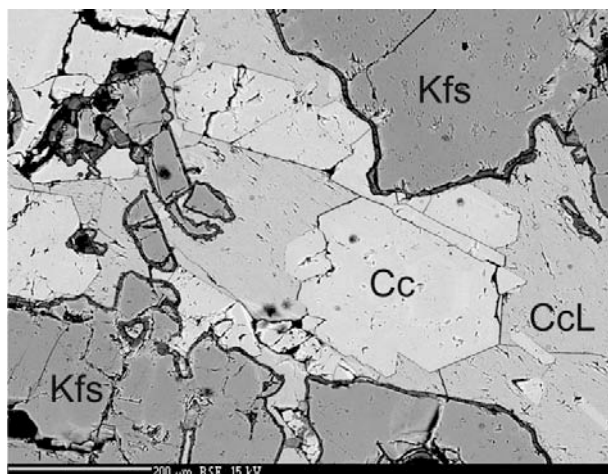
Fig. 2. Anorthoclasite xenolith with carbonatite melt (CcL) and calcite crystals (Cc) interstitial to alkali feldspars (Kfs).
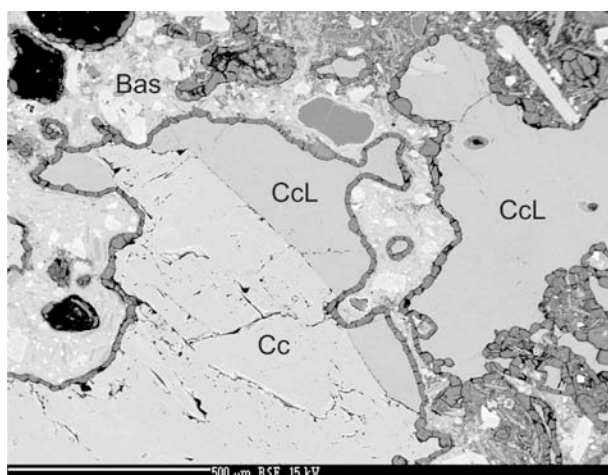

Fig. 3. Xenolith composed of carbonatite melt (CcL) and columnar calcite aggregates (Cc) resorbed from margins by alkali basalt (Bas).

Raman spectroscopy revealed that carbonate globules are well-crystallized phases with main fingerprint bands diagnostic of common low-pressure calcite Ipolymorph. In contrast, missing lattice modes and broader bands indicate alower crystallization degree of the coexisting phosphate globules, showing an isolated lattice mode at 131 cm^{-1} assigned to a Ca-PO$_4$ bond (Tsuda & Arends, 1994) and downshift of the main stretching $_1$PO$_4^{3-}$ mode of apatite from 962-964 cm^{-1} to 952-953 cm^{-1}. Vibrations at 1069 and 1017 cm^{-1} have been tentatively assigned to carbonate and sulphate components, respectively, although the latter is sometimes attributed to the triply degenerate antisymmetric stretching $_3$PO$_4^{3-}$ mode in carbonated hydroxylapatite (Antonakos *et al.*, 2007). A weak polarization-dependent band at 682 cm^{-1} was attributed to doubly degenerate $_4$ mode of CO$_3^{2-}$ ion integrated in the apatite lattice (Antonakos *et al.*, 2007). A weak band centred at 3561 cm^{-1} corresponds to OH-stretching, although the observed mode was substantially down-shifted from the values of 3572-3575 cm^{-1} typical of hydroxylapatite (Tsuda & Arends, 1994; Yu *et al.*, 2007). The shift may be due to substitution of the hydroxyl group by CO$_3^{2-}$ and/or O$_2^{2-}$.

Preliminary thermodynamic modelling with Perple_X software package (Connolly 2005) and associated databases and solution models showed that crystallisation of plagioclase and alkali feldspar with the observed compositions may occur near solidus of strongly volatile (5 % H$_2$O, 1% CO$_2$) high alkaline (8 % in total) phonotephritic melt. Inferred *PT* parameters (720-790°C, 4-8 kbar) are consistent with low-to-middle crustal conditions and the observed assemblage of xenoliths and megacrysts is interpreted as a flotation cumulate from the top of differentiated alkaline basalt magma chamber ejected by later magma portions.

REFERENCES

Antonakos, A., Liarokapis, E., Leventouri, T.(2007) *Biomaterials* 28: 3043-3054.

Connolly J.A.D. (2005) *Earth Planet. Sci. Lett.* 236:524-541.

Konečný, V., Lexa, J., Balogh, K., Konečný, P.(1995) *Acta Vulcanol.* 7: 16-171.

Konečný, V., Kováč, M., Lexa, J., Šefara, J. (2002)*EGS Stephan Mueller Spec. Publ. Ser.* 1:165-194.

Seghedi, I., Downes, H., Vaselli, O., Szakács, A.,Balogh, K., Pécskay, Z. (2004)*Tectonophysics* 393: 43-62.

Tsuda, H., Arends, J. (1994) *J. Dent. Res.* 73,1703-1710.

Vass, D., Konečný, V., Túnyi, I., Dolinský, P.,Balogh, K., Hudáčková, N., KováčováSlamková, M., Beláček, B. (2000) *Geol.Carpath.* 51: 69-82.

Yu, H., Zhang, H., Wang, X., Gu, Z., Li, X., Deng,F. (2007) *J. Phys. Chem. Solids* 68: 18631871.

CO₂-SO₂-H₂O fluid inclusions in peridotite xenoliths from Jeju Island (South Korea)

Káldos, Réka*, Berkesi, Márta*, Hidas, Károly*,**, Yang, Kyounghee*** and Szabó, Csaba*

* Lithosphere Fluid Research Lab, Eötvös University (ELTE), Budapest, Hungary
**Instituto Andaluz de Ciencias de la Tierra, CSIC-UGR, Granada, Spain
***Dept. of Geological Sciences, Pusan National University, Busan, South Korea

Representative peridotite xenoliths have been selected for detailed study from three different alkali basaltic outcrops of Jeju Island (South Korea). Based on the modal composition, the majority of the studied xenoliths here is spinel lherzolite with minor amount of spinel harzburgite. All of them shows coarse grained protogranular-porphyroclastic texture.

Fluid inclusions in every xenolith are intergranular, crosscutting the rock-forming mantle silicates, and applying the definition of Roedder (1984) are considered as secondary ones with respect to the formation of the host minerals. The fluid inclusion associations always consist of several hundred negative crystal shaped fluid inclusions ranging in size from 2 to 60 µm. Furthermore, small-sized fluid inclusions (<10 µm), even in olivine, are usually of one-phase at room conditions and show no indication for any decrepitation, whereas the large, partially decrepitated ones contain one (liquid) or two phases (vapor and liquid phase with various volume proportions).

Combined microthermometric and laser Raman microspectroscopic techniques were used to investigate the fluid compositions. By using a Linkam heating-freezing stage we observed the solid phase melts at -56.6°C (±0.3°C) with no other observable melting events indicating that the trapped fluid is dominantly CO_2. In contrast, the homogenization temperatures show a much wider range. As a general rule the smaller the fluid inclusion, the lower the homogenization temperature, regardless of the host mineral.

Fluid inclusions with high density (1.03-1.10 g/cm³) were found in every xenolith, where sufficient number of heating-freezing experiments could be done. Microthermometric data on Jeju xenoliths did not succeed to identify other volatile components than CO_2. Hence, Raman analyses were carried out to determine other volatile components at room and elevated temperatures (~170°C). At room temperatures CO_2 and SO_2 was detected, whereas at high temperatures, beside the CO_2, and SO_2 the peaks of H_2O dissolved in CO_2 (*e.g.* Sterner & Bodnar, 1991, Diamond, 2001) were also observed resulting in an average composition of the CO_2-rich phase at around 170 ºC as follows: CO_2 94,2 mol%, H_2O 5,72 mol% and SO_2 0,1 mol%. It is noteworthy to mention that SO_2 in mantle fluids is not a common volatile component therefore further investigations are necessary to interpret its presence.
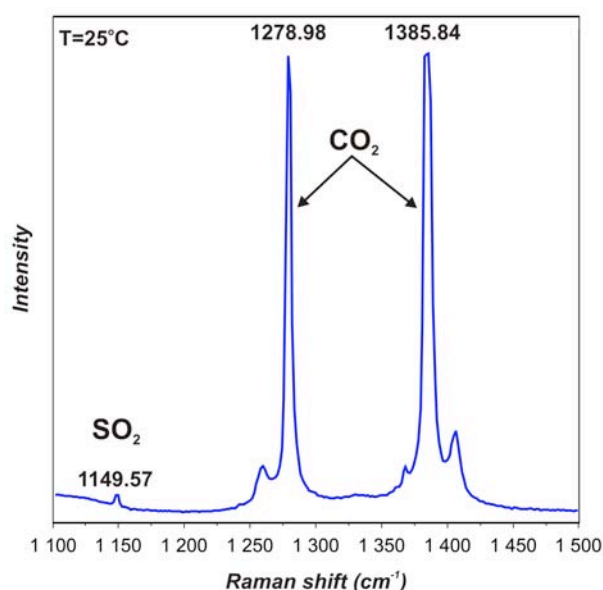

Fig. 1. Representative Raman spectra of CO_2 and SO_2 in orthopyroxene-hosted fluid inclusion taken at room temperature. Peak positions are determined by fitting with Gaussian-Lorentzian function

As summarized, fluid inclusions entrapped at upper mantle conditions in the deep sub-continental lithospheric conditions contain small

amount of H_2O and SO_2. The widespread occurrence of fluid inclusions in the Jeju peridotite series also indicate that the upper mantle is crosscut by several C-O-H-S bearing fluid inclusion zones, which could significantly affect the mantle rheology beneath the island, however, based on the petrographic evidences, the fluid entrapment can be regarded as a late stage event in the evolution of the shallow sub-continental lithospheric mantle.

Acknowledgement

REFERENCES

Roedder E. (1984) Reviews in Mineralogy, 12, 1646.

Sterner S. M., Bodnar R. J. (1991 American Journal of Science 291, 1-54.

Diamond L. W. (2001) Lithos 55,69-99.

The role of fluids in the formation of a clinopyroxene-rich pegmatoid vein in a migmatised granitic gneiss: Söndrum Stenhuggeriet, Halmstad, SW Sweden

Kerkhof, Alfons M. van den*, Harlov, Daniel E.** and Johansson, Leif***

*Geowissenschaftliches Zentrum der Universität Göttingen, Goldschmidtstrasse 3, 37077 Göttingen, Germany
**GeoForschungsZentrum Potsdam, Telegrafenberg, 14473 Potsdam, Germany
***Department of Earth and Ecosystem Sciences, University of Lund, Sölvegatan 12, 22362 Lund, Sweden

A clinopyroxene-rich pegmatoid vein along the eastern wall of the Söndrum stone quarry, Halmstad, SW Sweden has been investigated. The quarry is located in the Eastern Segment of the Sveconorwegian Orogen in SW Sweden. The study is accomplished by investigating the petrology, mineralogy, mineral chemistry, and fluid inclusions from a series of samples collected along a 1080 cm symmetrical traverse centred on the clinopyroxene-rich pegmatoid vein and including the surrounding coarsened granitic gneiss and subsequent surrounding regional migmatised gneiss. The obvious structural and geometric relationship between these three rock types makes this association ideally suited for the study of fluid-rock interaction under high-grade conditions.

The zone consists of a 0.5 m-wide, dark green, orthopyroxene-absent clinopyroxene-rich pegmatoid vein, which is characterized by an intergrown mass of megacrystic, semi-euhedral to anhedral clinopyroxene crystals up to 5-10 cm in size. This pegmatoid vein is surrounded on either side by a 0.5 meter-wide, coarsened overprint of red-pink, granitic gneiss, which grades into the unaltered regional migmatised granitic gneiss. Similar but smaller clinopyroxene-rich pegmatoid veins as well as clinopyroxene-bearing coarse patches in the migmatised granitic gneiss are also found in other parts of the Halmstad area.

EMP analysis of garnet, clinopyroxene, biotite, amphibole, and fluorapatite across the traverse indicates various mineral chemical trends including high Cl and low F values, low Fe and Ti values, and high Mn values in the pegmatoid dyke relative to the surrounding coarsened granitic gneiss and migmatised granitic gneiss. With the exception of Cl, diffusive trends are seen for these elements in the coarsened granitic gneiss. All minerals, with the exception of clinopyroxene are ubiquitous showing the same modal mineralogy both in the coarsened gneiss zone as well as in the surrounding granitic gneiss with the proviso that in the case of those samples containing clinopyroxene, modal amounts of hornblende and biotite are relatively less than in samples devoid of clinopyroxene.

Garnet-clinopyroxene and garnet-biotite geothermometers suggest an approximate temperature for the formation of the clinopyroxene-rich zone of 650-700°C. Subsequently, garnet-clinopyroxene-plagioclase-quartz barometry indicates a mean pressure of 750-820 MPa.

The fluid inclusions show a series of striking differences along the traverse. The regional migmatized granitic gneiss contains only aqueous inclusions, whereas the clinopyroxene-rich vein contains dominantly carbonic inclusions (ca. 76% of the fluid inclusion inventory) and subordinate water inclusions. The transitional coarse-grained granitic gneiss between the two contains carbonic and aqueous inclusions, but the aqueous inclusions are more abundant here compared to the clinopyroxene-rich vein (ca. 41% instead of ca. 22% of the fluid inclusion inventory).

The fluid inclusions can be grouped in (1) low-salinity solutes (ca. 8 mass% NaCl), (2) essentially pure water, (3) high-salinity $CaCl_2$-rich brines (20-21 mass% $CaCl_2$), (4) pure CO_2, and (5) aqueous-carbonic fluids. Mixtures between all types occur. CO_2 is found only in the clinopyroxene-rich and red gneiss zones, with the largest quantity in the clinopyroxene-rich zone, where it also has the highest densities.

The carbonic inclusions are always closely associated with the H_2O-NaCl inclusions with salinities of ca. 78 mass% NaCl, suggesting that these fluids were derived from one H_2O-NaCl-CO_2 fluid, which may have been present during granulite-facies metamorphism. This would concur with the finding of primary, peak-metamorphic fluid inclusions of the same composition in Opx-Cpx-Bt-Amph-Gt dehydration zones in the western wall of same quarry (Harlov et al. 2006). In the present Cpx-rich pegmatoid vein however, the original fluid seems to be poorly preserved. Rare aqueous-carbonic inclusions found in the pegmatoid vein are interpreted as samples of the original fluid. These inclusions show water volume fractions of 0.7 to 0.8 and have an estimated composition of $H_2O(87)CO_2(10)NaCl(3)$. The corresponding isochores cross-cut the peak-metamorphic conditions. Rock deformation (shearing) must have resulted in secondary pure carbonic inclusions trapped in healed microfractures (Fig. 1), whereas aqueous inclusions remained as clusters.
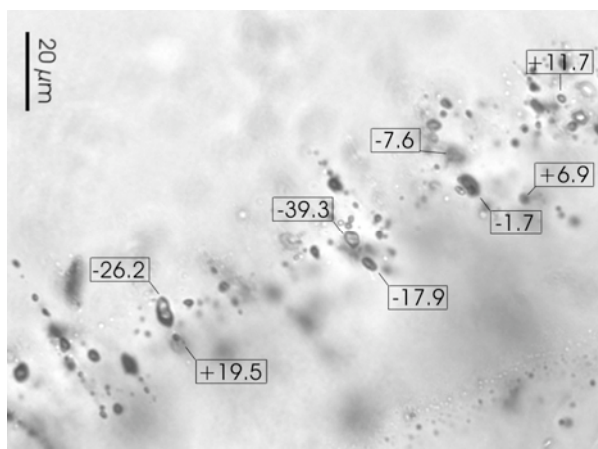
Fig. 1. Sheared carbonic inclusions in quartz from the Cpx-rich pegmatoid vein. Note highly scattering homogenization temperatures (°C).

In the clinopyroxene-rich vein the pure CO_2 inclusions are not only most abundant, but also best preserved. The homogenization temperatures of these inclusions concentrate between ca. −10 and 0°C, whereas homogenization temperatures in the reddish gneiss concentrate between ca. +12 and +24°C. The fluid inclusions in the clinopyroxene-rich vein are assumed to be trapped during an early stage of uplift, the ones with highest density of 1.114 g/cm^3 (T_h −39.3°C) must originate from conditions close to the metamorphic peak and survived uplift. Most of the carbonic inclusions in the reddish gneiss are likely to be re-trapped at low temperatures. This is also in accordance with the general lower total homogenization temperatures found for the aqueous inclusions in the reddish gneiss, which points to retrograde re-equilibration.

The homogenization temperatures of the migmatized granite are generally low $T_h$total <220°C. This is the only rock which contains $CaCl_2$-bearing brines. The homogenization temperatures of these brine inclusions are the lowest found (ca. 98 to 123°C) or the inclusions are monophase, suggesting re-equilibration below ca. 200°C 200 MPa. The $CaCl_2$ brines are considered the result of extreme retrograde rock alteration.

It can be concluded that the Cpx-rich pegmatoid vein must have formed at granulite-facies conditions in a tectonic fracture flushed with CO_2-rich fluids. The differences in the fluid inclusion inventory observed for the different rock types was strengthened by the different retrograde developments: the "dry" Cpx-rich vein best preserved the carbonic fluid inclusions, together with the aqueous inclusions with highest homogenization temperatures, and also some peak-metamorphic H_2O-NaCl-CO_2 inclusions. The fluid inclusions in the surrounding "wet" rocks were most intensively equilibrated at low temperatures.

REFERENCES

Harlov D.E., Johansson L., Van den Kerkhof A.M.Förster H.-J. (2006). *Journal of Petrology*47: 3–33.

Fluid inclusions in datolite from siliciclastic peperite in a Jurassic pillow basalt series of a dismembered Dinaric mélange in NE-Hungary

Kiss, Gabriella*, Molnár, Ferenc* and Zaccarini, Federica**

*Department of Mineralogy, Eötvös Loránd University, Pázmány P. stny. 1/c, 1117 Budapest, Hungary
**Department of Applied Geosciences and Geophysics, University of Leoben, Peter Tunner Str. 5, 8700 Leoben, Austria

The pillow basalt blocks of the Szarvaskő Unit in the SW-Bükk Mountains are parts of an accretionary mélange which was displaced from the Dinarides to its current position in NE-Hungary by the Mid-Hungarian fault system during the Alp-Carpathian collision (e.g. Haas & Kovács 2001; Dimitrijević et al. 2003). The origin of the basalt is related to a back-arc-basin or marginal sea environment in the Mesosoic Vardar Ocean (e.g. Harangi et al. 1996; Aigner-Torres & Koller 1999).

The Egerbakta quarry in the Szarvaskő Unit exposes a pillow basalt block from a submarine basaltic volcano, in which the so-called peperitic facies **s.l.** (i.e. local admixture of siliciclastic sediments into the pillow sequence) occurs among the closely packed pillows and some pillow fragmented hyaloclastite breccia volcanic facies (Kiss et al. 2011). A quite limited seawater-rock interaction resulted in precipitation of hydrothermal minerals, such as quartz, calcite, chlorite and prehnite. They occur in every volcanic facies, mainly in short veinlets within the pillows, however, the matrix of the pillow fragmented hyaloclastite breccia facies contains the best example of this kind of hydrothermal mineralization. The upheated seawater related origin is proven by fluid inclusion data obtained from calcite, where 4.59 mass% NaCl salinity was detected. These elevated salinities are results of seawater-rock interaction. Formation temperature-pressure conditions of 160 °C and 0.5 kbar were determined by combining results of fluid inclusion microthermometry with chlorite thermometry (Kiss et al. 2011). Another mineral association of prehnite, calcite, quartz and chlorite, as results of the later Alpine low grade metamorphism (Sadek et al. 1996) are confined to veins cross-cutting the basalt pillows.

Occurrence of datolite $[CaBSiO_4(OH)]$ is restricted to cross-cutting veins in the peperitic facies only, together with prehnite and minor chlorite, calcite and albite. The prismatic and more isometric datolite crystals are anhedral to euhedral (in cavities of the veins) and their size can reach up to 7 mm. Close to the walls of the vein crystals are dull, due to the presence of large amount of fluid inclusions, while they are water clear in the cavities of the central parts of the veins. Prehnite formed earlier and also together with datolite, while chlorite precipitated synchronously with it.
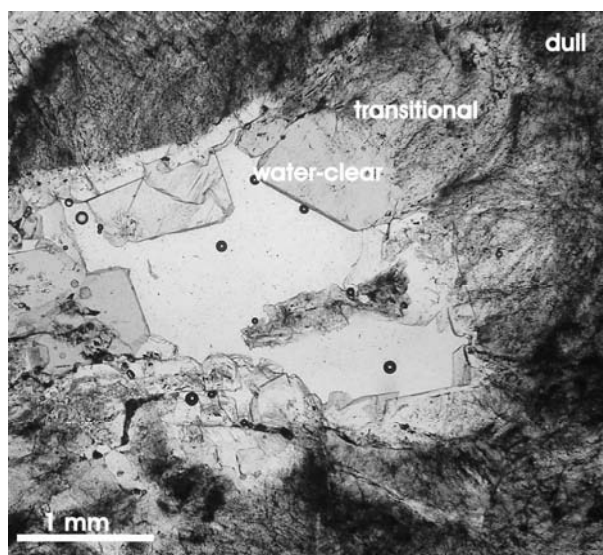

Fig. 1: Different types of datolite around a cavity in a vein.

The electron microprobe analysis revealed that there is no significant compositional difference among the different types of datolites. All of them consist of typical datolite constituents; Ca, B, Si with minor Al (most probably as substitution of Si, as shown by slight negative correlation between Si-Al), K, Na, F and Cl.

The primary fluid inclusions of 5-30µm size in datolite form an: (P1) water-rich $L_{aq}+V_{CH4}$ inclusions and (P2) liquid methane-rich L_{CH4} inclusions, thus petrography suggests their entrapment from an immiscible fluid system. A minor amount of invisible aqueous phase may occur in the P2 type primary inclusions. The estimated volume fraction of V_{CH4} in P1 type inclusions varies between 5 and 20 %. Salinities estimated from the ice melting temperatures are between 0.4 and 1.8 mass% NaCl Calculations based on the Raman spectra of the aqueous fluid also proved low salinities (around 1.22 mass% NaCl) for P1 inclusions. These low salinities are sensibly lower than values of seawater. This observation confirms that datolite (and the host hydrothermal veins) does not represent a product of seawater-rock interaction. Raman spectroscopy of the P1 inclusions proved the presence of methane in the vapour phase of aqueous inclusions, however, its amount is rather small as it is illustrated by absence of methane peak in the homogenized liquid at the T_h and by the absence of observable clathrate formation during freezing experiments. A slight decrease of the Raman shift was found in relation to vapour methane in the P2 inclusions confirming the liquid state, but no trace of water was detected even at the T_h of P1 inclusions. Therefore the thermodynamic behaviour of the P2 inclusions is modelled by properties of pure methane.

Entrapment conditions of P1 and P2 inclusions are obtained by intersections of $T_h(LV{\rightarrow}L)$ for P1 inclusions and representative isochors of P2 inclusions. Results indicate increasing temperature and pressure during the crystallization from dull (180-200 °C, 0.5 kbar) through the transitional (200-230 °C, 0.7-0.9 kbar) to the water-clear (~240 °C, 1.1 kbar). Composition of chlorite associated to the transitional datolite also suggests a formation temperature around 220 °C.

Datolite contains at least three generations of secondary inclusions. A group of $L_{aq}+V_{CH4}$ inclusions (S1) with uniformly $^{vap} \approx 10$ % and an average $T_h = 162°C$ and 0.9 mass% NaCl salinity. The other two generations of secondary inclusions (S2 and S3)) have apparently monophase L_{CH4} composition. Their average $T_h(LV{\rightarrow}L)$ is -85.2 °C

(S2) and -94.5 °C (S3). The presence of methane in the vapour phase of S1 and in the liquid phase of S2 and S3 was proven by Raman spectroscopy

The precipitation of datolite took place under conditions of increasing temperature and pressure. This could have happened during the progression of the low-grade Alpine metamorphism, when in the area of the SW-Bükk Mts. a maximum of 270-285 °C at 1.5-2 kbars was (Sadek et al. 1996, Péntek et al. 2006). The source of the boron and the methane was most likely the siliciclastic sediment in the peperitic facies of the submarine basaltic volcano. Methane was also present in fluids circulating in fractures of basalt after the datolite precipitation (S1, S2, S3 inclusions).

REFERENCES

Aigner-Torres M., Koller F. (1999) **Ofioliti** 24: 1-12.

Dimitrijević M. N., Dimitrijević M. D., Karamata S.,Sudar M., Gerzina N., Kovács S., DosztályL., Gulácsi Z., Less Gy., Pelikán P.(2003)**Slovak Geol Mag** 9/1: 3-21.

Haas J., Kovács S. (2001) **Acta Geol Hung** 44/2-3:345-362.

Harangi Sz., Szabó Cs., Józsa S., Szoldán Zs.,Árva-Sós E., Balla M., Kubovics I. (1996)**Internat Geol Review** 38/4: 336-360.

Kiss G., Molnár F., Koller F, Péntek A. (2011) **MittÖsterr Mineral Ges** 157: **in press**

Péntek A., Molnár F., Watkinson D. H. (2006) **GeolCarpath** 57/6: 433-446.

Sadek G. D., Árkai P., Nagy G. (1996) **ActaMineral Petrogr Szeged** 37: 99-128.

Small and large scale inhomogeneities in the magma chamber of the 18.6 ka Sarno plinian eruption of Mt. Somma-Vesuvius (Italy) based on melt inclusion studies in nodules

Klébesz, Rita*,**, Bodnar, Robert J.*, De Vivo, Benedetto**, Lima, Annamaria**, Petrosino, Paola**

*Dept. of Geosciences, Virginia Polytechnic Institute and State University, 4044 Derring Hall, Blacksburg, VA24061, USA
**Dept. of Earth Sciences, University of Naples "Federico II", Via Mezzocannone 8, Naples 80134, Italy

The Sarno eruption is one of the oldest and largest eruptions of Mt. Somma- Vesuvius, but it has been little studied. Nodules (coarse-grain "plutonic" rocks) were collected from the phreato-magmatic phase of the Sarno eruption in C. Traianello quarry, located on the NE slope of Mt. Somma. These nodules are interpreted to be wallrock or previously crystallized material that was transported to the surface by the Sarno magma. Based on the mineral composition, most of the rocks can be classified as monzonite-monzogabbro, only one sample is more evolved with a syenitic composition. The nodules consist of An-rich plagioclase, K-feldspar, clinopyroxene (ferro-diopside), mica (phlogopite-biotite) ± olivine and amphibole. Unlike most of the nodules from the other eruptions, these samples do not have typical cumulative texture, but rather display a porphyrogranular texture. The phenocrysts are large (up to few mm) with variable compositional zoning, most commonly normal or reverse zoning, but irregularities and resorbtion surfaces are not observed. The phenocrysts are often partially to completely enclosed by later poikilitic feldspars. Sometimes irregular intergrowths of alkali feldspar and plagioclase and smaller mica, Fe-Ti oxides and/or clinopyroxene crystals can be observed. These features are interpreted as crystallized melt pockets. Based on their textures, the nodules may represent the *in situ* crystallizing melt on the walls of the magma chamber. The lack of the interstitial glass, which is common in nodules from similar environments, can be explained by the time difference between the plinian and the phreatomagmatic phase. The relatively long time difference might have provided sufficient time for the interstitial melt in Sarno samples to crystallize.

Minerals, especially clinopyroxenes, are abundant in crystallized silicate melt inclusions. They are usually 20-30 µm, but their size ranges between 5 and 60 µm. They have rounded to angular shape. Two types of melt inclusions can be distinguished. Type I consists of mica, Fe-Ti-oxide minerals and/or dark green spinel, clinopyroxene, feldspar and bubble. No volatiles (CO_2, H_2O) could be detected in the bubbles by Raman spectroscopy. Type II Inclusions are generally lighter in and they contain subhedral feldspar and/or glass and several dark phases which are possibly oxide minerals and/or tiny bubbles. The melt inclusions are randomly distributed in the crystals or they appear along a growth zone and are therefore interpreted to be primary. While the two types of inclusions are spatially associated and appear in the same zone, which would suggest a genetic relationship, the nature of any genetic relationship between the two types of MI is unclear.
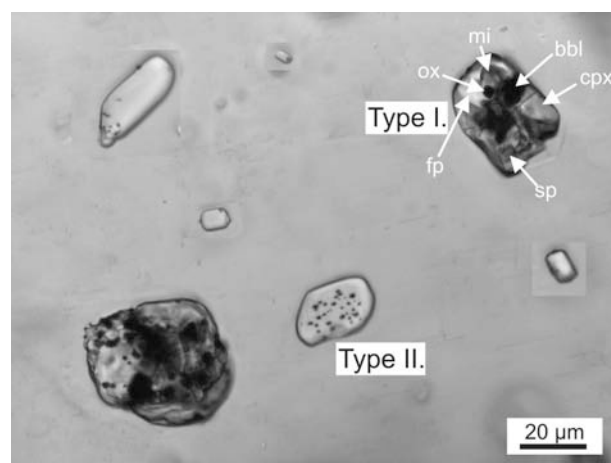

Fig. 1. Crystallized melt inclusions in clinopyroxene host. Cpx – clinopyroxene, sp – spinel, mi – mica, ox – Fe-Ti-oxide, fp – feldspar, bbl – bubble.

Heating experiments have been carried out to rehomogenize the inclusions for further analyzes. The two types of inclusions have similar homogenization temperature, ranging from 1205°C to 1250°C, based on their size. Larger MI homogenize at slightly higher temperatures compared to smaller MI. All crystals were quenched immediately after homogenization. In some cases a bubble reappeared during quenching, indicating that the homogenization probably was not complete, or the inclusion leaked during heating, or that the melt was close to volatile saturation and re-exsolved the dissolved volatiles during the quench. During reheating inclusions started melting at about 1050-1100°C. Mica starts melting just slightly above 1100°C, and it disappears about 1150°C. The bubbles become smaller during heating and they are the last phases to disappear, unless spinel is present, then that is the last phase to melt.

Crystallized melt inclusions in clinopyroxenes have been analyzed by LA-ICP-MS. Even though the two types of inclusions behave similarly during the heating experiment, they have significantly different compositions. Type I. (phono-tephrite – tephra-phonolite, similar to the products erupted during the plinian phase) are enriched in alkaline and incompatible elements compared to type II MI (basalt-basaltic andesite). Plotting the composition on MgO vs. SiO_2, Na_2O and CaO diagrams, a continuous trend can be observed indicating the evolved inclusions likely represent a melt that differentiated from the basaltic melt represented by type II inclusions. On the other hand, trace element contents of the inclusions define two distinctive groups that appear to be unconnected. This and the spatial distribution of the melt inclusions indicate that the melts are not differentiated from each other. Based on the calculated distribution coefficient between the host and the melts represented by the inclusions, only type I MI compositions are in or close to equilibrium with the host clinopyroxene. There is no indication that the composition of type II MI has been modified by entrapped solid phases, however it cannot be excluded. Type II inclusions may represent inhomogeneities within the crystallizing melt, but their high portion (about 20-30%) of the inclusions and their uniform composition makes it unlikely and suggest another origin. Further analyzes will be carried out to determine the volatile content and the major and trace element composition of the rehomogenized melt inclusions in order to explain the observed inhomogeneities and estimate a minimum crystallization depth.

Fluid inclusions in Sarno samples are usually single phase, secondary in origin, and not associated with melt inclusions, unlike in other nodule samples from Mt. Somma-Vesuvius. The observed differences in textures and melt and fluid inclusion populations in the samples from Sarno eruption compared to those from other eruptions of Mt. Somma - Vesuvius may indicate different pre-eruptive conditions and processes.

Phase state of NaF-containing fluid from synthetic fluid inclusions at 700ºC and 100–300 MPa

Kotelnikov, Alexey* and Kotelnikova, Zoya**

*Institute of Geology of ore deposits, Mineralogy, Petrology and Geochemistry of RAS. Staromonetny, 35.Moscow. Russia.
**Institute of Experimental Mineralogy of RAS. Chernogolovka, Institute av., 4. Russia

Fluid inclusions in quartz were synthesized by the method of crack healing at temperature 700ºC and pressures 100, 200 and 300 MPa from 0.5M solutions, containing sodium fluoride. Fluid inclusions study result in fluid was heterogeneous at run conditions.

Experiments at a pressure of 100 MPa
Two- and three-phases inclusions runs.Two forms of   under heating of multiphase inclusions observed: 1 no changes take place in inclusions under cooling to −90ºC and heating up to 450ºC inclusions were frozen at −90ºC. The precise measur of temperatur and melting failed over similarity of the coefficients of the rejection. At 170–180ºC the of crystals precipitated from solution, but subsequent heating up to 210–220ºC result in its partial re-solution. Precipitated crystals disappeared at 350ºC. t 170–350ºC the salt solubility is lower tha at room temperature. At temperature 250ºC the liquid separation on two phases in the presence of vapor and solid occurred in the inclusions. ew liquid appeared around vapor bubble and was absorbed at 387–389ºC.L+V inclusions show two different way of phase transformation under heating liquid separationtemperatures were −0.2 −2.1ºC; homogenization in L and V at 386−394ºC.
*Experiments at a pressure of 200 MPa.*L+V inclusions   er   run. Temperatures of the homogenization with critical phenomena were 354–361ºC, −1.9 o −2.3ºC. un conditions correspond to vicinity of critical point

*Experiments at a pressure of 300 MPa.*V+L and V+Gl (glasslike phase) re observed after run. V+L inclusions homogenize at 348–372ºC. V+Gl inclusions show two different style of phase transformation: 1 At 350ºC the liquid separation on two phases in the presence of vapor occur in the inclusions. New liquid appeared around vapor bubble, partial homogenization in L take place at 365–373 C 2 in under heating (Fig. 1). Bubbles coalesc and at approximately at 350ºC the liquid immiscibility . Vapor dissolved at 385–389ºC and then inclusions .
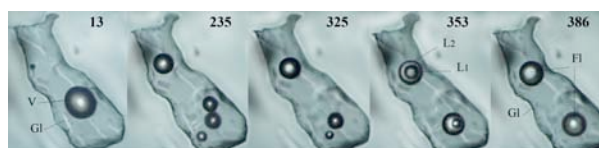
Fig. 1. Phase transformation under heating in Gl+V inclusion, synthesized at 700ºC and 300MPa.

bservations Such compositions are known. For example,

The significant peculiarity of studied system is re-immiscibility of the liquid, entrapped in higher heterogeneous area. Then heterogenization may take place in two (or more for multicomponent systems) stages at large scale of *TP*-parameters. The immiscibility is mode of matter re-distribution between immiscible phases. multistage of is important the enrich or deplet the fluid phase

The separation of the liquid in the presence of vapor and solid are described for natural inclusions too [1, 2].

REFERENCES
Kaluzsnyi V.A. (1956) Mineralog. Sbornik LvovUniversity (in Russian). N10: 77–80.
Ahmad S.N., Rose A.W. (1980). 75:229-250

Formation conditions of the Bystrinskoe Cu-Au skarn-porphyry deposit (Eastern Transbaikalia, Russia): The first results of mineralogical and fluid inclusion studies

Kovalenker, Vladimir, Yazykova, Yulia and Krylova, Tat'ana

Institute of Geology of Ore Deposits, Petrography, Mineralogy, and Geochemistry (IGEM) RAS, Staromonetny per. 35, Moscow 119017, Russia

The Bystrinskoe Cu-Au skarn-porphyry deposit is located in Gazimuro-Zavodsky ore district (Eastern Transbaikalia). It is confined to Bystrinsky structure of central type composed of terrigenous and carbonate formations of Paleoproterozoic to Mesoproterozoic and Mesomesozoic (limestones, sandstones, argillites, aleurolites, less often conglomerates) which are cut by diorites, diorite-granodiorites, granites and their porphyries, andesites and dacites of Bystrinsky stock. The dike suite is represented by granodiorite-porphyries, granite-porphyries, lamprophyres, and basalts. The large ore bodies are located along the contact of magmatic and terrigenous-carbonate sedimentary rocks in southern and eastern parts of the stock. The commercial mineralization is represented by disseminated (80 %) and streaky (20 %) ore types.

The history of hydrothermal mineralization is considered to include three phases.

I. The magmatic phase comprised the magnesium skarn formation synchronized with the injection of diorite porphyries.

II. The postmagmatic phase included retrograde alteration of Mg skarns, formation of Ca skarns and diaphtoric transformation of them. At this phase, there was a formation of potassium (K-feldspar and biotite) metasomatites (in magmatic rocks) synchronous with skarns formation.

III. In a hydrothermal (ore) phase, the following mineralization types were consecutively formed: the scheelite-molybdenite, ide (pyrrhotite-pyrite-arsenopyrite-chalcopyrite), base metal (galena-sphalerite), antimonite and quartz-carbonate mineralization which overprinted both skarns and magmatic rocks and were accompanied by zonally distributed quartz-sericite metasomatites, argillizites, and secondary quartzites.

Similar relations are typical of Cu-porphyry systems with various (porphyry, epithermal, skarn) mineralization (Sillitoe, 2010), however, though, within the limits of the Bystrinskoe deposit, the epithermal mineralization was not discovered yet (could have been destroyed by erosion), its ore-forming system can be qualified as skarn-porphyry-epithermal one.

The most widespread ore mineral in skarn is magnetite which is represented by monomineral cryptocrystalline accumulations. It is less widespread in ide assemblages of the ore-bearing phase where it develops at the expense of hematite and pyroxene. A ide mineralization is composed of pyrite, chalcopyrite, pyrrhotite and marcasite (result of pyrrhotite diidization), and also arsenopyrite and earlier not reported at the deposit cobaltite, which form inclusions in pyrite and chalcopyrite. This mineralization is productive on gold, presented here as native gold which is one of the latest minerals of this assemblage. It was observed in the form of fine inclusions in pyrite, on border between pyrite and chalcopyrite, magnetite and chalcopyrite. Share of Ag in native gold varies from 18.1 to 33.7 at%.

The first results of fluid inclusions (FI) study for the deposit (based on the THSMG-600, Linkam device), characterize mainly FI in amphibole, scheelite, quartz and calcite from skarn-ore mineralization. They are summarized on diagrams T_h - C and T_h - T_e. (Fig.1).

The *amphibole* contains three-phase (gas + solution + a solid isotropic phase) and two-phase (gas + solution) inclusions. Their major T_h range is from 421 to 382°C. Any detailed freezing studies were impossible because of too small FI sizes. Some indirect data (freezing temperature of solution near 90°C) testify that some bivalent cations were

present in solutions of FI and the concentration of solutions was rather high (a gas phase essentially increases its size during cooling). A solid phase in three-phase FI was dissolved at 244°C, that corresponds to concentration of 34.5 % NaCl The pyroxene comprises mainly two-phase (gas + solution) FI with the solutions of NaCl composition and 8.4 5.0 concentration.

The *scheelite* has only two-phase FI (gas + solution), with T_h ranging in 335 - 277 and 195 -149°C intervals. All of them have NaCl composition and concentration from 22.4 to 6.5 %. Correlation between T_h and C is not observed (Fig. 1)
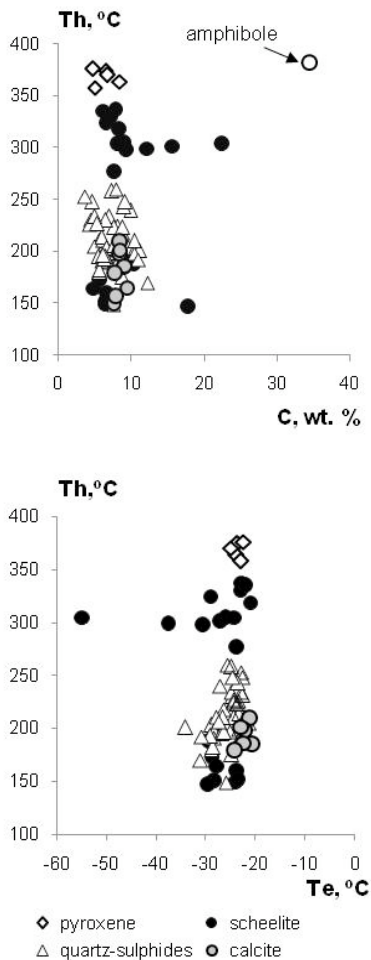
Fig. 1. The results of FI studies of skarn-ore mineralization of the Bystrinsky deposit.

In *quartz* there are two-phase FI of two types: 1 with the gas phase comprising up to 10 % of FI, and 2 essentially gaseous FI, usually with a film of solution at FI walls. The FI of the first type contain water-salt fluid of NaCl composition with concentration 11.2 - 6.2 % and T_h=248 -170°C. The inclusions of the second type are filled with practically pure liquid CO_2 (T_m = ‒-56.7 ‒57°C) or with the carbonic acid containing some other gases – impurity (T_m = ‒60.4 58.8°C). The CO_2 homogenizes into a liquid phase at the temperature range from 30.2 to 7.3°C. In calcite, all FI have two-phase composition (gas + solution) and NaCl solutions with concentration 9.17.7 % and T_h = 210 179°C (Fig.1).

The FI pressure was calculated using FLINCOR (Brown, 1989) code. For FI with CO_2 T_m from -60.4 to -58.8 which contain up to 0.5 1% of methane (samples 107-107), the CO_2 partial pressure at 200°C 310 - 320 bar. For FI with CO_2 T_m from ‒57 to ‒56.7°C, containing CH_4 less than 0.03 - 0.04%, pressure was calculated as pressure of pure CO_2. According to this estimate, the pressure during mineralization could vary from 1600 to 600 bars.

The obtained data show that a skarn-ore mineralization was formed in a wide range of temperature (420 170°C) and pressure (1600 - 310 bar). The fluids had mainly NaCl composition and moderate concentration (6 - 22 % NaCl). The CO_2 prevailed in the gas phase of fluids. Together with the data of mineralogical research considered above these parameters can testify that studied skarn-ore mineralization of the Bystrinskoe deposit is quite comparable by its features to mineralization formed as a result of activity of skarn-porphyry-epithermal ore-forming systems (Heinrich, 2005; Sillitoe, 2010), that essentially expands a potential ore capacity of the given deposit at the expense of porphyry and, probably, epithermal ore types.

REFERENCES

Brown P.E. (1989.) Am. Mineral. 74: 1390-1393

Heinrich C.A. (2005.) Miner.Deposita. 39: 864-889

Sillitoe R.H. (2010.) Econ. Geol. 105: 3-41

Characteristics of the ore fluids during magnesite metasomatism in the Satka Ore Field (Veitsch type, Urals, Russia)

Krupenin, M. T.*, Garaeva, A. A*., and Prochaska, Walter**

* Zavaritskii Institute of Geology and Geochemistry, Ural Division, Russian Academy of Sciences, Pochtovyi per. 7, Yekaterinburg, 620151, Russia
** Geology and Economic Geology, Department of Applied Geology and Geophysics, Montanuniversitaet Leoben, Peter-Tunner-Str. 5, 8700 Leoben, Austria

Of crucial importance in studying the "sparry magnesite problem [Aharon, 1988]" are the thermodynamic conditions of formation this type of deposis. The investigation of fluid inclusions in magnesites and host rocks along with other geochemical methods allows to specify the parameters of the replacement mechanisms. We investigated some features of fluid inclusions in the stratiform Satka ore group (coarse-grained "Veitsch Type" magnesite deposits) from the Southern Urals magnesite province in Russia. 90 % of the Russian periclase production comes from the Satka ore field.

The study of the chemical composition of the fluid inclusion (crush-leach analysis) showed an evaporitic trend for the magnesites in the Na/Br-Cl/Br diabram for the Satka deposits and for other sparry magnesite deposits of Southern Urals province. The host limestones in this plot are in the area of sea water Krupenin Prochaska, 2005. This method is very useful in the case of very fine size of fluid inclusions in host rocks. A series of special structural features like pseudomorphs after sulphates, tepee-structures and angle-shaped coarse-grained white dolomite, sometimes with chert in fine-grained grey dolostones are developed in the magnesite-bearing horizon of the Satka formation (Mezoproterozoic age) indicating pre-evaporitic conditions during sedimentation. Buried evaporitic brines in this sequence may be the original source of magnesium for the metasomatic fluids. It proposes to use a seepage reflux model for magnesite precipitation, similar to the proposed formation of the sparry magnesites of Austria Prochaska, 2000.

Microcryometric and microthermometric study of fluid inclusions in the magnesites and adjacent metasomatic minerals are very important for understanding of the physico-chemical conditions of metasomatic process. Nests and clusters of dolomites and quartz can be found in the magnesites. It seems that the studied mineralizations were formed at one single stage of metasomatism. At preliminary stage about 130 inclusions were studied. The inclusions of the magnesites and of the dolomite/quartz clusters are more of less the same (>15 % NaCl. with ice melting temperature from -10C to -28C) and temperatures of homogenization varies from 120C to 400C.

The inclusions were studied with successive microcriometric and heating study of every inclusion. We used a THMSC-600, «Linkam» equipment which allows to measure temperatures of phase transitions from -196C to +600C. We used samples from the quartz nests from a dolomite collaps-breccia in a distance of 8-10 m laterally from magnesite body contact. Quartz precipitated in the collaps-breccia as secretions (fine-bended agate-like filling of the nest) and is a perfect mineral for keeping primary inclusions in comparison with carbonates [Goldstein, Reynolds, 1988]. These thin lays were formed during high alkaline magnesium metasomatism in external parts of magnesite bodies.

The majority of the studied inclusions are of primary or primary-secondary type. They occur as gas-liquid 2-phase vacuoles the different forms like orbicular and negative crystals in the size of 5-15 microns. The majority of the considered inclusions contain a saline solution and the gas phase amounts 10-25 %, higher filling rates are rare. Only in four cases we found 3-phase inclusions with liquid CO_2. In three cases we found 3-phase inclusions with a solid phase in the vacuoles which turned out to be halite.

The salt content of the solutions was defined by the temperature of eutectic fusion [Borisenko,

1977]. Concentration of salts in inclusions was estimated on temperature of last ice melting for the salt system $CaCl_2$ Goronovsky et al., 1987. The salinity of the liquid phase is calculated as $CaCl_2$ as the temperature of fusion of ice is in most cases below the eutectic point of NaCl (-212C). For the overwhelming majority of inclusions a salinity of 28-32 % $CaCl_2$ is calculated, only 11 inclusions (with mainly secondary inclusions) have a salinity of 5-8 % $CaCl_2$ (see 1). Prevailing temperatures of liquid-vapor homogenization of inclusions are in the range from 85 to 235C, (median 149C). Temperature calculations based on cation exchange thermometers (Na/Li) indicate a formation temperature of the magnesites of ~ 130°C which confirms the average temperatures of homogenization of the fluid inclusions. In one sample 3 inclusions with liquid-vapor homogenization in an interval 386-440C were obtained. For the sample having high-temperature inclusions, the presence $MgCl_2$ and KCl is supposed. This means, that the original brines had elevated temperatures and contained chlorides of magnesium and potassium. We assume, that the fluids from the quartz –dolomite nests in the outer zone of the magnesite bodies contain a fractionated residual fluid from which the major amounts of magnesium has already been fixed in the areas of the magnesite precipitation. Therefore the prevalence of $CaCl_2$ in the brines of this external zone is quite naturally.

The calculation of the fluid pressure has shown comparable results in an interval between 590-664 bar. If to admit, that the fluid during Mg-metasomatism was under lithostatic pressure the calculated pressure of a fluid phase corresponds to a depth of about 20 km. This depth corresponds to the overall thickness of the magnesite-bearing horizon of the Satka Formation and the overlying Bakal Formation. Then a large break in sedimentation with a pronounced unconformity, connected with the formation of the Mashak riftogenic structure (volcano-terrigenous graben) to the east of Satka ore field follows. The riftogenic event was accompanied with crustal extension, regional development of a diabasic formation and the penetrating of granitoids, including Berdyaush rapakivy granite in the northern periphery of the Satka ore field (1371.3 ± 26 Ma, Sm–Nd method Ronkin et al., 2007). The homogenization temperatures of the fluid inclusions, obtained in the present research, mismatch temperatures of heating of country rocks as a result of immersing into depths of 15-20 km, and it is probable that additional heating of the fluids from an additional heating source occurred with the Berdyaush rapakivy pluton being the heat-source. The results obtained well fit into the concept of Mg-metasomatism as a result of riftogenic heating of buried evaporitic brines in the permeable dolomitic collaps-breccias of Satka Formation Krupenin Prochaska, 2005.

References:

Aharon P. (1988) Chem. Geol 1988. 69 127–145.

Borisenko A.S. (1977) *Geol Geoph* 8 16-27.

Goldstein R.H., Reynolds T.J. (1988) *SEPM short course.* 31 195 p.

Goronovsky I.T. et al., (1987) The Brief Directory in Chemistry. Kiev, Naukova Dumka. 828 p.

Krupenin M.T., Prochaska W., (2005) *Doklady Earth Sciences*, 403A 838–840.

Prochaska W. (2000) Min Slov 32 543-548.

Ronkin Yu. L., Maslov A. V., Kazak A. P. et al. (2007) *Doklady Earth Sciences*, 415A 835–840.

A revised model for the interpretation of pressure and salinity from fluid inclusions that homogenize by halite disappearance

Lecumberri-Sanchez, Pilar, Steele-MacInnis, Matthew and Bodnar, Robert J.

Department of Geosciences, Virginia Tech, 4044 Derring Hall, Blacksburg, VA, 24061, USA

Fluid inclusions that homogenize by halite disappearance at a temperature higher than the liquid-vapor homogenization temperature are reported in many ore deposits. Becker et al. (2008) developed a model to estimate the pressure at the halite melting temperature based on the temperature of bubble disappearance and T_m(halite) for inclusions that homogenize by halite disappearance. The model is generally consistent with the available experimental data for the liquidus at P above 100 MPa and above 300°C. However, for PTX conditions outside of that range, the model of Becker et al. (2008) yields inconsistent results – for example, if pressure and/or homogenization temperature are below 300°C, the pressure obtained from Becker et al. (2008) for a given and differs significantly from the known halite liquidus (Bodnar, 1994).

In the present study, we extend the model of Becker et al. (2008) to T_h(LV→L) and conditions that are outside of the range of experimental conditions of the earlier model. The model is based on the fact that as fluid inclusions are heated from the temperature of liquid-vapor homogenization to the temperature of halite disappearance, the inclusion must follow an isochoric path. Assuming that no leaking or stretching takes place, this path has to satisfy three main conditions: (1) the volume of the fluid inclusion is constant, (2) the masses of H_2O and NaCl in the inclusion do not change, and (3) the P-T conditions remain on the halite liquidus at all times (liquid is in equilibrium with halite until halite disappears at).

Using these constraints, the PTX evolution of FI along the liquidus has been calculated. For any composition, a and combination produces a single P-X point. The model has been tested for between 100 and 600°C and pressures between the liquid-vapor-halite (L+V+H) three-phase equilibrium curve and 300 MPa. Each - combination produces a single P-X data point.

Pressure P, halite disappearance temperatures and liquid-vapor homogenization temperatures combinations obtained from the mass and volume balance calculations have been regressed to generate an equation that predicts pressure as a function of and (Fig 1). In the same way, composition – - data have been regressed and provide an equation that predicts the inclusion salinity as a function of and (Fig 2).
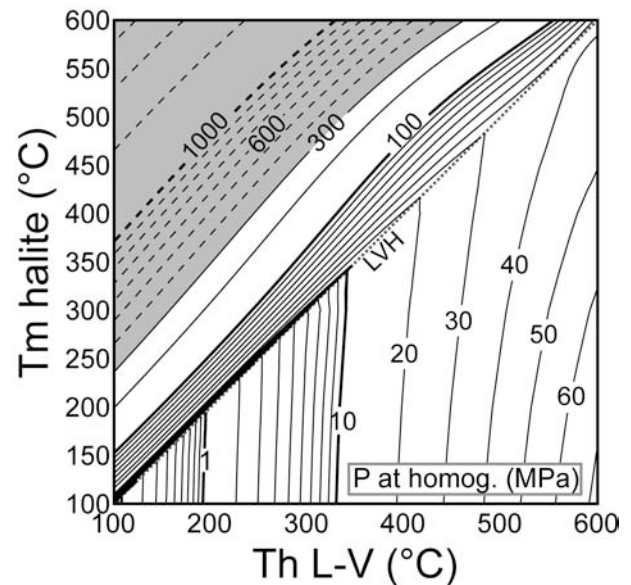
Fig. 1. Isobars predicted by the model as function of –. The grey area is beyond the limits of the data used in this model
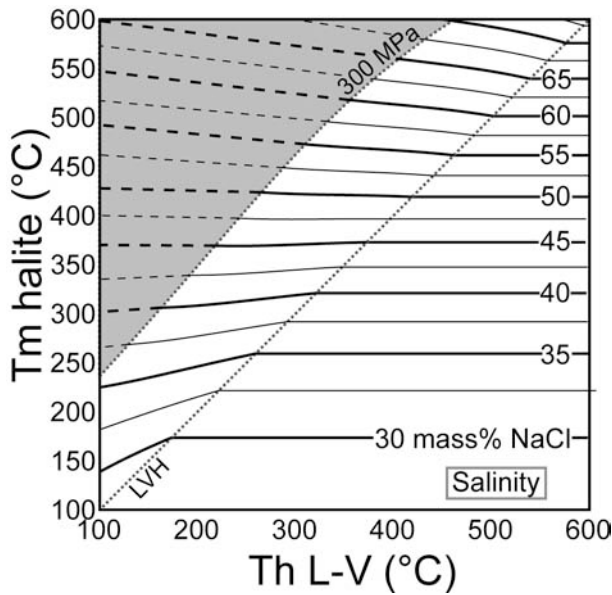
Fig. . Isopleths predicted from $T_hLV - T_mhalite$ using the model. The grey area is beyond the limits of the data used in this model and has been obtained from extrapolation of the trends below 300 MPa.

The resulting model is consistent with the available experimental data for the halite liquidus (Becker et al., 2008; Bodnar, 1994 and references therein). The equations remove the anomalies present in the previous model of Becker et al. (2008). The equations provide a tool to calculate pressure at homogenization and salinity for fluid inclusions that homogenize by halite disappearance. These equations are valid for inclusions in which is between 100-600°C and pressure at the temperature of halite disappearance is between the L+V+H equilibrium curve and 300 MPa.

REFERENCES

Becker, S.P., Fall, A., Bodnar, R.J. (2008) *Econ.Geol* 103: 539-554.

Bodnar R.J. (1994) *Geochim Cosmochim Acta* 58:1053-1063

PTX evolution of mineralizing fluids in the porphyry copper-high idation epithermal system at Red Mountain, AZ

Lecumberri-Sanchez, Pilar*, Bodnar, Robert J.* and Kamilli, Robert**

*Geosciences Department, Virginia Tech, 4044 Derring Hall, Blacksburg, VA, USA
**US Geological Survey 520 North Park Avenue, Suite 355, Tucson, AZ, USA 85719

Red Mountain is a Laramide-age porphyry copper deposit located in southern Arizona near the border with Mexico. Porphyry copper systems are abundant in this region and, due to a complex structural evolution, the various deposits show variable degrees of erosion. Within this context Red Mountain, with its shallow level of erosion and well-preserved lithocap, provides an exceptional example of the transition from the deeper porphyry copper environment to the shallow high-idation epithermal system.

Two main mineralization zones occur in this deposit: a chalcopyrite-bornite zone in the deeper porphyry system and an enargite-chalcocite zone in the shallow high-idation epithermal system.

In the present study, we have conducted detailed petrographic and microthermometric analysis of fluid inclusions (FI) related to specific mineralization and alteration types to characterize fluid evolution in the Red Mountain magmatic-hydrothermal system.

FI petrographically associated with chalcopyrite mineralization typically contain chalcopyrite daughter minerals and large vapor bubbles and are classified as inclusion type "B60" (according to the classification of Rusk et al., 2004, Fig. 1). These inclusions have homogenization temperatures (T_h) between 350 – 380 °C and salinities between 3 and 5 eq mass% NaCl. Later fluid inclusions in chalcopyrite-bearing samples are frequently characterized by halite-bearing FI that homogenize by halite disappearance at temperatures of 350 - 420°C (Fig. 2).

FI within well-defined fluid inclusion assemblages (FIA) in chalcopyrite-mineralized samples often have constant T_h but T_m that varies by as much as 80°C. The constant T_h implies that no stretching has occurred. The variability in T_m could be a result of halite entrapment or necking down after halite began to precipitate in the FI but before a vapor phase had nucleated. If the variability in T_m is a result of halite entrapment, this indicates that FI were entrapped under halite-saturated conditions and the maximum pressure of entrapment would be between 70 MPa and 200 MPa. If the variability in T_m is due to necking, 70 - 200 MPa constitutes a range of *minimum* pressures of entrapment. Corn (1975) proposed that a few thousand meters of volcanics were probably eroded from Red Mountain following the mineralization event. If that eroded material was added to the sample depths (1 – 1.5 km) the expected lithostatic pressure at the given depth would be on the order of 100 MPa.
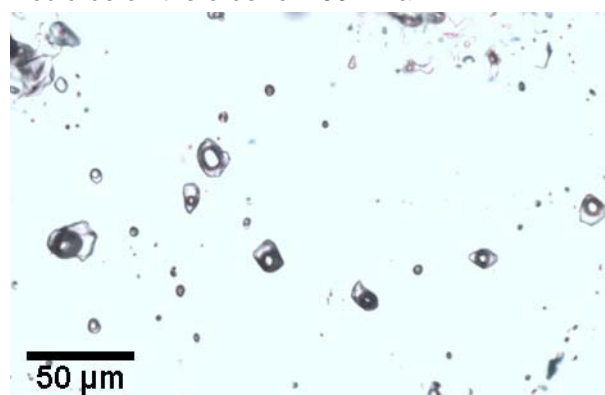
Fig. 1. FIA of chalcopyrite-bearing B60 FI in a chalcopyrite-bearing sample.
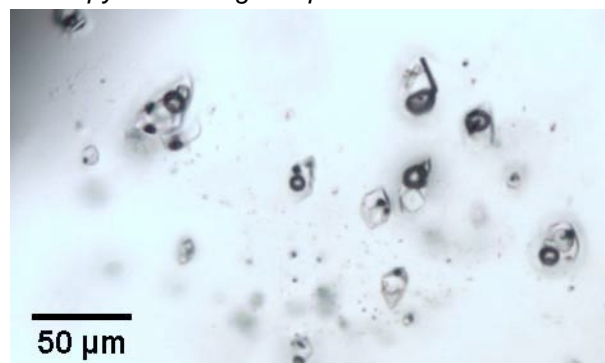
Fig. 2. FIA in a chalcopyrite bearing sample, containing halite-bearing FI that homogenize by halite disappearance.

Fluid inclusions spatially associated with enargite-chalcocite mineralization frequently show evidence of boiling (Fig. 3). A reconnaissance study of FI in this part of the system has yielded T_h values above 480 °C and salinities between 30 - 35 mass% NaCl. While these inclusions are spatially associated with enargite mineralization, a genetic relationship is yet to be identified. Slow ascent of fluids through the host rock would result in thermal equilibration between rocks and fluids and result in lower fluid temperatures. The existence of high temperature fluids in the shallow part of the system indicates a rapid fluid ascent from depth. These high temperatures observed in the high-idation part of the system are also consistent with recent observations by Mavrogenes et al. (2010).

Fig. 3. Coexisting liquid-rich and vapor-rich inclusions in an FIA from the shallow, high-idation part of the system (100 m present day depth).
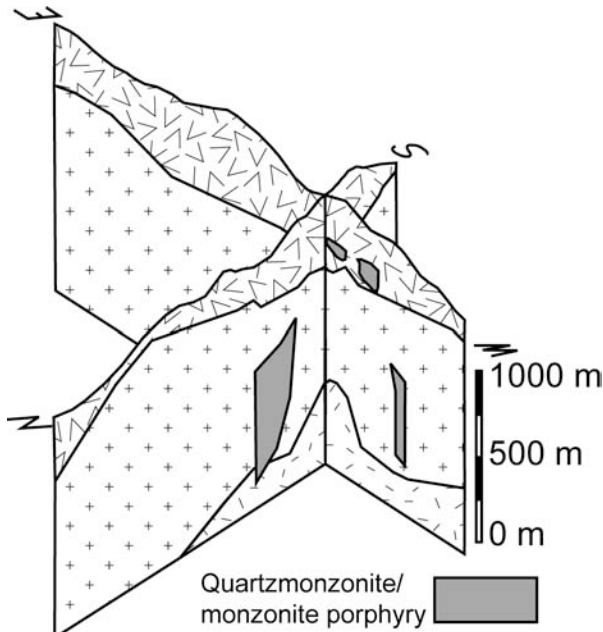
Fig. 4. Spatial distribution of porphyritic dykes and sills intersected during drilling at Red Mountain. The lithologies cut by the porphyry are from the surface downwards: trachyte, andesite and latite.
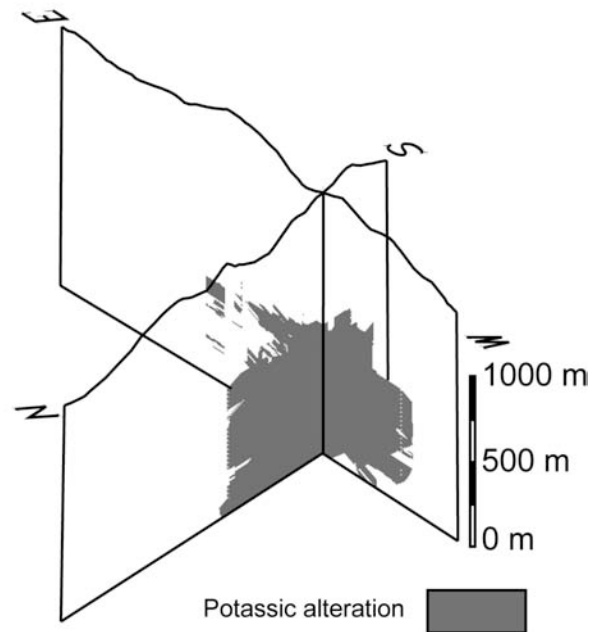
Fig. 5. Spatial distribution of potassic alteration at Red Mountain.

A three-dimensional model of Red Mountain (Fig. 4 & 5) shows that the alteration zones are not on the intersected porphyry dikes or sills. Therefore, a deeper porphyry intrusion may be the major contributor of mineralizing fluids to the system and the core of the Cu mineralization may be below the current depth of exploration.

Fluid inclusions at Red Mountain indicate that the observed chalcopyrite mineralization occurred at temperatures around 350°C and likely at pressures below 100 MPa. However, the lithology and alteration distribution indicates that the drill core has not intercepted the main porphyry intrusion. Therefore deeper chalcopyrite mineralization may occur at Red Mountain. The enargite-mineralizing fluid has not been conclusively characterized although spatially related fluids have temperatures above 480°C.

REFERENCES

Corn R. M. (1975) *Econ Geol* 70: 1437-1447

Mavrogenes J., Henley R. W., Reyes A. G., Berger, B. (2010) *Econ Geol* 105: 257-262

Rusk B. G., Reed M. H., Dilles J. H., Klemm L. M., Heinrich C. A. (2004) *Chem Geol* 210:173-199.

Carbon and nitrogen isotope measurements of gas-bearing fluid inclusions

Lüders, Volker and Plessen, Birgit

Helmholtz Centre Potsdam GFZ German Research Centre for Geosciences, Telegrafenberg Potsdam,Germany

For simultaneous measurement of natural gases (N_2, CH_4, and CO_2) in fluid inclusions a sample crusher and an Elemental analyser (EA) combustion-IRMS system was used, including an EA, ConFlo III and Delta^{plus}XL mass spectrometer (Fig. 1). The general design of the crusher and its connection to an EA was adopted from Vonhof et al. (2006) and developed by GFZ machinists. The crusher is coupled to the EA via a He carrier gas line from which the carrier gas, He 5.0, passes through the crusher with 300 ml/min. The crusher consists of a special hardened steel chamber and piston which is not only useful for soft minerals, such as calcite, fluorite and ates but also for quartz and other silicates. Similar to the Amsterdam device, the GFZ crusher is equipped with a septum port for direct injection of gases for blank runs. The crusher volume of about 2 cm^3 allows crushing of up to 1g of sample material.
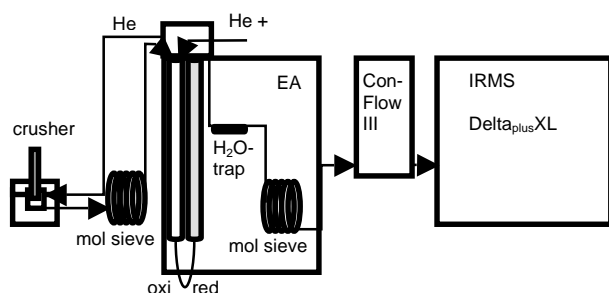
Fig. 1. Schematic diagram of the crusher-EA-IRMS line for simultaneous measurement of N_2, CH_4, and CO_2 gases released from fluid inclusions by crushing.

After crushing of sample chips (which have been used for microthermometry and laser-Raman spectroscopy before), the He – gas mixture passes through a mol sieve and separates N_2, CH_4 and CO_2 from each other. The gas species enter the oxidation column of the EA, where CH_4 gets oxidized to CO_2 with simultaneous injection of O_2 at 960°C. In order to obtain complete oxidation of CH_4, a 25 ml oxygen loop was used for the He-O_2 purge line. After passing the reduction column and water trap, the gas species N_2, CO_2 from CH_4 oxidation and original CO_2 from inclusions are separated again in a second mole sieve and enter the isotopic ratio mass spectrometer (IRMS) via a Conflo III.
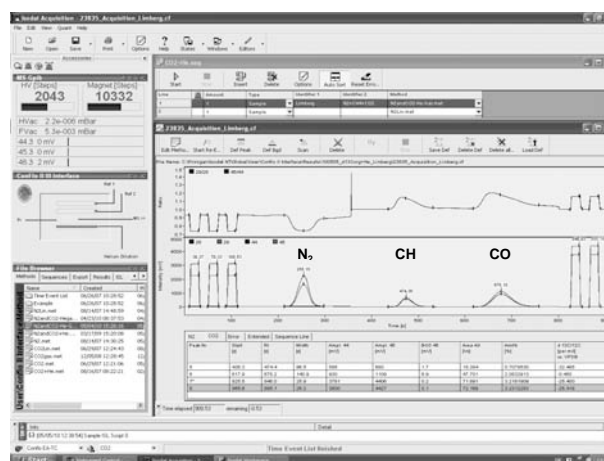
Fig. 2. Signal intensity trace of m/z 28 and 29 until 350 sec and 44 and 45 after of CH_4-CO_2-N_2-bearing fluid inclusions in quartz hosted by Jurassic sandstone (LSB, Germany)

The rapid high precision magnetic jump of the mass spectrometer, the injection of two different reference gases (N_2, CO_2), and the He-mode of the ConFlo III allow the simultaneous measurement of $\delta^{15}N$ and $\delta^{13}C$ of N_2, CH_4 and CO_2, respectively. The first three peaks shown in Fig. 2 are reference gas peaks for N_2, and the fourth peak is the N_2 peak of natural gas released from fluid inclusion by crushing. After jumping to the CO_2 option within 300 seconds, the CH_4 peak of the fluid inclusion gas appears well separated from the following CO_2 peak. The last two peaks are the reference gas peaks for CO_2 (Fig. 2). The intensity of the gas peaks, and the peak shape

indicate effective gas release and separation of N_2, CH_4, and CO_2. The complete gas separation and oxidation of CH_4 to CO_2 has been proven by multiple injections of gas mixtures with known isotopic compositions into the crusher followed by several blank measurements. The $\delta^{15}N$ and $\delta^{13}C(CH_4, CO_2)$ values of gases being released from fluid inclusions in individual chips of quartz from a sample site in the Lower Saxony Basin are shown in Table 1. The excellent reproducibility of $\delta^{13}C$ values for CH_4 and CO_2 indicates complete gas separation and oxidation of CH_4 to CO_2.

Sample	$\delta^{15}N$	$\delta^{13}C$ CH_4	$\delta^{13}C$ CO_2
Chip 1	-8.5	-33.6	-0.2
Chip 2	-6.9	-33.4	-0.8
Chip 3	-8.9	-32.9	-0.5
Chip 4	-7.9	-32.2	-0.3

Table. 1. ^{13}C and ^{15}N isotopic composition of fluid inclusions in quartz hosted by Jurassic sandstone (Lower Saxony Basin, Germany).

REFERENCES

Vonhof H.B., van Breukelen M., Postma O., RoweP.J., Tim C., Atkinson T.C., Kroon D.(2006) *Rap. Comm. Mass Spec.* 20: 25532558.

A preliminary fluid inclusion study of Vejin Pb-Zn ore of Tiran region from Sanadaj-Sirjan zone, Central Iran

Mackizadeh, Mohammad Ali[*] and Taghipour, Batoul[**]

*Geology Department, University of Isfahan, Isfahan, Iran
**Department of Earth sciences, Faculty of Sciences, Shiraz University, Shiraz, Iran

The Vejin deposit is one of the three known carbonate rock-hosted Pb-Zn deposits in Tiran region, NW Isfahan. The deposits occur within the Sanadaj-Sirjan metamorphic zone at the margin of the Central Iranian microplate between the NW-SE trending Zagros fold belt and the Uromieh-Dokhtar Belt (Cenozoic magmatic belt of Central Iran) (Fig. 1). The stratabound ore occurs as replacement bodies within the lower Cretaceous (Barremian-Aptian) limestone, as well as along major NW-SE faults with no apparent association with magmatic bodies. The carbonate host rock that formed within a fore-arc environment unconformably lies on metasediments of Triassic-Jurassic age. The ore consists of galena and sphalerite with subordinate amounts of pyrite and is associated with quartz and calcite alteration. Microthermometric studies of fluid inclusions in sphalerite indicates the presence of brines with 16 eq mass% NaCl, T_m(ice) = -11 °C, that precipitated at temperature of 150 ± 10 °C.

Fluid inclusion data, the carbonate composition of the host rock, the replacement style of mineralization and the geotectonic setting unrelated with magmatic activity show close similarities with MVT type mineralization for the Vejin Pb-Zn deposit as proposed for other Pb-Zn deposits of the region (e.g. Ghazban, 2003). The ore fluids may have been generated as basinal brines due to the compaction of the Sanadaj-Sirjan metamorphic formations during the Cretaceous Neo-Tethyian continental collision between the Iranian and the Arabian plates.
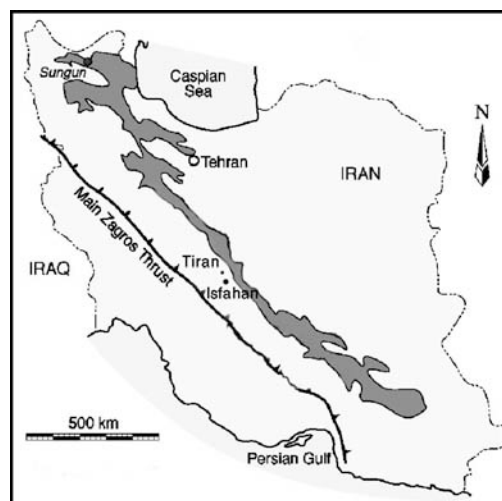
Fig. 1. Sketch map showing the position of the Central Iranian volcanic belt and the study area (Tiran).

REFERENCES

Ghazban F, Hajikazemi E (2003) *Diagenesis, hydrocarbon migration and MVTmineralization in Cretaceous carbonates of west Central Iran Mineral exploration and sustainable development*, P 1161 - 1164.

Contrasting fluids on similar vein-type Pb-(Zn-Cu) deposits in Portugal

Marques de Sá, Carlos and Noronha, Fernando

CGUP - GIMEF, DGAOT-FCUP, Rua do Campo Alegre s/n, 4169-007 Porto, Portugal

Introduction

Fluid inclusion (FI) studies of Pb-(Zn-Cu) deposits are being carried out in 8 deposits in NE and W Portugal: 4 in the Bragança district (NE Portugal): Ferronho (F), Vale da Madre (VM), Estevais (E) and Olgas (O); and 4 in the Aveiro District (W Portugal): Moinho da Pena (P), Carvalhal (C), Palhal (PA) and Telhadela (T). The study of these deposits encompasses mineralogical, geochemical and petrographical studies together with fluid inclusions studies. We now present preliminary results of the petrographic and microthermometric FI studies and the contrasting evolution of their *T-x* paths.

Geology and Mineralogy

The studied deposits are low temperature vein type deposits, formed in late to post-Variscan fractures. In the Bragança district the veins cross Ordovician phyllites and quartzites. The deposits form a lineament parallel to the main NNE-SSW Vilariça regional fault. The deposits of the Aveiro district occur in E-W fractures related to late stages of the Variscan and early Alpine orogenesis. They occur along a NE-SW fault which is a tributary of the main NW-SE Porto-Tomar regional fault. The veins cut across gneisses and mica-schists of lower Ordovician age. On both regions the veins are not spatially related to the synorogenic Variscan granites. All the veins are brecciated and composed of several generations of the main gangue, quartz with calcite (Cc) occurring in the Aveiro district deposits Palhal (PA) and Telhadela (T). In general there are three main quartz generations: earlier massive milky quartz (QI); translucent subhedral quartz (QII) contemporaneous with main ore stages; and late quartz in clear euhedral crystals with comb texture (QIII). Different quartz generations accompany different paragenetic stages. These paragenetic stages are: stage 0 (s0; QI, pre-ore); stage 1 (s1; QI-QIIa, Fe-As); stage 2 (s2; QIIa-QIIb, Cu-Zn); stage 3 (s3; QIIb-

QIIc and Cc, Pb); stage 4 (s4; QIII, late). Main sulphides are s1: arsenopyrite and pyrite; s2: sphalerite and chalcopyrite; s3: galena. Several other rarer sulphides, sulphosalts, sulphates, carbonates and oxides occur earlier and later in the paragenesis.

Fluid Inclusion Petrography

Most of the studied FI are hosted by quartz except a few cases of FI in calcite from Palhal and Telhadela mines. All studied FI are two-phase aqueous inclusions (L_w) and present frequently an oval, rectangular or negative crystal shape, with sizes ranging from 5 to 100 μm (most common 10 μm). Petrographical studies enabled us to identify different assemblages of FI: isolated, defining crystal growth zones or in intragranular planes or swarms (primary or pseudosecondary in the last case); in transgranular planes or trails (secondary) (Roedder, 1984; Van den Kerkhof & Hein, 2001). The assemblages were correlated with the host quartz generation and by this way with the paragenetic stage. Flw is constant in most cases within one assemblage, although there are some cases of variable vapour bubble size within the same assemblage.

Microthermometry Results

About 100 FI were microthermometrically analyzed in each deposit, although in some cases results for the pair ice melting temperature - T_m(ice) - and homogenization temperature - T_h - were not possible to obtain, due to decrepitation, leakage or other undesirable irreversible phenomenons. Microthermometric results are summarized in Table 1. For each deposit T_e, T_m(ice) and T_h means with standard deviation are presented according to paragenetic stage. Presence of Ca^{2+} is probable as indicated by most of T_e temperatures (Goldstein & Reynolds, 1994). Plotting a diagram (Fig. 1) of T_m(ice) versus T_h (L and V) of the inclusions allowed us to observe: 1) different fluid "paths" for each district; 2) a distinct

separation between the fluids related to PbS deposition in the Bragança district and those from the Aveiro district (Fig. 2). The following bivariate plots are self explanatory.

	Stage 0 Pre-ore			Stage 1 Fe-As			Stage 2 Cu-Zn			Stage 3 Pb			Stage 4 Late		
	T_e	T_{mi}	T_h	T_e	T_{mi}	T_h	T_e	T_{mi}	T_h	T_e	T_{mi}	T_h	T_e	T_{mi}	T_h
Moinho da Pena (108)				-54.3 (6.4)	-1.2 (1.5)	261.2 (57.7)	-60.1 (5.6)	-22.5 (2.1)	164.2 (28.1)	-57.5 (7.6)	-20.6 (4.6)	99.6 (8.9)	-55.7 (5.7)	-17.2 (5.4)	68 (4.4)
Carvalhal (106)				-59.4 (6.3)	-1.2 (1.6)	228.6 (50.3)	-63.7 (7.9)	-24.6 (1.6)	122.2 (30.6)	-62.9 (5.5)	-23.2 (2.6)	101.6 (11.1)	-62.2 (3.8)	-22.2 (2.7)	83.6 (13.5)
Palhal (112)	-65.7 (3.3)	-0.3 (0.2)	337.7 (18.9)	-53.5 (8.2)	-0.5 (1.1)	196.5 (34.3)	-67.1 (5.3)	-24 (2.4)	108.1 (16.1)	-59 (1)	-22 (1.6)	92.8 (2.5)	-71.3 (3.2)	-18.6 (3)	70.2 (4.8)
Telhadela (90)				-55.3 (5)	-1.8 (1.8)	255.5 (86)	-59 (4.8)	-23 (2.2)	104 (14.8)	-65.4 (4.1)	-23 (1.8)	107.3 (9.8)			
Ferronho (123)	-53.3 (3.4)	-4.9 (4.8)	325.8 (51.4)	-54.2 (4.6)	-1.1 (0.5)	226.7 (14)	-53.2 (3.4)	-6.9 (2.6)	154.4 (15)	-55.6 (6.3)	-0.9 (0.4)	156.8 (19.9)	-57.4 (3.4)	-16.1 (3.2)	103.1 (8.8)
Vale da Madre (110)	-54.3 (12)	-3.9 (3.1)	295 (53.9)	-55.6 (7.4)	-3.5 (0.4)	253 (18.3)	-55.3 (5.2)	-0.8 (0.7)	213.2 (27.4)	-56.9 (5.8)	-2.3 (1.5)	129.1 (11.1)			
Estevais (110)	-56.8 (4.6)	-10 (7.6)	335 (46.7)	-51.7 (3.6)	-8.6 (0.9)	244 (18.3)	-57.6 (6.3)	-6.8 (1.3)	147 (21.9)	-56.5 (6.8)	-0.7 (0.7)	141.4 (25.6)	-61.3 (4.4)	-15.4 (7)	93.4 (10.5)
Olgas (97)	-54.3 (6.1)	-0.4 (0.3)	264 (22.5)	-46.7 (11.2)	-4.1 (1.5)	178.1 (37.1)	-52.8 (7)	-0.3 (0.2)	177.8 (23.2)	-44.6 (9.7)	-0.2 (0.1)	119.8 (11)			

Table. 1. Microthermometric data according to paragenetic stages. Values are means with std. dev. in parenthesis; all values in ºC. Total FI analysed in each deposit in parenthesis after the name of the deposit.
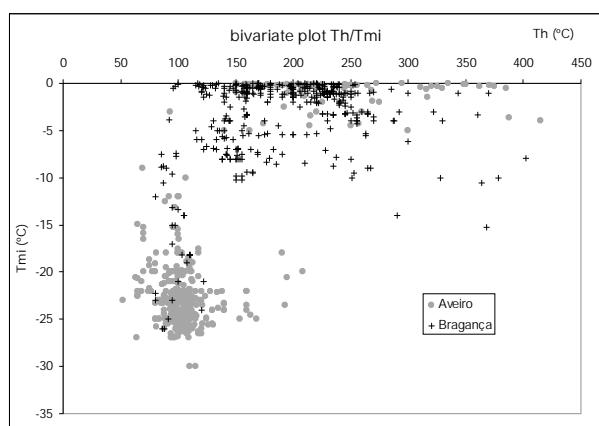
Fig. 1. T_h / T_m(ice) plot for all the FI analysed. Observe distinct paths of Aveiro vs Bragança deposits.
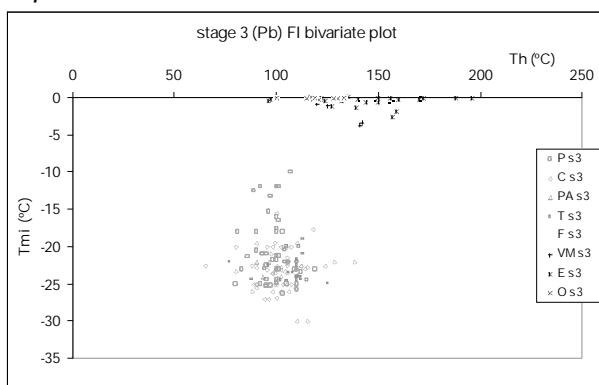
Fig. 2. T_h/ T_m(ice) plot for Pb stage FI in each deposit. Observe contrast Aveiro vs Bragança deposits.

Conclusions

The fluids responsible for the galena deposition in the Aveiro district deposits have different characteristics (temperature and salinity) from those of the Bragança district. The different "fluid paths" (T_h/T_m(ice) plot) suggest that different series of reactions were responsible for ore deposition. Boiling is evidenced in some cases by similar values of T_h (L) and T_h (V), by the dispersion of the T_h values, variable Flw and petrographical textures (Roedder, 1984; Bodnar et al., 1985). Aveiro district deposits have similar "fluid path" to other Pb-Zn deposits studied before (Marques de Sá, 2008). The "fluid path" in the Bragança district is similar to the one registered on later stages of W-Sn vein deposits in northern Portugal (Noronha, 1984). Recently obtained stable isotopes results also point out contrasting characteristics of these otherwise mineralogically and texturally very similar deposits.

REFERENCES

Bodnar, R.J., Reynolds, T.J., Kuehn, C.A. (1985). Rev. in *Econ. Geol.,* 2: 73-97.

Goldstein, R.H., Reynolds, T.J. (1994). SEPM *Short Course* 31: p.99 (198)

Kerkhof, A.M. van den, Hein, U.F. (2001). *Lithos*, 55: 27-4.

Marques de Sá, C. (2008). MD thesis FCUP, 215p.

Noronha, F., (1984). *Bull. Minéral.*, 107: 273-284.

Roedder, E., (1984). *Rev. in Mineralogy,* vol.12, (ed. Ribbe, P.H.), Min. Soc. of America,644p

Boiling as a mechanism for emerald colouration from the Emmaville and Torrington emerald deposits, Australia.

Marshall, Dan*, Loughrey, Lara* and Millsteed, Paul**

*Earth Sciences, Simon Fraser University, Burnaby, BC, Canada
**Earth Sciences Research School, Australia National University, Canberra, ACT, Australia

The Emmaville emeralds were the first emeralds discovered in Australia during the late nineteenth century. The nearby Torrington emerald deposit was discovered a century later. Both deposits appear to be typical granitoid-related emerald deposits and are associated with the nearby Moule Granite of the New South Wales Fold Belt.

The emeralds are zoned (Fig. 1) and display alternating bands of emerald green and clear growth zones within individual crystals at the millimetre scale. The zoning is seen optically but can also be observed via other imaging techniques such as backscattered electron, cathode luminescence, and chemically via electron microprobe analyses. Additionally, there is a correlation between the presence of a population of primary vapour-rich fluid inclusions within the clear growth zones (Fig. 2) and a second population of highly saline three-phase (liquid + vapour + halite) fluid inclusions in the darker or coloured growth zones.

Fig. 1. Photomicrograph of a zoned emerald crystal from the Emmaville-Torrington deposit.

The two fluid inclusion populations appear to represent conjugate sets of a boiling system with the three-phase highly saline fluid inclusions having an average salinity of approximately 33 eq mass% NaCl. This population undergoes total homogenisation into the liquid and probably represents fluids trapped in the liquid system of a two-phase (boiling) system. The vapour-rich population of fluid inclusions (Fig. 2) have an average salinity of approximately 6 eq mass% NaCl and homogenise into the vapour phase at higher temperatures.

Fig. 2. Enlarged area of the photomicrograph of primary fluid inclusions Figure 1 showing alternating coloured and clear areas in the zoned emerald crystal. The clear zones correspond to growth zones dominated by primary vapour rich fluid inclusions.

The correlation of colour versus clear growth zones corresponding to highly-salinity liquid-dominant and vapour-dominant low-salinity primary fluid inclusions, respectively, indicates that the colour banding within the Emmaville and Torrington emerald is related to emerald precipitation in the liquid or vapour portion of a boiling fluid system. Although other emerald deposits worldwide display similar growth banding this is the first time it has been documented as a consequence of boiling during emerald formation.

The effect of surface tension on liquid-vapour homogenisation in low-temperature fluid inclusions

Marti, Dominik*, Krüger, Yves*, Fleitmann, Dominik**, Frenz, Martin* and Rička, Jaro*

*Institute of Applied Physics, University of Bern, Sidlerstrasse 5, Bern, Switzerland
**Institute of Geological Sciences, University of Bern, Baltzerstrasse 1 & 3, Bern, Switzerland

We present a thermodynamic model to analyse the effect of surface tension on the liquid-vapour homogenisation $(L + V \rightarrow L)$ for an isochoric pure water system. The model relies on the minimisation of the Helmholtz free energy of the inclusion system, derived from the IAPWS-95 formulation (Wagner & Pruß, 2002), and predicts the thermodynamic state, the vapour bubble radius, and the densities and pressures of the liquid and the vapour phase at a given temperature, volume, and bulk density.

The starting point of inclusion thermodynamics is a well known minimum principle: A closed isochoric system at equilibrium with a thermal reservoir assumes the minimum of Helmholtz free energy $F = U - TS$ with respect to any unconstrained internal variables. The following equation describes the Helmholtz free energy of an inclusion:

$$F = N_L \cdot f_L(\rho, T) + N_G \cdot f_G(\rho, T) + F_{LG}$$

where N_L and N_G denote the number of water molecules in the liquid and gas phase, respectively, f_L and f_G are the respective specific Helmholtz free energies that can be calculated using IAPWS-95, and F_{LG} denotes the interfacial energy arising from the surface tension. Assuming the bubble to be spherical, an assumption valid for small bubble volume fractions, the interfacial energy reads:

$$F_{LG} = 4\pi r^2 \, \sigma(T)$$

where r denotes the vapour bubble radius, and σ is the surface tension of water.

Figure 1 shows an example of the Helmholtz free energy as a function of the bubble radius for a hypothetical, truly isochoric pure water inclusion with a volume of 10^3 µm³ and a density of 999.1 kg/m³, corresponding to a nominal homogenisation temperature $T_{h\infty}$ of 15 °C. $T_{h\infty}$ denotes the homogenisation temperature of an
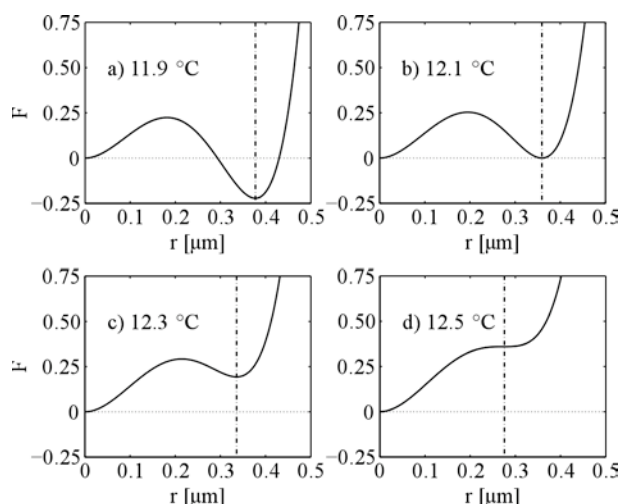
Fig. 1: The Helmholtz free energy of an inclusion of a volume of 10^3 µm³ and of a nominal homogenization temperature of 15°C at four different temperatures.

infinitely large inclusion, where the surface tension has no effect on the liquid-vapour equilibrium (Fall et al., 2009). The graphs indicate the presence of two distinct transitions between three different regimes: Below 12.1 °C (Fig. 1a), the vapour bubble is stable, the global minimum in the Helmholtz free energy is lower than the homogeneous liquid state with no bubble. At 12.1 °C (Fig. 1b) the two states are equally probable, therefore we denote this temperature as the "binodal temperature" T_{bin}. Between 12.1 and 12.5 °C (Fig. 1c) a vapour bubble can be present, but is in a metastable state. At 12.5 °C (Fig. 1d) we reach some kind of spinodal, where the bubble becomes unstable and must collapse from a non-zero radius, giving way to the stable homogeneous liquid state. Note that the spinodal temperature T_{sp} is 2.5 °C below the nominal homogenisation temperature. The actually observed homogenisation temperature $T_{h\ obs}$ of the inclusion must lie in the metastable region between T_{bin} and
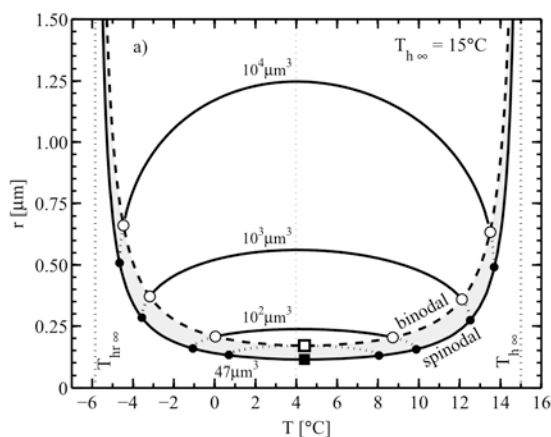
Fig. 3. Vapour bubble radii for different inclusion volumes vs. temperature.

T_{sp}, but can not be derived from the thermodynamic model.

The surface tension at the liquid-gas interface works towards a reduction of the bubble surface. Figure 2 shows the bubble radii as a function of the temperature for four different inclusion volumes. The prograde and retrograde binodal temperatures are indicated by open circles connected by the binodal curve (dashed line), the pro- and retrograde spinodal temperatures where the bubble must collapse are shown by filled circles connected by the spinodal curve (solid line). The bubble is metastable between these two temperatures, indicated with dotted lines.

It can be seen that, with decreasing volume, the spinodal temperature is shifted towards the density maximum of water. The difference ΔT between the observed homogenisation temperature (that must lie below T_{sp}) and the nominal homogenisation temperature $T_{h\infty}$ will therefore increase with decreasing inclusion volumes.

Figure 2 also shows that for a bulk density of 999.1 kg/m³ ($T_{h\infty}$ of 15 °C) and inclusion volumes between 28 µm³ (filled square) and 47 µm³ (open square) only a metastable vapour bubble can exist in the inclusion, whereas below 28 µm³ no vapour bubble can exist at all.

Figure 3 summarises these limits for various $T_{h\infty}$. The dark grey area denotes the $T_{h\infty}$/volume pairs for which there can be no stable or metastable bubble and therefore no T_h measurements can be conducted. The square indicates the case explained in Figure 2 for the
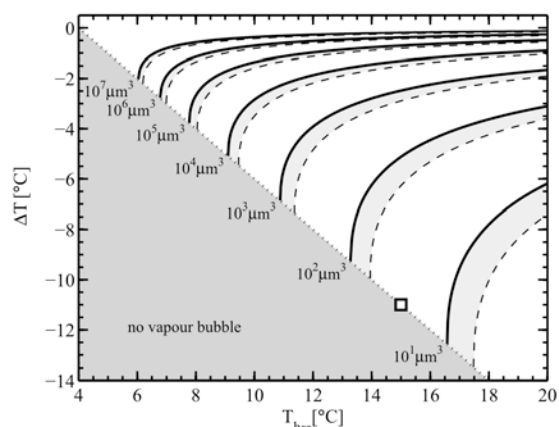
Fig. 2. Temperature difference between the spinodal temperature T_{sp} and the nominal homogenisation temperature $T_{h\infty}$ (solid lines) and between the binodal temperature T_{bin} and $T_{h\infty}$

nominal homogenisation temperature $T_{h\infty}$ of 15 °C. The solid lines in Figure 3 indicate the temperature difference ΔT between T_{sp} and $T_{h\infty}$ for different volumes, whereas the dashed lines denote ΔT between T_{bin} and $T_{h\infty}$. It can be seen that ΔT increases with decreasing inclusion volume and increasing bulk density.

From Figure 2 it can be seen that, when measuring the vapour bubble radius in an inclusion at different temperatures, the nominal homogenisation temperature $T_{h\infty}$ and the inclusion volume can be calculated by fitting the radius curve to the measured data. However, measurements of bubble radii from microphotographs are prone to systematic errors that can severely alter the resulting formation temperature and volume, especially in small inclusions. It is therefore necessary to develop a reliable bubble radius measurement routine.

REFERENCES

Fall, A., Rimstidt, D., Bodnar, R.J. (2009) *Am Min.* 94: 1569 – 1579

Wagner, W., Pruß, A. (2002) *J Phys Chem ref Data.* 31(2): 387 – 485

Fluid inclusion study of the Arcos Deposit, Lugo, Spain: preliminary results

Martínez-Abad, Iker, Cepedal, Antonia and Fuertes-Fuente, Mercedes

Department of Geology, University of Oviedo, Arias de Velasco s/n, 33005, Oviedo, Spain.

Introduction

The Arcos deposit (Lugo, NW of Spain) was discovered in 2001 by the Outokumpu company. This deposit along with the mineralization of Castro de Rey and Valiña constitutes the Villalba Gold District (Martínez-Abad et al., 2011a), is a newly defined gold mineralized area in the NW of Spain. Two types of ore deposits were distinguished in the district, a gold skarn with Bi-Te-Au metal assemblage and low temperature polymetallic deposits with Au-As-Sb and Ag-Pb-Zn±Cu±Au geochemical signatures. While both deposit styles are present in the Castro de Rey area, only the latter is present in Valiña and Arcos. Based on the geological and mineralogical characteristics of the mineralized areas, Martínez-Abad et al. (2011a) proposed an intrusion-related gold system (Lang et al., 2000) for the Villalba Gold district, where the Arcos deposit would represent the type of deposit formed peripheral to intrusions. In this paper we present a preliminary fluid inclusion study of the Arcos mineralization to establish the composition of the fluids involved in the mineralizing process and the P-T conditions during this event.

Geological setting

The Arcos deposit is located in the West Asturian Leonese Zone (Julivert et al., 1972) of the Iberian Massif. The sedimentary rocks in Arcos consist of sandstones, slates and impure limestones of Lower Cambrian age that were folded, thrusted, faulted and metamorphosed during the Variscan Orogeny (Martínez Catalán et al., 1990). During the Late-Variscan, the area was affected by N-S, E-W and NE-SW trending fault systems. Several rhyolitic dikes intruded along N-S faults, showing near vertical dips and low angle-sub-horizontal dips in sill-like apophyses. Spatially related to the rhyolites, low temperature polymetallic mineralization occurs disseminated in altered host rocks and within veins (centimetrical in scale) located along fractures, bedding and cleavage planes.

Arcos deposit

The Arcos mineralization was developed in at least two phases. The first consists of fine-grained sulphides: pyrite, arsenopyrite and gold bearing As-rich pyrite, in a matrix of quartz and/or calcite. This stage occurs disseminated in silicified impure limestone and calcareous slates (jasperoids) as well as infilling veins and fault breccias. Gold mainly occurs as refractory in the As-rich pyrite (Martínez-Abad et al., 2011b). In the second stage, which replaces the early one, base metals, Ag-rich tetrahedrite and Pb/Sb sulphosalts occur along with quartz, carbonate and chlorite. Eventually, younger veins with fluorite, carbonate and chlorite crosscut the mineralization stages cited above as well as the rhyolites dikes.

Fluid inclusion study

This preliminary fluid inclusion study was carried out in samples of quartz from a mineralized jasperoid and samples of fluorite from the later veins cited above. Two types of aqueous-carbonic fluid inclusions were defined: type Lw-(c) in the jasperoid and type Lw-c in the fluorite.

Type Lw-(c) inclusions occur as small clusters or, sometimes, isolated in the quartz crystals. We consider them as primary according to Roedder´s criteria (1984). Their morphologies are irregular, prismatic and elongated with sizes of between 8 and 16 µm. They contain two phases at room temperature and the volumetric fraction of the aqueous phase is from 65 to 75%. From the microthermometric results, T_e was around -20.8 ºC. The main interval of T_m(ice) is between -5.1 and -3.6 ºC. T_m(cla) was between 7.1 and 9.1 ºC. T_h(total) was between 187 and 268 ºC to the liquid state, with the most values lying between 230 and 240 ºC.

Type Lw-c inclusions occur in clusters and isolated in the fluorite crystals. We consider them as primary. Their morphologies are prismatic, elongated and negative crystals with sizes of between 30 and 60 µm. They contain three phases at room temperature and the volumetric fraction of the aqueous phase is between 45 and 80%. Some of these inclusions contain a crystalline solid, which may be a carbonate. There is no sign of dissolution during the heating experiments and this solid is anomalously large compared to its host inclusion, therefore we interpreted it as a trapped mineral. From the microthermometry results, $T_m(CO_2)$ was between -57.1 and -56.6 ºC. $T_h(CO_2)$ varied from 25.6 to 30.5 ºC to both liquid and vapour state. T_{eut} was around -20.8ºC. The main interval of $T_m(ice)$ was between -0.5 and -3.7 ºC. $T_m(cla)$ was between 8.1 and 9.9 ºC. $T_h(total)$ was between 186 and 265 ºC to the liquid state, with most values lying between 220 to 230 ºC.

Discussion

In type Lw-(c), the presence of a volatile component is only detected from clathrate formation. Since $T_m(cla)$ is below 10 ºC, the main volatile in this type of inclusion is probably CO_2. Salinity from $T_m(cla)$ is between 2.7 and 6.1 mass% NaCl. In type Lw-c, the $T_m(CO_2)$ close to -56.6 ºC and $T_m(cla)$ below 10 ºC indicate that the main volatile is CO_2. In this case, salinity from $T_m(cla)$ is between 2.9 and 5.3 mass% NaCl. In both types, T_{eut} indicates NaCl as the most probable solute in the aqueous phase, according to Potter & Brown (1977).

Bulk composition, density and isochores of representative fluid inclusions were calculated to estimate the minimum P-T conditions and composition of the fluid related to ore deposition in the studied jasperoid and the fluid related to later fluorite deposition. These data were calculated using the "Clathrate" and "Fluids 1" packages (Bakker, 1997, 1998, 2003). The composition of the fluid involved in the ore deposition in jasperoids and trapped by type Lw-(c) inclusions is $x(H_2O)$ = 0.91-0.94, $x(CO_2)$ = 0.036-0.046, $x(NaCl)$ = 0.008-0.016 with a density range of 0.69-0.78 g/cm^3. Isochores show that for a minimum trapping temperature of 300 ºC, the minimum corresponding pressures are below 500 bars.

The composition of the fluid involved in the fluorite deposition and trapped by type Lw-c inclusions is $x(H_2O)$ = 0.80-0.89, $x(CO_2)$ = 0.07-0.15, $x(NaCl)$ = 0.008-0.015 with a density range of 0.83-0.89 g/cm^3. Isochores show that the trapping of this low-salinity aqueous carbonic fluid took place under the minimum conditions (T_h,P_h) of between 210 and 242 ºC at pressures from 275 to 605 bars.

Carbonic and aqueous carbonic fluids characterize the intrusion-related gold systems environment. The temperatures and pressures attending precipitation of gold and related metals span broad ranges of <200 ºC to >600 ºC and <0.5 to >3.0 kbar (Lang et al., 2001). According to these authors, the metallic assemblage described in Arcos and the composition and P-T conditions of the fluids related to ore deposition in the studied jasperoids are those expected in deposits formed peripheral to intrusions. Moreover, the fluid related to fluorite deposition represents a later stage of aqueous carbonic fluid circulation under similar P-T conditions.

REFERENCES

Bakker RJ. (2003) *Chem. Geol.* 194: 3-23.

Bakker RJ. (1997) *Comp. & Geo.* 23: 1-18.

Bakker RJ. (1998) *Geol. Soc. Lon.* 137: 75-105.

Julivert M., Fontbote JM., Ribeiro A., Nabais Conde LE. (1972) *Mapa Tect. Esp. E. 1:1000 000*

Lang JR., Baker T., Hart CJR., Mortensen JK. (2000) SEG Newsl. 40: 6-15.

Lang JR. and Baker T. (2001) *Min. Dep.* 36: 477 489.

Martínez-Abad I., Cepedal A., Arias D., Martín Izard A. (2011a) in press.

Martínez-Abad I., Cepedal A., Arias, D., Martín Izard A. (2011b) in press.

Martínez-Catalán JR., Pérez-Estaún A., Bastida, F., Pulgar JA., Marcos A. (1990) Premesozoic Geol. of Iberia. 103-114.

Potter, R.W., Brown, DL. (1977). *US Geol. Surv.Bull.*, 1421-C: C1-C36

Roedder E. (1984) *Mineral. Soc. Am. Rev. Mineral.* 12: 646.

Fluid inclusions in high sulphidation gold deposits: what can we learn from them about conditions of ore deposition?

Mavrogenes, John A., Henley, Richard W., and Tanner, Dominique

Research School of Earth Sciences, Australian National University, Building 61, Mills Rd., Canberra, Australia

Popular ore deposit models (e.g. Hedenquist and Lowenstern, 1994) require that high sulphidation gold deposits form at temperatures below 300°C. However, stable isotope data consistently link these ores with high proportions of magmatic fluids. This presents a paradox, in that magmatic fluids by their nature are high temperature.

In their classic paper, Bethke et al. (2005) said that; "A number of planes of inclusions with large vapour bubbles were seen but not measured because of the difficulty in determining temperatures of homogenisation to vapour on small inclusions. Thus, vapour-rich inclusions are much more abundant than they appear to be from Table 2." This highlights the problem we have with vapour-rich fluid inclusions. Because we cannot measure them accurately, should we ignore them? Analogously, since liquid-rich inclusions are easy to measure should we measure them with impunity?

We have separated euhedral quartz crystals from sulphosalt "feeder-zone" ores from the El Indio Au-Ag-Cu deposit, Chile; and the Summitville Au-Ag-Cu deposit, Colorado in order to characterise the fluid inclusions present during enargite-gold deposition. These euhedral ~200 μm crystals either grow into vugs in the sulphosalt ore, or are encased by sulphosalts.
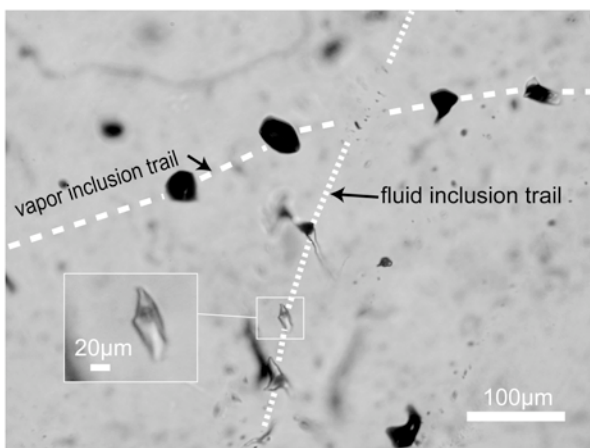
Fig. 1. Crosscutting trails of secondary vapour and secondary fluid inclusions in sulphosalt-ore stage quartz from the Summitville Au-Ag-Cu deposit, Colorado.
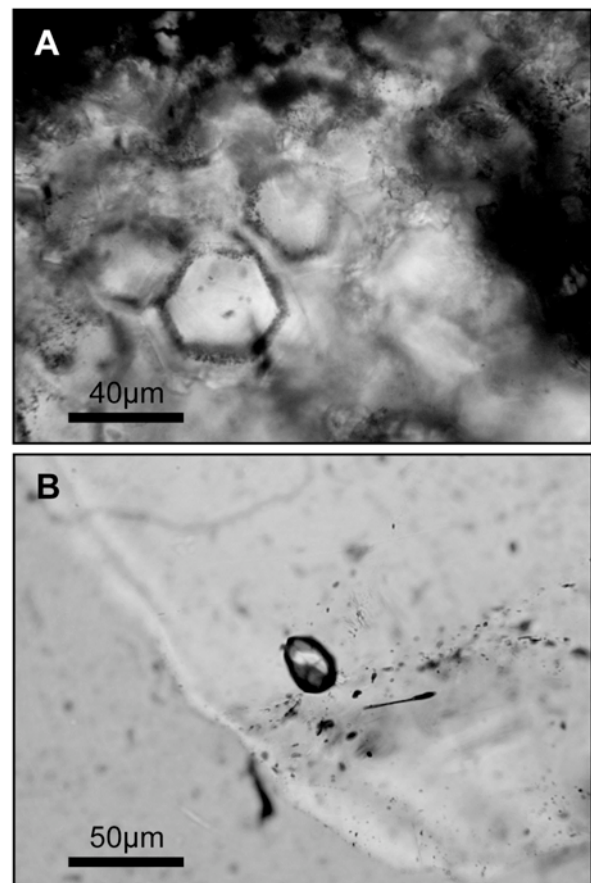
Fig. 2. Fluid and vapour inclusions in sulphosalt-ore stage quartz from the Summitville Au-Ag-Cu deposit, Colorado: (A) primary inclusions (<1 μm) mantling growth bands in euhedral quartz; (B) An isolated low-density vapour inclusion in quartz.

All the high-density fluid inclusions (those that homogenise to the liquid) found in these crystals are secondary, occurring in multiple generations of healed fractures. Low-density (vapour) vapour-rich inclusions are present as both primary and secondary inclusions.

We interpret the well-formed, isolated vapour inclusions as pre-dating the higher density (liquid) fluid inclusions because they are spherical, concentrated in the middle of quartz crystals and are not along healed fracture planes (Fig. 2B). Yet the preponderance of high-density (liquid-rich) inclusions is somehow interpreted as playing a more significant role than the rarer, vapour-rich fluid inclusions by most workers (e.g. Hedenquist et al., 1998). Yet, these may be the only direct evidence of the original magmatic fluid.
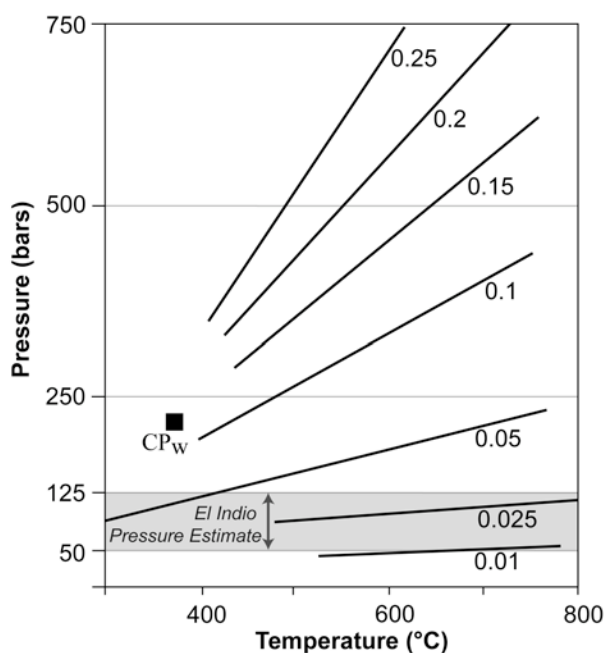
Fig. 3. A pressure-temperature plot of low-density water isochors (from the Steam Tables). Gray strip represents pressure estimates for deposition of the El Indio Au-Ag-Cu deposit. CP_w denotes the critical point of pure water.

El Indio, Chile formed as a sequence of veins at about 650 – 1150 meters below the surface of a dacitic volcanic complex (Jannas et al., 1999). Stable isotope data indicate a dominance of magmatic fluid and there is an absence of significant brecciation indicating that vein fluid pressure was greater than hydrostatic; giving pressures between 50 and 125 bars. Visual estimates of vapour-rich fluid inclusion densities from El Indio (such as those shown in Fig. 1) and Summitville are so low (inclusions appear empty) that quantitative measurement is impossible, but densities less than 0.05 g/cc are the norm. Isochoric plots of low-density isochors (Fig. 3) intersect the pressures appropriate for El Indio deposition at temperatures significantly above 300 °C. For instance, vapour inclusions of 0.01 g/cc would have been trapped at temperatures above 600 °C, consistent with independent estimates based on sulphosalt stability data (Henley and Mavrogenes, in review).

Fluid inclusion studies are not popularity contests where the most abundant win, as is often claimed, but should focus on independently linking fluid inclusion generations to specific geological events.

REFERENCES

Bethke, P.M., Rye, R.O. Stoffregen, R.E. and Vikre, P.G. (2005) *Chem. Geol.* 215: 281 - 315.

Jannas, R.R., Bowers, T.S., Petersen, U. and Beane, R.E. (1999) *Jour. Geochem. Expl.* 36: 233-266.

Hedenquist J. W. and Lowenstern J. B. (1994) *Nature* 370: 519-527.

Hedenquist, J.W., Arribas, A., Reynolds, T.J. (1998) *Econ. Geol.* 93: 373-404.

Henley R.W. and Mavrogenes, J.A. (2011) Geofluids, in review.

Mineral textures and fluid inclusion characteristics of ore samples from the Guanajuato district, Mexico

Moncada, Daniel, Bodnar, Robert J., Fedele, Luca

Dept. of Geosciences, Virginia Tech, Blacksburg, VA 24061, USA

Successful exploration for mineral deposits requires tools that the explorationist can use to distinguish between targets with high potential for mineralization and those with lower economic potential. In this study, we describe a technique based on petrographic and fluid inclusion characteristics that may be applied in exploration for precious metal deposits to identify areas of high-grade mineralization.

The Guanajuato mining district in Mexico is one of the largest silver producing districts in the world with continuous mining activity for nearly 500 years. Ore shoots in the district are localized along three major northwest trending vein systems, the La Luz, the Veta Madre and the Vetas de la Sierra. Mineralization in the district shows much variability between and within individual deposits, from precious metal-rich to more base-metal-rich zones, and from gold-rich to silver-rich zones. Ore textures also vary and include void space that formed during multiple fissuring events, banded quartz veins, massive quartz veins and stockworks. More than 1,400 samples representing all the different mineralization styles were collected from all three vein systems in the Guanajuato mining district, and the mineral textures and fluid inclusion characteristics of each sample have been defined. In addition, each sample was assayed for Au, Ag, Cu, Pb, Zn, As and Sb.

Selected mineralized samples from the central part of Veta Madre that contain up to 249 g/t of Au and 13,600 g/t Ag shows homogenization temperatures from 184 to 300 °C and salinities of 0 to 5 mass% NaCl. Barren samples show the same range in homogenization temperature but slightly lower salinities of 0 to 3 mass% NaCl. Fluid inclusions in the mineralized samples contain detectable Au and Ag, using laser ablation ICP-MS (Fig. 1).

Samples from the Guanajuato district show a wide range in silica textures. Some of these textures, including colloform texture, plumose texture and jigsaw texture, are indicative of rapid precipitation, such as occurs when fluids boil. Other mineral phases, including illite, rhombic adularia and bladed calcite are also indicative of rapid growth and are characteristic of boiling systems. Because boiling is an effective mechanism for precipitating gold and silver from hydrothermal fluids, the presence of mineral textures indicative of boiling is a desirable feature in exploration. In many samples, textural evidence for boiling is supported by coexisting liquid-rich and vapour-rich fluid inclusions, or Fluid Inclusion Assemblages consisting of only vapour-rich inclusions, suggesting "flashing" of the hydrothermal fluids. Textural and fluid inclusion evidence for boiling has been observed in the deepest levels of the Guanajuato mining district, suggesting that additional precious metal resources may occur beneath these levels.
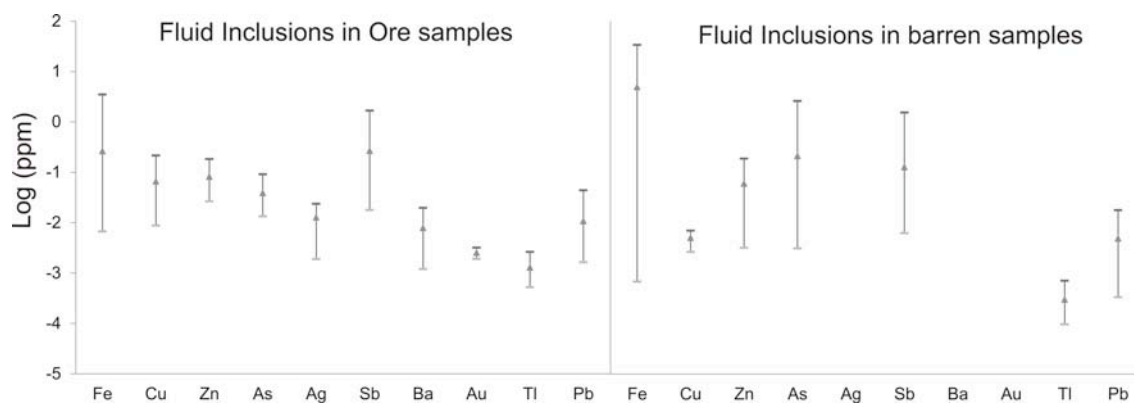
Fig. 1. Laser ablation ICPMS analysis of individual fluid inclusions assemblages in mineralized samples (left) showing the presence of Au and Ag. Inclusions from barren samples (right) do not show Au or Ag.

The study of microorganisms in the natural quartz fluid inclusion

Naumov, Vladimir B.*, Prokofiev, Vsevolod Yu.** and Vapnik Ye.***

*Vernadsky Institute of Geochemistry, Russian Academy of Sciences, Kosygin str. 19, Moscow, Russia
**Institute of Geology of Ore Deposits, Petrography, Mineralogy, and Geochemistry, Russian Academy of Sciences, Staromonetnyi per. 35, Moscow, Russia
***Department of Geological and Environmental Sciences, Ben-Gurion University of the Neger, Beer-Sheva 84105, Israel

The fluid inclusion (12 x 28 μm), which presumable contains microorganisms (we will call them bacteria) had been studied from 1985. This inclusion was classified as a secondary inclusion as it is located in the intersecting fissure within the quartz crystal from metamorphic rock, i.e. amphibolite of Ladoga region, Russia. The inclusion contains aqueous solution, a vapour bubble (about 10 vol.%) and several dark elongated phases with a length between 2.5 - 3.5 μm and a thickness between 0.6 - 0.8 μm. These phases are immovable at room temperature, but after freezing and subsequent thawing of the aqueous solution a chaotic movement in the inclusion is observed. This movement does not occur only in a single plane of the inclusion, it takes place in the whole volume thus the quantity of particles can not be accurately counted. Up to 13 - 14 of those phases are observed in the field of vision. The velocity of movement gradually diminishes up to a complete stopping during different time intervals in different observations. The phenomenon is being reproduced every time after the fluid inclusion was frozen. Such freezing was performed about 100 times during last 25 years. The duration of bacteria movement was found to decrease from 10 days in 1987 up to about 24 hours beginning from the end of 2009 until now. Thus, it could be assumed that the bacteria movement is not a result of physical processes such as the Brownian motion movement.

The aqueous solution in this fluid inclusion freezes at -30 °C, with the complete disappearance of the vapour bubble and the ice occupies the complete volume of the inclusion. This indicates that the liquid has a low salinity. After heating, the ice disappears completely at +2

°C within the metastable region, stimulating the intensive bacteria movement. At slow cooling down to -28 °C, the movement is observed down to the freezing temperature of -30 °C. After thawing the movement of bacteria was also observed in all other experiments. In 2010 the inclusion was stated at +4 °C during 24 hours, but the duration of bacteria movement did not increase.

During heating the inclusion up to the homogenization temperature (gaseous bubble disappears at +130 °C) the bacteria movement was not slowed down but perhaps accelerated. The movement was practically the same at the temperature of inclusion heterogenization (+106 °C). During the homogenization experiment, where the bacteria do not move, it was found, that after heterogenization they began to move, but substantially less actively than after freezing.

Such behaviour of microorganisms in fluid inclusions was not observed in any objects and never reported in publications. But some data on moving particle observations of the above mentioned type and dimension is interpreted as microorganisms activity and can be found in Bargar et al., 1984 and 1985. The particles were observed in quartz crystals from the depth of 102.1 m obtained in bore holes in Yellowstone National Park. The authors assumed that the microorganisms (bacteria?) were incorporated some months or even years before the inclusions were studied.

The bacteria studied in our experiments are presumably rather ancient, but the dating could not be performed accurately. If the bacteria were enclosed in a obscured space for a long time, their living products (CO_2 or other gases?) could be accumulated and lead to decrease of their activity. The freezing could be responsible for the formation

of clathrates and the temporary decrease of gas concentration inside the inclusion succeeding the bacteria activity. The restoration of gas-liquid equilibrium inhibits the living activity of microorganisms. The un-reversible accumulation of gases in the inclusion could be interpreted as the cause of gradual decrease of bacteria activity duration in the cryometric experiments. Our knowledge on the microorganism existence within the obscure space could be markedly extended if our hypothesis is valid.

The bacteria activity during freezing, thawing and heating experiments was documented by a vision camera.

REFERENCES

Bargar, K.E. et al. (1984) *Geol. Soc. Am.*, 16: 436-437.

Bargar, K.E. et al. (1985) *Geology*, 13 :1, 483-486.

Unusual acid melts at unique epithermal Roşia Montană (Romania) gold deposit

Naumov, Vladimir B.*, Prokofiev, Vsevolod Yu.**, Kovalenker, V.A.**, Tolstykh, M.L.*, Damian, G.*** and Damian, F.***

*Vernadsky Institute of Geochemistry, Russian Academy of Sciences, Kosygin str. 19, Moscow, Russia
**Institute of Geology of Ore Deposits, Petrography, Mineralogy, and Geochemistry, Russian Academy of Sciences, Staromonetnyi per. 35, Moscow, Russia
***Universittiea Nord Baya Mare, Victoriel 134 48000, Baia Mare, Romania

Roşia Montană is known as one of the largest gold ore deposits in Europe. It is located at the Northern part of the Southern Apuseni mountains and also called as "The Golden Quadrangle". The deposit was discovered in pre-Roman times and is mined nowadays having large ore stocks (218 mln ton with 1.52 g/ton Au and 7.5 g/ton Ag) (Manske et al., 2006). The main aim of our studies was the determination of the chemical composition of silicate melt inclusion, the former being in quartz porphyry phenocrysts.

Roşia Montană can be compared with well known gold deposits in Au-Ag diatreme-hosted epithermal ore deposits in Acupan (Philippines) and Kelian (Indonesia) (Manske et al., 2006). The deposit is connected with the Miocene intrusions of intermediate and acid composition and neck breccia of the maar-diatreme complex. The ore mineralization is spatially associated with dacites, presented by biotite and amphibole-bearing hypabyssal rocks with rare quartz phenocrysts. Those intrusions form two main bodies (Cetate and Cârnic) which protrude into a large explosive breccia body and maar sediments and include the predominant stocks of Au and Ag. The hydrothermal processes had cyclic character and were interrupted by eruptions within the maar-diatreme complex and were responsible for alteration of country rocks as well as for the ore mineralization.

The main gold ore mineral of the deposit is electrum, being well known by famous large crystals and dendrites. The andesite and dacite intrusions were dated by geological mapping and isotopic geochronology (U-Pb, magmatic zircon) and Ar-Ar (hydrothermal adularia). It was shown, that the magmatic intrusions accompanied by the phreatomagmatic brecciation and epithermal ore formation was performed within narrow time intervals between 13.6 and 12.8 Ma (Wallier et al., 2006). These data indicate the tight temporal connection of magmatism and the Roşia Montană epithermal mineralization.

This deposit is thoroughly studied in terms of its geology, mineralogy and geochemistry of ores and altered country rocks as well as in age, physico-chemical mineral-forming process parameters and ore fluid sources (Cook et al., 2004 etc). Recently the fluid inclusion data, obtained from the studies of large bipyramidal magmatic ß-quartz crystals in Montană dacites were published (Wallier et al., 2006). Those dacites are spatially associated with Au-Ag ore mineralization. The existence of high-temperature (above 460 °C) and high saline (32-55 eq mass% NaCl) fluid inclusions was found, which are interpreted as magmatic fluid relics.

We took some samples of bipyramidal magmatic quartz at two Montană dacite exposures, the former being analogous to those investigated by Wallier et al. in 2006. We studied the primary silicate melt inclusions as well as crystal inclusions. The crystal inclusions were observed as plagioclase (An_{51-62}), orthoclase, amphibole (F = 0.19 mass%, Cl = 0.04 mass%), zircon, magnetite (TiO_2 = 2.8 mass%) and iron sulphide. The melt inclusion dimensions are usually not above 10 - 15 µm, rarely near 30 µm. Melt inclusions were heated in muffle furnace (Naumov, 1969) up to their homogenisation, chilled and exposed to the surface by grinding on the diamond paste. The glasses were analysed by the X-ray microprobe SX-100 (Vernadsky Institute, Moscow) and by ion microprobe IMS-4f (Yaroslavl', Russia). Two types

of melts were established (see Fig. 1). The first type is very unusual in chemical composition. The 19 studied inclusions are represented by the following average composition (in mass%): 76.3 SiO_2, 0.37 TiO_2, 6.37 Al_2O_3, 4.55 FeO, 0.09 MnO, 1.61 MgO, 2.90 CaO, 2.79 Na_2O, 3.77 K_2O, 0.07 P_2O_5, 0.02 Cl. The second type of inclusions are typical for the acid melts and the 21 studied inclusions have a composition as follows (in mass%): 79.4 SiO_2, 0.16 TiO_2, 11.25 Al_2O_3, 0.65 FeO, 0.09 MnO, 0.30 MgO, 1.88 CaO, 3.53 Na_2O, 2.66 K_2O, 0.07 P_2O_5, 0.05 Cl. The comparison of these data shows the remarkable variations in Ti, Al, Fe, Mg, Ca, Na and K. High values of the total sums, being near to 100 % (98.8-99.1 mass%) are indicative of a low water content in these melts. Two inclusions of Type I and two inclusions of Type II were analysed by the use of the ion microprobe and it was found that those are largely different in terms of their rare element composition. Respective values are as following (in ppm): 10.0 and 0.69 Be, 29.3 and 5.7 B., 6.4 and 1.4 Cr, 146

and 6.9 V, 74 and 18 Cu, 92 and 29 Rb, 45 and 15 Zr, 1.7 and 0.6 Hf, 10.3 and 2.3 Pb, 52 and 1.3 U. Such results support the assumption of probable contamination of magmatic melt by unusual crustal rocks (sedimentary rocks?). The specific ore mineralization could be responsible for such contamination.

REFERENCES
Naumov, V.B. (1969). *Geokhimiya*, 4: 494-498.
Manske S.L. et al. (2006), *SEG Newsletter*, 64: 1, 9-15.
Wallier, S., et al. (2006). *Economic Geology*, 101: 923-954.
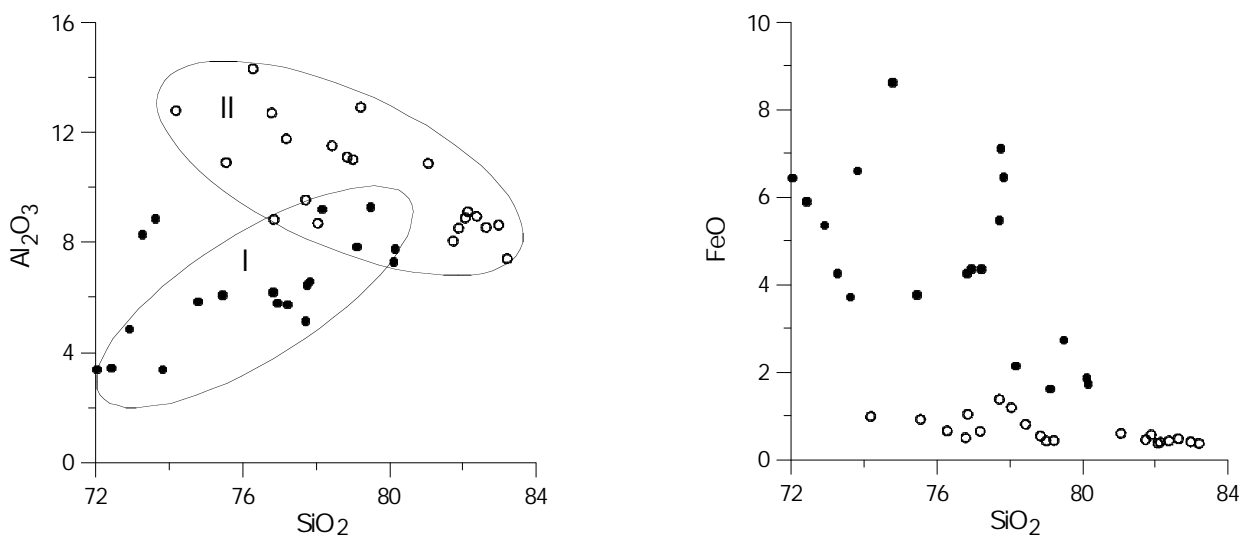
Fig. 1. Variation diagrams SiO₂ – Al₂O₃ and SiO₂ - FeO

Fluid–rock interactions in mafic granulite xenoliths from Bakony – Balaton Highland Volcanic Field

Németh, Bianca*,**, Török, Kálmán ** and Szabó, Csaba*

*Lithosphere Fluid Research Lab, Department of Petrology and Geochemistry, Institute of Geography and Earth Sciences, Eötvös University, Budapest, Hungary
** Eötvös Loránd Geophysical Institute of Hungary

1. INTRODUCTION

The Pannonian Basin is famous of its xenolith localities hosted by Plio-Pleistocene alkaline basalts, where several kinds of ultramafic, mafic and other kinds of xenoliths from different depths of the lithosphere were found and studied. In this work we present the first results of fluid-rock interaction studies in mafic garnet granulite xenoliths from the Bakony-Balaton Highland Volcanic Field (BBHVF) specifically from Sabar-hegy (Káptalantóti), from Szigliget and from Mindszentkálla. We made petrography, microthermometry, electron microprobe analyses and Raman spectroscopy on silicate melt inclusions to find out their composition and origin to assess the interaction between the granulitic lower crust and the migrating melts.

2. DESCRIPTION OF THE SAMPLES, GENERAL CHARACTERISTICS

The main rock forming minerals in the studied xenoliths are Pl, Cpx, Grt ± Opx, while the most common accessory is sphene, with some Zrn, Ilm, Rt and Ap crystals (mineral abbreviations after Kretz, 1983) as well. Some xenoliths contain amphibole and rarely biotite. This is the oldest mineral assemblage which could be detected. Texturally younger minerals originating from different reactions like melting and subsequent crystallisation (i.e. fluid-rock interaction) occur in some samples. E.g. reaction of sphene with melt produced Cpx + Ilm ± Pl or the breakdown reaction of Amp which produced Cpx and Pl ± Grt ± Opx.

The metamorphic peak temperature of the granulite xenoliths is between 800 and 1050 °C and the peak pressure varies between 1.0 and 1.6 GPa based on geothermobarometric calculations (Dégi, 2010).

3. SILICATE MELT INCLUSIONS

Two generations of SMIs were observed in the samples. There are primary silicate melt inclusions, in the original granulite facies rock forming minerals (plagioclase, clinopyroxene and sphene). Some of the minerals which were formed during later fluid-rock interactions (e.g.: Ilm, Cpx and Opx, new Amp and Pl) also trapped SMIs during their growth.

Both types of SMIs in plagioclase show negative crystal shape, with sizes of 10 - 90 μm and consist of a colourless glass phase and a fluid bubble. Due to the dark occurrence of the bubbles, microthermometry was not possible. Raman analyses of the fluid bubbles indicate CO_2+CO in the inclusions. Clinopyroxene also contains both types of SMIs with irregular forms and sizes between 10 and 20 μm. The observed SMIs contain brown coloured glass ± bubble(s). The last melting points suggest pure CO_2 (-56.6 °C). The homogenization temperatures (T_h = 29.9 °C) show that low-density gas is present in the bubble, which always decrepitated. Bubbles contain CO_2+H_2O according to Raman analyses. SMIs in sphene, are around 10 μm and show negative crystal forms. They contain brown glass phase ± fluid bubble. Because of the small size of bubbles (<1 μm), we were not able to analyse them with microthermometry. Ilmenite hosts 10-50 μm SMIs which were observed by SEM.

4. COMPARISON OF EXPERIMENTAL DATA WITH ELECTRONMICROPROBE DATA OF SMIS

We measured the composition of the glass phase in SMIs by electron microprobe and compared them with experimental data to find out the origin of the melts. The results are shown in the TAS (total alkali-silica) diagram (see Fig. 1). The glass phases of SMIs of plagioclase and clinopyroxene are trachydacitic-dacitic-rhyolitic and

show similar compositions to the rhyolitic-dacitic melts derived by the melting of biotite-quartz-plagioclase assemblage (Patiño-Douce and Beard, 1995) or melting of metagreywacke (Montel and Vielzeuf, 1994 and 1997). Melts with similar composition were derived also by the melting of mafic granulites (Springer and Seck, 1997).

The composition of the glass in SMIs trapped in ilmenite is trachybasaltic to trachydacitic and close to the composition of glass derived from melting of alkaline basalt in the presence of H_2O and CO_2. (Kaszuba and Wendlandt, 2000; Fig. 1).

The composition of the glass in SMIs trapped in sphene are trachyandesitic or rhyolitic in composition. The trachyandesitic ones show similarities to melts from partial melting of alkaline basalt as in the case of ilmenite hosted ones (Fig. 1). The rhyolitic ones have composition close to glasses from quartz-amphibolite melting (Patiño-Douce and Beard, 1995), or by melting of granulite (Springer and Seck, 1997) (Fig. 1).

5. SUMMARY

The comparison of SMI compositions and the experimental data suggests that the SMIs originated from partial melting of different lower crustal rocks of mafic and metasedimentary origin with an occasional presence of fluids such as H_2O and CO_2. According to the two different generations of host minerals and primary melt inclusions trapped, we can establish at least two stages when melt was present in the lower crust and interacted with the lower crustal rocks.

The Ttn contains SMIs from the oldest detected mineral assemblages, which belongs to the formation of the granulite facies in the lower crust. The crystallizing parent melt of the granulite what was in the lower crust seems to be trachyandesitic to rhyolitic. SMI compositions in the later reaction products, such as Pl, Cpx and Ilm show that younger melts have different compositions. One part of them has trachydacitic-dacitic-rhyolitic compositions. The origin of this melt can be melting of biotite-gneiss or quartz-amphibolite. Other parts of these melts have andesitic, basaltic trachyandesitic compositions, which suggest a melting event of an alkaline basalt

in the presence of fluids. Our results show that melts of different composition percolated the lower crust at least two times during its evolution.
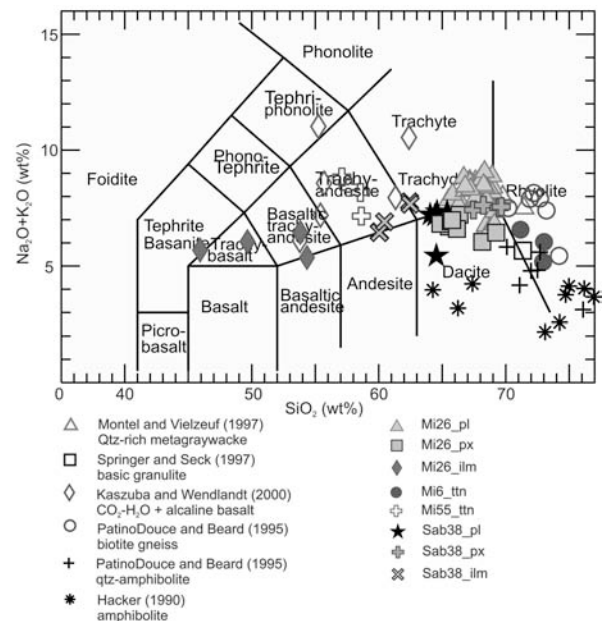
Fig.1. TAS-diagram of the electron microprobe analyses of the glass phases of silicate melt inclusions comparing with the data in the literature on experimental works.

REFERENCES
Dégi J (2010): *Unpubl. PhD Thesis* Eötvös University, Budapest
Kaszuba J.P. and Wendlandt R.F. (2000): *J. Petrology* (41) 3: 363–386.
Kretz R. (1983): *Am Mineral* (68): 277-279
Montel J-M. and Vielzeuf D. (1997): *Contrib Mineral Petrol* (128): 176-196.
Patiño-Douce A.E. and Beard J.S. (1995): *J. Petrol.* (36) 3: 717-738.
Springer W. and Seck H.A. (1997): *Contrib Mineral Petrol* (127): 30-45.
Vielzeuf D. and Montel J-M. (1994): *Contrib Mineral Petrol* (117): 375-393.

Generation and crystallization conditions of the Colle Fabbri melilitite melt, Italy: melt inclusion data

Nikolaeva A.T.

V.S. Sobolev Institute of Geology and Mineralogy SB RAS, Koptyuga 3, Novosibirsk, Russia

The Colle Fabbri volcano consists of 4 m thick freatomagmatic breccia and volcanic neck of fine-medium grained leucite - wollastonite melilitolite. The wollastonite – anortite – pyroxene igneous rocks are located at the contact of the melilitolite body and the pelite country-rock. (Stoppa and Sharygin, 2009; Stoppa and Rosatelli, 2009).

The Colle Fabbri melilitolites are rocks of the kamafugite series (Stoppa et al., 2002). However, they differ with the presence of wollastonite, which is not characteristic of common kamafugites.

Leucite – wollostonite melilitolite contains almost equal amounts of (35 – 40 vol%) melilite and wollastonite, as well as small amount of leucite, plagioclase, Ti-garnet, apatite, magnetite and Fe-Ni-sulphides. The chemical composition of leucite – wollastonite melilitolites is Si-undersaturated (about 42 mass% SiO_2) with a low content of Al_2O_3 (10.7 – 11.2 mass%) and extremely high content of CaO (37.3 – 38.5 mass%). Despite the presence of leucite in the rock, the total amount of Na_2O+K_2O is low (about 1.4 – 1.9 mass%.) The contents of MgO (1.6 – 2.4 mass%) and FeO (3.3 – 3.7 mass%) are also low.
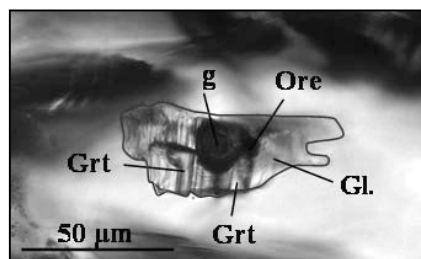
Fig. 1. Inclusion in melilite (transmission light).

The single partly crystallized melt inclusions are found in the grains of melilite (up to 50 μm). Their phase composition is glass, garnet, ore phases, and a gas bubble (Fig. 1). T_h = 1320 ± 15 °C.

The chemical composition of unheated glasses varies considerably in the contents of (mass%) 36.76 – 58.69 SiO_2, 19.89 – 29.65 Al_2O_3, 2.17 – 11.42 CaO, 0.23 – 1.68 FeO, 0.03 – 0.58 MgO and 7.79 – 26.42 K_2O. The amounts of TiO_2 (up to 0.67 mass%), Na_2O (up to 0.59 mass%), BaO (up to 0.98 mass%), P_2O_5 (up to 2.91 mass%) and SO_3 (up to 1.84 mass%) are also appreciable.

The chemical composition of heated glasses varies as well and are compared to unheated ones characterized by lower values (mass%) of SiO_2 (38.04 – 39.57), Al_2O_3 (mostly 14.4 – 17.6), K_2O (mostly 0.21 – 5.7) and higher CaO (21.63 – 30.59), FeO (5.59 – 6.65), MgO (0.44 – 2.83), Na_2O (0.37 – 0.75) and SO_3 (up to 1.29).

Wollastonite also contains single, partly crystallized melt inclusions (< 40 μm). Their phase composition is glass, garnet, ore phases and gas bubble (Fig. 2). T_h is higher than 1230 °C.
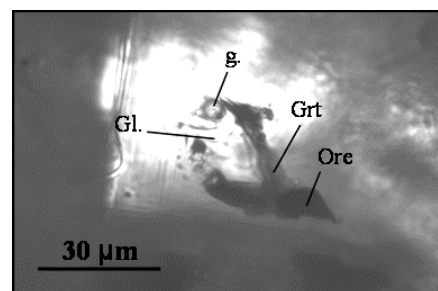
Fig. 2. Inclusion in wollostonite (transmission light).

The glasses of unheated inclusions contain (mass%): 43.37 – 47.49 SiO_2, 10.78 – 16.71 Al_2O_3, 0.78 – 0.97 FeO, 0.06 – 0.09 MgO, 20.79 – 29.92 CaO, 3.94 – 5.75 K_2O, 1.18 – 2.24 Na_2O and minor TiO_2 (up to 0.17), P_2O_5 (up to 0,10) and SO_3 (up to 0.09).

The chemical composition of heated glass compared to unheated ones are characterized (mass%) by high FeO (4.27 – 14.39), MgO (0.14 – 0.45), TiO_2 (up to 4.75), P_2O_5 (up to 1.17) and SO_3

(up to 0.78), equal Al_2O_3 (11.62 – 25.03), CaO (25.18 – 36.64) and low SiO_2 (28.61 – 36.7), K_2O (0.31 – 1.63) and Na_2O (0.80 – 1.83).

It is noteworthy that the chemical composition of heated glass in wollostonite compared to ones in melilite has less amounts of Si, Al, K and more values of Fe, Mg and Ti at similar Ca and Na contents.

According to the geochemical data melilite (gehlenite – akermanite) contains about an order of magnitude more LILE and much less HFSE compared to the primitive mantle (PM). The pattern for melilite (Fig. 3) normalized to primitive mantle has a negative slope with positive anomalies of Ka and Sr and negative anomalies of Nb, Zr and Ti.
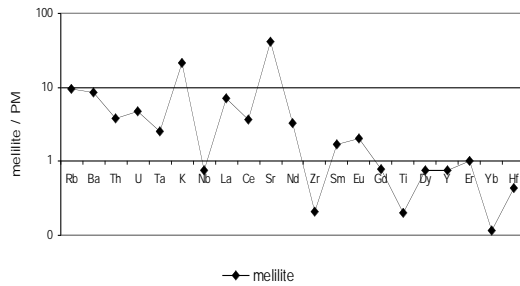
*Fig. 3. Primitive mantle-normalized (*Taylor, McLennan, 1985*) spider-diagram for melilite.*

The content of trace elements in the rock and in the glasses of heated inclusions in melilite are similar (Fig. 4). They are considerably enriched in incompatible elements, whose concentrations are 2 for Rb and Ba, 1,5 for K or 1 of HFSE orders of magnitude higher than the mantle norm. The patterns of the rock and the glass of heated inclusion have a negative slope owing to the high LILE and LREE and low HREE. This indicates the possible presence of garnet in the mantle source. It is known that in the primitive melt LREE increase and HREE remain in the garnet during partial melting of a garnet-bearing source located at the depth between 30 – 60 km (Sklyarov et al., 2001).

The considered pattern (Fig. 4) as well as the pattern for melilite (Fig. 3) display negative Nb and Ti anomalies, which possibly indicate the involvement of crustal material in magmatic

process. Moreover, on the Nb/Ta - La/Nb diagram (Barth et al., 2000) the rock and melilite-hosted melt are localized in the same region of the continental crust influence.
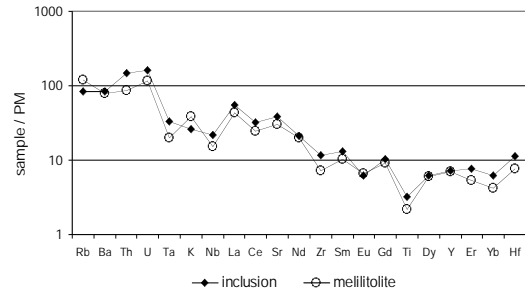
*Fig. 4. Primitive mantle-normalized (*Taylor, McLennan, 1985*) spider-diagram for melilitolite and melt inclusion in melilite.*

Thus, thermometric data suggest that the crystallization of melilite in the studied rocks started at 1320 ± 15 °C and crystallization of wollostonite occurred above 1230 °C.

The initial magma for leucite – wollostonite melilitolite was a Ca-enriched melilitite melt.

Geochemical data indicates that the studied rocks are enriched in trace elements and the crustal material was involved in the magmatic process during their formation.

REFERENCES

Barth M.G., McDonough W.F., Rudnik R.L. (2000) *Chem. Geology*, 165:197-213.

Taylor S.R., McLennan S.M. (1985) *Blackwell*, Oxford.

Sklyarov E.V. et al. (2001) *Interpretation of geochemical data*. Moscow (in Russian).

Stoppa F., Rosatelli G. (2009) *Journal of Volcanology and Geothermal Research* 187: 85 – 92.

Stoppa F., Sharygin V.V. (2009) *Lithos* 112S: 306 - 320.

Stoppa F., Whooley A.R., Cundari., (2002) *Mineralogical Magazine* 66(4): 555 – 574.

Fluid inclusion microthermometry in coexisting quartz and wolframite – a case study from Morococha, Peru

Ortelli, Melissa and Kouzmanov, Kalin

Earth and Environmental Sciences, University of Geneva, 13. Rue des Maraîchers, Geneva, Switzerland

In the ore deposit research, most fluid inclusion studies are conducted on transparent gangue minerals which are "co-genetic" with the mineralization according to textural evidence. However, ore-precipitating fluids can be more directly studied by analyzing fluid inclusions found in transparent ore minerals, like Fe-poor sphalerite (e.g. Simmons and Browne 1997; Bonev and Kouzmanov, 2002) or wolframite. Commonly, wolframite-hosted fluid inclusions are studied by infra-red light microscopy and microthermometry (Campbell and Robinson-Cook, 1987; Bailly et al., 2002), but some Mn-rich wolframite (huebnerite) can be transparent in visible light due to its low iron content.

In this study we present and compare microthermometric measurements of fluid inclusions in huebnerite (Mn-rich wolframite) and syn-genetic quartz from Cordilleran polymetallic veins of the Morococha district in Peru, which overprint the giant Toromocho porphyry Cu-Mo deposit (Catchpole, 2011). The huebnerite, which precipitated after enargite and other Cu-sulphosalts, occurs intergrown with pyrite and quartz. A growth zonation highlighted by reddish-orange bands is visible in transmitted light microscopy (Figs. 1 and 2a).

Electron microprobe analyses (EMPA) and X-ray mappings reveal growth banding controlled by variable Fe and Mg content (Fig. 1), which substitute for Mn in the wolframite structure (Bailly et al., 2002). Iron and Mg content in huebnerite (Fig. 1.d-f) are often below the detection limit of 0.2 mass% and 0.07 mass%, respectively, but three analyses yield compositions of 0.7 to 1.65 to mass% Fe and 0.13 mass% Mg.

Microthermometric measurements have been performed on huebnerite and quartz using a Linkam THMSG 600 heating-freezing stage mounted on a DMLB Leica microscope. Primary (along growth bands) and secondary fluid inclusion assemblages (FIAs; Goldstein and Reynolds, 1994) were found in the wolframite, while numerous secondary fluid inclusions were observed along trails in quartz crystals (Fig. 2). Both, primary and secondary fluid inclusions in wolframite are liquid-rich (30 % vapour). Post-entrapment modifications due to necking-down or leaking are common for secondary fluid inclusions in quartz and wolframite.
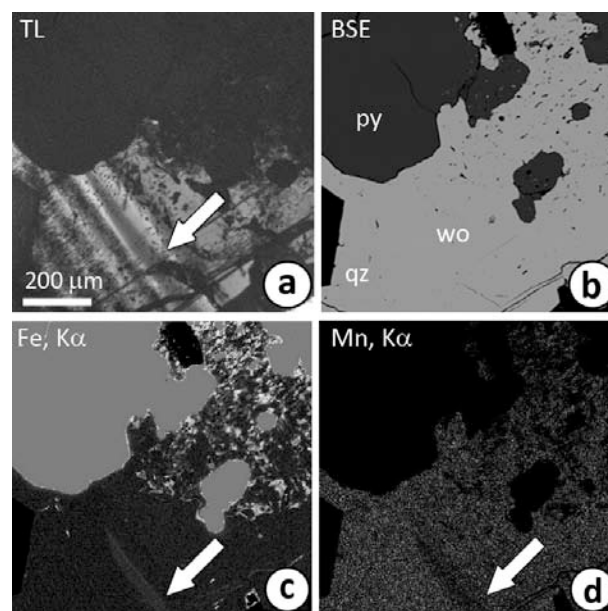
Fig. 1. Wolframite textures: a) Transmitted light photomicrograph of growth zoning in wolframite; b) BSE image showing no zonation; c-d) EMP X-ray maps of Fe and Mn. Iron and Mg are enriched in the dark growth bands (white arrows), whereas Mn is slightly depleted. Abbreviations: py - pyrite, qz – quartz, wo - wolframite.

Primary FIAs in wolframite yield homogenization temperatures of around 300 °C and low salinity (1-1.3 eq mass% NaCl) and are representative for the wolframite deposition conditions (Fig. 3). Secondary fluid inclusions in wolframite have similar or slightly lower homogenization temperatures but higher salinity reaching 4.3 eq mass% NaCl.

Secondary fluid inclusions in quartz usually yield lower homogenization temperatures between 180 to 280 °C with salinities similar to those found in the secondary FIAs in the wolframite (Fig. 3).
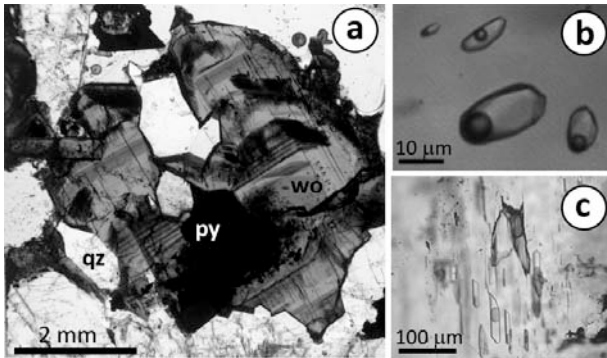
Fig. 2. *Transmitted-light photomicrograph of wolframite-quartz-pyrite vein from the Morococha district: a) Growth zones are highlighted by dark growth bands; b) Large secondary liquid-rich fluid inclusions in quartz; c) Primary fluid inclusions in wolframite.*
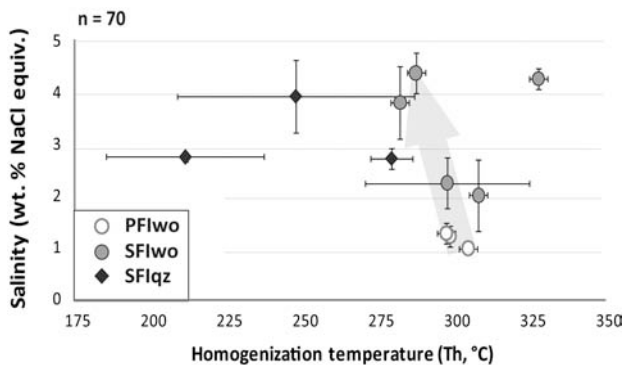
Fig. 3. Microthermometry data for fluid inclusions hosted in quartz (diamonds) and wolframite (circles). Seventy single fluid inclusion measurements have been collected from 11 FIAs. The arrow indicates the T-X evolution of the fluid from a low salinity (1 eq mass% NaCl) at 300 °C which cools with time and undergo boiling as revealed by secondary FIAs in wolframite and quartz with higher salinities. X-error bars are mostly reflecting the effect of post-entrapment re-equilibration of the fluid inclusions (e.g., necking-down). Abbreviations: PFIwo – primary fluid inclusions in wolframite, SFIwo – secondary fluid inclusions in wolframite, SFIqz – secondary fluid inclusions in quartz.

Fluid boiling could explain the evolution of the fluid salinity of wolframite-hosted inclusions from an early high-temperature low-salinity fluid (primary FIAs) to later lower temperature fluid (secondary FIAs) with a higher salinity (Fig. 3, light arrow). Finally, fluid mixing between the cooling fluid and meteoric water could explain the decrease of homogenization temperatures and salinity of the two secondary FIAs in the quartz. The data are in agreement with reported microthermometric results for Cordilleran polymetallic veins from the central Morococha district (Catchpole, 2011).

This fluid inclusion study on wolframite and quartz reveals that microthermometric measurements on ore and gangue minerals can complement each other, bringing more information concerning the fluid evolution. LA-ICP-MS analyses of the fluid inclusions will be undertaken in order to compare the metal, alkalis and sulphur content of quartz- and wolframite-hosted FIAs in the studied samples.

ACKNOWLEDGMENTS

REFERENCES

Bailly L., Grancea L., Kouzmanov K. (2002) *Economic Geology* 97: 415-423.

Bonev I., Kouzmanov K. (2002) *European Journal of Mineralogy* 14: 607-620.

Campbell A.R., and Robinson-Cook S. (1987) *Economic Geology* 82: 1640-1645.

Catchpole H. (2011) *PhD thesis*, University of Geneva, Switzerland.

Goldstein R.H. and Reynolds T.J. (1994) *Systematics of fluid inclusions in diagenetic minerals.* SEPM Short Course 31.

Simmons S.F. and Browne P.R.L. (1997) *Economic Geology* 92: 485–489.

Preliminary study of CO$_2$-rich fluid inclusions in upper mantle xenoliths from the Rio Grande rift, New Mexico

Park, Munjae*, Haemyeong Jung*, Youngwoo Kil**, Berkesi, Márta*** and Szabó, Csaba***

*School of Earth and Environmental Sciences, Seoul National University, Seoul, Korea
**Geological Museum, Korea Institute of Geoscience and Mineral Resources, Daejeon, Korea
***Lithosphere Fluid Research Lab, Eötvös University, Budapest, Hungary

Introduction

Study of fluid inclusions in mantle xenoliths can provide useful information on fluids that interact with the mantle lithosphere (e.g. Andersen and Neumann, 2001; Hidas et al., 2010). Knowledge of their existence and composition is essential in understanding mantle processes (e.g. Roedder, 1984).

In our study mantle xenolith-hosted fluid inclusions have been investigated to get information on fluids in a rift tectonic setting.

Sampling

The studied spinel peridotite xenoliths were collected at the Rio Grande rift (New Mexico, USA) far from the rift axis; occurrence is called Adam's Diggings. The age of the host basalt has been determined up to 15 million years.

Fluid inclusions petrography

Host minerals of fluid inclusions are orthopyroxenes and clinopyroxenes. Two fluid inclusion generations were distinguished on the basis of textural appearance. According to definition of Roedder (1984), one generation is the petrographically primary and psuedosecondary, whereas the other one is petrographically secondary. The primary inclusions can be characterized by having negative crystal shapes with a size ranging between 2 and 14 microns and are randomly distributed and isolated. The secondary inclusions have elongated shapes and occur along healed fractures. Their size varies from 13-80 microns.

In this study we are focusing only on the negative crystal shaped fluid inclusions. These inclusions have mainly one visible fluid phase at room temperature, but solid phase could also be rarely seen.

Microthermometry

We conducted microthermometry to determine composition and density of the inclusions' fluid phase. The melting (dissolution) temperatures are consistently –56.9 °C (± 0.1 °C, n=40).Homogenization into the liquid phase is observed between –30.2 °C and –16.5 °C. These observations indicate that the trapped fluid is dominated by CO$_2$. The density of CO$_2$ was calculated between 1.015 and 1.077 g/cm^3 using the equation of state developed by Span and Wagner (1996).

Raman spectroscopy

Raman spectroscopy show Raman peaks at 738.5 and 1094.0 cm^{-1} (when focusing with the laser spot on the solid phase) indicating the presence of magnesite. However, indication for any other fluid molecules than CO$_2$ was not found, even at high temperature (150 °C).

Conclusions

The presence of fluid inclusions indicates that high-density CO$_2$ were entrapped in the lithospheric mantle beneath Rio Grande rift.

Acknowledgement

REFERENCES

Andersen T., Neumann E-R., (2001) *Lithos* 55: 01-320.

Hidas K., Guzmics T., Szabó C., Kovács I., Bodnar R.J., Zajacz Z., Nédli Z. Vaccari L. & Perucchi A. (2010) *Chem. Geol.* 274: 1–8.

Roedder, E. (1984) *Rev. Mineral.* 12: 1-646.

Span R., Wagner W. (1996) *J. Phys. Chem. Ref. Data* 25: 1513-1558
.

Unique phlogopite and amphibole-bearing fluid inclusions in upper mantle xenoliths from Cameroon Volcanic Line

Pintér, Zsanett*, Kovács, István**, Berkesi, Márta*, Szabó, Csaba*, Tene Djoukam, J. F. ***, Tchouankoue, J.P. *** and Perucchi, Andrea****

*Lithosphere Fluid Research Lab, Eotvos University (ELTE) Budapest, Hungary
**Eötvös Lorand Geophysical Institute of Hungary
***Department of Earth Sciences, University of Yaounde I, Yaounde Cameroon
****ELETTRA Syncrotron Light Laboratory, Trieste, Italy

Introduction

Phlogopite and amphibole play great role in understanding the role of H_2O-bearing CO_2-rich fluids/melts in the lithospheric upper mantle (e.g. Sato et al., 1997). The presence of the H_2O in mantle fluid inclusions (Berkesi et al., 2009) as well as amphibole-and/or phlogopite-bearing ultramafic xenoliths (e.g. Szabó et al., 2009) shed lighten on the importance of understanding the fluid properties in the mantle. We have studied fluid inclusions hosted in upper mantle xenoliths from alkali basalts outcropped at Nyos and Barombi Lakes, which are situated at the Cameroon Volcanic Line (CVL). We found both phlogopite and amphibole (pargasite) within the fluid inclusion, beside the C-O-H-S system providing an insight into the fluid/peridotite reaction.

Ultramafic xenoliths

The studied amphibole-bearing peridotite xenoliths are spinel lherzolites with protogranular and porphyroclastic texture showing lithologies and mineral chemistries similar to the other xenoliths from the continental sector (Lee et al., 1996; Dautria and Girod, 1986) along the CVL, and also to the average sub-continental lithospheric mantle (Downes, 2001).

Petrography of fluid inclusions

Based on fluid inclusion petrography, two main generations of fluid inclusions can be distinguished in the xenoliths as Type 1 and 2 (Fig. 1). Type 1 fluid inclusions can be seen randomly in olivine and orthopyroxene in Nyos peridotites. These fluid inclusions have negative crystal shape with an average size of 50 μm, and they are partially or completely decrepitated. This population of fluid inclusions is considered as older

generation fluid inclusions relative to the Type 2 ones, which occur in all the mantle silicates, (including clinopyroxene, orthopyroxene and olivine) in both Barombi and Nyos xenoliths. These inclusions are trapped along healed fractures in sizes of 8 - 30 μm. In the Nyos peridotites, however, they can also be found in neighbourhood of the older decrepitated inclusions. This population of fluid inclusions is considered as younger generation fluid inclusions. They can be divided into two subgroups: generation 2A fluid inclusions showing negative crystal or spherical shapes, and generation 2B fluid inclusions which have irregular, oval or vermicular shape. Solid phases in the younger generation (2A) fluid inclusions were identified under polarized microscope.

Microthermometry and Raman analyses

Microthermometric measurements were carried out only on generation 2A fluid inclusions because they show textural equilibrium with the host silicates in mantle xenoliths. In the generation 2A fluid inclusions for both Barombi and Nyos peridotites similar last melting temperatures were observed. In the Barombi xenoliths melting temperature shows a very narrow range between -57.9 and -56.6 °C, and in the Nyos samples the range is between -58.1 and -56.6 °C. The homogenization temperatures are between -48.2 and -27.8 °C in the Barombi xenoliths and between -50.9 and -30.1 °C in the Nyos xenoliths. Based on the density of CO_2-rich inclusions in ortho- and clinopyroxenes (1.12 - 1.03 g/cm^3), the estimated minimum trapping pressure conditions correspond to a range between 8.4 and 11 kbar (Holloway & Blank, 1981).

Raman analyses were conducted at room and elevated temperatures (+150 °C) after Berkesi et al. (2009). At room temperatures the CO_2, H_2S and small peak of H_2O as a dissolved component in CO_2 were detected, whereas at elevated temperatures, beside the Fermi-diad of CO_2, the peaks of H_2O dissolved in CO_2 were also observed in higher ratio than at room temperature. Presence of H_2S is in good accordance with the distribution of the observed CO_2 melting temperatures. With Raman spectroscopy solid phases were also detectable, which show magnesitic composition (Type 2A).

SR-FTIR on the fluid inclusions

The main advantage of the use of the Fourier Transform Infrared Spectroscopy coupled with Synchrothron Radiation (SR-FTIR) is twofold: 1) enables high resolution (5x5 microns aperture size) mapping of the phases in the mantle fluid inclusions and 2) able to detect OH-bearing, microns sized, solid phases easily. By the use of SR-FTIR we detected and mapped fluid inclusion compositions, especially H_2O next to the major CO_2 (Fig.1). Solid phases were also identified inside the fluid inclusion. Their absorbance characteristics are a combination of both pargasite and phlogopite (Green et al., 2010) in the OH stretching range (Fig.1). It is important to mention that by the use of Raman spectroscopy, the identification of these latter phases is more ambiguous.

Conclusion

Our results suggest that the CO_2-rich fluid inclusions, occurring in both Barombi and Nyos upper mantle xenoliths, trapped at lithospheric mantle condition in the mantle silicates. The application of the infrared spectroscopy coupled to synchrotron radiation is confirmed to be a great tool for mapping the fluid phases and identify OH-bearing solid phases (phlogopite and amphibole), that play a great role in the metasomatized upper mantle.

Acknowledgement:
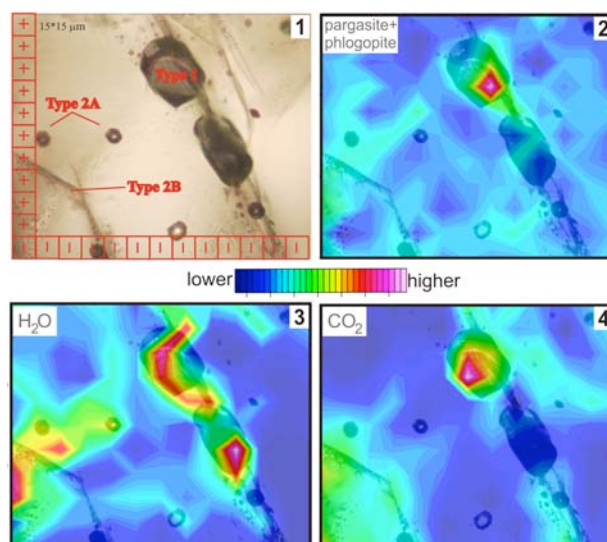
Fig. 1. Orthopyroxene-hosted fluid inclusions (Type 1, 2A and 2B) (1) and the distribution of OH-bearing solid phases (2), H_2O (3) and CO_2 (4) inside the fluid inclusions.

REFERENCES

Berkesi, M., Hidas, K., Guzmics, T., Dubessy, J., Bodnar, R. J., Szabó, C., Vajna, B. & Tsunogae, T.(2009) *J. Raman Spectrosc.* 40: 1461–1463.

Dautria, J.M. & Girod, M. (1986) *Bull. Minéral.* 109, 3:275–288.

Downes, H. (2001) *J. Petrol.* 42: 233-250.

Holloway, J.R. & Blank, J.G. (1981) In Hollister: L.S., Crawford, M.L.,(Eds.). Mineralogical Association of Canada, Short Curse Hadbook 6: 13-38.

Green, D. H., Hibberson, W. O., Kovács, I. & Rosenthal, A. (2010) *Nature* 467: 448-452.

Lee , D.-C., Halliday, A. N., Davies, G. R., Essene, E. J., Fitton, J. G. & Temdjim, R. (1996) *J. Petrol.,* 37: 415-441.

Sato, K., Katsura, T. & Ito, E. (1997) Earth *Planet. Sci. Lett.* 146: 511-526.

Tanyileke, G.Z., Kusakabe, M. & Evans, W.C. (1996) J. of African Sciences, 22: 433-441.

Touret, J., Grégoire, M. and Teitchou, M. (2010) C.R. *Geoscience* 342: 19-26.

Fluid inclusions in the Outokumpu Deep Drill Core: implications for paleofluid evolution and composition of modern deep saline fluids

Piribauer, Christoph J.*, Meyer, F. Michael*, Sindern, Sven*, Vennemann, Thorsten W.** and Prochaska, Walter***

*Institute of Mineralogy and Economic Geology, RWTH Aachen University, Wüllnerstraße 2, D-52056 Aachen
** Institut de Minéralogie et Géochimie, Université de Lausanne, BFSH-2, CH-1015 Lausanne
***Department of Applied Geoscience and Geophysics, University of Leoben, 8700 Leoben

The drill hole, which was finished in January 2005 at a depth of 2516 metres, transects the Paleoproterozoic Outokumpu formation and was intended to encounter the Archaean basement. The Outokumpu formation represents a 1-5 km thick remnant of folded and imbricated overthrust terrain, consisting of mica schist with black schist interlayers, serpentinite, skarn rocks, and pegmatitic gneisses, which are underlain by Archaean basement. The formation was strongly deformed during the Svecofennian orogeny (1.9 Ga) (Gaal et al., 1975).

Mica schist, biotite mica schist, and biotite gneiss contain quartz, biotite, chlorite, and feldspars as main components and accessory minerals like hematite, pyrrhotite, garnet, and tourmaline. Fine-grained quartz is oriented along bedding planes and/or foliation. Some grains show undulous extinction and incipient recrystallisation. Biotite defines bedding planes and/or foliation and is partly replaced by chlorite. Plagioclase is rarely replaced by white mica and alkali feldspar shows signs of incipient alteration. The mineralogy and texture of the ultramafic rocks of the Outokumpu assemblage show an amphibolite facies overprint (Peltonen et al. 2008). The samples studied are addressed as serpentinites. Microscopically serpentine, calcite, Mg-chlorite, and sericite can be distinguished. Because of the strong serpentinisation and the metamorphic conditions, no relicts of the primary magmatic minerals could be identified. In addition, magnetite and pyrite occur as opaque phases. The skarn rock mainly consists of diopside and tremolite, which are arranged in a herringbone pattern. Talc, carbonates, and opaque phases are also present. The opaque phases, like pyrrhotite and chalcopyrite, replace the primary minerals. The

skarn rocks are often penetrated by calcite veins (Piribauer et al. 2011)

In addition to these main lithologies other strongly carbonatized rock types were found. The pegmatites and pegmatitic granites consist of alkali feldspar, plagioclase, muscovite, quartz, and garnet. Apatite, epidote, and opaque phases occur as accessories. Quartz shows partly undulous extinction and no recrystallisation has been observed. The strip-shaped plagioclase shows beginning alteration and a myrmekitic intergrowth with quartz. Alkali feldspar is not as strongly altered as plagioclase and muscovite forms large crystals within the interstices (Piribauer et al. 2011).

The primary, pseudosecondary, and secondary fluid inclusions observed in quartz veins contain up to three different phases: vapour phase (V), liquid phase (L), and sometimes a solid phase (S) as accidentally trapped crystals. Within the veins, fluid inclusions occur on intragranular trails, on transgranular trails, in clusters or as single inclusions in the veins. Fluid inclusions within the carbonate veins are smaller than 5 μm and cannot be analysed with microthermometry. Four different types of primary isolated fluid inclusions can be distinguished within the quartz veins, based on their composition:

Type 1: LV = H_2O-NaCl
Type 2: LV = H_2O-$CaCl_2$-NaCl
Type 3: L = CO_2
Type 4: LL = H_2O-CO_2

Type 1 fluid inclusions show a melting temperature (T_m) between -2 and -22 °C, which corresponds to a salinity of 2 – 22 eq mass% NaCl. The size of the inclusions range from <2 μm

to 40 μm. The homogenisation temperatures (T_h (LV→L)) of the type 1 fluid inclusions plot between 100 and 400 °C. Type 2 fluid inclusions have a lower eutectic melting (T_e) than type 1 fluid inclusions. T_e is between -30 and -60 °C, which suggests the presence of $CaCl_2$ in addition to NaCl. Final melting occurs between -45 and -5 °C, which points to a variable salinity of the fluid inclusions next to a variable composition of the $CaCl_2$-rich type. The CO_2 bearing, type 3, inclusions are characterised by a Tm(ice) between -57° and -60°C, which indicates the presence of another gas phase, most likely CH_4. They show different homogenisation temperatures $T_h(CO_2$ LV→L) between -11 °C and +6 °C. The homogenisation of the CO_2 occurs into the liquid phase. Type 4 H_2O-CO_2 fluid inclusions show melting temperatures of CO_2 between -57.9 and -62.5 °C, CO_2 homogenisation occurs into the liquid phase between 8.7 and 22.6 °C. It was not possible to measure T_h(total) due to decrepitation. Ice and clathrate melting temperature also suggest the presence of an additional salt component within the H_2O, which is assumed to be NaCl (Piribauer et al. 2011).

The results of crush-leach analyses show cation ratios of Ca/Na (0.255 – 0.948 molar), K/Na (0.097 – 0.204 molar), Li/Na (0.001 – 0.085 molar), and Mg/Na (0.024 – 0.344 molar), which are partially higher than seawater (Ca/Na 0.022; K/Na 0.021; Li/Na >0.001; Mg/Na 0.113; seawater values from Turekian, 1968). The Li/Na ratio rises in the vicinity of the deeper pegmatites, which suggests an influence of magmatic water. Within the Cl/Br-Na/Br diagram most of the crush-leach samples differ significantly from the seawater evaporation trajectory (SET). They also plot mainly below the 1:1 line, indicating a change of the Cl/Br-Na/Br ratios during halite precipitation and halite dissolution. The molar Cl/Br ratios range from 100 to 400 and are significantly lower than seawater, suggesting a higher Br concentration than seawater. The molar Na/Br ratios are between 80 and 580 and are similar to seawater ratios (Piribauer et al. 2011).

The $\delta^{18}O$ values of the fluid inclusions were calculated under the assumption of isotopic equilibrium between the fluid phase and the host mineral (quartz, Hu & Clayton 2003) at a temperature of 500 - 540°C, as indicated by geothermometry. The δD values of the fluid inclusions show a broad scatter; however, all values plot in the field of metamorphic fluids with the biotite values being distinctly lighter in $\delta^{18}O$ straddling the field of magmatic fluids. In contrast, the isotopic composition of the Outokumpu groundwater (Nurmi et al., 1988) plots to the left of the meteoric water line (Piribauer et al. 2011).

Deep groundwaters in the Outokumpu crystalline basement deviate significantly from fluid inclusions in their stable isotope ratios, which plot to the right of the global meteoric water line in a δD - $\delta^{18}O$ diagram. This suggests that they may have formed as a mixture of meteoric and saline waters. In addition, Cl/Br and Na/Br ratios point to chemical exchange with the host rocks. Many models have been proposed to account for the enhanced salinity of deep groundwaters and the shift in the stable isotopes, but our data indicate that the saline fluids are derived primarily through water–rock interaction. The role of fluid inclusions as important contributors to the saline fluids is not supported (Piribauer et al. 2011).

REFERENCES

Bottinga, Y, Javoy, M. (1975) *Rev. Geoph. Space Phys.* 13 (2), 401-418.

Gaál, G., Koistinen, T., Mattila, E. (1975) *Geological Survey of Finland, Bulletin* 271, 67p.

Koistinen, T.J. (1981) *Trans. Royal Soc. Edinb.: Earth Sciences* 72, 115-158.

Hu, G., Clayton, R. N. (2003) *Geochim. Cosmochim. Acta* 67 (17), 3227–3246.

Nurmi, P. A., Kukkonen, I. T., Lahermo, P. W. (1988) *Ap. Geochem.* 3 (2), 185-203.

Park, A. F. (1988) *Precambrian Research* 38 (2), 131-146.

Peltonen, P., Kontinen, A., Huhma H., Kuronen, U. (2008) *Ore Geol. Rev.* 33 (3-4), 559-617.

Piribauer, C. J., Sindern, S., Meyer, F. M., Vennemann, T. W., Prochaska, W. (2011) *Geological Survey of Finland, Special Paper* 51, 169–180

Säntti, J., Kontinen, A., Sorjonen-Ward, P., Johanson, B., Pakkanen, L. (2006) *Int. Geol. Rev.* 48 (6), 494-546.

Turekian, K.K. (1968) Oceans. Prentice-Hall, 149 pp

Postmagmatic evolution of the Caeiras-Pegmatite – a new occurrence and its potential for high-tech-metals in the Borborema Pegmatite Province, NE-Brazil

Piribauer, Christoph J.*, Sindern, Sven*,Mashev, Dobromir*, Meyer, F. Michael*, Hellmann, André*, Havenith, Vanessa J.*, Bakker, Ronald J.**, Lima, R. F. S.***, Petta. R. A.*** and Campos, T. F. C.***

*Institute of Mineralogy and Economic Geology, RWTH Aachen University, Wüllnerstrasse 2, 52056 Aachen, Germany

** Resource Mineralogy, Department of Applied Geoscience and Geophysics, University of Leoben, 8700 Leoben, Austria

*** Departamento de Geologia, Universidade Federal do Rio Grande do Norte, Rio Grande do Norte, Brazil

The Caeiras-Pegmatite is one of numerous pegmatite occurrences in the Borborema Pegmatite Province in NE-Brazil. It is exposed in three quarries and exploited by an artisanal operation since 2007. The effect of mineral alteration and redistribution is of interest for the assessment of the economic potential of the rare metal Caeiras-Pegmatite.

The heterogeneous pegmatite consists of a core of quartz, enveloped by meter-sized perthitic feldspars. Within the wall zone texturally different units can be distinguished, generally dominated by quartz and feldspar. In addition to quartz and feldspar from the core zone, other minerals such as tantalite, beryl, and tourmaline are extracted in minor amounts from both the intermediate zone and the wall zone. Tantalite mineralization is a salient feature of the general pegmatite zonation pattern known in the province. Ratios of K/Rb vary between 91 and 294 in K-feldspar. Caesium ranges from values < 2 ppm in the presence of ceramic-type feldspar in the central areas, up to 60 ppm in association with rare metal occurrences in the wall zones.

Potassium-rich alkali-feldspar crystals have the composition $Ab_{22.7-30.7}Or_{69.0-77.0}An_{0.3}$. Their perthitic exsolution texture is characterised by the occurrence of different Or-rich domains showing either fine or coarse irregular microcline. Ab-rich domains are either fine coherent lamellae or irregular elongated to patchy areas. Compositional data of these domains indicate a first exsolution event at approximately 550 °C, followed by a second at 400 to 300 °C. Irregular and partly patchy perthitic exsolutions reveal the presence of a fluid phase at the lower temperature stage, as is indicated by secondary low-salinity aqueous inclusions. The post-magmatic hydrothermal fluid overprint resulted in the alteration of primary magmatic phases and in the formation of secondary minerals. The alteration of tantalite and the ubiquitous distribution of secondary U-minerals is attributed to the late fluid overprint.

Primary, secondary, and pseudosecondary fluid inclusions within quartz contain up to three different phases: liquid, vapour, and sometimes solid as accidentally trapped crystals. These aqueous solutions show salinities up to 21 mass% NaCl eqv.; homogenisation occurs into the liquid phase at temperatures between 140 and 270 °C.

Raman spectroscopy identified CO_2 and N_2 as gaseous phases in fluid inclusions and LA-ICP-MS analyses of fluid inclusions in wall zone quartz revealed the presence of Li, in addition to Na and K. This particular fluid composition is a good indication of the rare metal potential of the wall zones.
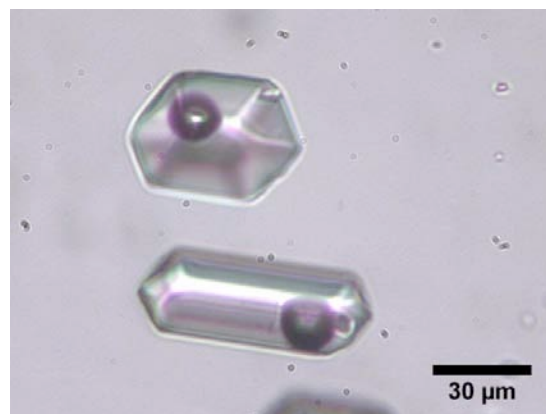
Fig. 1. High saline aqueous fluid inclusions with accidentally trapped crystals.

Cerny (1992) defines the P-T conditions of LCT-type pegmatites between 2 and 4 kbar and 500 – 650 °C. The metamorphic conditions within the Borborema province are between 3.5 – 5 kbar and 560 – 600 °C (Beurlen et al., 2001). Feldspar analyses show minimal formation temperatures above 550 °C.

None of the calculated isochors plot within the P-T range (3.5 – 4 kbar and 600 – 650 °C, which has been defined in the literature. The trapping temperatures at the given pressures correlate partly with the temperatures of the second event exsolution event within the feldspars.

REFERENCES
Cerny, P. (1992) *Geosc. Canada* 18, 49-67
Beurlen, H., Da Silva, M. R. R., De Castro, C. (2001) *Chem. Geol.*, 173: 107-123.

Formation conditions and chemical compositions of ore-forming fluid of Butarnoye gold deposit (North-East of Russia)

Prokofiev, Vsevolod Yu.*, Cherepanova, Natalia V.**, and Trubkin Nikolay V.*

*Institute of Geology of Ore Deposits, Petrography, Mineralogy, and Geochemistry, Russian Academy of Sciences, Staromonetny per. 35, Moscow, 119017 Russia
** Department of Geology, Lomonosov Moscow State University, Vorob'evy gory, Moscow, 119899 Russia

The Butarnoye gold deposit is situated on Chukotka, in the Hurchan-Ortukanskoy zone of tectonic-magmatic activation. The gold deposit is localized in granodiorite of the late-jurassic Butarninsky granitoid stock. Host rocks of the stock are presented by terrigenic sediments: argillites, alevrolites and sometimes by sandstone. The ore bodies are presented by gold bearing quartz veins and veinlets. Ore veins associated with metasomatites are presented by albite-sericite-quartz and sericite-quartz rocks developed on granodiorites and dikes of diorite porphyrites.
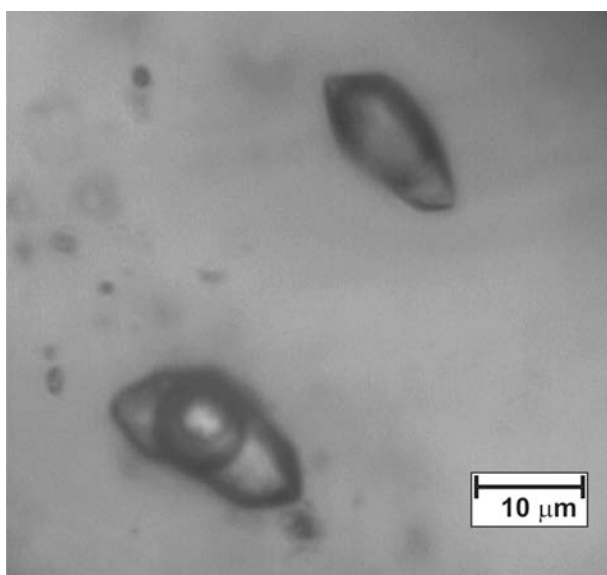
Fig. 1. Fluid inclusions in the ore vein quartz: type I three-phase fluid inclusions with H_2O liquid, CO_2 vapour and CO_2 liquid and type II is vapour-rich CO_2 fluid inclusions.

The ore was formed in two stages: arsenopyrite-pyritic and gold-bismuthic. Quartz is the main vein mineral in ore (more than 70%), whereas sericite, albite, K-feldspar, chlorite, epidote are the collaterally found. Arsenopyrite dominates among the ore minerals

Native gold, pyrite, native bismuth, stibnite, boulangerite, sphalerite and rare minerals like bismithinite, galena, chalkopyrite, pyrrotite are the secondary minerals.

The study of the chemical composition of the small mineral phases was conducted by scanning electronic microscope JSM5610LV with energy dispersion attachment Link ISIS in IGEM RAS. The presence of bismuthinite was confirmed and fineness of small gold particles was determined from 760 up to 908 ‰. In addition, two new minerals of bismuth: maldonite Au_2Bi and joseite A Bi_4TeS_2 was discovered in the ore deposit.

Fluid inclusions in quartz range from 1 to 30 μm in size and are in general irregular or have negative crystal shape forms. The primary and secondary inclusions are identified following the criteria outlined by Roedder (1984). Fluid inclusions are classified on the basis of phase compositions at room temperature (+21 °C). Type I are two-phase fluid inclusions consisting of H_2O liquid and CO_2 liquid and three-phase fluid inclusions with H_2O liquid, CO_2 vapour and CO_2 liquid. Type II is vapour-rich CO_2 fluid inclusions.

Fluid inclusion microthermometry was performed on a Linkam THMSG-600 heating-freezing stage attached to an Amplival microscope (Germany) and a monitoring video apparatus. The bulk salinity of the fluid was calculated from the combination of T_m(ice) and T_m(cla) (Distler et al., 2004). The identity of the species in the solutions was determined from eutectic temperatures (Borisenko, 1977). Quantitative chemical analyses of the inclusion fluid were carried out at the Central Institute of Geological Exploration for Base and Precious Metals of Moscow (analyst: Y.V. Vasyuta) using the technique reported by (Prokofiev et al., 2010).

Homogenization temperatures of Type I fluid inclusions in early quartz range from 334 to 245 °C. Clathrate melting temperatures at +15.1 to +9.0 °C were used to estimate a fluid salinity of 2.2 to 4.9 eq mass% NaCl. The estimated CO_2 content is 5.8 – 2.2 mole/kg in the solution. Eutectic temperatures of -24 to -35 °C infer that NaCl and $MgCl_2$ were the dominant soluble salts in the aqueous solution. The CO_2 melting temperatures of -57.1 to -59.7 °C indicate that the vapour phase contains CH_4. Vapour phase density in fluid inclusions of Type II, estimated from the CO_2 homogenization temperatures of 15.4 to 29.6 °C, ranges from 0.64 to 0.89 g/cm^3. Fluid pressures calculated by the intersection of the H_2O-CO_2 isotherms and the CO_2 isochors (Brown, 1989) varied from 80 to 140 MPa.

The chemical analysis fluid inclusions in quartz gave additional informations about ore-forming fluid composition. Carbonic acid (3.7 - 1.16 mol kg^{-1} water) and methane (0.18 - 0.05 mol kg^{-1} water) are detected in gas phase of fluid inclusions. Hydrocarbonate (0.03 - 0.02 mol kg^{-1} water) dominates among anions, whereas sulphate (0.01 mol kg^{-1} water) is discovered and chlorine is found in subordinated amount (0.004 - 0.003 mol kg^{-1} water) in the liquid phase of fluid inclusions. Na (0.06 - 0.02 mol kg^{-1} water) dominates among the cations, whereas K (0.004 - 0.0005 mol kg^{-1} water), Ca (0.002 – 0 mol kg^{-1} water) and Mg (0.0003 – 0 mol kg^{-1} water) are found in subordinated amount. In addition, following element concentrations are found in the inclusions (mmol kg^{-1} water): B: 28 – 12; As: 3.5 - 1.0; Br: 2.9 - 1.4; Li: 0.95 - 0.28; Fe: 0.7 - 0.009; Mn: 0.13 - 0.01; Zn: 0.12 – 0; Sb: 0.08 - 0.02; Ba: 0.05 - 0.0005; Co: 0.04 – 0; Cu: 0.03 - 0.0001; Sr: 0.02 - 0.004; Ni: 0.02 - 0.003; W: 0.01 – 0; Ge: 0.008 - 0.005; Rb: 0.008 - 0.003; Cs: 0.006 - 0.001; Bi: 0.005 – 0; Cr: 0.004 – 0; Sn: 0.003 – 0; Cd: 0.003 – 0; Ag: 0.003 – 0; Pb: 0.002 – 0; Mo: 0.002 - 0.0001; Au: 0.002 – 0; Hg: 0.001 – 0; Tl: 0.00005 – 0; and U: 0.00004 - 0. The value of K/Rb-relation changes from 62 up to 366, which indicate the participation of both, magmatic fluids and formation water in the ore-forming process.
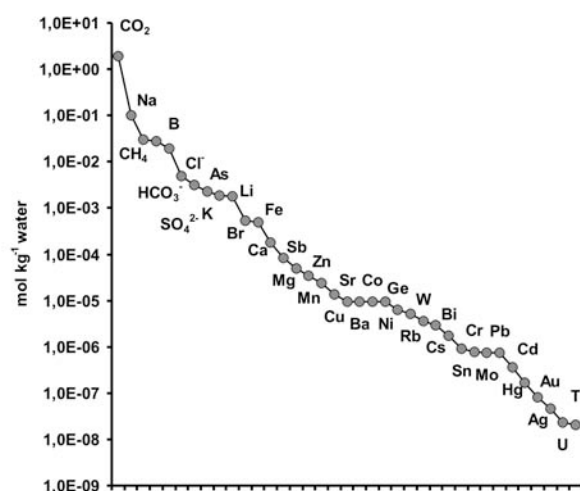
Fig. 2. The average chemical composition of fluid inclusions in the ore vein quartz.

The obtained data concerning the fluid inclusion particularities show the resemblance of ore-forming fluid of Butarnoye deposit with the fluids of orogenic gold deposits (Ridley, Diamond, 2000).

REFERENCES

Borisenko A. S. (1977) *Russian Geol. and Geof.* 8: 16 - 27.

Bodnar R. J., Vityk M. O. (1994) *Fluid inclusions in minerals: methods and applications*, Siena, taly, 1994: 117 - 130.

Brown P. (1989) *Amer. Mineral.* 74: 1390-1393.

Roedder E. (1984) *Rev. Mineral.* 12:, 646 p.

Distler V. V., Yudovskaya M. A., et al. (2004) *Ore Geol. Rev.* 24/1-2: 7 - 44.

Prokofiev V.Yu., Garofalo P.S., et al. (2010) *Econ. Geol.* 105: 395-416.

Ridley J.R., Diamond L.W. (2000) *Rev. Econ. Geol.* 13: 141 – 162

Crystallization conditions of the potassium alkaline melts on the Ryabinovyi massif (Central Aldan, Russia)

Rokosova E. Yu.

V.S.Sobolev Institute of Geology and Mineralogy SB RAS Koptyuga 3, Novosibirsk, Russia

The Ryabinovyi massif is an intricate volcano-plutonic structure (Kochetkov et al. 2006, Kostyuk et al. 1990). It consists of volcanic and vein rocks varied from ultrabasic to more siliceous compositions. The common feature of these rocks is a high alkalinity at pronounced potassium specialization. Several areas of gold mineralization were found within the Ryabinovyi massif (Kochetkov et al. 2006). Micaceous shonkinites are gold hosting, the high-magnesian, Si-undersaturated rocks of the massif with the age - K_1 — K_2. They contain clinopyroxene, Fe-Mg mica, potassium feldspar, albite, apatite, magnetite, sphene and rutile. The rock texture is hypidiomorphic-granular.

Clinopyroxenes are represented mainly by aegirine (Ae) (Fe# = 0.22 - 0.26; Na = 0.12-0.14), less often by subcalcium salite (Sal) (Fe# = 0.36 - 0.42; Na = 0.14-0.19) and subcalcium diopside (Di) (Fe# = 0.36 - 0.6; Na = 0.21-0.55). All clinopyroxenes are significantly enriched by trace elements.
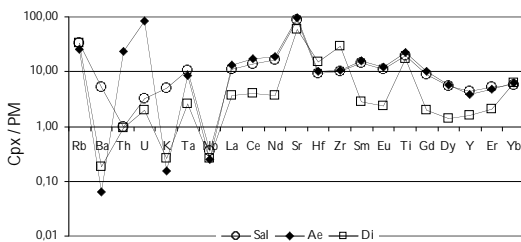
Fig. 1. Primitive mantle-normalized spidergram for grains of clinopyroxene.

Di has lower concentrations of trace elements in contrast with Sal, Ae (Fig.1). Di is different from Sal, Ae in indicator ratios Ce/Yb (2.1 vs. 8-10), Ti/Zr (7 vs. >20), La/Yb (0.81 vs. 2.7-2.9). During crystallization of clinopyroxene from Di to Sal, Ae there was an increase of the LREE relatively to HREE, what is evidence of the increase La/Yb, Ce/Yb ratios from Di to Sal, Ae. In addition, this crystallization for sequence clinopyroxene probably indicates the increase of fO_2, as evidenced by the increase Ti/V ratio from 4 (Di) to 6.7 (Sal, Ae)

Completely crystallized melt inclusions are observed in Sal, Ae. Silicate, silicate-carbonate, carbonate salt and carbonate inclusions were found among them.

Silicate-rich crystallized inclusions in Sal (Fig. 2) contain clinopyroxene, phlogopite, albite (Table 1), and rutile (99.3 mass% TiO_2).
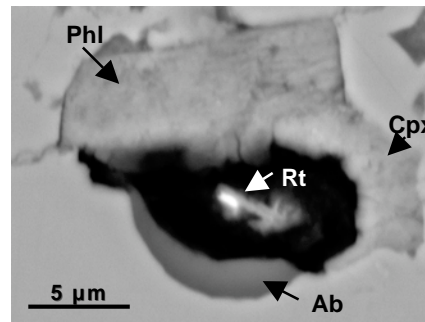
Fig. 2. Silicate-rich inclusion. Cpx – clinopyroxene; Phl – phlogopite; Ab – albite; Rt – rutile.

Component	Cpx	Phl	Ab
SiO_2	54.81	41.94	69.04
Al_2O_3	0.91	12.24	19.50
FeO	12.00	11.74	0.28
MgO	10.16	20.14	-
CaO	18.88	0.19	0.12
Na_2O	3.26	0.10	11.33
K_2O	-	10.09	-
Total	100.20	96.44	100.27

Table. 1 Composition of daughter phases from inclusions, mass%

Silicate-carbonate inclusions in Ae (Fig.3) consist of clinopyroxene, phlogopite (Table 1), and

calcite (mass% - 53.48 CaO; 4.25 SrO; 0.52 FeO; 0.11 MnO; 0.12 MgO).
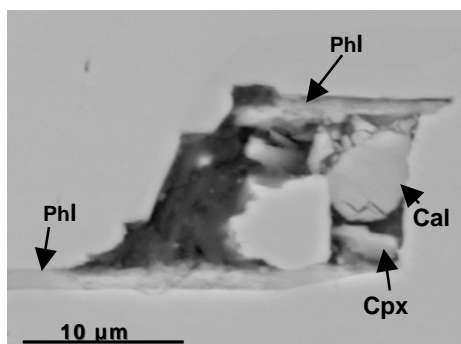
Fig. 3. Silicate-carbonate inclusion. Cal – calcite.

Carbonate-salt inclusions in Sal (Fig. 4) contain of crystals of calcite, alkali chlorides (mass% - 50.59 Cl; 18.48 Na; 9.54 K; 2.28 Ca) and sulphates (mass% - 31.4 SO_3; 29.35 SrO; 48.24 CaO), and sphene (mass% - 38.17 TiO_2; 30.20 SiO_2; 0.45 Al_2O_3; 27.02 CaO; 2.44 Fe_2O_3; 0.14 Na_2O; 0.03 MgO; 0.12 SrO).
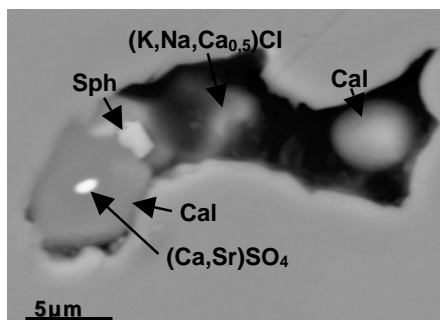
Fig. 4. Carbonate-salt inclusion. Sph – sphene.

Carbonate inclusions in Ae (Fig. 5) are rich in calcite, and portlandite (mass% - 73.64 CaO; 0.41 SrO; 0.6 FeO; 0.04 MnO; 0.09 MgO).
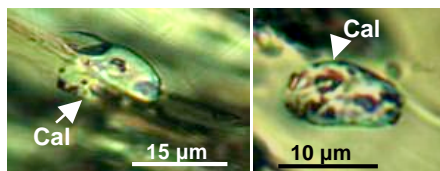
Fig. 5. Carbonate inclusion.

In *silicate*-rich inclusions daughter phases started to melt at above 900-1000 ºC and a gas bubble appeared. At 1150 – 1160 ºC daughter phases melted completely and the gas bubble disappeared. The composition of quenched homogenized glass of inclusion is as follows (mass% - 45.22 SiO_2; 2.48 TiO_2; 3.37 Al_2O_3; 13.93 FeO; 0.41 MnO; 5.62 MgO; 19.23 CaO; 3.84 Na_2O; 1.19 K_2O; 0.4 SrO; 0.84 P_2O_5). In carbonate-salt inclusions salt phases partly melted at 390-420 ºC but above 650 ºC the inclusions decrepitated even at slow increasing of temperature. We failed to completely homogenize such inclusions

Chromatographic analysis showed that fluid in clinopyroxene of shonkinites at 1000 ºC containing mainly CO_2 (3400 mg/kg), H_2O (2500 mg/kg).

Conclusions:

1. Shonkinites crystallized from magmatic melt enriched in CO_2 - H_2O fluid.

2. During crystallization of clinopyroxenes the melt was heterogeneous and represented by immiscible silicate, silicate-carbonate, carbonate-salt, and carbonate fractions. The carbonate-salt and carbonate melts separated from silicate magma were enriched in Ca, alkalies, CO_2, S, Cl and were, undoubtedly, an immiscible carbonatite fraction.

3. Homogenization temperature of silicate inclusions was 1150-1160 ºC, and that of carbonate-salt melts was much higher than 650 ºC.

4. Low-temperature sulphate-chloride and sulphate-carbonate fluids are commonly associated with gold mineralization (Borisenko et al. 2010). Thus, we can assume that on the magmatic stage carbonate-salt melts, which are spatially separated from carbonatite magma, could be transporters of gold.

REFERENCES

Borisenko A.S., Borovikov A.A., Vasyukova E.A., Pavlova G.G., Palessky S.V. (2010) *ACROFI III*. Novosibirsk. 34-35.

Kochetkov A.Ya. (2006) *Russian Geology and Geophysics*, 7 (47), 850-863.

Kostyuk V.P., Panina L.I., Zhidkov A.Ya., Orlova M. P., Bazarova T. Yu. (1990) Novosibirsk, "Nauka", (in Russian).

Fluid inclusion studies on the determination of mineralization environment and classification of a Red-Bed type Cu deposit in Yozgat, Turkey

Sezerer Kuru, G.*, Çiftçi, E.** and Sakitaş, A.***

*TMA, Turkey Mineral Exploration,06520, Ankara, Turkey
**İstanbul Technical University, Maslak, İstanbul, Turkey
***General Directorate of Mineral Research and Exploration, Ankara, Turkey

Red-wine red coloured sedimentary rocks of Oligo-Miocene in the Yozgat region (Turkey) are described as Red-bed type beds. Sedimentary rocks include volcanic conglomerates, sandstones and marls. Descloizite, $PbZn(VO_4)(OH)$, is firstly observed in Turkey within these three lithological units (Sezerer et al., 2011). This mineral is widely observed in this region. Beside descloizite, other ore minerals are not observed in this field. This mineral is found in the matrix of sandstones and within andesite and basalt fragments.

Based on detailed petrographic and microthermometric analyses on these rocks, two types of fluid inclusion series are determined. These are CO_2-rich and water-rich fluid inclusion assemblages. Two different CO_2-rich fluid inclusion assemblages are traced, one of which has a homogenization temperature of 230 °C and as salinity of 1.8 eq mass% NaCl and the other with 320 °C and 12.6 eq mass% NaCl. Water-rich fluid inclusions comprise two separate fluid inclusion assemblages. One of these has a homogenization temperature of 150 °C and other one with a homogenization temperature of 250 °C. These two low-temperature fluid inclusions have low salinity as 3.9 eq mass% NaCl and as 25 eq mass% NaCl, respectively.

This system is generated by a deposit formed in a hydrothermal system that involved both extra-basinal, deeply sourced CO_2-rich fluid and basinal, aqueous fluid.

REFERENCES

Sezerer Kuru G., Çiftçi E. and Sakitaş A., (2011)
   Congress of Turkey geology, Ankara, Turkey.

Comparative study of systemic methods in geochemical data optimization, Ghoulan area, E-Azerbaijan, Iran

Shahinfar, Hamid

Department of Geology, Faculty of Sciences, Tabriz Branch, Islamic Azad University, , Tabriz, Iran

Detection of optimized geochemical patterns requires Orientation Survey (O.S.) in which one of its important layers is selecting an effective data analysis method.

In order to detect favourable potentials in Ghoulan area, discrimination of mineralized and blind ore zones using advanced techniques with presenting a suitable geochemical pattern and relative pathfinders is the scope of this study. In this respect, 233 stream sediment samples were collected from the area and analyzed for base metals (Cu, Mo, Cr, Co, Ni, Pb, Zn, As, Y) and their indicator elements.

The anomalous zones in the area were detected using two systemic methods such as principal component analysis (PCA) and Fractal (F) methods. Application of F method on geochemical data leads to detection of two anomalous zones of Cu in Gharachilar and W-Loutkeh, with Mo appearance in Namnigh. The separation of these two anomalous zones (Cu & Mo) probably is due to acidity of area formed by solubility of sulphides from outcrops and migration of Mo in the form of molibdate which caused the precipitation of Cu and Mo in two different zones.

The results show that both methods (F & PCA) have similar detection zones but the capability of PCA in enhancement of halos and detection of blind ore zones is more effective than F method. As in this case, it could detect strong blind anomalous zone of Mo in Namnigh in addition to Cu & Mo trend. Overall, the characterization of methods also revealed that the PCA is more reliable in rejecting the syngenetic effects and the results can be more precisely used in the area.

Groundwater quality assessment in Marand Region, northwest Iran

Shahinfar, Hamid

Department of Geology, Faculty of Sciences, Tabriz Branch, Islamic Azad University, Tabriz, Iran

To study hydrochemical characteristics of groundwater, water samples were collected in an area of 40 km^2 and 17 locations from Marand plain, Eastern Azerbaijan province. Samples analysed for major cations and anions and processed by statistical methods. While carrying out factor analysis, three major parameters of groundwater composition were extracted. Piper diagram and correlation matrix results indicate that the main type of groundwater is bicarbonate with influential role of alkaline earths. Studying Isoelectrical conductivity, total dissolved solid contours, and a Pie chart in hydrochemical maps shows an increase in EC, TDS and Chloride concentration in the groundwater located in the northeast of the region. Changes in the spatial interpretation of the groundwater parameters indicate that the quality and geochemical characteristics of groundwater have a close correlation with topography, Geology, and hydrograph of Marand plain. Samples which have been obtained from southern parts of the region (near to aquifer recharge centre) show very suitable quality, but the composition of the groundwater changes in the northeast because of an increase of ionic constituents and the existence of fine grain sediments in aquifer zones. We can conclude that factors such as groundwater flow paths, water level increase and human influences (urban wastewater and agricultural activities) made this part of the region sustainable.

Formation conditions of labuntsovite group minerals from the Kovdor massif (Kola Peninsula, Russia)

Sokolov, Stanislav V.

All-Russian Scientific-Research Institute of Mineral Resources (VIMS) 109017, Staromonetny, 31, Moscow, Russia

Minerals of the labuntsovite group were found in the Kovdor massif in various settings (Chukanov et al., 2003): labuntsovite-Mg is often present in younger hydrothermal associations related to veins of dolomite carbonatites that cut pyroxenites; labuntsovite-Fe and lemmleinite-Ba were found in a zeolite-calcite vein hosted in ijolites; nenadkevichite and korobitsynite (± labuntsovite-Mg) were identified in calcite-dominated veinlets in fenites.

Our samples contained various minerals of the labunstovite group, which were identified by N.V. Chukanov. Two of the samples represented veins of younger Fe-dolomite carbonatites. One of the veins is hosted in a carbonatite-phoscorite stock at an apatite-magnetite deposit (sample I), and the other one cuts pyroxenites (sample IV). Both veins contain vugs and caverns whose walls are lined with rhombohedral dolomite-2 with higher iron and manganese concentrations (5.5 mass% FeO and 0.53 mass% MnO) than those of the rock-forming dolomite-1 (~3 and 0.35 mass%, respectively). Labuntsovite-Mg, ancylite, and catapleiite crystals occur as ingrowths in the outer zones of dolomite rhombohedras or overgrow them. The youngest dolomite-3, calcite, and strontianite crystallized at a later time.

Sample II was taken from the central part of a zonal natrolite-calcite vein in ijolites, whose caverns contained lemmleinite-Ba in association with major minerals and catapleiite.

Zeolite-calcite and anchimonomineralic calcite veins of analogous composition at the Kovdor massif cut across the silicate rocks (ijolites and fenites), phoscorites, and even the younger carbonatites and are thought to be products of the post-carbonatite stage. Calcites in these veins differ from this mineral in all older rocks in containing very low concentrations of typomorphic minor elements, such as Mg, Mn, Fe, Sr, Ba, and

REE. This exactly calcite occurs as veinlets and pockets in the fenites (sample V). Associated with it labuntsovite-Mg is found in the marginal zones of large calcite rhombohedrons (up to 5-7 mm) and also grows on them.

The mineralogy of the samples and the chemistry of the carbonates were examined under an optical microscope and by X-ray phase and quantitative spectral analyses. Inclusions were examined in transparent minerals (labuntsovite, calcite, dolomite, and natrolite). Thereby inclusions suitable for determining their homogenization temperatures (T_h) were found only in carbonates.

The rock-forming dolomite-1 from carbonatite veins (samples I and IV) contains primary melt inclusions (single inclusions or unzoned groups spatially separated from secondary inclusions) and accompanying fluid inclusions (FI) of various phase composition (Fig. 1a, 1b, 1c). The dolomite also contains abundant secondary gas-liquid inclusions.
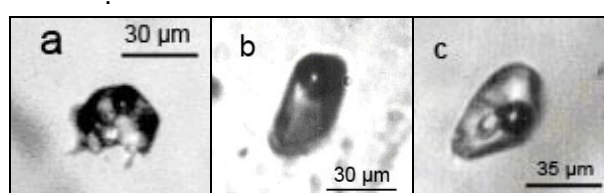
Fig. 1. Inclusions in dolomite-1: a. melt inclusion, b. two-phase fluid inclusion (V + L), c − multiphase fluid inclusion (V + L + S_{is} + S_{an}).

The melt inclusions (MI) consist of recrystallized aggregates of solid phases (partially isotropic) and two-phase fluid segregations, which homogenize (LV→L) at 190-220 °C. This and the simultaneous occurrence of primary gas-liquid ± solid inclusions in the host mineral suggest that the carbonatite melt was saturated with respect to a water-rich fluid.

We failed to homogenize these inclusions because of the intense decrepitation of the

secondary gas-liquid inclusions with low T_h (≤270 °C), which resulted in the destruction of both the MI and their host mineral at 320-460 °C.

The daughter solid phases of the primary FI in dolomite-1 (as in the other examined carbonates) are optically isotropic, with only a few exceptions, (sub)cubic or short-prismatic, and account for approximately 5 to 7 % of the inclusions by volume. The relatively high temperatures at which dissolution begins (120-130 °C) suggest that the solid phases are halite. The undisturbed inclusions homogenized into liquid at 290-360 °C.

Rhombohedral dolomite-2 from vugs and caverns contains primary FI (V + L ± S_{is}) and rare crystal-fluid inclusions (CFI), which contain up to 35-45 vol% vapour and liquid (Fig. 2), and the inclusions eventually decrepitated from 290 to 410 °C.
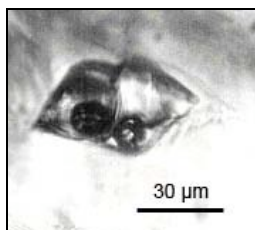
Fig. 2. Crystallofluid inclusions in dolomite-2.

Primary FI in dolomite-2 have a phase composition analogous to those of inclusions in dolomite-1. A few of these inclusions decrepitated at 185-270 °C, and the rest of them homogenized to liquid at 265-335 °C.

In calcites from samples II and V, primary gas-liquid inclusions dominate over FI with solid daughter phases (Figs. 3a, 3b). Almost all of inclusions did not leak in the heating stage and homogenized into liquid at similar T_h = 180-210 °C in sample II and 175-225 °C in sample V.
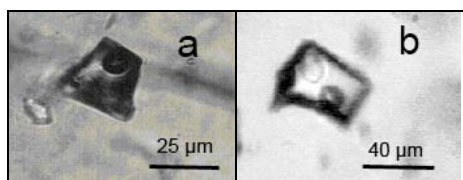
Fig. 3. Inclusions in calcite: a. gas-liquid inclusion, b. multiphase fluid inclusion (V + L + S_{is}).

The phase composition of the inclusions in the dolomites systematically evolved from fluidized melt to hydrothermal solution. Dolomite-1 crystallized in the course of the magmatic process, and dolomite-2 started to crystallize in vugs from fluid with residual portions of the melt-brine, which was trapped by minerals in the form of CFI. Younger minerals (labuntsovite-Mg, ancylite, catapleiite, dolomite-3, calcite, and strontianite) precipitated from solution as the P-T parameters decreased.

The decrease in the fluid pressure (P_{fl}) during the development of the hydrothermal associations in vugs is indirectly confirmed by the fact that the dolomite contains progressively less primary FI, which decrepitated independently of the effect of secondary inclusions. This baric trend first induced an increase in the acidity of the solutions (Shcherbina, 1967), as follows from the increase in the concentrations of Fe and Mn (as more acidic components than Ca and Mg) in dolomite-2. However the replacement of the later dolomite by calcite testifies to an increase in the alkalinity that is agreement with manifestation of acidic wave in the carbonate-forming systems.

The virtual absence of the decrepitation of primary FI in calcites in samples II and V suggests that the calcite and zeolite-calcite veins were produced under P_{fl} no higher than 404 bar (Naumov et al., 1966) and hence the crystallization temperatures of these calcites (as well as the lemmleinite- Ba and labuntsovite-Mg) could not much higher than the T_h (175-225 °C). The formation of calcite (together with natrolite) in place of dolomite at these temperatures points to alkaline specialization of solutions. It cannot be ruled out that its source was the hydrothermas, the final evolutionary product of the carbonatite fluid.

REFERENCES

Chukanov N., Pekov I., Zadov A. et al. (2003) Moscow, Nauka, 323 p. [in Russ.]

Naumov V., Balitskiy V., Khetchikov L. (1966) *Doklady of the Academy of Sciences of the USSR.* 171: 183-185. [in Russ.]

Shcherbina V. (1967) Leningrad, Nauka: 61-67. [in Russ.]

Compositions of magmatic melts at formation of chemically heterogeneous rare-metal felsic dike in the East Kalguty dike belt (Gorny Altai, Russia)

Sokolova, Ekaterina[*], Smirnov, Sergey[*,**] and Annikova, Irina[*]

[*]V.S. Sobolev Institute of Geology and Mineralogy SB RAS, pr. Koptyga, 3, Novosibirsk, Russia
[**]Novosibirsk State University, Pirogova, 2, Novosibirsk, Russia

Introduction

East Kalguty dike belt is a part of Kalguty ore-magmatic system along with biotite granite pluton, leukogranite stocks and Mo-W ore deposit. The belt consists of more than a hundred dikes, extends by about 10-15 km and spatially overlaps with Mo-W hydrothermal vein stockwork. The ages of the dike rocks, determined by SHRIMP on magmatic zircon (200 Ma) are close to the Ar-Ar ages of hydrothermal mineralization (200-204 Ma). This makes an opportunity to consider the dikes as a manifestation of deep magmatic source of rare metals for the hydrothermal deposit.

According to Na_2O/K_2O ratio the dike belt rocks are traditionally divided into ongonites (Na-rich) and elvans (K-rich). In the majority of dikes concentrations of Li are higher than 100 ppm with elevated amounts of Cs, Rb, Ta and Nb. Unlike typical Li-F granites and ongonites these rocks are low in F (0.3 – 0.4 mass%) and enriched in P (up to 0.4 mass% P_2O_5). One dike in the axial part of the belt differs from others by extreme enrichment in rare alkalis (up to 2500 ppm Li, 1050 ppm Cs and 1700 ppm Rb) and P (up to 0.79 mass% P_2O_5). The rocks of this dike show strong heterogeneity in Na_2O/K_2O ratio and appeared to belong both to ongonites and elvans. Elvan part of the dike is depleted in rare lithophyle elements compared to the ongonite one. No petrographic evidences for greisenization process were recorded. Such coexistence of K-rich and Na-rich magmatic rocks within the same magmatic body is unusual in nature. In this work the study of melt inclusions in quartz phenocrysts was aimed at the chemical features of melts, which are parental for chemically heterogeneous magmatic body.

Melt and fluid inclusions

Quartz phenocrysts from ongonite and elvan portions of the dike contain numerous fluid (FI) and melt (MI) inclusions. MI are filled with aggregate of daughter crystals and fluid segregation which typically is distributed within interstices between crystalline phases. Mica (muscovite), feldspars, apatite and monazite were identified among crystalline phases in MIs before heating (Fig.1a). Primary aqueous FI that appear in the same part of crystals with MI are believed to represent the fluid phase, coexisting immiscibly with the melt when quartz phenocrysts were growing.

The entrapment temperature for melt inclusions was estimated within 600-670 °C after their heating in autoclave under external D_2O pressure 1-3 kbar. After the high temperature exposure inclusions were quenched along the isochore. Quenched inclusions were checked for leak-tightness by FTIR spectroscopy within D-O vibration region.
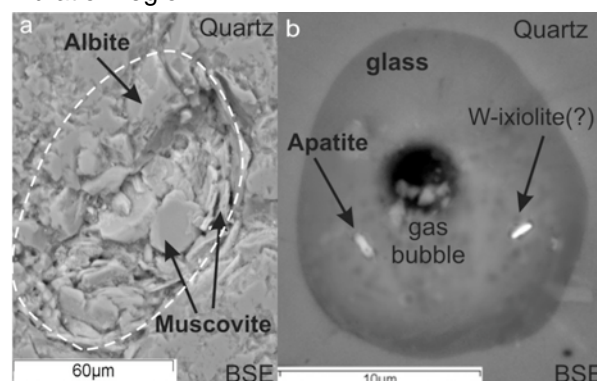
Fig.1. (a) Melt inclusion before heating. Dash line marks border of inclusion. (b) Melt inclusion after heating under 640 °C and 1 kbar.

The heated inclusions contain transparent silicate glass, sometimes with remnants of crystalline phases (muscovite, feldspar, apatite, Fe-Ti and

Ta-Nb oxides) and fluid bubble (Fig.1b). Homogeneous glasses were studied by EMPA and SIMS analyzes.

The quench glasses of MI show major element compositions typical for granites: SiO_2 70-74 mass%, Al_2O_3 12.3-13.5 mass%, total alkali 6.0-6.6 mass%. The silica, alumina, P and F contents in general are comparable with concentrations in the dike rocks. Alkali contents are somewhat lower than in the rock. It is important to note that Na_2O/K_2O ratio of the quenched glasses is close to 1. The MI glasses in elvan and ongonite quartz phenocrysts are comparable in K_2O content but elvan MIs are depleted in Na_2O. F and P contents in elvan MIs are higher than in ongonite MIs. Mis from elvan quartz have lower totals, suggesting possible higher water contents in comparison to ongonite melts.

Trace element analyzes shows that MI glasses are enriched in Li (350-500ppm), Rb (300-400 ppm), Cs (30-130 ppm), Ta (2-8 ppm) and Nb (7-35 ppm). However, it is easy to see that MI glasses are depleted in rare lithophyle elements in comparison with the host rocks. On the other hand concentrations of these elements in the MI glasses from both types of rocks are similar.

Discussion

The data obtained on melt inclusions show that compositions of entrapped melts differ from compositions of the rocks. This suggests that the dike and inclusions represent different stages of evolution of magmatic source, which produced East Kalguty dike belt. In the previous study it was shown that quartz phenocrysts from the dike belt rocks crystallized from the water-saturated rare-metal felsic magma in the chamber that was located at the level of the bottom part of the Kalguty biotite granite pluton (Sokolova et al., 2011). Quartz phenocrysts from the studied dike have similar crystallization T-P range. Primary fluid inclusions that accompany the studied melt inclusions indicate that crystallization of quartz proceeds in the system where water-saturated silicate melt coexisted with aqueous fluid. Thus we suggest that despite the composition difference the rare-element-enriched dike originated from the same magmatic source as for other dikes in the belt. This is supported by large overlaps between MI compositions from quartz in the studied dike and from other dikes showing less enrichment in rare elements. The depletion of MIs in rare elements compared to the bulk rock suggests that the studied inclusions do not represent the primitive melts. Some elements like Ta and Nb can be extracted from initial melt by crystallization of Ta-Nb oxides, while other like Li and Cs may not reach high concentration levels at the quartz phenocryst crystallization.

On the basis of the studied MI compositions one can come to the conclusion that the difference between ongonite and elvan melts already existed at the quartz phenocryst crystallization. The most important differences between MI and the bulk rock composition are in the K-content and Na/K ratio. Elvans are more enriched in K_2O than MI. There are no reasonable ways for K enrichment of the residual melts, as K-feldspar and muscovite exist as phenocrysts in the rocks. Thus we should suggest K enrichment in the course of process, which took place after the MI entrapment and before solidification of dikes.

The most possible agent for K enrichment is a fluid phase which coexists with the melt in the magmatic source. However, the absence of evidences for greisenization leads us to conclude that K enrichment occurred as a result of element exchange between aqueous fluid and crystallizing felsic melt. High viscosity of the felsic melt and fast crystallization prevented uniform change of the melt composition within the dike. This resulted in formation of K-rich elvan portions, slightly depleted in rare-elements from strongly altered melt and Na-rich ongonite portions enriched in rare-elements from less altered melt.

Conclusion

The formation of chemically heterogeneous ongonite-elvan dike strongly enriched in rare elements occurred from magmas, which originated from the same source, but were subjected to interaction with K-rich fluid before solidification.

REFERENCES

Sokolova E.N., Smirnov S.Z. Astrelina E.I., et al (2011). *Russian Geol. and Geoph.* (in press).

Formation of Na/Ca – F/Cl salt melts in the pantellerites magmas, Island Pantelleria, Itali

Solovova Irina, Girnis Andrey

Institute of Geology of Ore Deposits, Mineralogy, Petrology and Geochemistry of RAS. Staromonetny, 35, Moscow, Russia.

In the last decades, increasing evidence has appeared for the occurrence of immiscible chloride melts in natural magmatic systems. In contrast, findings of fluoride melts are still very rare (Andreeva et al., 2007), although experimental evidence indicates the existence of a wide silicate-fluoride liquid immiscibility field (e.g. Gramenitskiy et al., 2005; Dolejs & Baker, 2007). We report new data on the formation of Na/Ca-F/Cl melts in the pantellerites of the Island of Pantelleria, Italy (samples were provided by V. Kovalenko). Previously, immiscible chloride melts were reported from groundmass glasses and melt inclusions in these rocks (Solovova et al., 1991; Lowerstern, 1994). Melt inclusions were studied in anorthoclase phenocrysts from the pantellerites using a Linkam TS-1500 heating stage and electron and ion microprobes.

Silicate melt inclusions contain daughter crystals of anorthoclase, glass, fine-grained multiphase salt globules and H_2O-bearing low-density vapour, in which liquid water was occasionally observed. The composition of salt melt globules are $NaCl$-$CaF_2 \pm NaF$ and show only minor admixtures of Mg and Fe and never Al. Two groups of globules are clearly distinguished: (1) $NaCl$-CaF_2 and (2) NaF-$NaCl$-CaF_2 with variable Cl/F proportions. Globules of these two types may coexist in a single inclusion, although they were never observed in direct contact.

Upon heating, the salt phases were completely melted between 500 and 800 °C (Figure 1). The salt melt gradually dissolved in the silicate melt and completely disappeared at 850 to 1020 °C. The complete homogenization of the melt inclusions with the dissolution of daughter anorthoclase and vapour bubbles was attained at 1020–1080 °C. Rapid quenching (~2 s to 100 °C) produced homogeneous glasses in the inclusions, whereas cooling at rates of 1-20 °C/min resulted in the reappearance of salt globules embedded in silicate glass.
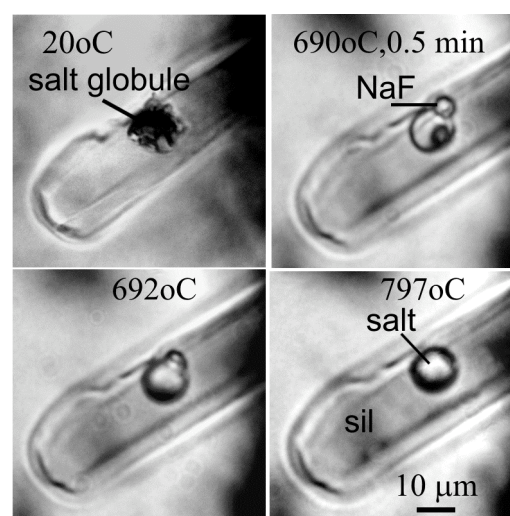
Fig. 1. Micrographs of the behaviour of the silicate glass + salt globule inclusion during heating. sil – silicate and salt – salt melts.

The homogeneous melt of inclusions contained up to 72 mass% SiO_2 and up to 10 mass% $Na_2O + K_2O$ (Na/K mol. up to 2). Average concentration of $Fe_2O_{3\ tot}$ is 7.4 mass%. These melts are rich in F (up to 0.6 mass%), Cl (up to 1.2 mass%) and H_2O (0.3 - 0.93 mass%). SIMS analysis revealed high contents of Zr (up to 4300 ppm), Nb (up to 1400 ppm), and Hf (up to 67 ppm), but only minor Ba (70–740 ppm) and Sr (4.5–38 ppm). $NaCl$-$CaF_2 \pm NaF$ salt melt is characterized by maximum concentrations of Ba and Sr (intraplate continental settings, Figure 2). $NaCl$-CaF_2 salt melt with minimum concentrations of Ba and Sr is typical for acid igneous rocks of island arcs and active continental margins.

Residual silicate melts coexisting with salt globules and daughter anorthoclase are very distinguished from the homogeneous melt of

inclusions. A main features of these melts are 1) the sharp increase of $(Na+K)/Al$ ratios (up to 14) and 2) reduction of Al_2O_3 concentration (up to 1 mass%) while increasing Fe_2O_3 concentration (up to 18 mass%) (Figure 3). Residual silicate melts contain up to 1.3 mass% F, and 2.1 mass% Cl that can be considered as the limit of saturation.
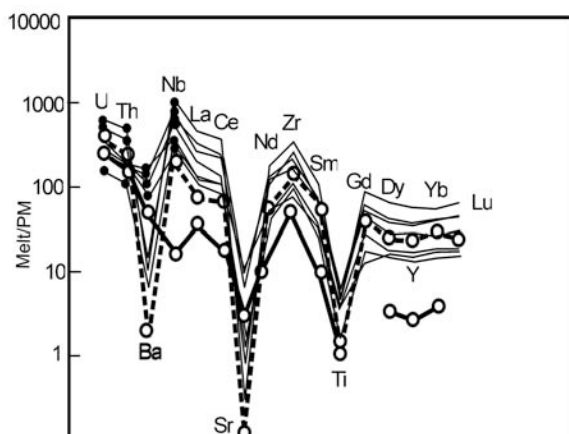
Fig. 2. Primitive mantle-normalized trace-element patterns of homogeneous melt inclusions: thin lines - glasses of inclusions, thick dotted line – the peralkaline silicic melts of intraplate continental settings and thick solid line - island arcs and active continental margins (Kovalenko et al., 2009).
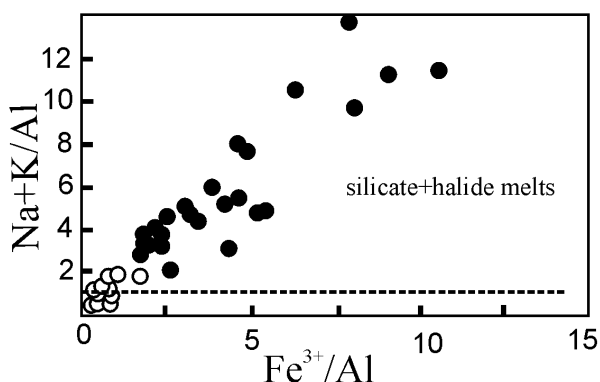
Fig. 3. Correlations of the Al=(Na+K)/Al ratio with the Fe^{3+}/Al ratio in the homogeneous (open circles) and residual (solid circles) melt inclusions.

The relationships between the two halide melts remain obscure. The $NaCl-NaF-CaF_2$ system shows no liquid immiscibility field (e.g. Sydykov et al., 2004), but the additional components (H_2O, SiO_2, Al_2O_3, Fe_2O_3, etc.) may affect phase relationships. This problem is a topic of future studies. Our investigation showed that fluoride–chloride melts may separate from peralkaline silicic melts containing about 2.1 mass% Cl and 1 mass% F at temperatures about 1000°C. The SIMS analysis of fluoride globules indicated that $NaF-NaCl-CaF_2$ melts are strongly enriched in incompatible trace elements relative with the coexisting silicate melts.

REFERENCES

Andreeva, I.A., Kovalenko, V.I., Yarmolyuk, V.V.,Listratova, E.N. & Kononkova, N.N.(2007). *Doklady Rarth Sciences* (in Russian). V. 414 (4): 655-660.

Dolejs, D. & Baker, D.R. (2007). *J. Petrology. V.* 48: 785-806.

Gramenitskiy, E., Shchekina, T & Deviatova, V. (2005). In book: Phase relations in the fluorine-bearing granite and nepheline syenite systems and the element distribution between phases (experimental research). *M. GEOS*. 188 (In Russian).

Kotelnikova, Z.A. & Kotelnikov, A.R. (2008). *Geochemistry International*. N 1: 54-68.

Kovalenko, V.I., Naumov, V.B., Girnis, A.V., Dorofeeva, V.A. & Yarmolyuk, V.V. (2009). *Petrology. V.* 17 (4): 410–428.

Lowerstern, J. (1994). *American Mineralogist*, V. 79: 353-369.

Solovova, I.P., Girnis, A.V., Naumov, V.B., Kovalenko, V.I. & Guzova, A.V. 1991. *Doklady Rarth Sciences*. V. 320 (4): 982- 986 (In Russian).

Sydykov, A., Friedrich, B., Milke, E. & Arnold, A. (2004). VII International Conference on Molten Slags Fluxes and Salts, *The South African Institute of Mining and Metallurgy*.

Veksler, I.V., Dorfman, A.M., Kamenetsky, M., Dulski, P.& Dingwell, D.B. (2005). *Geochimica et Cosmochimica Acta*. V. 69: 2847–2860.

Melt inclusions in olivine from New Caledonia boninites: initial melts and post-entrapment oxidation effects

Solovova, Irina and Girnis, Andrei

Institute of Geology of Ore Deposits, Mineralogy, Petrography and Geochemistry, Russian Academy of Sciences, Staromonetny 35, Moscow 119017, Russia

Boninites are Mg-rich high-Si volcanics enriched in water and strongly depleted in other incompatible components. Their magmas are believed to be derived by melting of depleted mantle rocks under the influence of water fluids produced by dehydration of subducted materials.

Melt inclusions were investigated in olivine phenocrysts (mg = 0.89 - 0.92, NiO up to 0.4 mass% and CaO < 0.2 mass%) from boninite dikes in New Caledonia (samples were provided by D. Ohnenstetter). The main distinctive features of these rocks are low CaO and very high Na_2O contents.

The inclusions contain glass, gas, and daughter orthopyroxene (Fig. 1) with high CaO (up to 2.7 mass%) and Al_2O_3 (up to 3.7 mass%). Daughter olivine always occurs on the inclusion walls, which is indicated by up to 17% increase in inclusion volume during heating up to 1250-1370 °C.
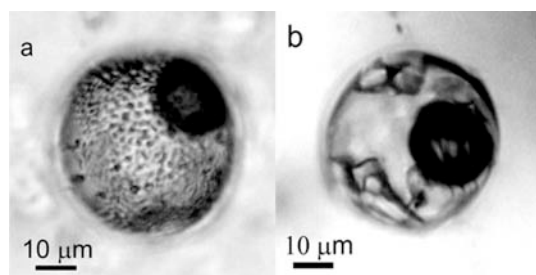
Fig. 1. Photomicrographs of melt inclusions.

In order to eliminate effects related to olivine-groundmass interaction, monomineralic olivine grains were separated for heating experiments. Crystalline phases within the inclusions were dissolved at 1200–1250 °C. Complete homogenization was never attained, because the vapour bubble remained undissolved up to 1370 °C. Two (vapour and liquid) phases were observed in the fluid phase of some melt inclusions. The liquid was frozen at –52 °C, and the beginning of melting was detected between -22.2 and –20.3 °C, i.e. near the eutectic of the H_2O–NaCl system. The ice melting temperature was close to 0°C, indicating low solute content.

The major and trace element compositions of reheated melt inclusions were determined using electron and ion microprobe analysis. The melts contain 56–63 mass% SiO_2, up to 16 mass% MgO, and 2.6–5.0 mass% Na_2O + K_2O at a molar Na_2O/K_2O of up to 11. The melts show low Nb, Ti, and Th contents and are enriched in Sr, Zr, Hf, and LREE relative to HREE (La_N/Sm_N 2–3 and Sm_N/Yb_N 1.4–2.0). SIMS analysis indicated no more than 1.4 mass% H_2O in heated melt inclusions. Residual glasses from unheated melt inclusions contain up to 3.5 mass% H_2O. The H_2O content of fresh groundmass glasses is much higher and may reach 8.7 mass%.

Electron microprobe analysis revealed an increase in the Mg of olivine directly near the glass–host olivine interface (Fig. 2). Such variations in olivine composition are in apparent conflict with the observed olivine crystallization on the walls of inclusions, which usually results in a gradual increase in the fayalite mole fraction of olivine in contact with the residual melt. We believe that this peculiar effect is related to the diffusion migration of H_2 outside the inclusions, which results in Fe oxidation in the melt via the reaction $2FeO+H_2O=Fe_2O_3+H_2$. The loss of only 0.1 mass% H_2O will result in the oxidation of 0.8 mass% FeO to Fe_2O_3 and, correspondingly, an increase in the Mg of equilibrium olivine. Assuming that $K_d = (Fe/Mg)^{Ol}: (Fe^{2+}/Mg)^{Gl}$ remains constant, the effect of oxidation of 0.8 mass% FeO in boninite melt can be counterbalanced by the fractionation of 7 mass% olivine (i.e. the composition of crystallizing olivine will remain constant). At higher rates of H_2 escape and melt oxidation, the Mg of olivine will increase during crystallization.

The composition of melt trapped during olivine crystallization was estimated by modelling simultaneous fractional crystallization and FeO oxidation providing the observed variations in olivine composition at K_d = 0.3. These exercises showed that the initial trapped melts contained 0.5–1.0 mass% less MgO compared with estimates based on the fractionation model ignoring the effect of Fe oxidation.
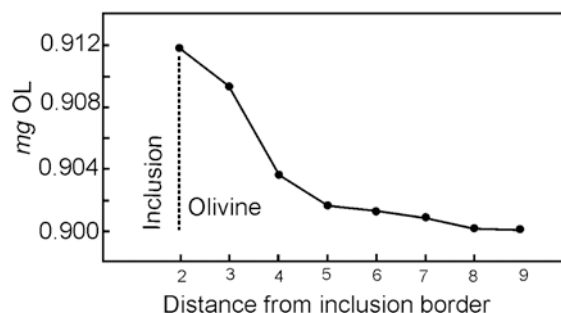
Fig. 2. Increase in the mg of olivine directly near the glass–host olivine interface. Distance from point 2 to point 9 is 20 μm.

Most of the estimated melt compositions show moderate MgO contents of 8-12 mass%. One melt inclusion showed MgO ~ 16 mass% and the highest FeO content of 10.2 mass%. This inclusion falls on the same trends as the other compositions with significantly lower MgO contents. Intriguingly, there is no correlation between MgO content in melt and the *mg* of host olivine, which suggests that MgO and FeO variations in the melts are not controlled by olivine fractionation and could be related to different degrees and depths of melting. This is supported by the analysis of correlations between other elements. The major- and trace-element characteristics of the boninite melts are similar to those of low-Ca boninites from the slope of the Marianna trench. Noteworthy is the relatively high Na_2O content in the New Caledonia magmas, which is not typical of low-Ca boninites from other regions (usually <2 mass%). The obtained melt inclusion evidence indicates that the enrichment in Na_2O is a specific feature of primary melts rather than the result of secondary alterations.

Isotopic fluid composition of rare-metal pegmatites, Sierra de San Luis, Argentina

Sosa, Graciela M.*, Kerkhof, Alfons M. van den*, Lüders, Volker**, Plessen, Birgit** and Montenegro, Teresita***

*Geoscience Centre of the University of Göttingen, Goldschmidtstr. 3, 37077 Göttingen, Germany
**GeoForschungsZentrum, Telegrafenberg, 14473 Potsdam, Germany
***CONICET & Universidad de Buenos Aires, Pabellón 2, Ciudad Universitaria, Argentina

Fluid inclusion studies and stable isotope measurements of fluids from small (ca. 0.5 grams) samples have been carried out on rare-metal (Be, Li, Nb, Ta, Sn) granitic pegmatites from the Sierra de San Luis (Argentina) in order to trace the source and evolution of the mineralizing fluids. The granitic pegmatites are related to syn-tectonic, meta- to peraluminous S-type granites (Sosa et al. 2007). They were emplaced during the Ordovician magmatism during the Famatinian Orogeny. Nb-Ta-pegmatites are concordantly emplaced in fine-grained quartz-mica schist of the Conlara Metamorphic Complex in the east, while Sn-bearing pegmatites are emplaced in the westerly schist of the Pringles Metamorphic Complex (Sosa, 2002; Sims et al, 1998). The sedimentation age was ca. 587 to 498 Ma for the Conlara Complex (Steenken et al. 2006) and significantly younger (ca. 530 to 498 Ma) for the Pringles Complex (Sims et al. 1998). The Nb-Ta-pegmatites were dated (K-Ar) ca. 404-444 Ma, the Sn-pegmatites slightly younger ca. 398-411 Ma (Sosa et al. 2002). The metamorphic grade of the country rocks varies from greenschist to lower-amphibolite facies. The concordant textural relation between the pegmatites and country rocks indicates a plastic behaviour of the schist during the pegmatite intrusion. The larger Nb-Ta pegmatites show a clear internal fractionation, whereas the smaller Sn pegmatites are homogeneous.

Fluid inclusions are present in most pegmatite minerals (apatite, beryl, cassiterite, columbite-tantalite, plagioclase, quartz) and, except in quartz, show primary features like the occurrence in growth zones. In apatite, cassiterite, beryl and plagioclase, the majority of the fluid inclusions are mixtures of H_2O-NaCl-CO_2-CH_4-N_2, and the rest are H_2O-NaCl (Van den Kerkhof et al. 2005). In contrast, columbite-tantalite contains almost only aqueous inclusions. Non-aqueous carbonic inclusions are found in quartz and plagioclase. In all minerals the salinity of the aqueous inclusions is typically 4 to 7 eq mass% NaCl, whereas the aqueous-carbonic inclusions have higher salinity. High CH_4 and N_2 contents were found in cassiterite, plagioclase and quartz with highest contents in cassiterite (up to 58 mol% CH_4, incidentally pure CH_4, and up to 32 mol% N_2; Fig. 1). The carbonic inclusions in the quartz show always much higher CH_4-concentrations in the Sn-pegmatites compared to Nb-Ta-pegmatites.
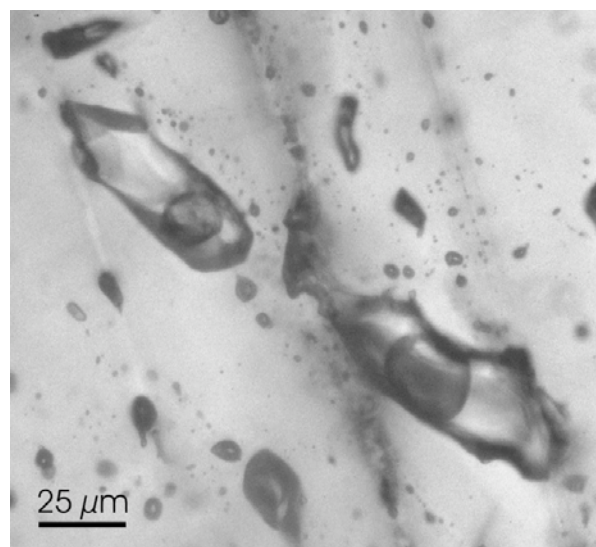
Fig. 1. Primary aqueous-carbonic inclusions in cassiterite (Yolanda pegmatite). The larger inclusion shows $T_m(CO_2)$ = -63.2; $T_m(ice)$ = -5.4; $T_m(cla)$ = +10.7; $T_h(LV{\rightarrow}V)$ CO_2 = +0.4 °C. The gas phase contains $CO_2(61)CH_4(14)N_2(25)$. The isotopic composition of this sample is $\delta^{13}C(CO_2)$= -12.4°/oo; $\delta^{13}C(CH_4)$= -47.7°/oo VPDB and $\delta^{15}N(N_2)$= +0.4°/oo.

Rare high-salinity inclusions (29-32 eq mass% NaCl) in quartz may originate from the magmatic stage, but most fluid inclusions

represent later hydrothermal fluids. The pegmatite minerals must have crystallized from a H_2O-NaCl-CO_2 ($\pm CH_4$-N_2) dominated fluid, preserved as primary inclusions in beryl and plagioclase (trapped at 400-500 °C /2-3 kbar as estimated from isochores). These conditions are in agreement with regional metamorphism and the liquidus conditions of rare-metal pegmatite crystallization. Subsequently, columbite-tantalite or cassiterite crystallized at 300-400 °C, and finally apatite at 200-300 °C. The CO_2-concentration became progressively lower, resulting in $H_2O \pm CO_2$ preserved in apatite. Fluid inclusions in quartz represent the full temperature range with the latest fluids (re)trapped in the immiscible aqueous-carbonic field at 100-150°C/0.5 kbar. The different modified fluid inclusions reflect the mineral-specific properties of preserving fluids. Halo textures in quartz indicative of implosion-decrepitation testify isobaric cooling. Methane-bearing inclusions indicate reducing conditions during cassiterite crystallization, or re-equilibration of aqueous-carbonic inclusions (graphite-bearing inclusions in plagioclase and quartz). Late low-salinity water found in all minerals must have been introduced after crystallization and represent meteoric water.

Stable isotope ($\delta^{13}C$ and $\delta^{15}N$) studies were carried out on gas-rich inclusions in quartz from both types of pegmatites and in cassiterite (analysis of tantalite in progress) using crusher which is connected to an elemental analyzer and isotopic mass spectrometer. CO_2 in quartz from Nb-Ta-pegmatite (Conlara Complex) shows $\delta^{13}C$ values between ca. -10 and $+4^o/_{oo}$ VPDB, with frequency maximums around -4 and $-9^o/_{oo}$. The magmatic signatures of ca. $-4^o/_{oo}$ are found for 3 pegmatites (Los Chilenitos, La Beatriz, La Violeta), all situated in the central easternmost part of the Sierra de San Luis; the lower $\delta^{13}C$ values are found for pegmatites more to the west. The CO_2 in quartz from the westernmost Sn- pegmatites in the Pringles Complex shows lightest $\delta^{13}C$ values (ca. -8 to -17 $^o/_{oo}$ VPDB) suggesting that the main oxide-silicate stage fluid was contaminated with carbon derived from the meta-sedimentary country rock. The $\delta^{13}C$ values of CO_2 in cassiterite coexisting with the quartz is slightly higher compared to the CO_2 in quartz (e.g. -9.3 $^o/_{oo}$ and -14.7$^o/_{oo}$ for cassiterite and quartz, respectively;

Neutrón pegmatite), but in one example (Irene pegmatite) we found clearly lower $\delta^{13}C$ (-16.4 $^o/_{oo}$) than for the CO_2 in cassiterite (-8.6 $^o/_{oo}$ PDB), suggesting the local uptake of organic carbon during cassiterite crystallization.

The $\delta^{13}C$ values of the abundant CH_4 in cassiterite are very low ($-47.7^o/_{oo}$ VPDB), but also the quartz in Nb-Ta-pegmatites with magmatic CO_2 contains minor CH_4 with low $\delta^{13}C$ (ca. -42 $^o/_{oo}$ VPDB). These values suggest that a part of the carbonic fluid must be of thermogenic origin (from kerogen at elevated temperatures) in both Conlara and Pringles metamorphic complexes.

The $\delta^{15}N$ values of N_2 which occurs as a minor constituent in the carbonic inclusions is ca. +3 to +6 $^o/_{oo}$ for quartz and slightly lower, i.e. ca. 0 to +3 $^o/_{oo}$ for cassiterite. These values confirm the contamination of the mineralizing fluid with organogenic material.

Based on regional isotopic variation of carbon in fluid inclusions we can distinguish between fluids with a magmatic signature, which correlate with Nb-Ta-pegmatite mineralization, and fluids which changed their isotopic composition due to interaction with the surrounding metasediments. The abundance and isotope compositions of CH_4 and N_2 suggest that the uptake of organic material in the mineralizing fluids must have been much larger in the western part of the Sierra de San Luis (Pringles Complex) and resulted in Sn-pegmatite mineralization.

REFERENCES

Sims J., Ireland T., Camacho A., Lyons P., Pieters P., Skirrow R., Stuart Smith P., Miró R. (1998) In: Pankhurst R., Rapela C. (Eds.) *Geological Society of London, Special Publications* 142: 259-281.

Sosa G.M., Augsburger M.S., Pedregosa J. (2002) *Eur. J. Mineral.* 14: 627-636.

Sosa G.M., Van den Kerkhof A.M., Lopez de Luchi M., Ortiz Suarez A. (2007) *ECROFI-XIX Bern*: 204.

Steenken A., Siegesmund S., López de Luchi M.G., Frei R., Wemmer K. (2006) *J. Geol. Soc.* 163: 965-982.

Van den Kerkhof A.M., Sosa G.M., Montenegro T. (2005) *ECROFI XVIII-Siena* Abstract ebook.

Fluids in the metamorphic stage of Krivoy Rog iron deposit evolution, Ukraine

Sośnicka, Marta*, Bakker, Ronald J.**

*AGH University of Science and Technology, 30 Mickiewicza Av., 30-059 Kraków, Poland
**Resource Mineralogy, Department of Applied Geosciences and Geophysics, Montanuniversitaet Leoben, Peter-Tunner-Str. 5, Leoben, Austria

Krivoy Rog deposit is situated in the Ukrainian crystalline shield and represents one of the biggest accumulations of iron ore within banded iron formation in Europe. Its complex evolution was initiated by sediment deposition in Early Proterozoic and formation of metaterrigenous-ferruginous complex that has undergone several episodes of ductile and brittle deformation as well as metamorphic and metasomatic events. Orogenic movements in Late Proterozoic ultimately determined the present shape of Krivoy Rog structure and completed the tectogenesis. Krivoy Rog iron deposit is classified as metamorphosed genetic type. Its origin is emphasized to be strictly associated with metamorphic processes that in majority influenced the iron ore formation. Metamorphic conditions determine extent of low-grade and high-grade iron ores. Samples, examined in the study, were collected from Skelevatske-Magnetitove deposit (Yugok open pit) in the interval of one year. The studied jaspilites (low-grade iron ore) belong to metaterrigenous-ferruginous complex corresponding to Saksaganskaya Suit of Kryvorizka Series in the local stratigraphy (Gurskiy, 2002). The rocks are composed of silicate, carbonate, magnetite and magnetite-martite bands. Circulation of residual metamorphic solutions during metamorphic stage was responsible for material migration within jaspilites. Fluids were generally transported along cracks and fractures. It resulted in formation of metamorphic veins, crosscutting iron ore bands. They contain fluid inclusion providing information about fluids present after peak metamorphic conditions. Studied veins are composed mainly of quartz, a younger style calcite and specularite assemblages. Fluid inclusions were observed in quartz veins excluding quartz bands in iron ore due to their small size. Fluid inclusions can be grouped in four types: primary one-phase aqueous, secondary one-phase CO_2, secondary two-phase or three-phase (CO_2-H_2O) and secondary three phase (CO_2-H_2O-nahcolite). Small in size (<1 µm), primary fluid inclusions are distributed in trails, parallel to the vein walls and may represent crystal growth surfaces. Their distribution indicates entrapment resulting from vein crack-seal mechanism. One-phase, liquid CO_2 inclusions are usually very irregular but in some cases they occur as negative crystal shaped, arranged in single trails. Some of the inclusions seem to be one-phase CO_2 but they may contain a thin aqueous rim, not always visible. This type often coexists with H_2O-CO_2 inclusions, distributed along microfractures. Secondary CO_2-H_2O inclusions comprised of aqueous and liquid CO_2 phases may contain additional vapour CO_2 phase present at room temperature. Three-phase inclusions with an aqueous liquid, CO_2 liquid and a solid nahcolite phase are randomly scattered among two-phase inclusions. Elongated or oval crystals of solid phase occur entirely inside inclusion (Fig. 1) or crosscut its wall (Fig. 2). Laser Raman spectroscopy revealed that it is nahcolite (peaks at: 1046 cm^{-1}, 685 cm^{-1}, 659 cm^{-1}), accidentally trapped during the inclusion formation. Veins that experienced more complex thermal history contain fluid inclusions grouped in decrepitation clusters and dense clouds indicating that part of inclusions had leaked due to the pressure increase in surrounding rock. It marks condition changes after vein formation and may indicate episodes of fracturing during late deformation events experienced by the rock. Two consistent data sets, corresponding to two quartz veins (vein1 and vein2), were obtained from microthermometry measurements. Studied two-phase inclusions were approximated by H_2O-CO_2-NaCl system, based on Raman spectroscopy that confirmed CO_2 and H_2O

content. Salts were not detected but according to decreased clathrate melting temperatures, T_m(cla) = 6.0-8.6 °C, salt is present in the aqueous solution. Properties of fluids were calculated using computer packages FLUIDS (Bakker, 2003). The total molar volume of inclusions ranges between 20.49 and 30.78 cm^3/mol with mode close to 21.5 cm^3/mol. Densities of carbon dioxide, fluctuating in the interval: 0.89-1.04 g/cm^3, were determined from microthermometry data and from Raman spectroscopy, based on the splitting of the Fermi diad of CO_2 (Fall et al., 2011). Carbon dioxide density in individual fluid inclusions appears to be independent in relation to CO_2 volume fraction. This fact suggests that volume fractions diversity, φ^{vap} = 0.10 to 0.30 is not the effect of reequilibration processes but rather result of heterogeneous fluid entrapment. Post-metamorphic leakage of aqueous solution from unmixed CO_2-H_2O fluids is excluded because there is no density decrease compared with carbon dioxide phase size (Hollister, 1990). Moreover, pure CO_2 inclusions show higher densities than CO_2 phase present in CO_2-H_2O inclusions. Generally low salinities of aqueous solution varying between 2,5 and 7.5 eq mass% NaCl are typical for metamorphic fluids and exclude influence of basinal brines. The most frequent salinity values assigned to each vein differ insignificantly. Clathrate melting temperatures are lower in inclusions from vein 2, indicating about 1 mass% higher salinities. Quartz veins were formed in aqueous-rich environment in accordance with primary fluid inclusion trials resulting from crack-seal mechanism. Early post-formation condition changes caused fracturing and formation of several inclusion generations. They are characterized by various compositions, as well aqueous-rich as carbon dioxide-rich. Heterogeneous entrapment implies that during fracturing event two different fluids and nahcolite solid phase were present. The most important source of carbon dioxide was probably decarbonation reactions during metamorphism of banded iron formation (Perry&Ahmad, 1981). Decomposition of calcite and siderite caused expulsion of CO_2 during deformation. Each generation of secondary fluid inclusions represents different episodes in the thermal history of the

rock, after peak metamorphic conditions. Plotted isochores, constraining the possible fluid trapping conditions during retrograde metamorphism, overlap the greenschist and amphibolite facies on the P-T diagram. Fluid immiscibility of H_2O-CO_2 system might have occurred during these facies during retrograde metamorphism (Hollister, 1990). Entrapped low saline fluid inclusions, containing 10 mol% of CO_2, resulted from trapping of retrogressive fluids that are predicted to be driven through jaspilites in metamorphic conditions of greenschist or lower amphibolite facies. Studied veins represent probably one of the late stages of Early Proterozoic orogeny.

Fig. 1. Nahcolite crystal enclosed within inclusion comprised of aqueous phase (aq), liquid CO_2

Fig. 2. Three phase fluid inclusion comprised of aqueous phase (aq), liquid CO_2 and nahcolite crystal

REFERENCES

Bakker R.J. (2003) *Chemical Geology*, 194: 3-23

Fall A., Tattitch B. & Bodnar R.J. (2011) *Geochim. Cosmochim. Acta*, 75: 951-964

Gurskiy D.S., ed. (2002) Geological excursion guidebook, *Ukrainian State Geological Survey*

Hollister L.S. (1990) *Journal of Structural Geology*, vol. 12, 7: 895-901

Perry E.C., Ahmad S.N. (1981) *Lithos* 14:83-92

Preliminary analysis of fluid inclusions in Messinian Halite of Volterra basin and Crotone basin (Italy)

Speranza, G.*, Tecce, F.** and Faccenna, C.*

*Dipartimento di Scienze Geologiche, Roma Tre University, Rome, Italy
**Istituto di Geologia Ambientale e Geoingegneria - C.N.R., Rome, Italy

Typical neogenic sedimentary succession of Mediterranean Area comprises a thick evaporitic sequence of Messinian age, deposited during the "salinity crisis" between ≈6 and 5.33 Ma (Rouchy & Caruso, 2006), including thick Halite deposits.

To obtain information both on temperature at salt deposition time and on subsequent diagenetic transformation of Halite deposits, fluid inclusions analysis is a fundamental instrument.

We focused our attention on two areas of Italian peninsula: the Volterra basin (Tuscany) and the Crotone basin (Calabria) (Fig. 1). Both are filled by neogenic sedimentary sequences of Miocene to Pleistocene, including Messinian evaporites and Halite (Roda, 1964; Testa & Lugli, 2000).

In the Crotone area samples were collected directly from salt diapirs outcropping in the Vitravo river valley. Samples from Volterra basin come from cores from S1113 borehole made by Solvay Company for salt exploitation in the area.

Salt blocks were first cut using a diamond saw, then manually reduced to a thickness of about 500µm and manually polished using routine types of grinding papers. We watched out for samples temperature to not exceed roughly 25 °C.

Halite from Vitravo river is constituted by large, irregular crystals, up to 4-5cm, with portions of "clear" salt and portions of primary "cloudy" salt (chevrons, cubes and hoppers) (Hardie et al, 1983). These crystals contain many primary fluid inclusions, all liquid with cubic shape, often organized in typical growth bands (Fig. 2) (Counter Benison & Goldstein, 1999). Few inclusions contain daughter crystals which have been identified as gypsum and polyhalite by SEM investigations (Salvi & William-Jones, 1990).

Volterra samples consist of smaller (<1cm) crystals than Vitravo halite, with irregular shape. Cloudy halite, made up of countless minute inclusions, often take up the central area of the crystals, surrounded by clear halite. We recognized at least two generations of fluid inclusions (Goldstein, 2001; Kerkhof & Hein, 2001). Primary fluid inclusions, all liquid with cubic shape, are located at the edges of cloudy areas or isolated. Secondary fluid inclusions occur as planes or rows of more or less rounded inclusions, both liquid-rich and vapour-rich, clearly located into healed fractures. Large networks of tubular inclusions are also present

During the microthermometric runs (Linkam stage model THMSG 600), samples were first cooled until -25/-30 °C in order to avoid stretching and reaction with inclusion walls. For this reason no measures of fluid salinity could be possible. Samples were held at this temperature for about 30 minutes. In general, on cooling, vapour bubbles do not appear before ≅ 0 °C.
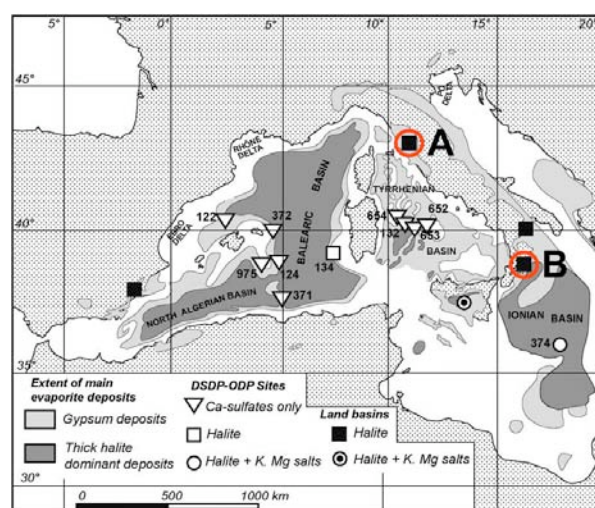
Fig. 1. Map showing distribution and extent of the Messinian evaporites in the Mediterranean area and location of samples (A: Volterra basin; B: Crotone basin). Modified from Rouchy & Caruso, 2006.
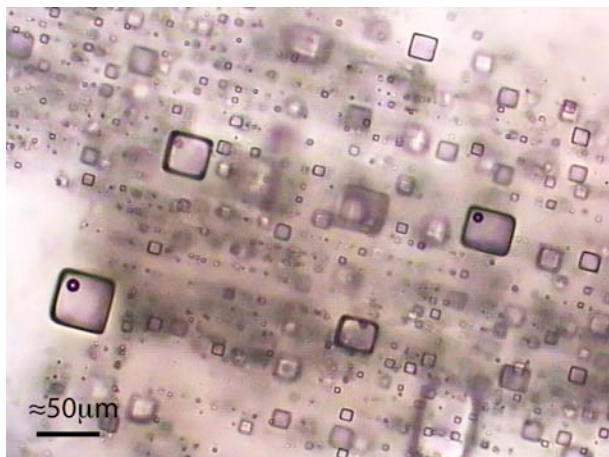
Fig. 2. Photomicrograph of fluid inclusions in halite from Vitravo 1 diapir (Crotone).

In general, bubbles appear earlier (i.e. at higher temperature) in Crotone inclusions than in Volterra ones, and usually earlier in larger inclusions than in smaller ones. The gas-to-liquid ratio appear constant within inclusions of the same generation. Then samples were heated at variable rate between 1 and 5 °C/min until T_h are reached.

T_h data vary between 12 and 42 °C (Fig. 3), in good agreement with previous works on primary fluid inclusions in Halite (Roberts & Spencer, 1995; Counter Benison & Goldstein, 1999). However, T_h data fall mostly in the range between 15 – 22 °C, a quite lower temperatures compared to those in Permian Halite as reported in Counter Benison & Goldstein, 1999. These data fit well with climatic conditions at salt deposition time, a glacial stage (TG 20 e TG 22 peaks) that, during Messinian salinity crisis, concurred in establishing evaporative conditions in the Mediterranean area (Rouchy & Caruso, 2006).

Furthermore, it can be noticed that Volterra samples exhibit Th slightly higher than Crotone samples. This can be due to local conditions at salt deposition time or to possible subsequent modification. In fact, during burial history of Volterra basin a high heat flow affected the area in Pliocene and Pleistocene, due to the emplacement of crustal and subcrustal magmatic bodies (Testa & Lugli, 2000).

We can conclude that T_h data from primary fluid inclusions are consistent with growth of halite crystals under evaporative conditions reported in Mediterranean area during Messinian (Rouchy & Caruso, 2006). Moreover we outline the fluid inclusion differences between Crotone and Volterra samples due to local conditions both at deposition time or during sin-depositional and post-depositional history. Observed differences can offer an important indication in order to explain different bulk properties of same rocks.

Analysis of secondary inclusions and samples from other rock salt mines (Sicily) are still in progress.
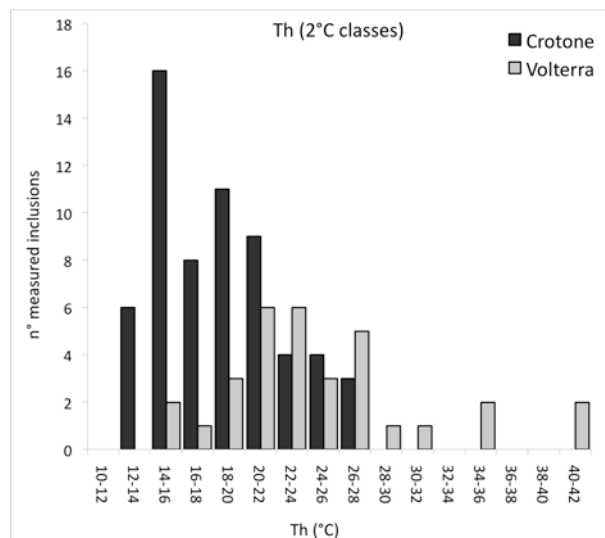
Fig. 3. Histogram of homogenization temperatures (T_h) of Volterra and Crotone halite primary fluid inclusions. Total number of measurements: 79 (Crotone 58; Volterra 21).

REFERENCES

Counter Benison K., Goldstein R. H. (1999) *Chem. Geol.* 154: 113-132.

Goldstein R. H. (2001) *Lithos* 55: 159-193.

Hardie L. A., Lowenstein T. K., Spencer R. J. (1983) *Sixth Int. Symp. on Salt* Vol.1.

Kerkhof A. M. van den, Hein U. F. (2001) *Lithos* 55: 27-47.

Roberts S. M., Spencer R. J. (1995) *Geoch. Et Cosm. Acta* 59: 3929-3942.

Roda C. (1964) *Geol. Rom.* III: 319-366.

Rouchy A. M., Caruso A. (2006) *Sed. Geol.* 188-189: 35-67.

Salvi S., William-Jones A. M. (1990) *Geoch. Et Cosm. Acta* 54: 2403-2418.

Testa G., Lugli S. (2000) *Sed. Geol.* 130: 249-268.

The role of fluid-phase immiscibility in quartz dissolution and precipitation in sub-seafloor hydrothermal systems: Implications for fluid inclusion studies of volcanogenic massive-sulphide deposits

Steele-MacInnis, Matthew, Han, Liang, Lowell, Robert P., Rimstidt, J. Donald and Bodnar, Robert J.

Department of Geosciences, Virginia Tech, 4044 Derring Hall, Blacksburg VA 24061 USA

Volcanogenic massive sulphide (VMS) deposits represent the fossil analogues of the active hydrothermal vents in the seafloor found at oceanic spreading centres (Galley *et al.*, 2007). Fluid inclusion (FI) studies of both active ("black smokers"; *e.g.* Vanko *et al.*, 2004) and fossil (*e.g.*, Pisutha-Arnond & Ohmoto, 1983) VMS systems have provided much information on the physical and chemical conditions of formation of these deposits. The vast majority of all FI studied from VMS deposits are hosted in quartz. Primary inclusions in quartz are trapped as quartz precipitates from hydrothermal fluid – primary inclusions are unlikely to be trapped where and when quartz is being dissolved. Therefore conditions of quartz dissolution will be under-represented in the primary inclusion record (although those conditions may be preserved in secondary inclusions). The properties of quartz-hosted FI can provide information on the physical and chemical conditions of quartz *precipitation*. Ideally those conditions should be related to hydrothermal processes, but sub-seafloor processes cannot be directly observed, and must therefore be modelled and/or inferred.

The occurrence of phase separation in sub-seafloor hydrothermal systems is now widely recognized based on vent chemistry data (*e.g.*, Von Damm, 2004), although less is known about how sub-seafloor immiscibility affects fluid-rock interaction in VMS deposits. Fluid inclusion assemblages in quartz from active VMS-forming systems sometimes contain coexisting liquid-rich and vapour-rich inclusions, revealing that the host quartz was precipitated from immiscible fluids (de Ronde, 1995; Vanko *et al.*, 2004). Halite-bearing inclusions are commonly found in VMS quartz, and may represent brine generated during phase separation, although they are usually found without coexisting vapour-rich inclusions.
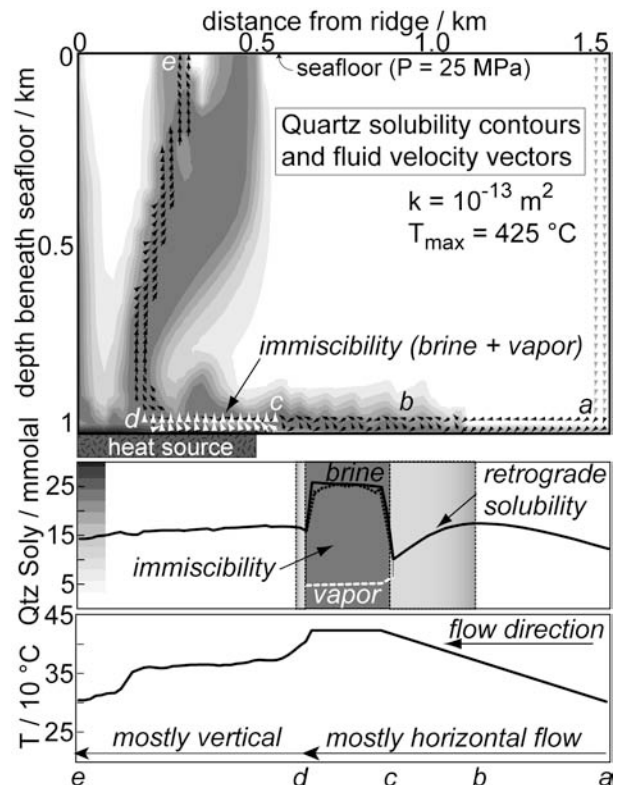
Fig. 1. Example flow path (small arrows are fluid flow vectors, top), and the quartz solubility (middle) and temperature (bottom) along the path. Points labelled a-e on the top diagram correspond to the x (distance) axis on the middle and bottom plots. Fluid flows from the lower right (a) towards the lower left (c-d, the heat source) and then flows upwards to vent at the seafloor (e). Quartz solubility first increases (a-b), then decreases (b-c), with increasing temperature. Immiscibility occurs at T > 410 °C (c-d), and quartz solubility is higher in the high-salinity brine and lower in the low-salinity vapour (white vectors). Bulk quartz solubility in the two-phase zone is dominated by the brine. There is an abrupt drop in quartz solubility going from two-phase to one-phase conditions (d).

In the present study, we couple numerical fluid flow modelling of sub-seafloor hydrothermal systems with a model for dissolution and precipitation of quartz, in order to predict where, when and by what mechanisms quartz is likely to be precipitated (and to trap FI in VMS deposits).

We model miscible and immiscible hydrothermal circulation using the code *FISHES* (Lewis and Lowell, 2009) which solves the conservation equations governing multi-component, multi-phase fluid flow in porous media. We calculate quartz solubility in H_2O-NaCl fluids (representing seawater and phase-separated seawater) using the model of Akinfiev and Diamond (2009). Quartz dissolves when the quartz solubility in the fluid increases along its flow path, and quartz precipitates in the opposite scenario.

Effects of retrograde quartz solubility and fluid-phase immiscibility are observed in this model (Fig. 1). Retrograde quartz solubility causes quartz to be precipitated as fluid heats along part of the flow path (elsewhere, quartz dissolves as the fluid heats). Immiscibility creates a region in which quartz solubility is significantly higher in the higher-salinity brine phase and lower in the lower-salinity vapour; overall quartz solubility in that region is controlled mostly by the brine (Fig. 1). Across the interface from two-phase to one-phase conditions, there is a steep decline in quartz solubility over a relatively short distance (Fig. 1), resulting in large amounts of quartz precipitation.

As fluid flows along the solubility gradients shown in Figure 1, quartz is precipitated and dissolved, and the rate of dissolution/precipitation depends on the solubility gradient as well as the fluid mass flux. Two examples of distribution of dissolution and precipitation are shown in Figure 2. In both examples, quartz is precipitated where fluid flows upward as hot plumes and vents at the seafloor. There is a significant difference between the two examples: in the upper example (Fig. 2, top) the bottom temperature is set just high enough so that phase separation occurs, whereas in the lower example (Fig. 2, bottom) the temperature is kept just below that needed for phase separation. Where immiscibility occurs (Fig. 2, top), a zone develops in which quartz is precipitated at the highest rates, along the two-phase to one-phase

interface (where immiscible brine and vapour flow upwards and re-mix). This outcome suggests that FI in quartz from VMS deposits may preferentially record conditions *just above* the two-phase region.
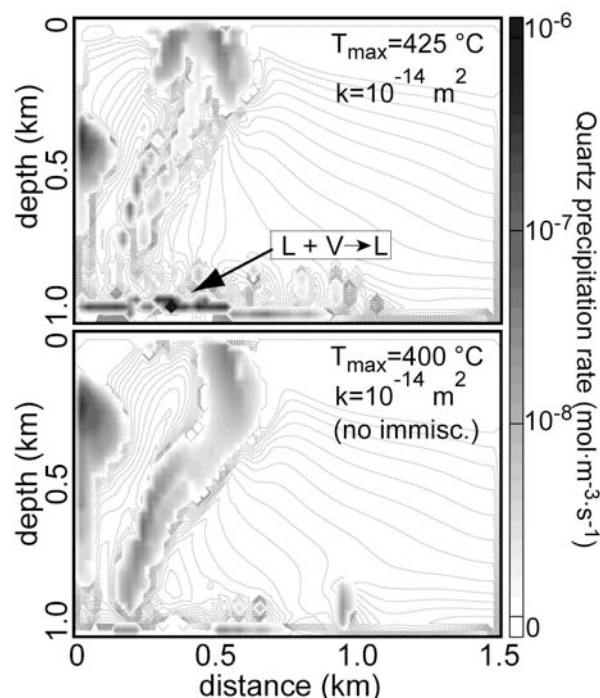
Fig. 2. Contoured rate of quartz precipitation throughout the system, comparing a simulation in which immiscibility occurs (top) with one in which immiscibility does not occur (bottom). Maximum rate of quartz precipitation is found in the simulation with immiscibility, at the interface between two-phase and one-phase conditions (L + V → L).

REFERENCES

Akinfiev N.N., Diamond L.W. (2009) *Geochim Cosmochim. Ac.* 73: 1597-1608.

de Ronde, C. (1995) in J.F.H. Thompson (ed.) *Magmas, Fluids and Ore Deposits* 479-509.

Galley A., Hannington M., Jonasson (2007) *Geol. Assoc. Can. Special Pub.* 5: 141-161.

Lewis, K.C., Lowell, R.P. (2009) *J. Geophys. Res.* 114: B05202

Pisutha-Arnond V., Ohmoto H. (1983) *Econ. Geol. Mon.* 5: 523-558.

Vanko D., Bach W., Roberts S., Yeats, C.J. Scott S.D. (2004) *Geochim. Cosmochim. Ac. 52: 2451-2456*

Von Damm, K. (2004) *Geophys. Mon.* 148: 285-304

The effect of post-entrapment crystallization on the H₂O and CO₂ concentrations of rhyolitic (silica-rich) melt inclusions, and implications for magma degassing paths

Steele-MacInnis, Matthew, Esposito, Rosario and Bodnar, Robert J.

Department of Geosciences, Virginia Tech, 4044 Derring Hall, Blacksburg VA 24061 USA

Concentrations of H_2O and CO_2 in silicate melt inclusions (MI) are often interpreted to represent magmatic "degassing paths," in which depressurization of the magma during ascent leads to vapour saturation and release of CO_2 and H_2O from the melt (*e.g.*, Lowenstern, 1994). This interpretation requires that melt inclusions are trapped under conditions of vapour saturation at various locations (depths) along the ascent path. If the trapped melt is saturated in volatiles, then the melt must exsolve a volatile phase if any post-entrapment crystallization occurs. As a result, the pressure inside the MI may differ from the confining pressure during post-entrapment cooling, and the PT path of the MI may be calculated knowing the solubility of H_2O and CO_2 in the melt as a function of T and P, as well as the PVT properties of the H_2O-CO_2 volatile phase, the partial molar volumes of H_2O and CO_2 in the melt, and the molar volumes of the melt phase and the crystallizing solid phase. Using PVTX data for the systems $NaAlSi_3O_8$-H_2O (Burnham and Davis, 1974) and $NaAlSi_3O_8$-H_2O-CO_2 (Holloway and Blank, 1994), we investigate the effect of small fractions of post-entrapment crystallization on the dissolved volatile content in an albitic melt inclusion entrapped under conditions of volatile saturation. The model is constrained to be a closed, isochoric system. As small amounts of albite crystallize on the inclusion walls, the melt becomes supersaturated in volatiles, and so nucleation and growth of an H_2O, CO_2 or H_2O-CO_2 vapour bubble occur and the pressure inside the MI is estimated from the difference between the molar volume of the volatile phase and the partial molar volume of the volatile in the melt using the EOS for H_2O-CO_2 (Holloway, 1977; Flowers, 1979).

Significantly different styles of PT and volatile evolution occur in MI that are saturated
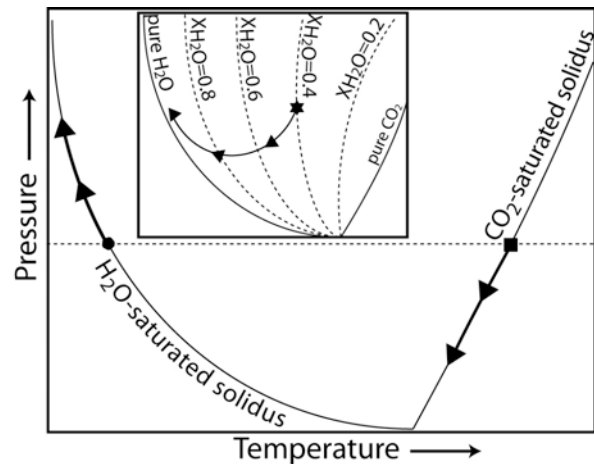
Fig. 1. Schematic PT trajectories followed by vapour-saturated MI during post-entrapment crystallization. Melt-volatile phase relations are shown by the H_2O- and CO_2-saturated solidus curves. The solid circle shows the PT point of entrapment of an H_2O-saturated melt inclusion at the same pressure (dashed line) as a CO_2-saturated melt inclusion shown by the solid square. Thick curves with arrows show the PT paths followed by both MI during PEC. The inset shows the PT path of a mixed H_2O-CO_2 saturated MI trapped at the PT point shown by the star, with isopleths of H_2O in the vapour phase shown as dashed lines).

with an H_2O-rich fluid versus a CO_2-rich fluid at the time of entrapment (Fig. 1). The differences are due to 1) the higher density of free CO_2 compared to H_2O at magmatic PT conditions, and the larger partial molar volume of CO_2 compared to H_2O in the melt phase; 2) the lower solubility of CO_2 compared to H_2O in the melt phase; and 3) the negative dP/dT slope of the H_2O-saturated solidus compared to the positive dP/dT slope of the CO_2-saturated solidus (Fig. 1). As a result, for CO_2-rich compositions the pressure in the MI and the dissolved CO_2 content of the melt phase both

decrease during post-entrapment crystallization. For H_2O-rich melts, the pressure and the dissolved H_2O concentration in the melt phase both increase during post-entrapment crystallization. Because the solubility of CO_2 in the melt is much lower than that of H_2O, MI with mixed H_2O-CO_2 initial volatile compositions undergo a transition from pressure decrease to pressure increase during post-entrapment crystallization, and the H_2O concentration in the exsolved volatile phase increases as crystallization proceeds (Fig. 1).

The evolution of H_2O and CO_2 contents in the melt (glass) phase during post-entrapment crystallization of volatile saturated MI in some cases reasonably reproduces the observed distribution of H_2O-CO_2 contents of natural MI (e.g., Fig 2). In particular, the dissolved CO_2 content in MI is highly sensitive to small fractions of post-entrapment crystallization, such that nearly all the dissolved CO_2 in the melt phase can be lost during crystallization of a few percent of the melt.

Model results show that dissolved volatile contents in the melt vary in a systematic manner during low degrees of post-entrapment crystallization. More importantly, the H_2O and CO_2 contents of the melt (glass) in the inclusion define trends similar to those produced during open-system degassing. Furthermore, the model predicts that the dissolved CO_2 in the melt phase may be almost completely lost to the vapour phase during post-entrapment crystallization, even though the vapour bubble occupies less than one volume percent of the melt inclusion (Fig. 2). Thus, melt inclusions that all trap a vapour-saturated melt with the same volatile concentrations, but experience varying degrees of post-entrapment crystallization on the walls, will define an H_2O-CO_2 concentration trend resembling an open-system degassing path.
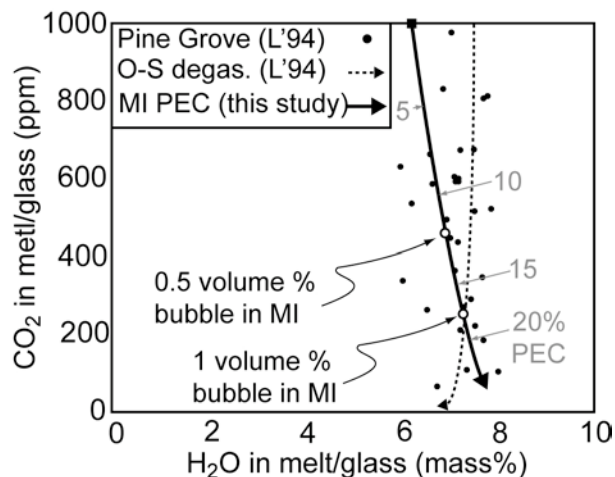
Fig. 2. H_2O-CO_2 contents of MI from Pine Grove, southwest Utah (solid circles, L'94 = Lowenstern, 1994; dashed curve, O-S degas. = open-system degassing; PEC = post-entrapment crystallization). Dashed curve represents open system degassing of a rhyolitic magma at 675 °C from Lowenstern (1994), and solid curve represents post-entrapment crystallization of a rhyolitic MI entrapped at 877 °C, calculated in the present study. Both trends start at 4 kbars. For post-entrapment crystallization, open circles show where the vapour bubble occupies 0.5 and 1 percent of the MI volume. Tic marks and numbers (5, 10, 15, 20%) on the PEC path show the proportion of the melt that has crystallized during PEC.

REFERENCES

Burnham C.W., Davis N.F. (1974) *Am. J. Sci.* 274: 902-940.

Flowers G.C. (1979) *Contrib. Mineral. Petr.* 69: 315-318

Holloway, J.R. (1977) in D.G. Fraser (ed.) *Thermodynamics in Geology*. 161-181

Holloway J.R., Blank J.G. (1994) *Rev. Mineral.* 30: 187-225

Lowenstern J.B. (1994) *Geology* 89: 893-896.

Enargite from the Lahóca high-sulphidation epithermal gold deposit at Recsk, Hungary: joint application of infrared microscopy – microthermometry and orientation imaging microscopy

Takács, Ágnes and Molnár, Ferenc

Department of Mineralogy, Eötvös Loránd University Pázmány Péter prom 1/C, Budapest, Hungary

Most of the ore minerals are opaque in the 400-700 nm wavelength (visible light) range and this sets limitations for routine microscopic methods for fluid inclusion studies of ore deposits. On the other hand, a number of opaque minerals are quite transparent to near-infrared (NIR) radiation (Campbell et al., 1984). The IR radiation has lower energy than the visible light and therefore its energy is not large enough to excite an electron from the valence band to the conduction band. Thus the light is not absorbed by the mineral, consequently the mineral is transparent in IR light (Shuey, 1975). Several opaque minerals, such as pyrite, enargite, stibnite, molybdenite, hematite, etc. have been found to be transparent in IR light (Campbell et al., 1984). Microthermometric studies on these minerals showed that their fluid inclusions preserved such stages of the ore forming processes which otherwise could not be reconstructed on the basis of conventional studies of fluid inclusions in transparent minerals (Campbell and Robinson-Cook, 1987; Lüders, 1996).

In the vicinity of Recsk in NE-Hungary, an intrusive-volcanic complex of Palaeogene age contains the Lahóca high sulphidation type epithermal Cu-As-Au ore deposit. The deposit consists of stocks of massive enragite-luzonite. Under the epithermal zones, porphyry copper deposit occurs at about 500 - 600 m depth.

Conventional fluid inclusion petrography and microthermometry of quartz-hosted fluid inclusions were completed on Olympus BX51 microscope with IR filters and Linkam FTIR 600 type stage. Infrared fluid inclusion petrography were carried out on enargite crystals using wide infrared radiation sensitive camera (Hamamatsu C2500) mounted on Olympus BX51 microscope without any light filter and using special objectives (Olympus MIRPlan) which are optimized for transmitting the infrared radiation. Infrared microthermometry on enargite was performed by using Linkam FTIR 600 type stage with sapphire windows together with the above described infrared microscopic system. The reproducibility of the measurements was ±1 °C at high temperatures and below 0 °C. The calibration measurements to avoid and eliminate IR radiation, which were carried out on quartz-hosted and enargite-hosted fluids, caused problems during fluid inclusion microthermometry which has been described by Moritz (2006). Results of calibration measurements proved that the "green house effect" has no significant effect on the measured homogenization and final ice melting temperatures by using the setup of our laboratory described above.

Our observations in the infrared microscope collude with the previous studies (Mancano and Campbell, 1995; Molnár et al. 2008), where enargite crystals show various transmittances under the IR microscope. Several times the crystals remained opaque in periodic zones or in inhomogeneous patches. The thickness of the sample and differences in the chemical composition (for example replacement of As by Sb in the structure) can influence the IR transmittance, but we couldn't explain the remained opacity by these effects. Because optical properties of minerals are highly influenced by the orientation of the crystal structure in relation to the incident beam, we investigated the IR transmittance in the connection to the crystal's orientation of enargite. Orientation imaging microscopy (OIM) is a powerful technique used to obtain crystallographic orientation from single and polyphase crystalline materials, based on the electron backscatter diffraction (EBSD) patterns in the scanning electron microscope (SEM). Results

of the comparison of the crystal orientation maps produced by the SEM-EBSD method with the IR transmittance of the samples under microscope suggest the validity of our approach. Further mapping the IR transparency of enargite crystals extended with NIR micro-spectrophotometric reflectance/transmittance measurements is in progress in order to define the exact relationship between the crystal orientation and absorption coefficients in near-infrared light.

The results of microthermometry for enargite-hosted primary fluid inclusions suggest that the ore forming stage in the Lahóca deposit took place in a temperature range between 170 and 230 °C. There is no quartz or other transparent mineral which precipitated synchronously with enargite and data for quartz which precipitated before crystallization of enargite indicate temperatures of 250 - 300 °C for the early stage of hydrothermal activity. Fluid inclusions in late stage quartz, formed during a syn-hydrothermal tectonic stage, homogenized between 130 and 170 °C. The defined decrease of the temperature between the hydrothermal phases is associated with an increase of fluid salinity, which probably reflects the increasing proportion of magmatic water in the epithermal zone of the intrusion-related hydrothermal system (Molnár et al., 2008). Data for enargite-hosted fluid inclusions also suggests that the decreasing temperature and increasing salinity (from ~1 to ~8 eq mass% NaCl) of the ore forming stage shows spatial changes from the NNW part to the SE part of the deposit. This direction does not point towards to the position of the porphyry copper ore bearing intrusion of the system.
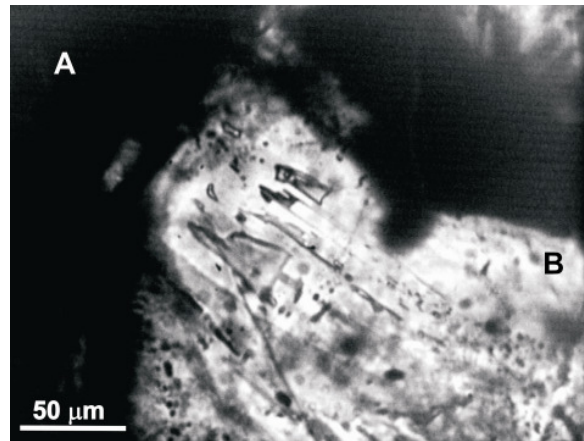
Fig.1. IR microscopic image of transparent (B) and opaque (A) enargite-crystals. The IR transmitting crystal contains secondary, mostly necked-down fluid inclusions.
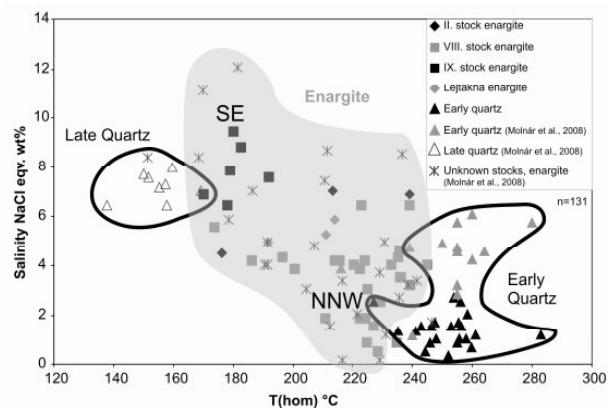
Fig.2. Fluid inclusion homogenization temperature-salinity data for the Lahóca epithermal gold deposit.

REFERENCES

Campbell A. R., Hackbarth C.J., Plumlee G.S., Petersen U. (1984) *Econ. Geol.* **79:** 1387-1392.

Campbell A. R., Robinson-Cook S. (1987) *Econ. Geol.* **82:** 1640-1645.

Mancano D.P., Campbell, A.R. (1995) *Geochim. Et Cosmochim. Acta* **29:** 3909-3916.

Molnár F., Jung P., Kupi L., Pogány A., Vágó E., Viktorik O., Pécskay Z., Hurai V. (2008) *Publ. of the Univ. of Miskolc Ser. A, Mining* **73:** 99-127.

Moritz R. (2006) *J. of Geochem. Explor.* **89:** 284 - 287.

Shuey R. T. (1975) *Semiconducting ore minerals* **Elsevier Scientific Publishing Company, 2**nd **edition, 415.**

Fluids in high-sulphidation gold deposits: Insights from *in situ* stable isotopes and noble gas analyses

Tanner, Dominique, Mavrogenes, John A. and Henley, Richard W.

The Research School of Earth Sciences, Australian National University, Building 61, Mills Rd., Canberra, Australia

In the past, the origin of fluids in high-sulphidation gold deposits has been based on stable isotopes (D, O and S) using the temperature of homogenisation of co-existing fluid inclusions (typically <300 °C).

We have separated euhedral quartz crystals from sulphosalt ore from the El Indio Au-Ag-Cu deposit, Chile; and the Summitville Au-Ag-Cu deposit, Colorado in order to investigate their isotopic composition. These euhedral ~200 μm crystals either grow into vugs in the sulphosalt ore, or are encased by sulphosalts.

All the high-density fluid inclusions found in these crystals are secondary, occurring in multiple generations of healed fractures. Low-density vapour inclusions are present as both primary and secondary inclusions. Often their paragenesis is unclear due to their small size (<1 μm), or isolation.

Sulphosalt-melt inclusions are abundant in quartz crystals from both deposits. They are mostly primary sulphosalt-melt inclusions, restricted to certain growth bands within the crystal (Fig. 1) - but rare secondary sulphosalt-melt inclusions have been identified.
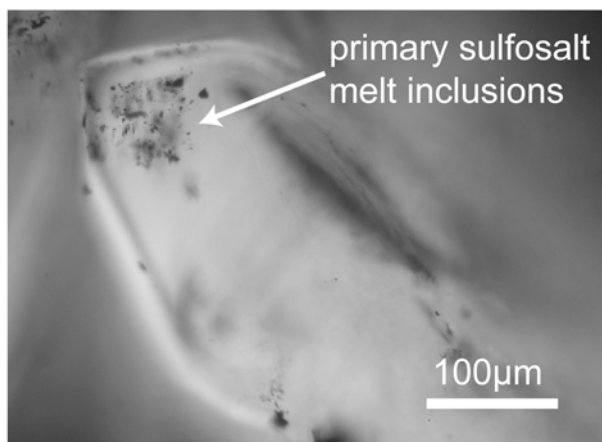
Fig. 1. Primary sulphosalt-melt inclusions restricted to distinct growth bands in euhedral quartz from the El Indio Au-Ag-Cu deposit, Chile.

Recent work has shown that sulphosalt melt assemblages co-existing with quartz crystals in high-sulphidation deposits are quenched at high temperatures ~675 °C (Mavrogenes et al., 2010; Henley and Mavrogenes, in review); suggesting that the quartz was sourced from a magmatic vapour.

In order to test this hypothesis, *in situ* stable isotopes were used to see whether the quartz had a magmatic ($\delta^{18}O$ ~ 5-10‰) or low-T hydrothermal ($\delta^{18}O$ ~ 5-10‰) signature. The noble gas chemistry of crushed quartz was also measured to test whether the fluid inclusions contain a crustal (He R/Ra <1) or magmatic (He R/Ra ~8) signature.

Cathodoluminescence (CL) imaging and Al-mapping using the electron microprobe (EMP) revealed that most quartz crystals displayed intricate euhedral growth bands (ranging from 1-40 μm thick), while a few samples displayed intricate sinter-like banding.

Oxygen isotopes were analysed using SHRIMP II at the Australian National University. The primary beam was ~25 μm in diameter, so many isotopic analyses within individual quartz crystals still provide a mix of isotopic compositions across two distinct growth zones (Fig. 2).

The isotopic composition of quartz from these deposits shows a wide range in isotopic compositions (3.7 - 17.1 ‰); with up to 11 ‰ variation within an individual crystal.

These data are compatible with published data from other high-sulphidation gold deposits. The $\delta^{18}O$ of whole quartz crystals from the Summitville deposit has been found to range between ~9.8 - 14.2 ‰ (Bethke et al., 2005). The $\delta^{18}O$ of one quartz crystal from the Pierina high sulphidation gold deposit was found to be ~17 ‰ (Fifarek and Rye, 2005).
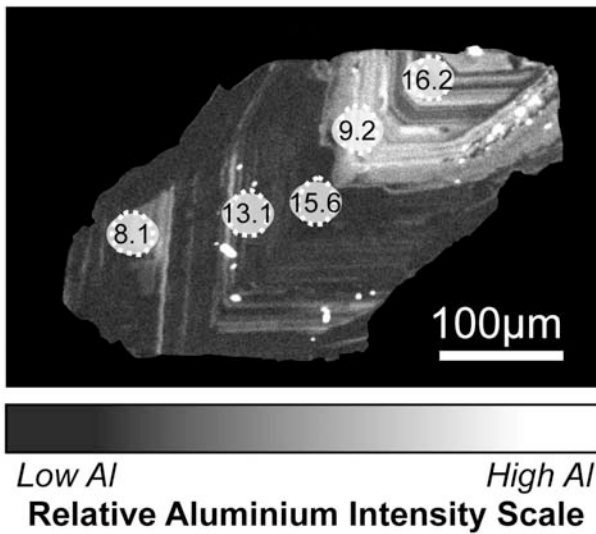
Fig. 2. Aluminium zoning in euhedral quartz from the El Indio Au-Ag-Cu deposit, Chile. The numbers show the measured variation in $\delta^{18}O$ (‰) within the crystal.

Such heavy and variable $\delta^{18}O$ compositions could suggest one of either two possibilities:

a)   the range in $\delta^{18}O$ values may be explained by *equilibrium* Rayleigh fractionation of a low-temperature fluid in a closed system with episodic pulses of fresh fluid; or

b)   the heavy oxygen may be explained by *kinetic* fractionation during progressive dehydration of a Si-O-OH-rich volcanic gas condensate. The range in $\delta^{18}O$ can therefore be explained by various degrees of dehydration from various Si-phases.

We do not consider option (a) to be plausible, as the entrapment of so many sulphosalt melt inclusions is not possible at low-temperatures.

Hypothesis (b) may also explain the origin of sinter-like banding evident in CL and EMP imagery – as residual evidence of an opaline phase.

Given that the isotopic composition of the quartz is controlled by kinetic, rather than equilibrium fractionation; and the fluid inclusions are not derived from the same fluid as the host mineral, isotopic calculations of the ore-bearing fluid cannot be made.

Noble gas analyses of 1g of crushed quartz from the El Indio Au deposit reveal that the fluid inclusions within the quartz have a crustal He signature (R/Ra <0.26). However, this contradicts the Ne isotopes, which suggest a more magmatic source (Ne/Ne = 9.27). The He and Ne values founding El Indio quartz are remarkably similar to vapour inclusions measured in alunite from other high-sulphidation deposits (Landis and Rye, 2005). These noble gas analyses suggest that the quartz preserves a fingerprint of both magmatic and crustal fluids.

These results show that the majority of fluid inclusions in quartz from the El Indio deposit are secondary and record evidence of a low-temperature, crustal-derived fluid.

REFERENCES

Berger B.R. (2010) *Econ. Geol.* 105: 257-262.

Bethke P.M., Rye R.O., Stoffregen R.E., Vikre P.G. (2005) *Chem. Geol.* 215: 281-315.

Fifarek R.H., Rye R.O. (2005) *Chem. Geol.* 215: 253-279.

Henley R.W. and Mavrogenes J.A. (2011) *Geofluids (in review)*.

Landis G.P. and Rye R.O. (2005) *Chem. Geol.* 215: 155-184.

Mavrogenes J.A., Henley R.W., Reyes A.G., (2010) *Econ. Geol.* 105: 257-262.

Modifications of fluid inclusions in quartz due to post-entrapment ductile deformation: Case study in the Aar Massif, Central Alps, Switzerland

Tarantola, Alexandre*, Diamond, Larryn W.**

*UMR-G2R, University Henri Poincaré, F-54506 Vandœuvre-lès-Nancy, France
**Institute of Geological Sciences, University of Bern, Baltzerstrasse 3, CH-3012 Bern, Switzerland

1. Introduction

Fluid inclusions in quartz are known to modify their shapes, textures, densities and in certain cases even their chemical compositions during shear deformation. These changes have been demonstrated in piston-cylinder experiments by Tarantola et al. (2010) and Diamond et al. (2010). In these experiments, natural fluid inclusions in quartz were deformed by uniaxial compression at high T and high confining P (σ_3) in the field of crystal plasticity. The experiments showed that intact inclusions (Fig. 1) preserve their original densities and compositions, whereas inclusions with strong changes in shape adopt new properties: relict inclusions lower their densities whereas neonate inclusions adopt the density corresponding to the maximum compressive stress (σ_1) during the non-hydrostatic deformation.

Here this experimental result is tested using a well-constrained natural sample of plastically deformed vein quartz from the Aar massif, Central Alps, Switzerland.
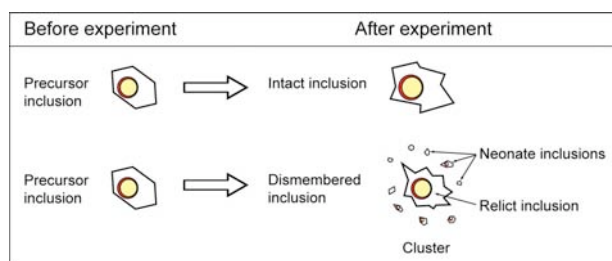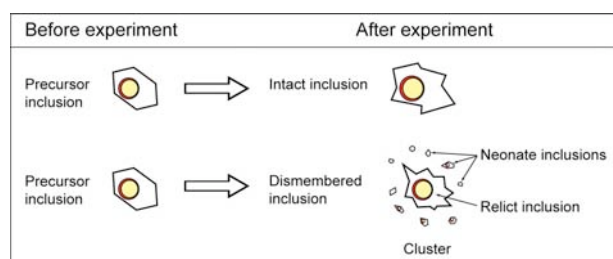

Fig. 1. Summary and nomenclature of shape changes accompanying ~1% plastic strain of the quartz host crystal. View looking down σ_1.

1. Grimsel sample description

A quartz vein within a ductile shear zone was sampled at the Grimsel Pass in the gneiss and schist zone between the Grimsel granodiorite and the southern Aar Granite. The area underwent Alpine greenschist metamorphism and deformation at 25-15 Ma. According to the Si content in phengites (3.2–3.3 p.f.u.) and to the $\delta^{18}O$ fractionation between biotite and quartz (Fourcade et al., 1989), the main shearing event occurred at $T = 450 \pm 30$ °C and $P_{lithostat} = 600 \pm 100$ MPa (Challandes et al., 2008) (top box in Fig. 3).
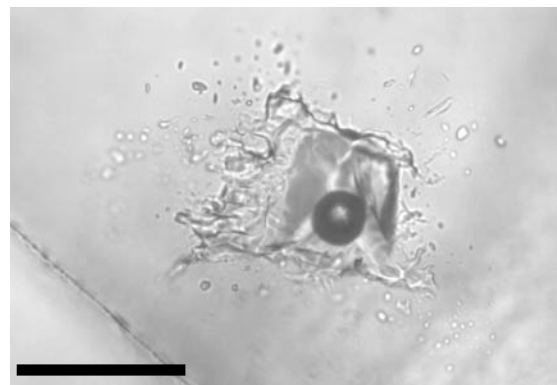
Fig. 2. Cluster of neonate inclusions surrounding their parent inclusion, viewed from direction of flattening. Scale bar is 50 µm.

2. Fluid inclusion petrography

In addition to post-shearing secondary inclusions (not discussed here), the quartz contains early, homogeneously trapped CO_2–H_2O–NaCl inclusions. At T_{lab} these consist of three fluid phases ($L_{aq}L_{car}V_{car}$) and various accidentally trapped minerals. In undeformed domains of the quartz the inclusions have euhedral shapes, and they are therefore classified as precursors (Fig. 1). In deformed domains the inclusions display the same variety of inclusion shapes as produced in the experiments. Some inclusions are deformed but intact, although most are flattened, stretched and dismembered (Fig. 2), defining a planar deformation fabric within the sample. Micro-cracks

emanate from acute angles of the inclusion walls, oriented parallel to the fabric. Within the dismembered clusters, abundant neonate inclusions surround the relict inclusions (Figs. 1 and 2).

3. Fluid inclusion *PVTX* properties

Compilation of the volumetric–compositional (*VX*) properties of the inclusions resulted in the *PT* interpretation in Fig. 3. The isochores of the undeformed precursor inclusions define a narrow band (extrapolated to the top-right corner of Fig. 3). The precise *PT* conditions of inclusion trapping within this band are not known, but this is not important to the present study; here the isochores simply serve to illustrate the pre-deformation *VX* properties of the inclusions. Inclusions that are deformed but intact have isochores that define a broader band, indicating that they largely preserve the *VX* properties of the precursors, but with some scatter to higher densities. As expected from the experimental study, the relict inclusions in the dismembered clusters display a wide range of densities, including many cases of significantly lowered densities. Their compositions remain unchanged compared to the precursors. Also in accord with the experiments, the neonates that surround the expanded relict inclusions all show much higher densities. Most of these isochores pass through the box that represents the independently determined conditions of ductile deformation. Recalling that the reconstructed pressure conditions represent mean stress (i.e. $P_{lithostat}$), it is quite conceivable that the densest isochores reflect the slightly higher value of σ_1.

4. Conclusions

The plastically deformed inclusions in this natural case study closely resemble the deformation-induced changes in shape, texture, density and chemical composition found in the cited experimental studies. This may open the way to interpret the meaning of fluid inclusions in other examples of ductilely deformed rocks, e.g. in shear-zone hosted hydrothermal ore deposits.
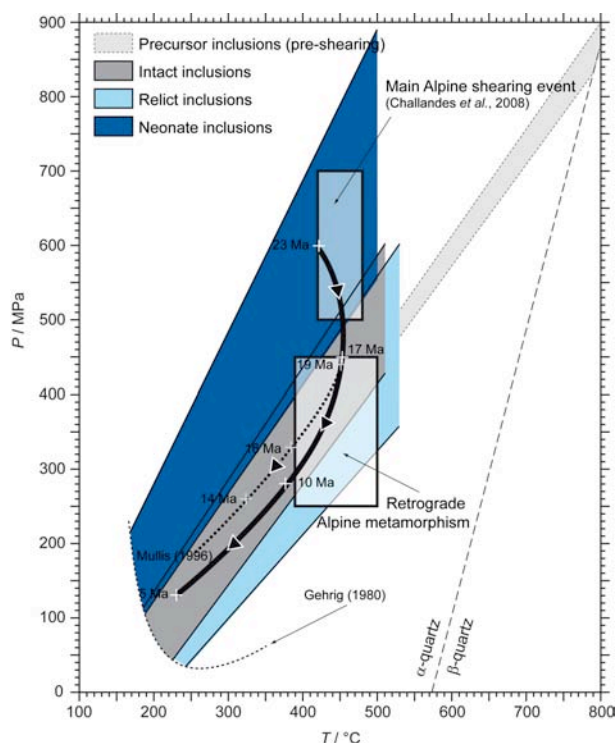
Fig. 3. PT plot of fluid inclusions in Grimsel quartz vein (excluding undeformed secondary inclusions).

REFERENCES

Bakker (2003) Chem. Geol. 194: 3-23.

Challandes N., Marquer D., Villa I.M. *(2008) Swiss J. Geosci.* 101, 269-288.

Diamond L.W., Tarantola A., Stünitz H. (2010) *Contrib. Min. Pet.* 160: 825-843.

Duan Z.H., Møller N., Weare J.H. (1995) *Geochim. Cosmochim. Acta* 59(14): 2869-2882.

Fourcade S., Marquer D. Javoy M. (1989) Chem. Geol. 77: 119-131.

Gehrig M. (1980) PhD thesis. Hochschulverlag Freiburg.

Tarantola A., Diamond L.W., Stünitz H. (2010) *Contrib. Min. Pet.* 160: 845-864.

Modification of natural H_2O–NaCl fluid inclusions under experimental deviatoric stress

Tarantola, Alexandre*, <u>Diamond, Larryn W.</u>**, Stünitz, Holger*** and Thust, Anja****

*UMR-G2R, University Henri Poincaré, F-54506 Vandœuvre-lès-Nancy, France
**Institute of Geological Sciences, University of Bern, Baltzerstrasse 3, CH-3012 Bern, Switzerland
***Department of Geology, University of Tromsø, Dramsveien 201, 9037 Tromsø, Norway
**** Department of Geosciences, Basel University, Bernoullistr. 32, CH-4056 Basel, Switzerland

1. Introduction

Deformed fluid inclusions are extremely common in rocks displaying moderate plastic strain, but no theoretical basis has been available on which to interpret their significance. The questions are (1) whether deformed inclusions retain information on the chemical composition and density of the pre-deformation paleofluids, and (2) whether they record conditions of the ductile deformation itself.

Recent experimental studies (Tarantola et al. 2010; Diamond et al., 2010) have managed to reproduce the microstructures of naturally deformed inclusions by subjecting single quartz crystals, which were rich in CO_2–H_2O–NaCl inclusions, to high deviatoric stresses at 700 °C and ~600 MPa confining pressure in a Griggs piston-cylinder apparatus. The results show that intact inclusions (Fig. 1 explains the new nomenclature), though irregular in shape, do indeed preserve the pre-deformation fluid properties. However, most of the inclusions in the experiments had become dismembered into discoid clusters of tiny, new-formed "neonate" inclusions, surrounding irregularly shaped relicts of the precursor inclusions (Fig. 1).

Fig. 1. Summary and nomenclature of shape changes accompanying ~1% plastic strain of the quartz host crystal. View looking down σ_1.

The thousands of discoid inclusions in each deformed sample define a planar fabric, which lies sub-perpendicular to σ_1. Tarantola et al. (2010) suggested that the direction of σ_1 can therefore be deduced from the corresponding fabric in natural samples. Whereas the relict inclusions preserve the original chemical composition, their densities bear no obvious relation to the *P–T* history of the sample. The neonates, in contrast, had lost H_2O and their densities had increased markedly, approaching the value consistent with the experimentally imposed principal stress, σ_1. Although there were some methodological ambiguities regarding the interpretation of the stress values, Diamond et al. (2010) suggested that this finding could be applied to natural samples. If the temperature of deformation is known, its intersection with the isochores of neonate inclusions defines the absolute magnitude of the principal stress, σ_1.

The latter result is of considerable interest to studies of rock deformation. However, owing to the uncertainty in the stress values in Diamond et al. (2010), the result needs confirmation. In the present study we report the results of 6 new experiments carried out using a similar approach of Tarantola et al. (2010) and Diamond et al. (2010), but on a different natural quartz crystal with compositionally simpler H_2O–NaCl inclusions. This permits an unambiguous interpretation of the stress conditions and of the resulting fluid inclusion isochores.

2. Experiments with H_2O–NaCl inclusions

Sample discs for the experiments were cut from a single quartz crystal from an Alpine cleft in the Aar Massif, Central Switzerland. Several generations of homogeneously trapped, liquid + vapour

inclusions are abundant. Eutectic melting, Raman and LA-ICP-MS analyses confirmed that their bulk properties can be well modelled as binary H_2O–NaCl mixtures.

The samples were loaded isochorically (stepped path in Fig. 2) to a radially symmetric confining pressure (σ_3) of 700–1011 MPa at 700 or 900 °C. A control experiment was held at these hydrostatic conditions for 39 hr, then retrieved and its fluid inclusions reanalysed. Their ice melting temperatures (T_m(ice) = –8.7 to –7 °C) homogenisation temperatures (T_h(LV→L) = 168–208 °C), and isochores match those of the precursors (Fig. 2A). No microstructural evidence was found for quartz plasticity. This demonstrates that simple loading and heating to P_{conf}, T_{exp} and retrieval of the sample produce no artifacts.

Five other samples were subjected to uniaxial compressive stresses (σ_1) of 940–1467 MPa (equivalent to differential stresses of 167–347 MPa) for 9–42 hr. All these samples showed undulatory extinction and bands of *c*-axis mismatch, demonstrating that the host quartz had deformed plastically. All the inclusions showed strong shape changes (as in Fig. 1), identical to those reported by Tarantola et al. (2010). All the neonate inclusions are markedly denser than their precursors, demonstrated by their lower T_h (116 to 166 °C) and T_m(ice) (–8 to –13 °C). Thus, the isochores that emanate from the T_h values at the base of the diagrams rise with steeper *P/T* slopes (shown in Fig. 2B–F by light shaded and stippled fans, truncated at T_{exp}). The most remarkable result is that, in each of the 5 deformation experiments, the densest of the neonate isochores (those with highest *P* at T_{exp}) intersects σ_1 at T_{exp}. These inclusions have thus equilibrated with $P = \sigma_1$ (not with $P = \sigma_{mean}$).

3. Conclusions

The deformation-induced changes in the fluid inclusions in the new experiments are consistent with the studies of Tarantola et al. (2010) and Diamond et al. (2010), but in part they represent more advanced steps along a progression in modifications of density, composition and shape. The plane of flattening of the intact and relict inclusions lies perpendicular to σ_1, and the isochores of the densest neonates pass through *P*

= σ_1 at $T_{shearing}$. These results confirm the idea that deformed fluid inclusions can serve as monitors of both the orientation and magnitude of σ_1 during low-strain, plastic deformation of rocks.
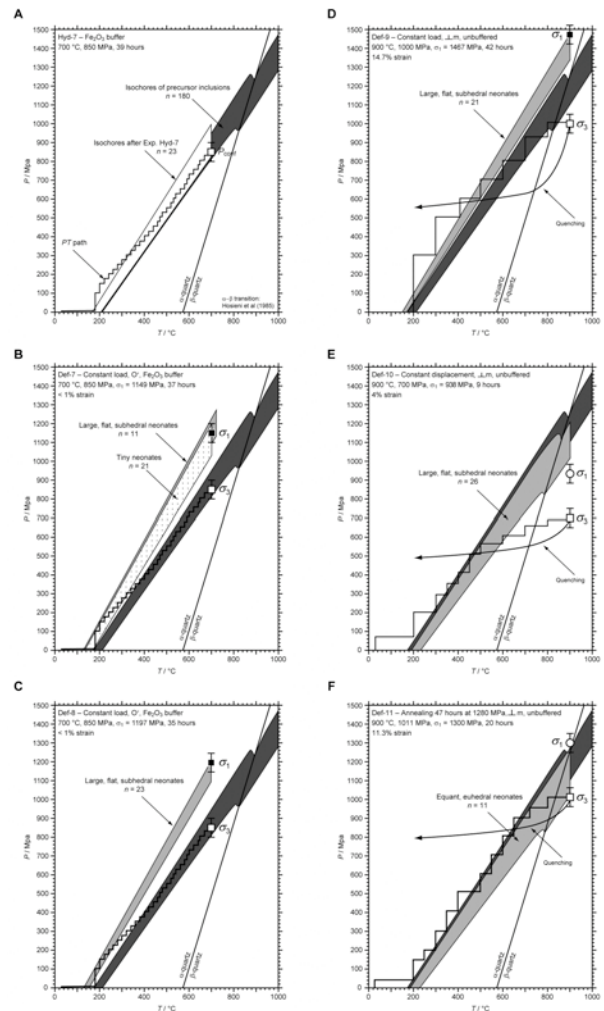
Fig. 2. Isochores of precursor inclusions used for the experiments (dark grey) and of resulting neonate inclusions following the experiments (white dotted and light grey). Isochores calculated from Bodnar and Vityk (1994). The stepped curves show the experimental PT paths.

REFERENCES

Bodnar R.J., Vityk M.O. (1994) *In De Vivo and Frezzotti (eds)*: 117-130.

Diamond L.W., Tarantola A., Stünitz H. (2010) *Contrib. Min. Pet.* 160: 825-843.

Tarantola A., Diamond L.W., Stünitz H. (2010) *Contrib. Min. Pet.* 160: 845-864.

On the two types of melts generating andesites of Gorely and Shiveluch volcanoes (Kamchatka)

Tolstykh, M.L.*, Naumov, V.B.* and Babansky, A.D.**

*Vernadsky Institute of Geochemistry, Russian Academy of Sciences, Kosygin str. 19, Moscow, Russia
**Institute of Geology of Ore Deposits, Petrography, Mineralogy, and Geochemistry, Russian Academy of Sciences, Staromonetnyi per. 35, Moscow, Russia

The genesis of andesitic rocks remains one of the most discussed problems in magmatic petrology (Dirksen et al., 2006; Reubi and Blundy, 2009). Melt inclusions in minerals from andesitic rocks may have different major and trace element composition (Humphreys and Edmonds, 2009; Tolstykh and Naumov, 2000). Plagioclase-hosted magmatic inclusions of two Kamchatka volcanoes demonstrate broad variations of melt composition, while compositions of the host rocks are similar.

Andesites of Gorely volcano are presented by dense lavas from the Young Gorely's edifice. They are represented by porphyric rocks with plagioclase being the main rock-forming mineral. Shiveluch andesites are presented by extrusion lavas and pumice lapilli. This pyroclastic material is represented by porous rock composed of frothed glass, Pl-Px-Amf paragenesis and basitic xenoliths.

The partially crystallized inclusions from Gorely volcano were homogenized before analyses. The naturally quenched glass melt inclusions from Shiveluch volcano were measured by electron microprobe without heating.

Majority of melts from Gorely volcano have andesitic composition ($SiO_2 < 59$ mass%) and are characterized by rather high contents of TiO_2 (1.5 - 2.5 mass%), MgO (2 - 2.5 mass%) and K_2O (about 3 mass%). Enrichment of SiO_2 is typical for all Shiveluch melts; they may be defined as water-rich dacites (SiO_2 68-71 mass%, $TiO_2 < 0.3$ mass%, MgO < 0.9 mass% and K_2O about 2.8 mass%).
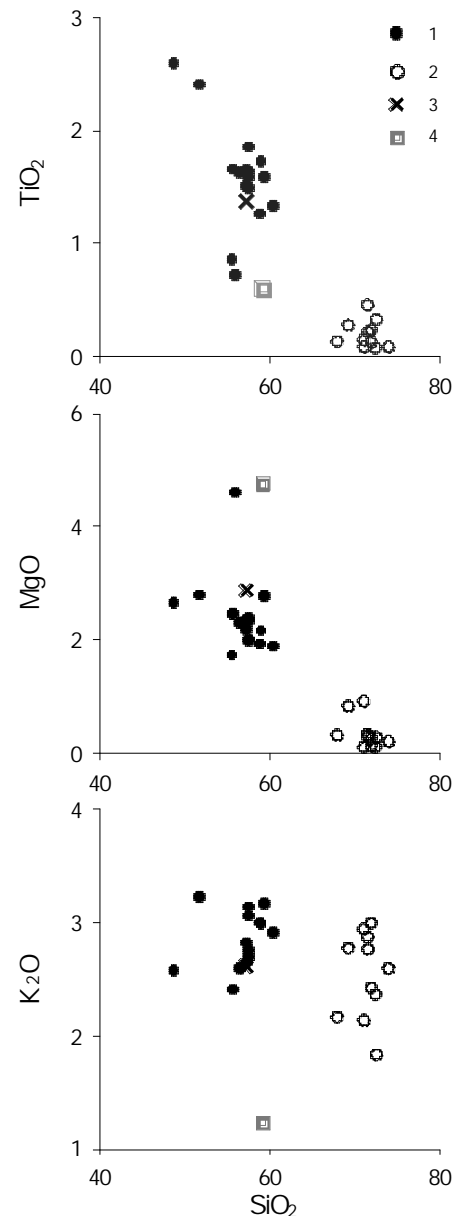
Fig. 1. Compositions of rocks (quadrates and crosses) and melt inclusions (circles) of Gorely (1, 3) and Shiveluch (2, 4).

However these differences can't be explained only by different degrees of fractionation. All melts of Gorely volcanic centre are enriched by trace elements (LILE, HFSE, HREE), while Shiveluch melts are REE-depleted.
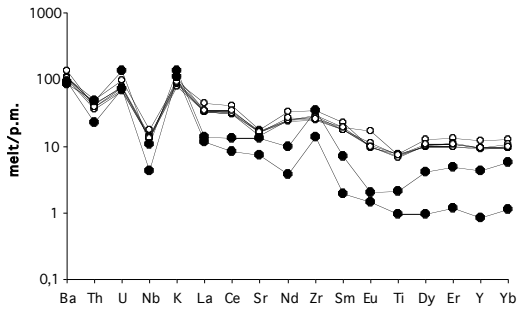
Fig. 2. Spider-diagram for melts of Gorely (empty circles) and Shiveluch (black circles) volcanoes.

The difference between the distribution patterns of trace elements could be explained by the association of these volcanoes with different magmatic sources. Therefore andesitic lavas of Gorely volcano are considered as the result of crystallization of the andesitic melt, while andesitic pumices of Shiveluch volcano are the result of mixing of water-rich dacitic and rhyolitic magmas and xenophases (olivine-spinel xenoliths).

REFERENCES
Dirksen O., Humphreys M.S.C., Pletchov P. (2006) *JVGR*. 155: 201-226
Humphreys M.S.C., Edmonds M. (2010) *GRL*. 37: L00E06.
Reubi O., Blundy J. (2009) *Nature.* 461: 1269-1274
Sun, S.-S., McDonough W.F. (1989) *GSSP*. 42: 313-345.
Tolstykh M., Naumov V. (2000) *Geochemistry International.* 38: 123-132.

Formation conditions and fluid component sources for volcanogenic massive sulphide deposits of the South Urals

Vikentyev, Ilya V.*, Karpukhina, Valentina S.** and Prokof'ev, Vsevolod Ju.*

*Institute of Geology of Ore Deposits, Petrography, Mineralogy and Geochemistry, Russian Academy of Sciences, Moscow, Russia

**Vernadskii Institute of Geochemistry and Analytical Chemistry, Russian Academy of Sciences, Moscow, Russia

Volcanogenic massive sulphide (VMS) deposits of the Urals are located inside ensimatic Tagil-Magnitogorsk trough (Prokin, Buslaev, 1999). Their formation relates to arc-related calc-alkaline rhyolite-dacite series S_1l_2 of Tagil Megazone and D_2e-gv_1 and Na-basalts D_2e_1 of Magnitogorsk Megazone (Table 1). World-class deposits with 3-10 MT of (Cu+Zn) reserves are located within the Magnitogorsk Megazone (Fig. 1). VMS deposits consist of semimassive to massive sulphide lenses underlain by discordant stockworks of quartz-sulphide veins and related quartz-phyllosilicate alternation. Localities of the VMS deposits of the Urals are controlled by paleovolcanic structures (calderas, troughs, local depressions) and are usually connected with rhyodacitic to calc-alkaline rhyolitic domes.

Fig. 1. Schematic map of Middle-South Urals and position of VMS deposits (Vikentyev, 2006).

Fluid inclusions (FI) in minerals from ore bodies and altered country rocks and melt inclusions (MI) and FI in quartz phenocrysts as well as stable (S, O, C, H) and radiogenic (Sr, Pb) isotopes for rocks and ores have been studied. Usually primary FI in minerals of ores (quartz, barite, sphalerite, carbonates) or secondary FI in quartz phenocrysts not exceed 10 μm. T_h range from 375 to 97 °C (routinely 300 – 200 °C). The pressure values range from 30 to 160 MPa that corresponds to buried, subbottom conditions of ore genesis for major deposits. Sulphur contents in fluid of vacuoles ranged from 160 to 250 mg/l, and copper from 0.3 to 1.2 g/kg in the solution. The CO_2 content may amount 40 mass%. Salinities range from 0.3 to 17 eq mass% Na^+ (Table 1). Minor phase separation occurred at deeper levels of some deposits. Na^+ and Mg^{2+} dominate among the cations in the fluid. For metamorphic-regenerated VMS deposits (Tarnjer, Degtyarsk, Tash-Yar, Dzhusinsk) T_h of FI were routinely higher (up to 440 – 465 °C), P = 100 - 180 MPa, w_{salt} = 1 - 18 eq mass% Na^+

Primary magmatic FI in quartz phenocrysts are round to negative crystal shaped and have a size between 25 to 100 μm. The gas bubbles have sizes between 8 to 40 μm. T_h of FI ranges from 124 - 245 °C with a salinity of w_{salt} from 1.2 to 6.2 eq mass% NaCl. Occurrences of sulphide globules (chalcopyrite, bornite, pentlandite and pyrrhotite) in some MI indicate an increased copper content in parent magmatic melt and are evidence of the important role of magma-derived metal components in ore formation. The concentrations of metals in glass of melt inclusion are 1100 ppm for Cu and 1400 ppm for Zn (LA-ICP-QMS).

The range of $(^{87}Sr/^{88}Sr)_o$=0.70597 - 0.70625 for carbonates, indicating a lower involvement of marine and higher input of

magmatic water, are characteristic for ores and host rocks. Deepseated mantle sources were the main ones for lead of galena (Chernyshev et al., 2008).

Isotope compositions of O and C of carbonates ($\delta^{18}O$= +13 to +26.5 ‰, $\delta^{13}C$= -28 to +1 ‰ for massive ores and $\delta^{18}O$= +9 to +27 ‰, $\delta^{13}C$= -20 to -1‰ for altered igneous rocks) testify to important addition of magma-derived components. Values of $\delta^{34}S$ in sulphides of ores ranging from -1 to +6 ‰ CDT for majority of VMS deposits confirm the dominant input of magmatic sulphur to hydrothermal fluid, with subordinated role of sea water sulphate and biogenic sulphur. Data for the δD and $\delta^{18}O$ of fluid deposited silicates and quartz of Aleksandrinsky, Uzelginsky and Uchalinsky deposits lie between marine and magmatic values.

Summary. The formation of the VMS deposits of the Urals related to shallow chambers of acidic magma. Ore bodies have been formed over discharge channels approaching sea floor or at subbottom position from moderately high temperature (up to 390 ^{o}C) hydrothermal solutions at pressure values ranged 30 – 160 MPa. Sr, Pb and stable isotope (S, O, C, H) studies revealed dual (oceanic and juvenile) nature of the ore-forming fluid source. The deposits are related to magmatic fluids as well as alteration of underlying felsic and basic volcanic rocks by circulating fluid system of evolved oceanic water. High amounts of CO_2 in fluid inclusions may also be indicative for a magmatic source of the hydrothermal fluids. This is also supported by high metal contents in primary fluid inclusions in quartz phenocrysts.

REFERENCES

Chernyshev I.V., Vikentyev I.V., Chugaev A.V. et al. (2008) *Doklady Earth Sci.* 418 (1): 178-183.

Karpukhina V.S., Baranov E.N. (1995) *Geochem. Int.* 1: 48-63.

Prokin V.A., Buslaev F.P. (1999) *Ore Geol. Rev.* 14: 1-69.

Simonov V.A., Kovyazin S.V., Terenya E.O. et al. (2006) *Geol.Ore Dep.* 48 (5): 369-383.

Vikentyev I.V. (2006) *Miner. Petrol.* 87: 305-326.

Zaykov V.V., Ankusheva N.N. (2008) *Proc. XIII Int. Conf. Thermobarogeoch.* 2: 41-44.

Age	Deposit type	Magmatic complexes	Main ore elements	Deposits	T_h, ^{o}C	w_{salt}, eq.% NaCl	Cations
S_1l_2	Cu-Zn-pyritic (Uralian type)	Sodium rhyolite-basalt	Cu $\geq$ Zn (Au, Ag)	Shemur	178-119	9.3-1.2	Mg, Na Na (+Mg)
			Zn > Cu (Au, Ag)	Yaman-Kasy [1], Valentor	290-110	16.9-0.6	Na, Mg Na (+Mg) Na
	Zn-Ag-pyritic	Potassium-sodium andesite-dacite	Zn, Au, Ag (Cu, Pb)	Galkinsk	170-114	4,0-1,4	Na, Mg Na (+Mg)
D_2e_1	Cu-Co-pyritic (Cyprus type)	Tholeite-basalt	Cu (Zn, Co)	Letnee, Levoberezhn	305-182		
D_2e-gv_1	Cu-Zn-pyritic (Uralian type)	Sodium rhyolite-basalt	Cu $\geq$ Zn (Au, Ag)	Safjanovsk, Podolsk	337-104	15.3-0.3	Na Na (+Mg)
			Zn > Cu (Au, Ag)	Uzelginsk, Uchaly, Novo-Uchaly, Chebach'e, West-Ozerny	375-97	7.8-0.3	Na К Na (+K) Na (+Ca) Na (+Mg)
	Cu-Zn-barite-pyritic	Sodium rhyolite-basalt	Cu, Zn, Ba (Pb, Au,Ag)	Alexandrinsk	340-160		
	Cu-Zn-Au-barite (Baymak type)	Potassium-sodium andesite-dacite	Cu, Zn, Au, Ba (Pb, Ag)	Tash-Tau [2], Uvarjazh	239-103	8-0.5	Mg (+Na) Na (+Mg) Na

Table. 1. Types of nonmetamorphosed VMS deposits of the South Urals and parameters of hydrothermal fluid (with use of data of Simonov et al., 2006 [1], and Zaykov, Ankusheva, 2008 [2]

REE in quartz fluid inclusions from gold deposits from North-East of Russia

Vikentyeva, Olga V.*, Gamyanin, Gennadii N.* and Bortnikov, Nikolay S.*

*Institute of Geology of Ore Deposits, Petrography, Mineralogy and Geochemistry, Russian Academy of Sciences, Moscow, Russia (ovikenteva@rambler.ru)

Fluid inclusions refer to the fluid entrapped during the formation of minerals. Rare earth elements (REE) are very useful tracers for a wide variety of geochemical processes. Inductively coupled plasma mass spectrometer (ICP-MS) was used to determine REE abundances in fluid inclusions. The samples analyzed in this study were fluid inclusion-bearing quartz concentrates. Object of this study are three major types of gold hydrothermal systems from North-East of Russia: polygenic (1) gold-quartz-sulphide (Au-Q, Nezhdaninsk) and (2) gold-antimony (Au-Sb, Sarylakh and Sentachan) and (3) intrusion-related gold-bismuth-siderite-polysulphide (Au-Bi-Sid, Arkachan) large deposits located in terrigeneous rocks of Verkhoyansk fold belt (Fig. 1). Quartz fluid inclusions from various types of ores have been studied: gold-quartz and Au-Mo-W-Bi veins and regenerated Ag-Pb ores from Nezhdaninsk deposit; Au-Q veins and regenerated quartz of Sb ores from Sarylakh and Sentachan deposit; metamorphic quartz and ore quartz from Arkachan deposit.

PT parameters and compositions of hydrothermal fluids of the deposits based on fluid inclusion studies are shown in Table 1. The data of inclusion types, phase compositions and microthermometry results have been adequately considered (Bortnikov et al., 2007; 2010; 2011).
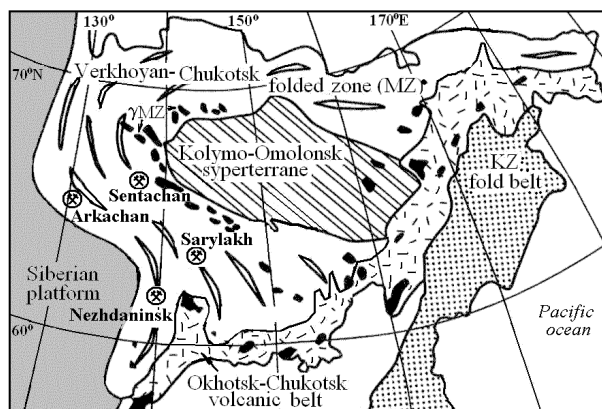
Fig. 1. The position of the studied deposit on the tectonic map of the North-Eastern Territory of Russia.

Our research is focused on the distribution of REE identified in aqueous solutions extracted from fluid inclusions. Analyses were performed by the uniform procedure published by Kryazhev et al. (2006). The procedure includes careful clearing of sample, breaking of inclusions in the quartz reactor by crushing or heating, gas chromatography of H_2O, CO_2, CH_4, preparation of aqueous extract (0,5 g of the sample + 7 ml of the cleansed water), ion chromatography of Cl^-, SO_4^{2-}, F^- and determination of other elements by ICP-MS. The sample washed out after the "working" extract is used for preparation of the "blank" extract.

Deposit	Stage	T_h, °C	P, kbar	w_{salt}, eq.%NaCl	CO_2/CH_4*	∑REE,* ppm	Au,* ppm	Cations*	Anions*
Au-Q	Au-Mo-W-Bi	374-199	1,4-0,4	31,1-1,9	0,1-0,5	5,5-52	0,8-1,3	K, Ca, Na	$Cl^->HCO_3^-$
	Au-Q	368-267	2,0-0,7	9,6-1,2	98-209	0,7-24,3	0,03-20	K, Na, Ca	$HCO_3^->>Cl^-$
	Ag-Pb	387-129	1,9-0,8	8,6-2,4	58-156	1,4-24,3	0,3	K, Ca	HCO_3^-
Au-Sb	Au-Q	340-232	3,4-1,2	8,3-1,6	47-54	0-0,8	0,05	Na, Ca	$HCO_3^->SO_4^{2-}$
	Sb	244-130	2,0-0,3	6,3-3,2	12-85	11,8-42	0,5-2,8	K, Ca	$SO_4^{2-}>HCO_3^-$
Au-Bi-Sid		385-261	1,7-1,3	26,3-3,7	20-137	0,2-4,0	0,5-2,2	Na	$HCO_3^->Cl^-$

*Table. 1. Parameters of hydrothermal fluids for the Nezhdaninsk (Au-Q), Sarylakh and Sentachan (Au-Sb) and Arkachan (Au-Bi-Sid) deposits. * - contents in fluid inclusions (TsNIGRI MNR, analyst Vasyuta Y.V.).*

REE are related to a group of elements-impurities, which arrive in the extract practically only from the matrix of the host mineral (quartz). Their concentration in the extract directly depends on the area of the surface of the sample and is identical in "blank" and "working" extracts. Between all elements of this group (Si, Al, Ga, Ti, Zr, Y, REE) strong positive correlations have been found (Kryazhev et al., 2008).

For samples of Nezdaninsk, Sarylakh and Sentachan deposits such correlation really exists, but for Arkachan deposit there is the opposite correlation. Comparison of total REE contents in the quartz and in the water extract shows enrichment of REE in the fluid inclusions compared to quartz.

The chondrite-normalized REE patterns of inclusion fluids for the Nezhdaninsk and Arkachan deposits are characterized by light rare earth elements (LREE) enrichment with a positive or negative Eu anomaly, whereas the patterns for the regenerated quartz from Sarylakh and Sentachan deposits are characterized by pronounced differentiation between both light and heavy lanthanides in fluid inclusions ($La_n/Sm_n = 12$ and 46, respectively). Only regenerated quartz contains HREE and has ratio La/Ce order higher than early milky quartz. The positive Eu anomalies in the fluid inclusions suggest that the hydrothermal fluids were relatively reduced. The total REE contents for studied deposits are shown on the Figure 2.

For Arkachan deposit the total REE contents are higher in the solutions having higher Na+K values. We interpret that REE concentrations increase, when the salinity the of inclusions becomes higher. Assuming that Cl^- content in the fluid inclusions increases together with the Na+K concentrations, our data suggest that REE could be transported as chlorine complexes in the Arkachan hydrothermal system. Values of Rb and Cs in fluid inclusions also show a positive correlation with the Na+K content.

The data presented here indicate that, indeed, markable amounts of rare earth elements may be transported in gold-bearing solutions.
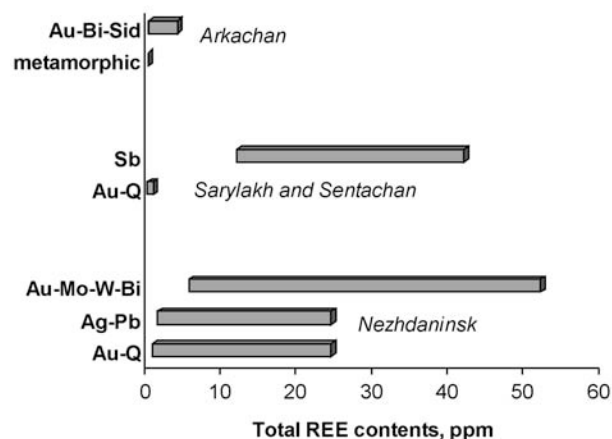
Fig. 2. The total REE contents in quartz fluid inclusions for varies types of deposits.

REFERENCES

Bortnikov N.S., Gamyanin G.N., Vikent'eva O.V. et al. (2007) *Geol. Ore Dep.* 49: 99-145.

Bortnikov N.S., Gamyanin G.N., Vikent'eva O.V. et al. (2010) *Geol. Ore Dep.* 52: 381-417.

Bortnikov N.S., Gamyanin G.N., Vikent'eva O.V., Prokof'ev V. Yu. (2011) *Proc. SGA Meeting, Chile.*

Kryazhev S.G., Prokof'ev V. Yu., Vasyuta Y.V. (2006) *Vestnik MSU. Geolog.* 4: 30-36

Kryazhev S.G., Prokof'ev V. Yu., Vasyuta Y.V. (2008) *www.minsoc.ru/2008-1-2-0*

An insight into the 'magnetite crisis' via magnetite hosted melt inclusions from the Pual Ridge.

Whan, Tarun H. E. and Mavrogenes, John A.

Research School of Earth Sciences, Australian National University, Building 61, Mills Rd., Canberra, Australia

The solubility of sulphur in silicate melts has been demonstrated by Jugo (2005) to be an order of magnitude higher as the oxidised sulphate species (SO_4^{2-}) than reduced sulphide (S^{2-}). Thus in relatively oxidised arc magmas, where sulphate is the predominant species, S solubilities are extremely high. However, the removal of Fe^{3+} from the melt consequent to fractional crystallisation of Fe-Ti oxide results in a shift in the redox exchange:

$$8FeO + SO_4^{2-} = 4Fe_2O_3 + S^{2-}$$
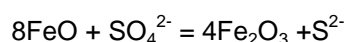
This relationship quantifies that the modest change in the Fe redox ratio can have great influence on sulphur speciation. During evolution of arc magmas, magnetite is the first phase to appear on the liquid line of decent during fractional crystallisation that significantly lowers the total Fe and Fe^{3+}/Fe^{2+} of the residual magma. This has led to the proposal that fractional crystallisation of magnetite may trigger sulphide saturation in the residual melt via the reduction of the Fe^{3+}/Fe^{2+} (i.e. the "magnetite crisis", Jenner et al., 2010).

Subaqueous quenched volcanic glasses provide the clearest record of magmatic evolution by fractional crystallisation. However, during the subaqueous eruption of oxidised arc magmas, significant concentrations of volatile species such as CO_2, S and some H_2O are lost from the resultant quenched glass. The behaviour of selenium has been traditionally thought to parallel that of sulphur in silicate melts (Palme and O'Neill, 2003) but has subsequently been shown to suffer less volatile loss upon quenching than S (Fig. 1).

In order to reconcile the observed chalcophile trace element behaviour during evolution by fractional crystallisation of oxidised arc magmas, precise determination of the sulphur speciation in the melt must first be obtained. However, as significant sulphur degassing occurs in oxidised arc magmas, the pre-eruptive sulphur content of the melt cannot be analysed directly from the quenched glasses.

To circumvent this problem, S* was established as the pre-eruptive ratio of S to Se. As Se is retained in oxidised arc magmas and can be measured in quenched glasses, it can be calibrated with the S/Se of MORBs and oxidised boninites to yield an estimate of the S* in oxidised arc magmas (Jenner et al., 2010).
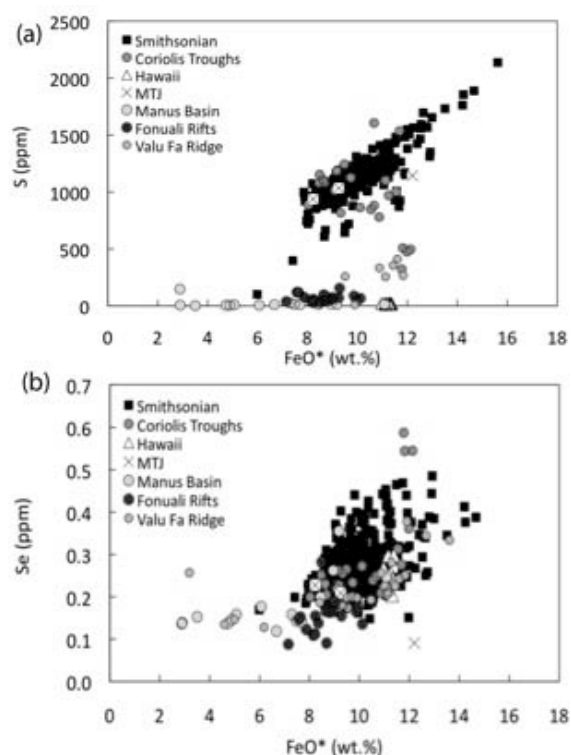
Fig. 1: Co-variation diagrams of (a) S and (b) Se vs. FeO* (mass%) for glasses from the Manus and Lau basins in comparison with the MORB. Demonstrates that oxidized magmas lose S upon degassing whilst reduced melts retain their pre-eruptive S content (Jenner, et al., 2010).

Analysis of melt inclusions contained within Fe-Ti oxide phases is advantageous as volatile and chalcophile elements such as S

behave incompatibly in magnetite-ulvöspinel solid solution. Thus the melt inclusions trapped at the time of oxide crystallisation preserve the original, un-degassed volatile content.

Furthermore the analysis of melt inclusions, contained in phases separated from the Pual Ridge glasses, provides a unique opportunity for the validity of the S/Se method for the determination of the S* to be tested. Electron Microprobe Analysis (EMPA) of melt inclusions contained within titanomagnetite separates from the Pual Ridge glasses (Fig. 2) have been shown to contain mean S concentrations of ~616 ppm, which is in accordance with the ~600 ppm predicted for the melt by the S/Se method.
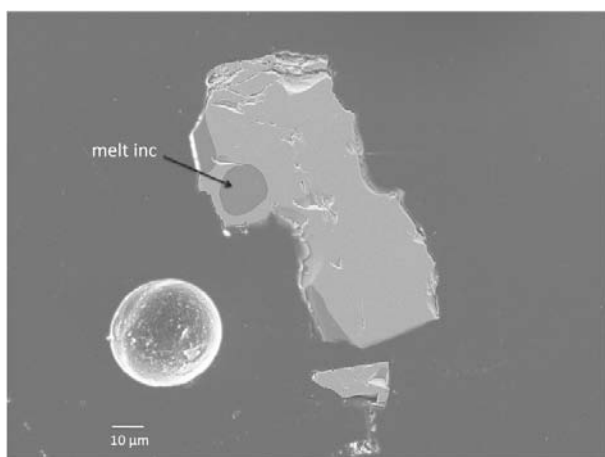
Fig. 2: Titanomagnetite phenocryst containing a silicate melt inclusion from the sample MD-7, Pual Ridge.

EMPA of melt inclusions contained in titanomagnetite phenocrysts from sample MD-7 evidence mean Cu concentrations of ~281 ppm, and is comparable with that measured for the quenched glass by LA-ICP-MS (Fig. 3; Jenner et al., 2010). The melt inclusions in the titanomagnetite phenocrysts record both the analysed peak Cu and the estimated peak S concentration in the melt immediately prior to sulphide saturation. This implies that magnetite crystallisation may trigger, but is not simultaneous with, sulphide saturation.

The Pual Ridge glasses record a fractional crystallisation sequence for which the major and trace element abundances of the residual melt have been thoroughly characterised (Jenner et al., 2010). However, only by the analysis of melt inclusions contained within phases separated from the quenched glasses may the concentrations of volatile elements such as S, CO_2 and H_2O be obtained directly.
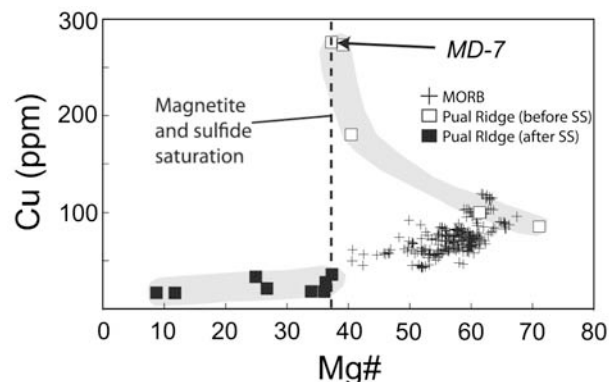
Fig. 3: Co-variation diagram of Cu vs. Mg#. Note the sharp decrease in Cu content of the melt at ~40 Mg#, representing magnetite induced sulphide saturation (Jenner et al., 2010).

Thus, in order to develop a greater understanding of the processes at play during evolution of arc magmas, the previously determined residual melt concentrations must be reconciled with melt inclusion data. Analysis of the melt inclusions contained within the phases separated from the subaqueous glasses over the fractionation interval evidenced by the Pual Ridge samples allows the validity of the 'magnetite crisis' to be rigorously tested. This is significant because it may relate to pre-enrichment of chalcophile trace elements and eventually to the formation of Cu-Au-Ag provinces and the development of the continental crust.

REFERENCES

Jenner, F. E., O'Neill, H. ST. C., Arculus, R. J., Mavrogenes, J. A. (2010) *J. Pet* 51: 2445-2464.

Jugo, P. J., R. W. Luth & J. P. Richards (2005) *J. Pet* 46: 783-798.

Palme, H., O'Neill, H. S. C. (2003). *Treat Geochem.* 2**:** 1-38.

Fluid inclusions in gold-rich ores in the Wulashan Gold Deposit, Inner Mongolia, China

Xu, Jiuhua*, Liu, Jianming**, Lin, Longhua* and Zeng, Qingdong**

*Department of Resource Engineering, University of Science and Technology Beijing, Beijing 100083, China
**Institute of Geology and Geophysics, Chinese Academy of Sciences, Beijing 100029, China

Located 50km west to Baotou city, the Wulashan gold deposit (239 – 276 Ma, Meng et al., 2002) is the largest one in Inner Mongolia, China. The gold-bearing vein systems are hosted by the Archean Wulashan group, which is composed of hypersthene granulite in the bottom, biotite-hornblende plagioclase-gneiss sandwiching magnetite quartzite and amphibolite in the middle, and quartzite and marble sandwiching in the top. There is a biotite granite intrusion in the west of the mine area, but it is not related to gold mineralization because of earlier SHRIMP zircon U-Pb age (353 Ma, Miao et al., 2001). Gold mineralization includes altered rock type and quartz vein type. Felsic pegmatite veins occur widely in the mine area, which are intersected by gold-bearing quartz veins.

There are four mineralizing stages at the Wulashan gold deposit: (K-feldspar)-white quartz stage (I); pyrite-grey quartz stage (II); polymetallic sulphides (chalcopyrite, pyrite, galena) –grey white quartz stage (III); and calcite-quartz stage (IV). Stages II and III are main gold mineralizing stages. Gold-rich veins are substantially polymetallic sulphides-quartz tiny veins filling in fractures of early white quartz veins (Fig. 1). Gold occurs as native gold or electrum along the margins of tiny chalcopyrite veins (Fig. 1A, D and E). Native gold, electrum or sylvanite can also be found in fissures of quartz (Fig. 1B). Some gold occurs in galena-chalcopyrite veins (Fig. 1F). Grey white quartz surrounding gold-bearing sulphides had been recrystallized and shows less deformed; whereas white quartz away from the sulphides had been fractured and deformed, and appears wavy extinction. It is clear that this white quartz had been formed in early stage and had been affected by tectonic stresses during gold mineralization.
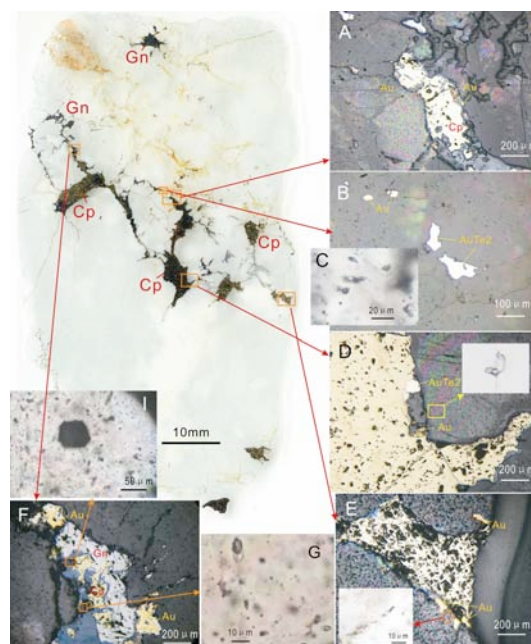
Fig.1. Gold-sulphides in tiny fissures and fluid inclusions in gold-rich quartz vein, the Wulashan gold deposit

Fluid inclusions can be frequently seen in both grey white quartz and early white quartz. Three types of fluid inclusions in quartz can be identified, and they are described as followings.

(1) CO_2-H_2O inclusions, composed of one aqueous phase and one CO_2 phase under room temperatures (Fig. 1C, G, I), dominate in gold-rich quartz vein that was examined. They have CO_2/H_2O volume ratios from 20 to 40%, with sizes of 5 to 30 µm. Sometimes three phases including liquid and gas CO_2 can be seen under room temperatures (Fig. 1D, I). They occur as isolated or random in quartz near gold-bearing sulphides, so they are of primary origin.

(2) CO_2 inclusions or carbonic (CO_2-CH_4-N_2) inclusions are composed of only one phase of CO_2 and are water-free inclusions. They occur occasionally with CO_2-H_2O inclusions in sulphide-

grey quartz veins (Fig. 1G), whereas they seem to be ruptured in early white quartz (Fig. 2). It is supposed that the fluid inclusions in early quartz had been broken during late gold mineralizing stages, because the pressure difference (internal minus external) can result in partial or complete decrepitating (Roedder, 1984).
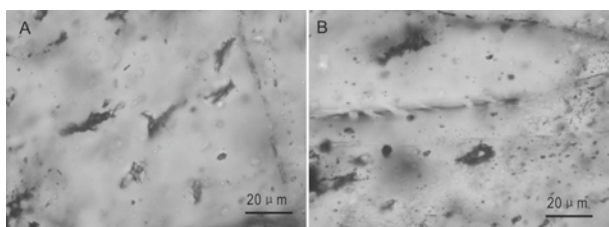
Fig.2.Broken CO_2-H_2O and CO_2 inclusions in early white quartz, the Wulashan gold deposit

(3) Aqueous inclusions, composed of a liquid water phase and a small bubble, occur in quartz outside of sulphide veins.

It is indicated from above petrographic evidence that gold has been introduced later than the bulk of the white quartz. Only those inclusions in recrystallized quartz near the sulphides are the actual gold-depositing fluid.

A microthermometry study shows that primary CO_2-H_2O inclusions in grey quartz near a galena-gold vein have similar melting temperatures of clathrate T_h(cla), i.e., from 5.3 to 7.3 °C (Fig. 3). The salinities are from 8.5 to 5.1 eq mass% NaCl according to Collins (1979). The total homogenization temperatures T_h(tot) are from 230.0 to 239.3 °C in the area of Fig. 3, but many inclusions decrepitated above temperatures of 215 to 273 °C. The partial homogenization temperatures of CO_2 phases in a few inclusions were observed to be between 27 - 31 °C, reflecting lower CO_2 densities of 0.66 - 0.47 g/cm^3. It can be estimated that mole fractions of CO_2 are 7.5 - 10.0% based on phase diagram of Diamond (2001). Hence, the trapping pressures would be at least 80 - 120MPa based on Takenouchi and Kennedy (1964). If we consider an average salinity of 6 eq mass% NaCl, the trapping pressures will be up to 250 MPa according to Brown and Lamb (1989). It is reasonable to speculate that many of inclusions decrepitate during heating because of high internal pressures.

We conclude that fluid inclusions occur in grey white quartz near gold and sulphides represent gold-depositing fluids. The precipitated T-P conditions for the gold-rich ores in the Wulashan gold deposit have been estimated to be at least 230 to 273 °C and 80 to 120 MPa.
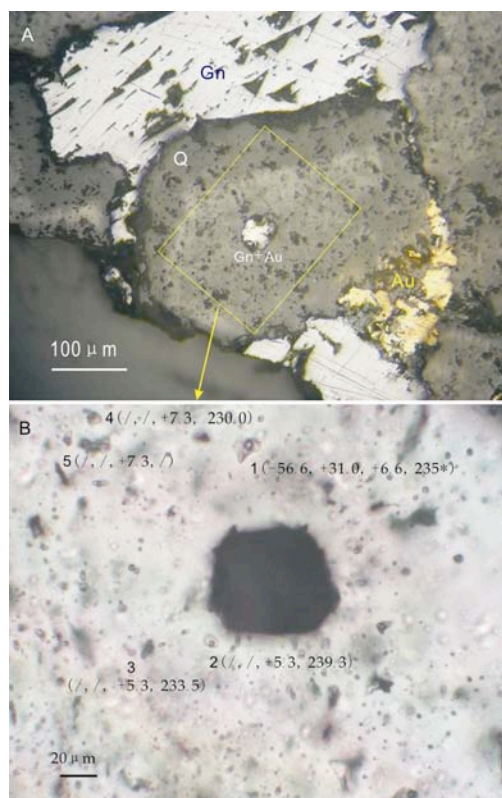
Fig.3.Thermometry of CO_2-H_2O inclusions in grey white quartz near gold-bearing sulphide vein, the Wulashan gold deposit. A: Au-gold; Gn-Galena; Q-Quartz; B: Number of inclusion ($T_m(CO_2)$, $T_h(CO_2)$, $T_h(cla)$,$T_h(tot)$)

REFERENCES
Brown PE., Lamb WM. (1989) *Geochim. Cosmochim. Acta,* 53: 1209-1221
Collins PLF. (1979) *Econ. Geol.,*74: 1435-1444
Diamond LW. (2001) *Lithos*, 55: 69-99
Meng et al.（2002）*Gold Geol.*, 8(4):13-17
Miao et al. (2001) *Geol. Review,* 47(2):169-174
Takenouchi S., Kennedy GC. (1964) Am J Sci., 262: 1055-1074

Bicarbonate-rich fluid inclusions and hydrogen diffusion in quartz gangue from the Libcice orogenic gold deposit, Bohemian Massif

Zacharias, Jiri*, Hrstka, Tomas* and Dubessy, Jean**

*Institute of Geochemistry, Mineralogy and Mineral Resources, Faculty of Science, Charles University in Prague, Albertov 6, Prague, Czech Republic
**G2R(UMR 7566), Faculté des Sciences, Université Henri Poincaré-Nancy Université, Vandoeuvre-les-Nancy Cedex, France

Unusual paleofluid composition is reported for the Libčice orogenic-type gold deposit located in a contact zone of the Central Bohemian Plutonic Complex, Czech Republic. Unexpected bicarbonate-rich fluids and their complex chemistry variations characterize primary fluid inclusions from the main gold-bearing quartz vein. A detailed microthermometry, Laser Raman Micro Spectroscopy and SEM cathodoluminescence study was used in order to decipher fluid history. The results (Zacharias, 2002; Hrstka et al., 2011) indicate the presence of H_2O and H_2O– CO_2–CH_4 ($\pm$ N_2; H_2S) fluids, the latter displaying variations of the CO_2/CH_4 ratio in the gaseous phase from 6.8 to 0.06. Variation of the CH_4 content across single grains and between different levels of the mine was recorded. The presence of nahcolite, H_2 (up to 6 mole%) and ethane (0–0.2 mole%) in the fluids were also discovered by Raman probe. Potential models for the formation of different types of fluids present in the deposit are discussed, including the genesis of HCO_3^- rich fluids as well as H_2 and C_2H_6 presence in the primary fluid inclusions. The potential influence of organic matter-bearing sediments, as well as the impact of the intrusion of CBPC, re-equilibration and/or re-speciation of fluid inclusions during the post-entrapment history is considered to have the main impact on the complex paleofluid chemistry. Based on the thermodynamic modelling, H_2 diffusion into the fluid inclusions was shown to be the main reason for the CH_4 variation on the scale of a single grain, as well as across the whole vein. Although the exact processes of production/formation of HCO_3^- and H_2 at the Libčice deposit remain open to discussion, reactions in the C–O–H system are considered to be a possible formation mechanism.

This work also contributes to our understanding of the importance of post-entrapment modifications and reactions in the C–O–H system on interpretation/ deciphering the processes in orogenic-type deposits.

REFERENCES

Zacharias J. (2002): J. Czech Geol. Society, 47: 123-132.

Hrstka T., Dubessy J., Zacharias J. (2011): *Chem. Geol.* 281: 313-332.

Author Index